

Aerosol Impacts on Climate Projections

Amy Helena Peace

Submitted in accordance with the requirements for the
degree of Doctor of Philosophy

University of Leeds

March 2022

Declaration of Authorship

The candidate confirms that the work submitted is her own, except where work which has formed part of jointly-authored publications has been included. The candidate confirms appropriate credit has been given within the thesis where reference has been made to the work of authors.

This thesis consists of an introductory chapter, three results chapters and a discussion chapter. Chapter 2 in this thesis has been published as a jointly-authored publication: Peace et al. 2020, Effect of Aerosol Radiative Forcing Uncertainty on Projected Exceedance Year of a 1.5 °C Global Temperature Rise, Environmental Research Letters, doi:10.1088/1748-9326/aba20c, jointly authored with Ken S. Carslaw, Lindsay A. Lee, Leighton A. Regayre, Ben B. B. Booth, Jill S. Johnson and Dan Bernie. The text was written by the candidate with the advice of all co-authors. Statistical emulation and sensitivity analysis code was adapted for use with help from Lindsay A. Lee and Jill S. Johnson. The candidate performed analysis of data, ran the simple climate model and prepared figures. The co-authors contributed in the interpretation of results.

Chapter 3 in this thesis has been submitted as a jointly-authored publication: Peace et al. submitted, Evaluating Uncertainty in Aerosol Forcing of Tropical Precipitation Shifts, jointly authored with Ben B. B. Booth, Leighton A. Regayre, Ken S. Carslaw, David M. H. Sexton, Céline J. W. Bonfils and John W. Rostron. The candidate wrote the manuscript with advice from all co-authors. The analysis of data and figure preparation were completed by the candidate. Ben B. B. Booth, David M. H. Sexton and John W. Rostron extracted data and performed additional aerosol forcing simulations for the HadGEM3-GC3.05 PPE. All co-authors provided discussion on the interpretation of results.

Chapter 4: Underestimating European Dimming, Overestimating European Brightening, is yet to be submitted for publication. The candidate wrote the manuscript, performed the analysis of model and observational data, and prepared the figures. The co-authors Leighton A. Regayre, Ken S. Carslaw and Ben B. B. Booth helped with scientific guidance and reviewing the manuscript.

This copy has been supplied on the understanding that it is copyright material and that no quotation from the thesis may be published without proper acknowledgment.

The right of Amy H. Peace to be identified as Author of this work has been asserted by her in accordance with the Copyright, Designs and Patents Act 1988.

© 2022 University of Leeds and Amy H. Peace

Acknowledgments

Firstly, I would like to thank my main supervisors Ken Carslaw, Leighton Regayre and Ben Booth for their support and guidance throughout my PhD. I am grateful for the insightful discussions we had, the time they invested to provide constructive feedback on my work, and their passion to advance the field. I would also like to thank Lindsey Lee and Jill Johnson for their support and guidance through the earlier stages of my PhD.

I would like to thank all the members of the aerosol research groups at Leeds for providing a fun and supportive environment throughout my PhD. For sharing ideas, discussing problems, and of course the many dinners. The climate projections group at the Met Office also welcomed me during visits to Exeter, and provided scientific and technical support throughout my PhD.

Thanks to my pre-pandemic office colleagues of 10.127 for making coming into the office a memorable experience, and to my other friends in ICAS and Leeds for the adventures along the way. Particularly, I would like to mention Ananth and Ben for being great friends and sharing the entire PhD process with me.

Lastly, I wish to thank my parents, Christine and Graham, and partner, Jack, for providing their continued and unconditional support throughout this process.

Abstract

Increasing anthropogenic aerosol emissions have profoundly impacted the climate over the industrial era. However, the radiative forcing of aerosols has persisted as one of the most uncertain aspects of present-day and industrial era climate modelling. This uncertainty in aerosol radiative forcing limits our ability to constrain estimates of climate sensitivity and regional climate changes. Over the coming decades reductions in anthropogenic aerosol emissions are expected in line with climate change and air quality mitigation policies. It is therefore vital to understand how the uncertainty in aerosol radiative forcing effects climate projections, and continue working towards reducing uncertainty in aerosol radiative forcing. The research in this thesis quantifies the range of changes in aerosol radiative forcing up to the mid-21st century for anthropogenic aerosol emission reduction scenarios. The effect of uncertainty in aerosol radiative forcing on future climate responses such as global mean temperature evolution and tropical precipitation shifts is explored. The usefulness of model performance in simulating observed surface solar radiation trends as a constraint on aerosol forcing is evaluated.

The results demonstrate anthropogenic aerosol emission reductions scenarios cause a positive global mean radiative forcing up to mid-21st century, relative to 2000. There is a large uncertainty in the near-term projections of aerosol radiative forcing due to both model parametric uncertainty and scenario uncertainty. Sea spray emissions and updraft velocity are the dominant causes of variance in near-term global mean aerosol radiative forcing for a middle of the road emission scenario in the modelling framework we explore. The uncertainty in near-term aerosol radiative forcing in the middle of the road emissions scenario alone can cause a 5-year window in projecting the exceedance year of a global temperature rise of 1.5 °C, which the Paris Agreement aims to limit temperature rise to. A correlation between the uncertainty in aerosol radiative forcing and climate sensitivity would increase the projected exceedance window by many years.

Observed shifts in tropical precipitation have been attributed to anthropogenic aerosol radiative forcing. Previous studies suggested the strength of the hemispheric contrast in aerosol radiative forcing can modulate the magnitude of tropical precipitation shifts. However, the results in this thesis show accounting

for parametric model uncertainty and a greater influence from internal variability can obscure such a relationship between anthropogenic aerosol forcing and tropical precipitation shifts over the 20th century. Yet, there is a clear influence of major volcanic eruptions on shifts. However, in the future, under a high greenhouse gas emission scenario, there is relationship between the magnitude of present-day aerosol forcing and tropical precipitation shifts up to mid-21st century.

The results in this thesis suggest that projections of both global mean temperature change and tropical precipitation shifts will be improved by reducing aerosol radiative forcing uncertainty. For tropical precipitation, any predictive gains may be offset by temporary shifts caused by potential future major volcanic eruptions. Trends in surface solar radiation are one line of evidence that has been suggested as a constraint on aerosol radiative forcing because the observations capture trends that coincide with the long-term evolution of aerosol emissions. The research in this thesis shows that caution is needed when using surface solar radiation as a model constraint because model performance, parameter influence and the relationship with aerosol radiative forcing varies between time periods when anthropogenic aerosol emissions increased compared to periods when emissions decreased, seasons, the degree of ocean coupling in the model, and the model ensemble size.

The results in this thesis provide insight into the important impacts that the uncertainty in aerosol radiative forcing has on future climate projections, and highlight areas of research needed to better understand and reduce the uncertainty of aerosol-driven responses in climate projections.

Table of Contents

Acknowledgments	III
Abstract	IV
List of Figures	IX
List of Tables	XII
Abbreviations	XIII
Chapter 1 Introduction	1
1.1 Atmospheric Aerosols	1
1.2 Aerosol-Radiation and Aerosol-Cloud Interactions	2
1.3 Evolution of Aerosol Emissions.....	4
1.4 Uncertainty in Aerosol Radiative Forcing	6
1.5 Climatic Effects of Aerosol Radiative Forcing	9
1.6 Constraints on Aerosol Radiative Forcing and Aerosol-Driven Climate Responses	12
1.7 Thesis Aims and Structure.....	14
Chapter 2 Effect of Aerosol Radiative Forcing Uncertainty on Projected Exceedance Year of a 1.5 °C Global Temperature Rise	26
2.1 Introduction	27
2.2 Methods	29
2.2.1 Climate Model: HadGEM3-UKCA	29
2.2.2 A Perturbed Parameter Ensemble of HadGEM3-UKCA	29
2.2.3 Using Statistical Emulation to Estimate Uncertainty in Future Aerosol Forcing.....	31
2.2.4 Shared Socioeconomic Pathways (SSPs)	33
2.2.5 Temperature Projection with a Simple Climate Model	34
2.3 Results.....	36
2.3.1 Quantifying Uncertainty in Near-Term Aerosol Radiative Forcing	36
2.3.2 Sources of Uncertainty in Near-Term Aerosol Radiative Forcing	38
2.3.3 Impact of Uncertainty in Aerosol Radiative Forcing on Temperature Projection.....	39
2.4 Discussion and Conclusion.....	43
Chapter 3 Evaluating Uncertainty in Aerosol Forcing of Tropical Precipitation Shifts	51
3.1 Introduction	52
3.2 Methods	55

3.2.1 Perturbed Parameter Ensemble of HadGEM3-GC3.05	55
3.2.2 Quantifying Shifts in Tropical Precipitation.....	56
3.2.3 Inter-Hemispheric Temperature and Radiative Forcing	57
3.3 Results and Discussion.....	59
3.3.1 Tropical Precipitation Shifts over the 20 th Century	59
3.3.2 Tropical Precipitation Shifts Up To Mid-21 st Century	68
3.4 Conclusion	72
Chapter 4 Underestimating European Dimming, Overestimating European Brightening.....	80
4.1 Introduction	81
4.2 Methods	83
4.2.1 Perturbed Parameter Ensemble of HadGEM3-GC3.05	83
4.2.2 Observations of Surface Solar Radiation.....	84
4.2.3 Model Evaluation Metrics and Parameter Relationships.....	86
4.3 Results.....	88
4.3.1 Solar Dimming Period: 1960 to 1980	88
4.3.2 Solar Brightening Period: 1985 to 2005	96
4.3.3 Multi-Year Average: 2005 to 2009	103
4.3.4 Surface Solar Radiation Trends as a Constraint on Anthropogenic Aerosol ERF	106
4.4 Discussion	107
4.5 Conclusion	111
Chapter 5 Thesis Conclusion.....	118
5.1 Summary of Main Results	118
5.1.1 Effect of Aerosol Radiative Forcing Uncertainty on Projected Exceedance Year of a 1.5 °C Global Temperature Rise	118
5.1.2 Evaluating Uncertainty in Aerosol Forcing of Tropical Precipitation Shifts	119
5.1.3 Underestimating European Dimming, Overestimating European Brightening	120
5.2 Thesis Limitations	121
5.3 Directions for Future Work	122
Appendix A.....	126
A.1 Description and Distributions of Perturbed Parameters.....	126
A.2 Aerosol Radiative Forcing Range in the PPE: in Context	131
A.3 Emissions Scalings.....	133
A.4 Extrapolation of Aerosol Radiative Forcing.....	136

A.5 Aerosol Radiative Forcing	137
A.6 Sensitivity Analysis of Aerosol Radiative Forcing	139
A.7 Temperature Projections in a Simple Climate Model.....	141
A.7.1 Temperature Projections Taking into Account Near-term Aerosol Radiative Forcing Uncertainty	141
A.7.2 Temperature Projections Taking into Account Near-Term Aerosol Radiative Forcing Uncertainty, Normalized at a 2000 Baseline to HadCRUT4	142
A.7.3 Temperature Projections Taking into account Near-Term Aerosol Radiative Forcing and Climate Sensitivity Uncertainty	143
A.7.4 Temperature Projections Taking into Account Near-Term Aerosol Radiative Forcing and Climate Sensitivity Uncertainty Normalized at a 2000 baseline to HadCRUT4	144
A.7.5 Limitations and Assumptions.....	145
Appendix B.....	147
Appendix C.....	168

List of Figures

- Figure 1.1 Example of black carbon aerosol emission sources, atmospheric processes and interaction with clouds and radiation. This figure is taken from Bond et al. (2013).3
- Figure 1.2 (a) Change in annual mean sulphate load between 1950 and 2000 and (c) evolution of annual mean sulphate load relative to 1850 for specified regions. This figure is taken from Skeie et al. (2011) and has been cropped to show the specified plots.4
- Figure 1.3 Changes in annual total (anthropogenic and biomass) global emissions (relative to 2015) of sulphur dioxide (SO₂), organic carbon (OC) and black carbon (BC) for SSP pathways. This figure is taken from Turnock et al. (2020).5
- Figure 1.4 Percentage contributions of uncertain aerosol and physical atmosphere model parameter to the variance for 1850-2008 (left) and 1978–2008 (right) global annual mean aerosol ERF. This figure was taken from Regayre et al. (2018) and cropped to show two time periods.8
- Figure 1.5 Emulated emissions to aerosol ERF curves for CMIP6 models. Aerosol ERF is shown relative to 1750. SSP2-4.5 is a middle of the road future emission scenario. This figure is taken from Smith et al. (2021)..9
- Figure 2.1 This schematic illustrates the steps used to quantify the uncertainty in near-term aerosol radiative forcing. The figure to the left shows a 2-dimensional example of a perturbed parameter ensemble. The middle figure illustrates a statistical emulator (blue cloud) trained from the perturbed parameter ensemble model output (blue dots), and validated against further model output (green dots). The figure to the right illustrates how by using the emulator, an anthropogenic emission scaling can be applied to predict a range of aerosol radiative forcing that represents the aerosol climate model uncertainty.....30
- Figure 2.2 Changes in anthropogenic SO₂ emissions between 2000-2050 for the Shared Socioeconomic Pathways scenarios SSP1-RCP2.6, SSP2-RCP4.5 and SSP4-RCP6.0 used (top row), in comparison to the scalings applied to our 2008 emissions from the PPE simulations (bottom row).....34
- Figure 2.3 Global mean radiative forcing relative to the year 2000 for anthropogenic aerosol emission (anthropogenic SO₂, carbonaceous fossil fuel, carbonaceous biofuel) reductions scaled to match three SSP emission scenarios. The solid line represents the mean of radiative forcing predictions, with the shaded area representing the 95% credible interval that represents the parametric uncertainty within the aerosol-climate model. The dashed line and lighter shaded areas represent where aerosol radiative forcing has been extrapolated.....37

Figure 2.4 Global mean temperature change relative to 1850-1900 for SSP2-RCP4.5. We prescribe our aerosol radiative forcing (RF) from 2000 for anthropogenic aerosol emissions changes. All other forcings are calculated by FaIR v1.4 from SSP2-RCP4.5 prescribed emissions. The top figure (a) shows the impact of model uncertainty in aerosol radiative forcing from 2000, with the darker shaded line representing our mean radiative forcing value translated to temperature and the shaded region representing the 95% credible interval (CI) for aerosol radiative forcing, with the black dashed line representing observations from HadCRUT4. The bottom figure (b) displays an illustrative range in exceedance year of 1.5 °C if a statistical relationship between uncertainty in aerosol radiative forcing and climate sensitivity is accounted for from 2000, for example if stronger values of our aerosol forcing range are paired with higher values of ECS and TCR, and weaker values of our aerosol forcing range are paired with lower values of ECS and TCR. The range of values selected for ECS and TCR in each projection is displayed in the figure legend.42

Figure 3.1 Time series of 5-year rolling mean Φ_{ITCZ} anomaly relative to the 1950 to 2000 reference period for (a) global, (b) Atlantic and (c) Pacific regional means. The ensemble mean time series is shown by the darker line, and the individual ensemble members in the lighter lines. Major volcanic eruptions are marked with grey vertical lines with maximum aerosol loading in the NH (El Chichón (1982, Mexico, 17.21° N) and Pinatubo (1991, Philippines, 15.08° N)) and in the SH (Mt. Agung (1963, Indonesia, 8.20° S)).60

Figure 3.2 Trend in 5-year rolling mean Φ_{ITCZ} for (a) 1950 to 1985 and (b,c) 2006 to 2060 for global (left), Atlantic (middle) and Pacific (right) regional means. The violin plots in light purple (in b) and red (in c) are equivalent. The black lines within the violin plots show individual ensemble members (13 in the PPE, 4 in the initial condition ensemble) and the white dashed line shows the ensemble mean.....61

Figure 3.3 Scatter plot of the 1950 to 1985 trend in 5-year rolling mean Φ_{ITCZ} against the 1950 to 1985 trend in inter-hemispheric (over 60 °S to 60 °N) surface air temperature (a), implied total radiative forcing (b) and anthropogenic aerosol ERF (c) for global (left), Atlantic (middle) and Pacific (right) regional means. Anthropogenic aerosol ERF is calculated over 1860 to 1975 for the PPE, and 1850 to 2014 for the initial condition ensemble. The Spearman’s rank correlation coefficient between variables is shown at top left of each plot.64

Figure 3.4 Scatter plot of trend in 5-year rolling mean Φ_{ITCZ} in 2006 to 2060 against the trend in inter-hemispheric (60 °S-60 °N) surface air temperature (a), and 1860 to 2005 anthropogenic aerosol ERF (b, c) for global (left), Atlantic (middle) and Pacific regional means (right). The Spearman’s rank correlation coefficient is shown at top left of each plot.71

Figure 4.1 Location of the 39 GEBA stations used in this study. The stations are partitioned into 5 European regions: North (N), North-West (NW), East (E), South (S), and Central (C) based on principal component analysis performed in Sanchez-Lorenzo et al. (2015).....85

Figure 4.2 1960 to 1980 linear trend of the 5-year rolling mean annual anomaly (from the 1960 to 1980 mean) in all sky SSR ($W m^{-2} year^{-1}$) across Europe. GEBA observations are overlaid in circles. The ensemble mean is shown at the top, followed by the individual ensemble members. The normalised RMSE is shown in the top left of each plot.	89
Figure 4.3 Density plots of the trend in the 5-year rolling mean SSR over 1960 to 1980 ($W m^{-2} year^{-1}$) at European GEBA stations. The rows of the plot labelled with numbers "0XXXX" represent PPE members where the model data has been interpolated to GEBA stations. The mean across the GEBA station locations is displayed by the dashed dark grey vertical line in each row, and the regional mean of PPE data over the whole of Europe is displayed with the light grey dashed line. Rows are ordered according to the magnitude of SSR trend at GEBA station locations.....	92
Figure 4.4 Histogram of the trend ($W m^{-2} year^{-1}$) in the five-year rolling mean time series of the annual anomaly in SSR for the average of the European GEBA stations over a) 1960 to 1980 and b) 1985 to 2005. .	93
Figure 4.5 1985 to 2005 linear trend of the 5-year rolling mean annual anomaly (against a 1985 to 2005 base period) in all sky SSR ($W m^{-2} year^{-1}$) across Europe. GEBA observations are overlaid in circles. The ensemble mean is shown in top left of the plot, followed by the individual ensemble members. The normalised RMSE is shown in the top left of each plot.	97
Figure 4.6 Density plots of the trend in the 5-year rolling mean SSR over 1960 to 1980 ($W m^{-2}$) at European GEBA stations. The rows of the plot labelled with numbers "0XXXX" represent PPE members where the model data has been interpolated to GEBA stations. The regional mean across the GEBA station locations is displayed by the dashed light grey vertical line in each row, and the regional mean of PPE data over the whole of Europe is displayed with the light grey dashed line. Rows are ordered according to the magnitude of SSR trend at GEBA station locations.....	99
Figure 4.7 a): 5-year rolling mean time series of the annual anomaly (against 1960 to 1985 and 1985 to 2005 base period) in SSR ($W m^{-2}$) for the average of European GEBA stations (green), the nearest model grid boxes to stations in the PPE (blue), and nearest model grid boxes to stations from HadGEM3GC-3.1 initial condition ensemble (red).The shading around each time series shows the spread in the ensemble mean for \pm the ensemble standard deviation b): PPE mean 5-year rolling mean time series of the annual anomaly (against 1960 to 1985 and 1985 to 2005 base period) in SSR ($W m^{-2}$) for all-sky (blue), clear-sky (pink) and cloudy-sky (green) for the nearest model grid boxes to GEBA stations. The shading around each time series shows the ensemble mean \pm the ensemble standard deviation.....	102

Figure 4.8 2005 to 2009 average in all sky SSR ($W m^{-2}$) across Europe for a) coupled ocean-atmosphere simulations and b) atmosphere-only simulations. 35 GEBA observations are overlaid in circles in circles. The ensemble mean is shown in top left of the plot, followed by the individual ensemble members. The normalised RMSE shown in the top left of each plot..... 104

List of Tables

Table 3.1 Table of Spearman’s rank correlation coefficients for the trend in global mean 5-year rolling mean Φ_{ITCZ} and global inter-hemispheric (60 °S to 60 °N) variables shown in Figure 3.3 with values for alternate time periods.....	67
Table 3.2 Table of Spearman’s rank correlation coefficients for the 1950 to 1985 trend in global mean 5-year rolling mean Φ_{ITCZ} and additional global inter-hemispheric (60 °S to 60 °N) variables.	68
Table 4.1 Regional mean 1960 to 1980 linear trend of the 5-year rolling mean annual anomaly in all-sky SSR ($W m^{-2} year^{-1}$) for GEBA, the PPE mean and initial condition ensemble mean when model data is interpolated to GEBA station locations. Linear trends in bold are statistically significant ($p < 0.05$) based on the Mann-Kendall test. The error is the standard error of the estimated trend. For the purpose of significance testing and error calculation, in the results shown in this table the regional mean for each year is calculated prior to trend calculation. In the other figures in this study, the regional mean is calculated following trend calculation.	90
Table 4.2 Spearman’s rank correlation coefficient between the trend in all-sky SSR in the given time periods and the perturbed parameters. Only parameters that have $r \geq 0.6$ are shown. The sign of the relationships in the dimming period have been reversed, so that for example, a positive relationship corresponds to decreasing model skill with an increasing parameter value in both time periods (because nRMSE is negative in the dimming period). Parameter descriptions are shown in Table B.1.	95
Table 4.3 Regional mean 1985 to 2005 linear trend of the 5-year rolling mean annual anomaly in all-sky SSR ($W m^{-2} year^{-1}$) for GEBA, the PPE mean and initial condition ensemble mean when model data is interpolated to GEBA station locations. Trends in bold are statistically significant ($p < 0.05$) based on the Mann-Kendall test. The error is the standard error of the estimated trend. For the purpose of significance testing and error calculation, in the results shown in this table the regional mean for each year is calculated prior to trend calculation. In the other figures in this study, the regional mean is calculated following trend calculation.....	100
Table 4.4 Table shows Spearman’s rank correlation coefficient between the 2005 to 2009 average in all-sky SSR in the given experiment types and the perturbed parameters. Only parameters that have $r \geq 0.6$ are shown. Parameter descriptions are shown in Table B.1.	105

Abbreviations

aci	Aerosol-Cloud Interactions
AMOC	Atlantic Meridional Overturning Circulation
AOD	Aerosol Optical Depth
ari	Aerosol-Radiation Interactions
CCN	Cloud Condensation Nuclei
CDNC	Cloud Droplet Number Concentration
CMIP	Coupled Model Intercomparison Project
ECS	Equilibrium Climate Sensitivity
ERF	Effective Radiative Forcing
ESM	Earth System Model
FaIR	Finite Amplitude Impulse Response model
GCM	Global Climate Model
GEBA	Global Energy Balance Archive
GHG	Greenhouse Gas
HadGEM	Hadley Centre Global Environmental Model
IPCC	Intergovernmental Panel on Climate Change
ITCZ	Intertropical Convergence Zone
MME	Multi-Model Ensemble
PPE	Perturbed Parameter Ensemble
RCPs	Representative Concentration Pathways
SSPs	Shared Socioeconomic Pathways
SSR	Surface Solar Radiation
TCR	Transient Climate Response
TOA	Top of Atmosphere
UKCA	UK Chemistry and Aerosol Model

Chapter 1 Introduction

1.1 Atmospheric Aerosols

Atmospheric aerosols have profoundly impacted the climate over the industrial era, and will continue to do so over the 21st century.

Atmospheric aerosols are a collection of solid, liquid or mixed phase particles suspended in air. Aerosols can either be emitted from a source directly into the solid or liquid phase (primary aerosol), or formed through gas-to-particle transformation (secondary aerosol) (Boucher, 2015). The sources of primary and secondary aerosol can be natural or anthropogenic. For example, primary natural aerosol includes sea spray, desert dust and biomass burning, whereas secondary natural aerosol can be formed from gaseous precursors such as dimethylsulphide (DMS) and volcanic SO₂. Anthropogenic aerosol mainly originates from fossil fuel and bio fuel combustion. For instance, fossil fuel combustion emits primary aerosol in the form of black and organic carbon, plus sulphate aerosol is formed from emitted SO₂.

Once emitted into the atmosphere, aerosols and their gaseous precursors undergo microphysical and chemical processes. These atmospheric processes effect the concentration, composition, size and mixing state of atmospheric aerosols (Randall et al., 2013). Gas phase molecules can transfer to another phase by clustering together (nucleation) which can lead to the formation of new particles, or by condensation onto the surface of pre-existing aerosol particles. Aerosol particles can amalgamate together to form larger particles (coagulation). Soluble aerosol species can dissolve in cloud water and undergo chemical reactions, being released into another phase when the cloud droplets evaporate (Boucher, 2015). While in the atmosphere, aerosols are mixed in the boundary layer, entrained or detrained into convective clouds, and transported by large-scale winds (Gong and Barrie, 2009). Aerosols are removed from the atmosphere through dry deposition at the surface, or by wet deposition, which includes in-cloud activation into cloud droplets or below-cloud scavenging by falling rain droplets (Pierce et al., 2015).

As a result of these processes, aerosols have a short atmospheric lifetime of days to weeks, depending on their composition and size (Kristiansen et al., 2016). For a residence time of 5 days, aerosols can be transported typically around 2000 km

from source (Bellouin et al., 2020). Consequently, aerosols are concentrated relatively close to or downwind of emission sources.

1.2 Aerosol-Radiation and Aerosol-Cloud Interactions

Atmospheric aerosols modify the Earth's radiation budget through their interaction with radiation, termed aerosol-radiation interactions (ari), and with clouds, termed aerosol-cloud interactions (aci).

Aerosol-radiation interactions (formerly the direct effect) refer to the scattering and absorption of radiation by aerosols. Scattering of solar radiation by aerosols reduces the amount of incoming radiation at the Earth's surface. The absorption of radiation by aerosols such as black carbon can modify the vertical temperature profile of the atmosphere which causes rapid atmospheric adjustments (formerly semi-direct effects) that affect atmospheric stability, relative humidity and consequently cloud formation (Bond et al., 2013). Absorbing aerosols that are deposited on snow can also affect surface reflectivity (e.g. Flanner et al., 2007).

Aerosol-cloud interactions refer to the alteration of the micro and macrophysics of clouds by aerosols acting as cloud condensation nuclei (CCN) or ice nuclei (IN) and the resulting cloud adjustments (Andreae and Rosenfeld, 2008). Aerosol-cloud interactions are diverse and complex, dependent on factors such as the cloud type, aerosol type, and meteorological conditions. For liquid clouds with a fixed amount of water, an increase in CCN generally leads to smaller but more numerous cloud droplets. The increase in cloud droplets increases the albedo of clouds (the Twomey or first indirect effect; Conover, 1966; Hobbs et al., 1970; Twomey, 1974). It has been hypothesised that clouds adjust to smaller droplets by slowing of the coalescence rate, which suppresses precipitation and thereby leads to prolonged cloud lifetime and extended areal coverage (the lifetime or second indirect effect; Albrecht, 1989). However, there is debate surrounding this effect as differences in the direction and magnitude of cloud lifetime have been observed in response to increased cloud droplets (Bellouin et al., 2020; Gryspeerdt et al., 2017; Malavelle et al., 2017; Possner et al., 2020; Toll et al., 2019).

An example of the sources of aerosol, the atmospheric processes, and interaction with clouds and radiation is shown in Figure 1.1 for black carbon. The air and aci described above alter the radiative balance of the atmosphere. Aerosol effective radiative forcing (ERF) is used to quantify the radiative forcing exerted by aerosols within the climate system. Forster et al. (2016) define ERF as the change in top of atmosphere (TOA) flux following a perturbation within the climate system.

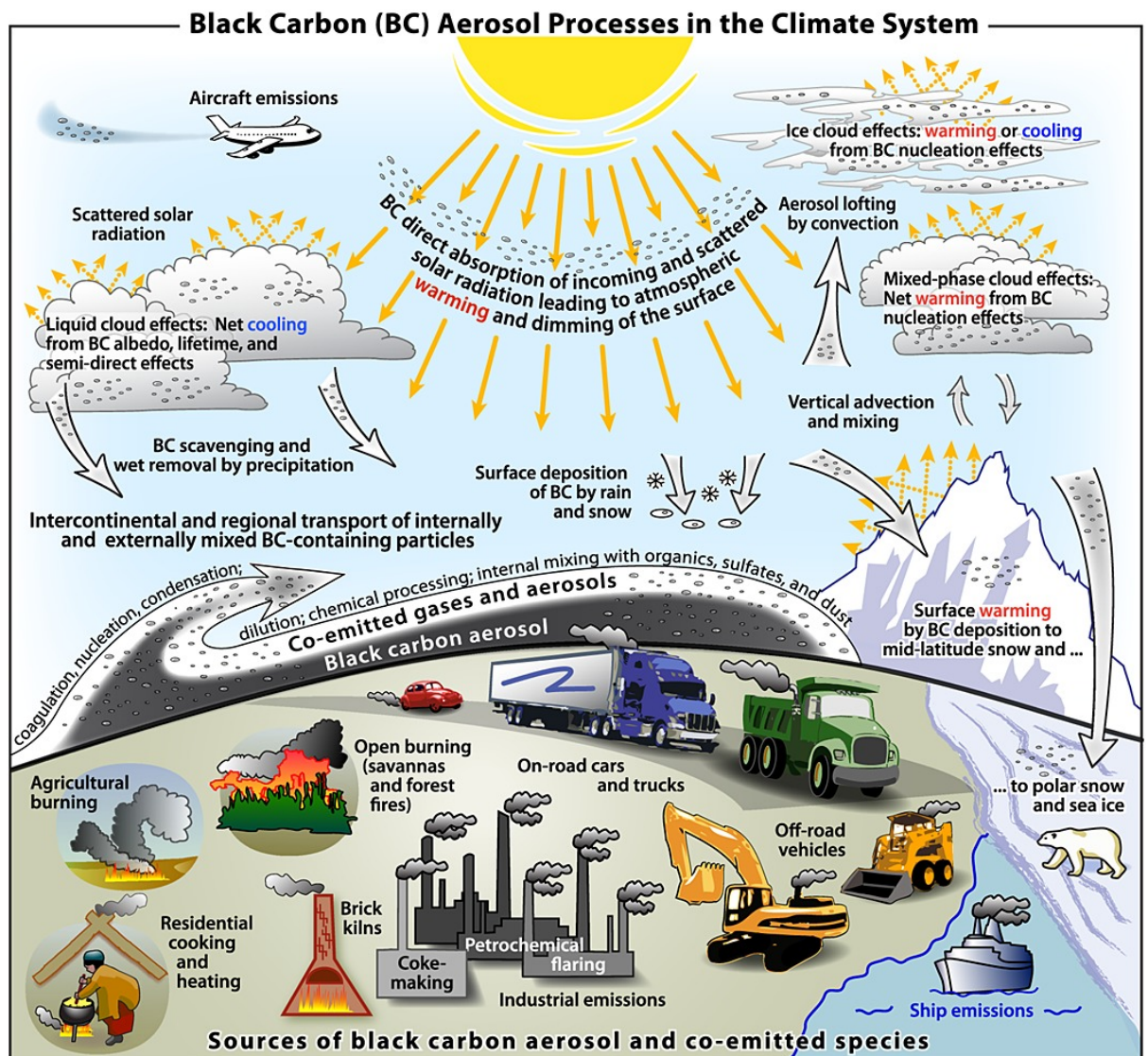


Figure 1.1 Example of black carbon aerosol emission sources, atmospheric processes and interaction with clouds and radiation. This figure is taken from Bond et al. (2013).

1.3 Evolution of Aerosol Emissions

Anthropogenic activities have substantially changed the abundance of atmospheric aerosols over the industrial era. Anthropogenic SO₂ emissions rose dramatically in the 20th century in line with increased fossil fuel combustion driven by growth in the energy transformation and industrial sectors (Hoesly et al., 2018; Lamarque et al., 2010; Skeie et al., 2011). In the beginning of the 20th century, emissions of anthropogenic SO₂ were dominated by Europe and North America, and began to increase in other regions by mid-20th century (Smith et al., 2011). Globally anthropogenic SO₂ emissions peaked in the 1980s driven by emission control policies in Europe and North America whilst Asian emissions continued to increase (Hoesly et al., 2018). In recent years (2005 to 2016) SO₂ emissions from China have gradually declined, whereas emissions from India continue to grow (Li et al., 2017). Hence, there has been a southward and eastward shift in SO₂ emissions over recent decades, as shown in Figure 1.2. Over the 20th century, emissions of organic and black carbon aerosol increased firstly due to residential sources, with other sectors such as agriculture and waste contributing after the mid-20th century (Hoesly et al., 2018). Unlike anthropogenic SO₂, emissions of black and organic carbon originate mainly from Asia and Africa, and have continued to increase up to present-day (Bond et al., 2007; Wang et al., 2014).

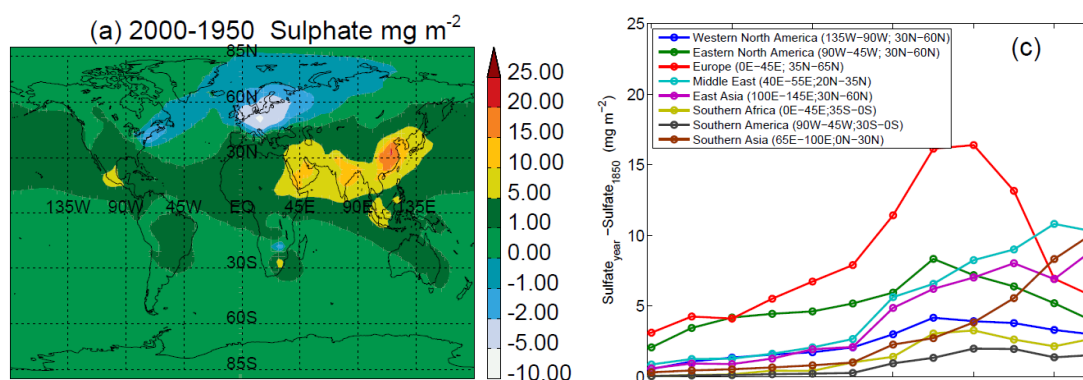


Figure 1.2 (a) Change in annual mean sulphate load between 1950 and 2000 and (c) evolution of annual mean sulphate load relative to 1850 for specified regions. This figure is taken from Skeie et al. (2011) and has been cropped to show the specified plots.

Over the coming decades anthropogenic aerosol emissions are projected to decrease in line with air quality and climate change mitigation policies. To explore the climate impact of changing anthropogenic aerosol emissions in the future (amongst other potential changes), common emission scenarios are used within

the climate modelling community. The Representative Concentration Pathways (RCPs) have been widely used in modelling studies of the Coupled Model Intercomparison Project Phase 5 (CMIP5) era. The RCPs prescribe emission scenarios based on a set of future scenario pathways that cover a range of four radiative forcing target values by 2100 (van Vuuren et al., 2011). The aerosol emissions pathways in the four RCP scenarios vary but are all based on the assumption of successful implementation of pollution control. Hence, the RCPs sample a relatively small range of aerosol emission changes that are not representative of the range of air pollution scenarios in current literature (Rao et al., 2017). In contrast, the more recently developed Shared Socioeconomic Pathways (SSPs) that are used in CMIP6 take into account different strengths of air pollution control and span a larger range of aerosol emission pathways than the RCPs (Rao et al., 2017). The SSPs are based on five different socio-economic narratives, and combine with the RCPs in a scenario matrix structure (Riahi et al., 2017). Aerosol emissions decline by up to 70% by the mid-21st century in SSP scenarios with strong air pollution control, but increase in the medium-term for SSP scenarios where air pollution control plans are not achieved (Rao et al., 2017; Turnock et al., 2020). Figure 1.3 shows the global mean evolution of aerosol emissions under selected SSP pathways. Hence, future emission scenarios provide an opportunity to explore relationships between emission changes and climate impacts, but the real world may well fall outside of the scenario range.

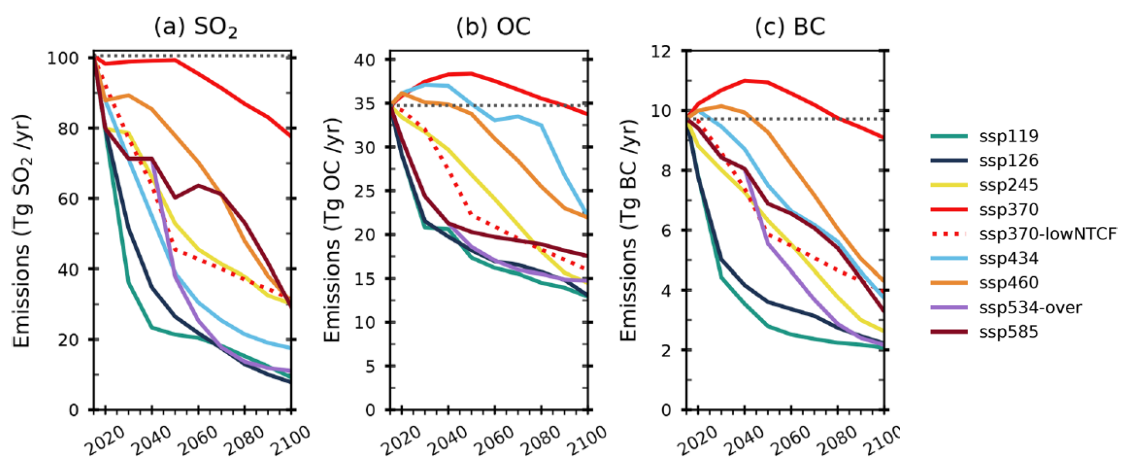


Figure 1.3 Changes in annual total (anthropogenic and biomass) global emissions (relative to 2015) of sulphur dioxide (SO₂), organic carbon (OC) and black carbon (BC) for SSP pathways. This figure is taken from Turnock et al. (2020).

In the coming decades, the emission fluxes of natural aerosols are also likely to change in response to a warming climate and land use change (Allen et al., 2016; Carslaw et al., 2010). For example, most models show a global mean increase in sea spray and biogenic volatile organic carbon (VOC) emissions in a warmer climate (Allen et al., 2016; Gettelman et al., 2016; Paulot et al., 2020; Scott et al., 2018; Thornhill et al., 2021).

1.4 Uncertainty in Aerosol Radiative Forcing

Increasing anthropogenic aerosol emissions over the industrial period have caused a net negative radiative forcing through the interactions of aerosols with clouds and radiation, as discussed in Section 1.2. The Intergovernmental Panel on Climate Change (IPCC) Sixth Assessment Report (AR6) used multiple lines of observational and modelling evidence to estimate a 1750 to 2015 global mean aerosol ERF of -1.3 (-2.0 to -0.6) W m^{-2} with medium confidence. ERF due to aerosol-cloud interactions (ERF_{aci}) was assessed to be -1.0 ± 0.7 W m^{-2} with ERF due to aerosol-radiation interactions (ERF_{ari}) assessed as -0.3 ± 0.3 W m^{-2} (Forster et al., 2021). In comparison, for a similar uncertainty interval (5-95% credible interval), Bellouin et al. (2020) estimated the 1850 to 2015 aerosol ERF to be in the range of -3.15 to -0.35 W m^{-2} . Changing from a 1850 to 1750 reference period would likely further shift this range by -0.2 to 0 W m^{-2} (Bellouin et al., 2020; Lund et al., 2019; Myhre et al., 2013). Due to the short atmospheric lifetime of aerosols, aerosol radiative forcing also has strong regional and temporal variations. This large uncertainty range has meant aerosol ERF has persisted as one of the most uncertain aspects of present-day and industrial era climate modelling (Bellouin et al., 2020; Randall et al., 2013). Aerosol-cloud interactions are the largest component of the uncertainty in aerosol ERF (Bellouin et al., 2020; Myhre et al., 2013; Regayre et al., 2018; Shindell et al., 2013), and represent one of the largest uncertainties in total radiative forcing in models submitted to the most recent inter-comparison project (CMIP6) (Smith et al., 2020).

Multi-model ensemble (MMEs) or perturbed parameter ensembles (PPEs) are important tools in quantifying the uncertainty range of aerosol radiative forcing. Multi-model ensembles sample the diversity in predictions across global climate models (GCMs). The spread in predictions is due to differing parameterizations and assumptions of physical process, and is classed as model structural

uncertainty. Perturbed parameter ensembles sample the spread in model predictions caused by uncertain model parameters and process representations in a GCM, which is termed parametric model uncertainty (Collins et al., 2011). There are limitations in using only MMEs to sample uncertainty in model output. For example, it is difficult to decompose the diversity into model processes (Stier et al., 2013) and GCMs often share common deficiencies so their output cannot be assumed statistically independent (Carslaw et al., 2018). An advantage of using PPEs is that a statistical emulator can be built from model output and used to predict a very large sample of model output for different model variants, allowing statistical methods to be used to decompose the model uncertainty to particular processes or assumptions (e.g. Lee et al., 2013).

Simple climate models are designed to represent the Earth system with aggregated variables and can be tuned to represent GCMs (Smith et al., 2018; Tsutsui, 2022). Simple climate models can also be used as tool to quickly predict large samples of regional mean variables such as aerosol radiative forcing or produce probabilistic climate projections, but offer limited insight into the processes causing uncertainty in projections.

The uncertainty in industrial era aerosol ERF has proved difficult to constrain because it depends on a variety of physical and aerosol processes, and the sources of model uncertainty can vary by region and time frame. The range of sources of uncertainty in aerosol ERF include emissions fluxes (Granier et al., 2011; Regayre et al., 2018; Wilcox et al., 2015), aerosol properties and removal processes (Croft et al., 2012; Kasoar et al., 2016; Regayre et al., 2014, 2018; Storelvmo et al., 2009; Textor et al., 2006, 2007), representation of aerosol-cloud interactions (Regayre et al., 2018; Seinfeld et al., 2016; Wilcox et al., 2015), plus representation of clouds and precipitation (Golaz et al., 2013; Haerter et al., 2009; Mülmenstädt et al., 2020; Neubauer et al., 2014), radiation calculations (Stier et al., 2013), and the pre-industrial state which aerosol ERF is calculated against (Carslaw et al., 2013, 2017; Wilcox et al., 2015). The sources of model parametric uncertainty in an aerosol-climate model are shown in Figure 1.4.

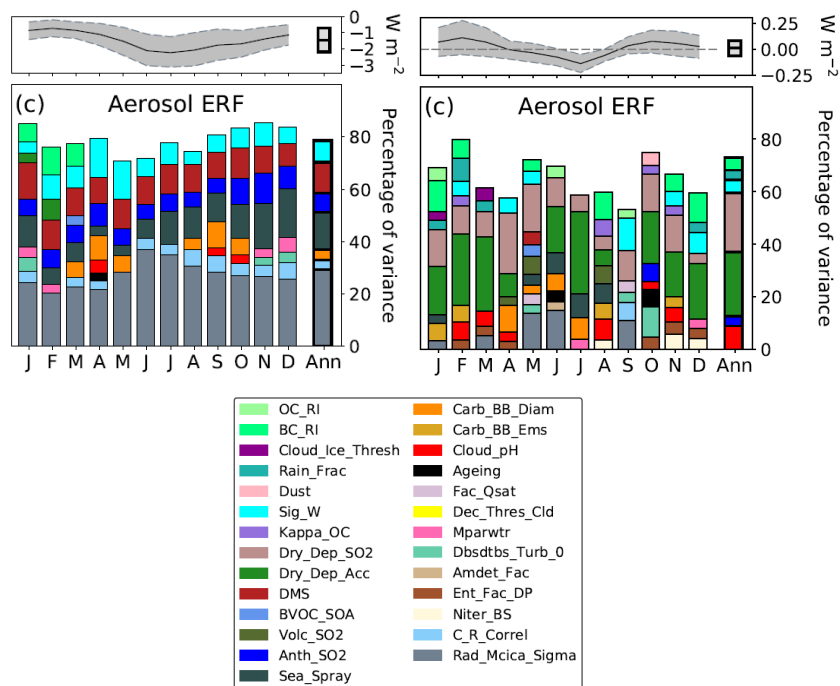


Figure 1.4 Percentage contributions of uncertain aerosol and physical atmosphere model parameter to the variance for 1850-2008 (left) and 1978–2008 (right) global annual mean aerosol ERF. This figure was taken from Regayre et al. (2018) and cropped to show two time periods.

Whilst it is well established increasing anthropogenic aerosol emissions caused a negative pre-industrial to present-day aerosol ERF of uncertain magnitude (e.g. Bellouin et al., 2020; Myhre et al., 2013; Randall et al., 2013; Smith et al., 2020; Zelinka et al., 2014), there is less research focused on how projected future emission reductions in anthropogenic aerosols will affect radiative forcing. Up until CMIP6, most studies on future aerosol radiative forcing projections used the RCPs that span a limited range of future aerosol emissions scenarios (Chalmers et al., 2012; Grandey et al., 2016; Hienola et al., 2018; Rotstayn et al., 2014; Samset et al., 2018; Shindell et al., 2013; Szopa et al., 2013; Westervelt et al., 2015). As an example, Shindell et al. (2013) assessed the radiative forcing by 2100 relative to 1850 in multiple models due to aerosol emission changes as prescribed by the RCPs. The radiative forcing in the CMIP5 models used, had an uncertain range of -0.85 to 0.05 $W\ m^{-2}$. More recent studies have used the SSPs to examine future projections of aerosol forcing (Fiedler et al., 2019; Lund et al., 2019; Smith et al., 2021). Figure 1.5 shows the global mean time series of aerosol ERF for historical and future periods (middle of the road emissions scenario) estimated from a climate model emulator.

Since the sources of parametric model uncertainty in aerosol ERF can vary dependent on the time period examined (Regayre et al., 2015), the sources of model uncertainty in future aerosol ERF could be different than recent decades or pre-industrial to present-day. Scenario uncertainty represents an additional source of uncertainty in future projections. Climate projections of aerosol forcing in the literature have briefly addressed scenario uncertainty, and structural uncertainty in climate projections using MMEs. However, there is considerably less research on the role of parametric model uncertainty in climate projections, warranting further research focused on both quantifying the uncertainty in future aerosol ERF and its sources.

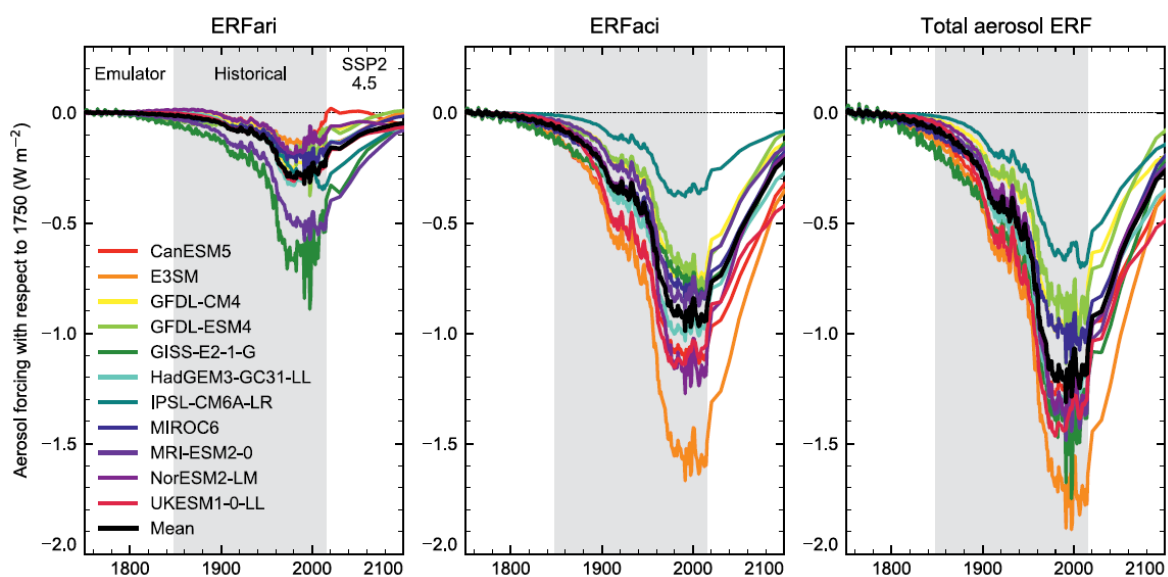


Figure 1.5 Emulated emissions to aerosol ERF curves for CMIP6 models. Aerosol ERF is shown relative to 1750. SSP2-4.5 is a middle of the road future emission scenario. This figure is taken from Smith et al. (2021).

1.5 Climatic Effects of Aerosol Radiative Forcing

The radiative forcing of anthropogenic aerosols has been attributed to causing a wide range of climate responses globally and regionally. Anthropogenic aerosol emission reductions will likely continue to cause aerosol-driven climate changes over the coming decades.

The negative anthropogenic aerosol ERF has substantially offset the radiative forcing of warming greenhouse gases (WMGHGs) over the industrial period (Myhre et al., 2013). Consequently, the net cooling effect of anthropogenic aerosols (0-0.8 °C) has masked some of the warming due to rising GHG concentrations (1-2 °C; 2010-2019 relative to 1850-2000) (Eyring et al., 2021),

and offset other warming-induced climate feedbacks such as Arctic sea ice loss, precipitation changes, and hot temperature extremes (Eyring et al., 2021; Mueller et al., 2018; Richardson et al., 2018; Seong et al., 2021). Reductions in global anthropogenic SO₂ emissions combined with increasing GHG emissions over recent decades have enhanced the overall positive total anthropogenic ERF but decreased the relative importance of aerosol forcing compared to other forcing agents (Gulev et al., 2021). Still, over the coming decades reductions in anthropogenic aerosol emissions will have important climate impacts and add to the warming effect of GHGs (Chalmers et al., 2012; Matthews and Zickfeld, 2012; Rotstayn et al., 2013; Westervelt et al., 2015). For example, a complete removal of anthropogenic sulphate and carbonaceous aerosol may add an additional global warming of 0.7°C (Samset et al., 2018).

Anthropogenic aerosol emissions also impact regional and global precipitation. Global precipitation is projected to increase with warming from GHGs (e.g. Allen and Ingram, 2002). However, increasing anthropogenic aerosols have caused a global drying, partially offsetting the global response of precipitation to historic warming (Levy et al., 2013; Zhang et al., 2021). In addition, anthropogenic aerosol forcing produces a larger change in global mean precipitation per degree of warming than GHG forcing (Forster et al., 2016; Salzmann, 2016). In the future, a removal of present-day anthropogenic aerosol emissions could cause a global mean precipitation increase of 2%–4.6% (Samset et al., 2018).

The heterogeneous spatial and temporal nature of aerosol ERF has led to differences in aerosol-driven climate response compared to longer-lived GHGs that have a more homogenous ERF and monotonic increase throughout time. Historic anthropogenic aerosol sources are predominantly located in the Northern Hemisphere, and therefore increasing aerosol emissions over the industrial period have caused a hemispheric imbalance in radiative forcing and surface temperature (Bonfils et al., 2020; Friedman et al., 2013).

The hemispheric contrast in aerosol forcing and temperature over the 20th century has been associated with modification of atmospheric circulation and a southward shift in the latitudinal position of the Intertropical Convergence Zone (ITCZ) (Allen et al., 2015; Hwang et al., 2013; Ridley et al., 2015; Rotstayn and Lohmann, 2002; Soden et al., 2017). Aerosol modulated shifts in the position of the ITCZ have been associated with rainfall changes in the Sahel (Ackerley et al.,

2011; Biasutti and Giannini, 2006; Chang et al., 2011; Haywood et al., 2013; Westervelt et al., 2018), and, in addition to local aerosol-driven circulation and precipitation changes, linked to a weakening and earlier onset of the South Asian Summer Monsoon (Bollasina et al., 2013, Guo et al., 2013, 2015; Wang and Wen, 2021). In recent decades, reductions of anthropogenic aerosol emissions have been associated with a reversal of some of these precipitation trends. For example, a northward recovery of the position of the ITCZ and associated tropical precipitation (Allen et al., 2015). In the future, aerosol emission reductions could lead to a northward shift in the position of the ITCZ and increases in Asian summer monsoon precipitation (Allen, 2015; Wilcox et al., 2020).

The heterogeneous distribution of aerosol forcing has been linked to further climate changes including modification of the Walker circulation (Amiri-Farahani et al., 2020; DiNezio et al., 2013), North Atlantic (Booth et al., 2012; Haustein et al., 2019; Undorf et al., 2018), and Pacific Sea Surface temperature variability (Smith et al., 2016; Verma et al., 2019), changes to the Atlantic Meridional Overturning Circulation (AMOC) strength (Menary et al., 2020) and changes in North Atlantic tropical cyclone activity (Villarini et al., 2013).

Despite the wide-ranging impacts of aerosols on climate, many aspects of the aerosol-driven climate responses remain poorly understood due to the large uncertainties in aerosol radiative forcing and diverse climate responses to aerosol forcing across models (Eyring et al., 2021). For example, the uncertainty in the magnitude of aerosol radiative forcing over the industrial period limits our knowledge of how sensitive historical temperature is to radiative forcing, and thus the accuracy of future temperature predictions (Andreae et al., 2005; Collins and Knutti, 2013). The lack of understanding of the magnitude, pattern and mechanisms by which aerosols influence precipitation change (Westervelt et al., 2018) leads to uncertainties in projecting future precipitation change (Lee et al., 2021). Reducing the uncertainty in aerosol radiative forcing and aerosol-driven dynamical feedbacks therefore remains a vital task for improving climate prediction since anthropogenic aerosol emission reductions will drive climate responses over the near to mid-term 21st century (Eyring et al., 2021; Rao et al., 2017; van Vuuren et al., 2011).

1.6 Constraints on Aerosol Radiative Forcing and Aerosol-Driven Climate Responses

Considerable effort has been put into using observational constraints to narrow the uncertain range of industrial era aerosol ERF.

The methods of constraint on aerosol ERF can be summarised into three main approaches that use different lines of evidence. The lines of evidence include estimating the sensitivity of clouds and radiation to aerosol perturbations, estimating large scale changes in cloud and radiation over the industrial era, and using energy budget considerations from observed changes of the overall Earth system (Bellouin et al., 2020). Process based constraint of aerosol ERF through estimating the sensitivity of clouds and radiation to aerosol perturbations is a “bottom-up” approach, whereas constraining aerosol ERF through observed large-scale changes in the Earth system is a “top-down” approach.

Aerosol ERF depends on a chain of processes involving cloud, aerosol and radiation terms, each of which has an associated uncertainty. Estimating the sensitivity between aerosol, cloud and radiation terms (i.e. expressed as $d\ln X/d\ln Y$) can reduce the uncertainty in parts of the process translating aerosol emissions to aerosol radiative forcing, or be used as an emergent constraint on aerosol ERF (Quaas et al., 2009). Some examples of relationships which are used to assess this sensitivity include, the relationship between emissions or aerosol optical depth (AOD) and cloud condensation nuclei (CCN), cloud droplet number concentration (CDNC), and cloud fraction (Christensen et al., 2022; Ghan et al., 2016; Gryspeerdt et al., 2017). These relationships are constrained using satellite or in-situ observations of the variables. A limitation of this technique, is that relationships derived from present-day observations may not extrapolate to pre-industrial conditions, where there is a different sensitivity of CDNC to aerosol emissions and which forcing is often calculated from (Carslaw et al., 2013; Ghan et al., 2016). Meteorological conditions can affect both aerosol concentrations and cloud properties (Quaas et al., 2010), and there are limitations in retrieving properties from satellites (Ma et al., 2018), both of which make establishing causal relationships difficult. It is also unclear how representative these relationships are for understanding larger-scale aerosol effects on climate (Christensen et al., 2022).

The second approach to constraint tests a model's ability to produce observable trends or climatological averages related to aerosols, clouds and radiation. Constraint on aerosol ERF through these large-scale changes then relies on selecting plausible model ensemble members based on their ability to reproduce the observed climate variables. For example, Cherian et al. (2014) used trends in surface solar radiation to constrain regional and global aerosol ERF in CMIP5 models (Cherian et al., 2014). McCoy et al. (2020) used the hemispheric contrast between the polluted Northern Hemisphere and more pristine Southern Hemisphere as a proxy for constraining pre-industrial to present-day CDNC changes and aerosol-cloud interactions in both a PPE and MME (McCoy et al., 2020). There are limitations in finding a subset of models in a MME that correlate well to observations because that does not necessarily reduce the underlying causes of uncertainty, and thus would not improve climate projections. In comparison, constraint using a PPE can reduce the underlying uncertainty in model parameters, but lacks a way to explore this in a broader range of potential parameterisations (Johnson et al., 2020; Regayre et al., 2020).

A top-down approach to constraining aerosol ERF relies on energy budget arguments that take into account the evolution of surface temperature and radiative fluxes (Booth et al., 2018; Kretzschmar et al., 2017; Rotstayn et al., 2015; Smith et al., 2021; Stevens, 2015). For example, plausible aerosol ERF ranges can be inferred from the historical temperature evolution if the ERF of GHGs and climate sensitivity are fairly well constrained. Limitations in using this approach are that the large regional effects of aerosol are not captured in a global mean energy budget analysis and that the constraint on aerosol ERF could be time period dependent (Kretzschmar et al., 2017).

Overall combining bottom-up constraints as applied in Bellouin et al. (2020) currently yields a global mean pre-industrial to present-day aerosol ERF of -2.2 to -0.6 W m⁻² and represents a similar range to the constrained aerosol ERF of the HadGEM3-UKCA PPE (Regayre et al., 2018). Including energy budget top-down constraints provides an additional constraint on the lower bound of aerosol ERF, suggesting an aerosol ERF more negative than -1.6 W m⁻² unlikely (Bellouin et al., 2020). The many limitations in the constraint approaches discussed continue to make reducing the uncertainty in industrial era aerosol ERF further a challenging task.

Whilst there is a large body of literature on constraint of industrial era aerosol ERF, there is considerably less on the use of historical constraints to reduce uncertainty in future aerosol-driven climate responses. Model parameters which reproduce present-day climate may not produce an appropriate prediction of climate change (Haerter et al., 2009). Hence, further research is needed on the applicability of historical constraints to future projections.

1.7 Thesis Aims and Structure

This thesis has focused on using a hierarchy of PPEs to quantify the parametric model uncertainty in aerosol radiative forcing over the coming decades, and investigate how the uncertainty in aerosol radiative forcing impacts future climate projections.

In Chapter 2, a statistical emulator was used to quantify the uncertainty in near-term aerosol radiative forcing out to 2050 for anthropogenic aerosol emission scenarios aligned with the Shared Socioeconomic Pathways (SSPs). The statistical emulator was built from a PPE that sampled the uncertainty in aerosol emissions and processes, and was composed of atmosphere-only simulations from the aerosol-climate model HadGEM3-UKCA. A simple climate model (FaIR) was then used to translate the uncertainty in near-term aerosol radiative forcing to global mean temperature change and examine the effect the uncertainty in aerosol radiative forcing has on predicting the exceedance year of a 1.5 °C temperature rise (the target set by the Paris Agreement to limit global mean temperatures to). This research which is published as Peace et al. (2020), examined the following questions:

- What is the magnitude of near-term aerosol radiative forcing for anthropogenic aerosol emission reduction scenarios?
- How large is the parametric model uncertainty in near-term aerosol radiative forcing, and how does that compare to scenario uncertainty?
- Which aerosol model parameters contribute to the uncertainty in near-term aerosol radiative forcing?
- How does the uncertainty in near-term aerosol radiative forcing alone affect the accuracy in predicting the exceedance year of the 1.5 °C? How does that compare to if the uncertainty in the relationship between aerosol radiative forcing and climate sensitivity is taken into account?

Chapter 3 used a PPE of a coupled ocean-atmosphere model (HadGEM3-GC3.05) with transient simulations over 1900 to 2100. This PPE samples the uncertainty across a range of model schemes, including the aerosol model. The set up allowed investigation of the role of aerosol radiative forcing uncertainty on tropical precipitation shifts over the 20th and 21st centuries which is one important, but uncertain, aerosol-driven climate response. The results from the PPE are compared to those of earlier multi-model studies that suggested the magnitude of tropical precipitation shifts is related to the hemispheric contrast in aerosol forcing. The following research questions were examined:

- How does the latitudinal position of tropical precipitation evolve in the PPE over the 20th and 21st centuries?
- In the CMIP5 multi-model ensemble there was a relationship between the magnitude of aerosol radiative forcing and the 20th century shift in tropical precipitation. Does this relationship exist in a PPE when we account for parametric model uncertainty and have a larger contribution from internal climate variability?
- Do aerosol emission reductions play a role in driving tropical precipitation shifts over the coming decades? If so, how does the single-model uncertainty in aerosol forcing affect the relationship?

In Chapter 4 performance of the coupled ocean-atmosphere PPE in simulating surface solar radiation trends over Europe when anthropogenic aerosol emissions increased and then declined was evaluated. Trends in surface solar radiation offer a long-term observational record related to aerosol radiative effects, yet climate models tend to underestimate the magnitude of observed trends. The observed surface solar radiation trend over Europe has been used as a constraint on aerosol ERF in the CMIP5 multi-model ensemble. The below research questions were explored in Chapter 4:

- How well does the PPE produce observed trends in surface solar radiation over Europe? What are the key perturbed parameters that influence model performance?
- Can we use model performance in simulating historical surface solar radiation trends to select plausible PPE members to be used in future projections? Is the observed surface solar radiation over Europe a useful constraint on aerosol ERF?

- Do the results from our analysis vary if we focus on a climatological mean rather than trends? Does the coupling of ocean to the atmosphere or a larger sample size affect our results for a climatological mean?

Chapter 5 synthesis the key results from this thesis, the necessary limitations and suggests directions for future work that build on the results presented in this thesis.

References

- Ackerley, D., Booth, B. B. B., Knight, S. H. E., Highwood, E. J., Frame, D. J., Allen, M. R. and Rowell, D. P.: Sensitivity of Twentieth-Century Sahel Rainfall to Sulfate Aerosol and CO₂ Forcing, *J. Clim.*, 24(19), 4999–5014, doi:10.1175/JCLI-D-11-00019.1, 2011.
- Albrecht, B. A.: Aerosols, cloud microphysics, and fractional cloudiness, *Science* (80-.), 245(4923), 1227–1230, doi:10.1126/science.245.4923.1227, 1989.
- Allen, M. R. and Ingram, W. J.: Constraints on future changes in climate and the hydrologic cycle, *Nature*, 419(6903), 228–232, doi:10.1038/nature01092, 2002.
- Allen, R. J.: A 21st century northward tropical precipitation shift caused by future anthropogenic aerosol reductions, *J. Geophys. Res.*, 120(18), 9087–9102, doi:10.1002/2015JD023623, 2015.
- Allen, R. J., Evan, A. T. and Booth, B. B. B.: Interhemispheric aerosol radiative forcing and tropical precipitation shifts during the late Twentieth Century, *J. Clim.*, 28(20), 8219–8246, doi:10.1175/JCLI-D-15-0148.1, 2015.
- Allen, R. J., Landuyt, W. and Rumbold, S. T.: An increase in aerosol burden and radiative effects in a warmer world, *Nat. Clim. Chang.*, 6(3), 269–274, doi:10.1038/nclimate2827, 2016.
- Amiri-Farahani, A., Allen, R. J., Li, K. F., Nabat, P. and Westervelt, D. M.: A La Niña-Like Climate Response to South African Biomass Burning Aerosol in CESM Simulations, *J. Geophys. Res. Atmos.*, 125(6), doi:10.1029/2019JD031832, 2020.
- Andreae, M. O. and Rosenfeld, D.: Aerosol-cloud-precipitation interactions. Part 1. The nature and sources of cloud-active aerosols, *Earth-Science Rev.*, 89(1–2), 13–41, doi:10.1016/j.earscirev.2008.03.001, 2008.
- Andreae, M. O., Jones, C. D. and Cox, P. M.: Strong present-day aerosol cooling implies a hot future, *Nature*, 435(7046), 1187–1190, doi:10.1038/nature03671, 2005.
- Bellouin, N., Quaas, J., Gryspeerdt, E., Kinne, S., Stier, P., Watson-Parris, D., Boucher, O., Carslaw, K. S., Christensen, M., Daniou, A. L., Dufresne, J. L., Feingold, G., Fiedler, S., Forster, P., Gettelman, A., Haywood, J. M., Lohmann, U., Malavelle, F., Mauritsen, T., McCoy, D. T., Myhre, G., Mülmenstädt, J., Neubauer, D., Possner, A., Rugenstein, M., Sato, Y., Schulz, M., Schwartz, S. E., Sourdeval, O., Storelvmo, T., Toll, V., Winker, D. and Stevens, B.: Bounding Global Aerosol Radiative Forcing of Climate Change, *Rev. Geophys.*, 58(1), doi:10.1029/2019RG000660, 2020.
- Biasutti, M. and Giannini, A.: Robust Sahel drying in response to late 20th century forcings, *Geophys. Res. Lett.*, 33(11), doi:https://doi.org/10.1029/2006GL026067, 2006.
- Bollasina, M. A., Ming, Y. and Ramaswamy, V.: Earlier onset of the Indian monsoon in the late twentieth century: The role of anthropogenic aerosols, *Geophys. Res. Lett.*, 40(14), 3715–3720, doi:10.1002/grl.50719, 2013.
- Bollasina, M. A., Ming, Y. and Ramaswamy, V.: Anthropogenic Aerosols and the Weakening of the South Asian Summer Monsoon, [online] Available from: <http://science.sciencemag.org/content/sci/334/6055/502.full.pdf> (Accessed 19 December 2017), n.d.
- Bond, T. C., Doherty, S. J., Fahey, D. W., Forster, P. M., Berntsen, T., Deangelo, B. J., Flanner, M. G., Ghan, S., Kärcher, B., Koch, D., Kinne, S., Kondo, Y., Quinn, P. K., Sarofim, M. C., Schultz, M. G., Schulz, M., Venkataraman, C., Zhang, H., Zhang, S., Bellouin, N., Guttikunda, S. K., Hopke, P. K., Jacobson, M. Z., Kaiser, J. W., Klimont, Z., Lohmann, U., Schwarz, J. P., Shindell, D., Storelvmo, T., Warren, S. G. and Zender, C. S.: Bounding the role of black carbon in the climate system: A scientific assessment, *J. Geophys. Res. Atmos.*, 118(11), 5380–5552, doi:10.1002/jgrd.50171, 2013.
- Bonfils, C. J. W., Santer, B. D., Fyfe, J. C., Marvel, K., Phillips, T. J. and Zimmerman, S. R. H.: Human influence on joint changes in temperature, rainfall and continental aridity, *Nat. Clim. Chang.*, 1–6, doi:10.1038/s41558-020-0821-1, 2020.
- Booth, B. B. B., Dunstone, N. J., Halloran, P. R., Andrews, T. and Bellouin, N.: Aerosols implicated as a prime driver of twentieth-century North Atlantic climate variability, *Nature*, 484(7393), 228–232, doi:10.1038/nature10946, 2012.

- Booth, B. B. B., Harris, G. R., Jones, A., Wilcox, L., Hawcroft, M. and Carslaw, K. S.: Comments on “Rethinking the lower bound on aerosol radiative forcing,” *J. Clim.*, 31(22), 9407–9412, doi:10.1175/JCLI-D-17-0369.1, 2018.
- Boucher, O.: Atmospheric Aerosols, in *Atmospheric Aerosols*, pp. 9–24, Springer Netherlands, Dordrecht., 2015.
- Carslaw, K., Lee, L., Regayre, L. and Johnson, J.: Climate Models Are Uncertain, but We Can Do Something About It, *Eos (Washington, DC)*, 99, doi:10.1029/2018EO093757, 2018.
- Carslaw, K. S., Boucher, O., Spracklen, D. V., Mann, G. W., Rae, J. G. L., Woodward, S. and Kulmala, M.: A review of natural aerosol interactions and feedbacks within the Earth system, *Atmos. Chem. Phys.*, doi:10.5194/acp-10-1701-2010, 2010.
- Carslaw, K. S., Lee, L. A., Reddington, C. L., Pringle, K. J., Rap, A., Forster, P. M., Mann, G. W., Spracklen, D. V., Woodhouse, M. T., Regayre, L. A. and Pierce, J. R.: Large contribution of natural aerosols to uncertainty in indirect forcing, *Nature*, 503(7474), 67–71, doi:10.1038/nature12674, 2013.
- Carslaw, K. S., Gordon, H., Hamilton, D. S., Johnson, J. S., Regayre, L. A., Yoshioka, M. and Pringle, K. J.: Aerosols in the Pre-industrial Atmosphere, *Curr. Clim. Chang. Reports*, doi:10.1007/s40641-017-0061-2, 2017.
- Chalmers, N., Highwood, E. J., Hawkins, E., Sutton, R. and Wilcox, L. J.: Aerosol contribution to the rapid warming of near-term climate under RCP 2.6, *Geophys. Res. Lett.*, 39(18), doi:10.1029/2012GL052848, 2012.
- Chang, C. Y., Chiang, J. C. H., Wehner, M. F., Friedman, A. R. and Ruedy, R.: Sulfate aerosol control of tropical atlantic climate over the twentieth century, *J. Clim.*, 24(10), 2540–2555, doi:10.1175/2010JCLI4065.1, 2011.
- Cherian, R., Quaas, J., Salzmann, M. and Wild, M.: Pollution trends over Europe constrain global aerosol forcing as simulated by climate models, *Geophys. Res. Lett.*, 41(6), 2176–2181, doi:10.1002/2013GL058715, 2014.
- Christensen, M. W., Gettelman, A., Cermak, J., Dagan, G., Diamond, M., Douglas, A., Feingold, G., Glassmeier, F., Goren, T., Grosvenor, D. P., Gryspeerdt, E., Kahn, R., Li, Z., Ma, P.-L., Malavelle, F., McCoy, I. L., McCoy, D. T., McFarquhar, G., Mülmenstädt, J., Pal, S., Possner, A., Povey, A., Quaas, J., Rosenfeld, D., Schmidt, A., Schrödner, R., Sorooshian, A., Stier, P., Toll, V., Watson-Parris, D., Wood, R., Yang, M. and Yuan, T.: Opportunistic experiments to constrain aerosol effective radiative forcing, *Atmos. Chem. Phys.*, 22(1), 641–674, doi:10.5194/acp-22-641-2022, 2022.
- Collins, M. and Knutti, R.: Long-term climate change: Projections, commitments and irreversibility, in *Climate Change 2013 the Physical Science Basis: Working Group I Contribution to the Fifth Assessment Report of the Intergovernmental Panel on Climate Change*, vol. 9781107057, pp. 1029–1136., 2013.
- Collins, M., Booth, B. B. B., Bhaskaran, B., Harris, G. R., Murphy, J. M., Sexton, D. M. H. and Webb, M. J.: Climate model errors, feedbacks and forcings: a comparison of perturbed physics and multi-model ensembles, *Clim. Dyn.*, 36(9–10), 1737–1766, doi:10.1007/s00382-010-0808-0, 2011.
- Conover, J. H.: Anomalous Cloud Lines, *J. Atmos. Sci.*, 23(6), 778–785, doi:10.1175/1520-0469(1966)023<0778:acI>2.0.co;2, 1966.
- Croft, B., Pierce, J. R., Martin, R. V., Hoose, C. and Lohmann, U.: Uncertainty associated with convective wet removal of entrained aerosols in a global climate model, *Atmos. Chem. Phys.*, 12(22), 10725–10748, doi:10.5194/acp-12-10725-2012, 2012.
- DiNezio, P. N., Vecchi, G. A. and Clement, A. C.: Detectability of changes in the walker circulation in response to global warming, *J. Clim.*, 26(12), 4038–4048, doi:10.1175/JCLI-D-12-00531.1, 2013.
- Eyring, V., Gillett, N. P., Achuta Rao, K. M., Barimalala, R., Barreiro Parrillo, M., Bellouin, N., Cassou, C., Durack, P. J., Kosaka, Y., McGregor, S., Min, S., Morgenstern, O. and Sun, Y.: Human Influence on the Climate System, *Clim. Chang. 2021 Phys. Sci. Basis. Contrib. Work. Gr. I to Sixth Assessment Rep. Intergov. Panel Clim. Chang.*, 2021.
- Fiedler, S., Stevens, B., Gidden, M., Smith, S. J., Riahi, K. and van Vuuren, D.: First forcing

estimates from the future CMIP6 scenarios of anthropogenic aerosol optical properties and an associated Twomey effect, *Geosci. Model Dev.*, 12(3), 989–1007, doi:10.5194/gmd-12-989-2019, 2019.

Flanner, M. G., Zender, C. S., Randerson, J. T. and Rasch, P. J.: Present-day climate forcing and response from black carbon in snow, *J. Geophys. Res. Atmos.*, 112(11), D11202, doi:10.1029/2006JD008003, 2007.

Forster, P., Storelvmo, T., Armour, K., Collins, W., Dufresne, J.-L., Frame, D., Lunt, D. J., Mauritsen, T., Palmer, M. D., Watanabe, M., Wild, M. and Zhang, H.: The Earth's Energy Budget, Climate Feedbacks, and Climate Sensitivity. In *Climate Change 2021: The Physical Science Basis. Contribution of Working Group I to the Sixth Assessment Report of the Intergovernmental Panel on Climate Change*, (In Press), 2021.

Forster, P. M., Richardson, T., Maycock, A. C., Smith, C. J., Samset, B. H., Myhre, G., Andrews, T., Pincus, R. and Schulz, M.: Recommendations for diagnosing effective radiative forcing from climate models for CMIP6, *J. Geophys. Res.*, doi:10.1002/2016JD025320, 2016.

Friedman, A. R., Hwang, Y.-T., Chiang, J. C. H., Frierson, D. M. W., Friedman, A. R., Hwang, Y.-T., Chiang, J. C. H. and Frierson, D. M. W.: Interhemispheric Temperature Asymmetry over the Twentieth Century and in Future Projections, *J. Clim.*, 26(15), 5419–5433, doi:10.1175/JCLI-D-12-00525.1, 2013.

Gettelman, A., Lin, L., Medeiros, B. and Olson, J.: Climate feedback variance and the interaction of aerosol forcing and feedbacks, *J. Clim.*, 29(18), 6659–6675, doi:10.1175/JCLI-D-16-0151.1, 2016.

Ghan, S., Wang, M., Zhang, S., Ferrachat, S., Gettelman, A., Griesfeller, J., Kipling, Z., Lohmann, U., Morrison, H., Neubauer, D., Partridge, D. G., Stier, P., Takemura, T., Wang, H. and Zhang, K.: Challenges in constraining anthropogenic aerosol effects on cloud radiative forcing using present-day spatiotemporal variability, *Proc. Natl. Acad. Sci.*, 113(21), 5804–5811, doi:10.1073/pnas.1514036113, 2016.

Golaz, J.-C., Horowitz, L. W. and Levy, H.: Cloud tuning in a coupled climate model: Impact on 20th century warming, *Geophys. Res. Lett.*, 40(10), 2246–2251, doi:10.1002/grl.50232, 2013.

Gong, S. and Barrie, L. A.: *The Distribution of Atmospheric Aerosols: Transport, Transformation and Removal, in Aerosol Pollution Impact on Precipitation*, pp. 91–141, Springer Netherlands, Dordrecht., 2009.

Grandey, B. S., Cheng, H. and Wang, C.: Transient Climate Impacts for Scenarios of Aerosol Emissions from Asia: A Story of Coal versus Gas, *Am. Meteorol. Soc.* [online] Available from: <https://journals.ametsoc.org/doi/pdf/10.1175/JCLI-D-15-0555.1> (Accessed 1 March 2018), 2016.

Granier, C., Bessagnet, B., Bond, T., D'Angiola, A., Denier van der Gon, H., Frost, G. J., Heil, A., Kaiser, J. W., Kinne, S., Klimont, Z., Kloster, S., Lamarque, J.-F., Liousse, C., Masui, T., Meleux, F., Mieville, A., Ohara, T., Raut, J.-C., Riahi, K., Schultz, M. G., Smith, S. J., Thompson, A., van Aardenne, J., van der Werf, G. R. and van Vuuren, D. P.: Evolution of anthropogenic and biomass burning emissions of air pollutants at global and regional scales during the 1980–2010 period, *Clim. Change*, 109(1–2), 163–190, doi:10.1007/s10584-011-0154-1, 2011.

Gryspeerd, E., Quaas, J., Ferrachat, S., Gettelman, A., Ghan, S., Lohmann, U., Morrison, H., Neubauer, D., Partridge, D. G., Stier, P., Takemura, T., Wang, H., Wang, M. and Zhang, K.: Constraining the instantaneous aerosol influence on cloud albedo, *Proc. Natl. Acad. Sci.*, doi:10.1073/pnas.1617765114, 2017.

Gulev, S. K., Thorne, P. W., Ahn, J., Dentener, F. J., Domingues, C. M., Gerland, S., Gong, D., Kaufman, D. S., Nnamchi, H. C., Quaas, J., Rivera, J. A., Sathyendranath, S., Smith, S. L., Trewin, B., von Shuckmann, K. and Vose, R. S.: *Changing State of the Climate System, Clim. Chang. 2021 Phys. Sci. Basis. Contrib. Work. Gr. I to Sixth Assess. Rep. Intergov. Panel Clim. Chang.*, 2021.

Guo, L., Highwood, E. J., Shaffrey, L. C. and Turner, A. G.: The effect of regional changes in anthropogenic aerosols on rainfall of the East Asian Summer Monsoon, *Atmos. Chem. Phys.*, 13(3), 1521–1534, doi:10.5194/acp-13-1521-2013, 2013.

Guo, L., Turner, A. G. and Highwood, E. J.: Impacts of 20th century aerosol emissions on the South Asian monsoon in the CMIP5 models, *Atmos. Chem. Phys.*, 15(11), 6367–6378,

doi:10.5194/acp-15-6367-2015, 2015.

Haerter, J. O., Roeckner, E., Tomassini, L. and von Storch, J.-S.: Parametric uncertainty effects on aerosol radiative forcing, *Geophys. Res. Lett.*, 36(15), n/a-n/a, doi:10.1029/2009GL039050, 2009.

Hansen, J. and Nazarenko, L.: Soot climate forcing via snow and ice albedos, *Proc. Natl. Acad. Sci. U. S. A.*, 101(2), 423–428, doi:10.1073/pnas.2237157100, 2004.

Haustein, K., Otto, F. E. L., Venema, V., Jacobs, P., Cowtan, K., Hausfather, Z., Way, R. G., White, B., Subramanian, A. and Schurer, A. P.: A limited role for unforced internal variability in twentieth-century warming, *J. Clim.*, 32(16), 4893–4917, doi:10.1175/JCLI-D-18-0555.1, 2019.

Haywood, J. M., Jones, A., Bellouin, N. and Stephenson, D.: Asymmetric forcing from stratospheric aerosols impacts Sahelian rainfall, *Nat. Clim. Chang.*, 3(7), 660–665, doi:10.1038/nclimate1857, 2013.

Hienola, A., Partanen, A. I., Pietikainen, J. P., O'Donnell, D., Korhonen, H., Matthews, H. D. and Laaksonen, A.: The impact of aerosol emissions on the 1.5 °C pathways, *Environ. Res. Lett.*, 13(4), 044011, doi:10.1088/1748-9326/aab1b2, 2018.

Hobbs P. V., Radke L. F. and Shumway S. E.: Cloud Condensation Nuclei from Industrial Sources and Their Apparent Influence on Precipitation in Washington State, *J. Atmos. Sci.*, 27(1), 81–89, doi:10.1175/1520-0469(1970)027<0091:ccnfis>2.0.co;2, 1970.

Hoesly, R. M., Smith, S. J., Feng, L., Klimont, Z., Janssens-Maenhout, G., Pitkanen, T., Seibert, J. J., Vu, L., Andres, R. J., Bolt, R. M., Bond, T. C., Dawidowski, L., Kholod, N., Kurokawa, J. I., Li, M., Liu, L., Lu, Z., Moura, M. C. P., O'Rourke, P. R. and Zhang, Q.: Historical (1750–2014) anthropogenic emissions of reactive gases and aerosols from the Community Emissions Data System (CEDS), *Geosci. Model Dev.*, 11(1), 369–408, doi:10.5194/gmd-11-369-2018, 2018.

Hwang, Y. T., Frierson, D. M. W. and Kang, S. M.: Anthropogenic sulfate aerosol and the southward shift of tropical precipitation in the late 20th century, *Geophys. Res. Lett.*, 40(11), 2845–2850, doi:10.1002/grl.50502, 2013.

Johnson, J. S., Regayre, L. A., Yoshioka, M., Pringle, K. J., Turnock, S. T., Browse, J., Sexton, D. M. H., Rostron, J. W., Schutgens, N. A. J., Partridge, D. G., Liu, D., Allan, J. D., Coe, H., Ding, A., Cohen, D. D., Atanacio, A., Vakkari, V., Asmi, E. and Carslaw, K. S.: Robust observational constraint of uncertain aerosol processes and emissions in a climate model and the effect on aerosol radiative forcing, *Atmos. Chem. Phys.*, 20(15), 9491–9524, doi:10.5194/acp-20-9491-2020, 2020.

Kasoar, M., Voulgarakis, A., Lamarque, J. F., Shindell, D. T., Bellouin, N., Faluvegi, G. and Tsigaridis, K.: Regional and global temperature response to anthropogenic SO₂ emissions from China in three climate models, *Atmos. Chem. Phys.*, 16(15), 9785–9804, doi:10.5194/acp-16-9785-2016, 2016.

Kretzschmar, J., Salzmann, M., Mülmenstädt, J., Boucher, O. and Quaas, J.: Comment on “rethinking the lower bound on aerosol radiative forcing,” *J. Clim.*, 30(16), 6579–6584, doi:10.1175/JCLI-D-16-0668.1, 2017.

Kristiansen, N. I., Stohl, A., Olivie, D. J. L., Croft, B., Søvde, O. A., Klein, H., Christoudias, T., Kunkel, D., Leadbetter, S. J., Lee, Y. H., Zhang, K., Tsigaridis, K., Bergman, T., Evangelidou, N., Wang, H., Ma, P. L., Easter, R. C., Rasch, P. J., Liu, X., Pitari, G., Di Genova, G., Zhao, S. Y., Balkanski, Y., Bauer, S. E., Faluvegi, G. S., Kokkola, H., Martin, R. V., Pierce, J. R., Schulz, M., Shindell, D., Tost, H. and Zhang, H.: Evaluation of observed and modelled aerosol lifetimes using radioactive tracers of opportunity and an ensemble of 19 global models, *Atmos. Chem. Phys.*, 16(5), 3525–3561, doi:10.5194/acp-16-3525-2016, 2016.

Lamarque, J. F., Bond, T. C., Eyring, V., Granier, C., Heil, A., Klimont, Z., Lee, D., Liousse, C., Mieville, A., Owen, B., Schultz, M. G., Shindell, D., Smith, S. J., Stehfest, E., Van Aardenne, J., Cooper, O. R., Kainuma, M., Mahowald, N., McConnell, J. R., Naik, V., Riahi, K. and Van Vuuren, D. P.: Historical (1850–2000) gridded anthropogenic and biomass burning emissions of reactive gases and aerosols: Methodology and application, *Atmos. Chem. Phys.*, 10(15), 7017–7039, doi:10.5194/acp-10-7017-2010, 2010.

Lee, J. Y., Marotzke, J., Bala, G., Cao, L., Corti, S., Dunne, J. P., Engelbrecht, F., Fischer, E., Fyfe, J. C., Jones, C., Maycock, A., Mutemi, J., Ndiaye, O., Panickal, S. and Zhou, T.: Future Global Climate: Scenario-Based Projections and Near-Term Information, *Clim. Chang.* 2021

- Phys. Sci. Basis. Contrib. Work. Gr. I to Sixth Assess. Rep. Intergov. Panel Clim. Chang., 2021.
- Lee, L. A., Pringle, K. J., Reddington, C. L., Mann, G. W., Stier, P., Spracklen, D. V., Pierce, J. R. and Carslaw, K. S.: The magnitude and causes of uncertainty in global model simulations of cloud condensation nuclei, *Atmos. Chem. Phys.*, 13(17), 8879–8914, doi:10.5194/acp-13-8879-2013, 2013.
- Levy, H., Horowitz, L. W., Schwarzkopf, M. D., Ming, Y., Golaz, J.-C., Naik, V. and Ramaswamy, V.: The roles of aerosol direct and indirect effects in past and future climate change, *J. Geophys. Res. Atmos.*, 118(10), 4521–4532, doi:10.1002/jgrd.50192, 2013.
- Lund, M. T., Myhre, G. and Samset, B. H.: Anthropogenic aerosol forcing under the Shared Socioeconomic Pathways, *Atmos. Chem. Phys.*, 19(22), 13827–13839, doi:10.5194/acp-2019-606, 2019.
- Ma, P. L., Rasch, P. J., Chepfer, H., Winker, D. M. and Ghan, S. J.: Observational constraint on cloud susceptibility weakened by aerosol retrieval limitations, *Nat. Commun.*, 9(1), 1–10, doi:10.1038/s41467-018-05028-4, 2018.
- Malavelle, F. F., Haywood, J. M., Jones, A., Gettelman, A., Clarisse, L., Bauduin, S., Allan, R. P., Karset, I. H. H., Kristjánsson, J. E., Oreopoulos, L., Cho, N., Lee, D., Bellouin, N., Boucher, O., Grosvenor, D. P., Carslaw, K. S., Dhomse, S., Mann, G. W., Schmidt, A., Coe, H., Hartley, M. E., Dalvi, M., Hill, A. A., Johnson, B. T., Johnson, C. E., Knight, J. R., O'Connor, F. M., Stier, P., Myhre, G., Platnick, S., Stephens, G. L., Takahashi, H. and Thordarson, T.: Strong constraints on aerosol-cloud interactions from volcanic eruptions, *Nature*, 546(7659), 485–491, doi:10.1038/nature22974, 2017.
- Matthews, H. D. and Zickfeld, K.: Climate response to zeroed emissions of greenhouse gases and aerosols, *Nat. Clim. Chang.*, 2(5), 338–341, doi:10.1038/nclimate1424, 2012.
- McCoy, I. L., McCoy, D. T., Wood, R., Regayre, L., Watson-Parris, D., Grosvenor, D. P., Mulcahy, J. P., Hu, Y., Bender, F. A. M., Field, P. R., Carslaw, K. S. and Gordon, H.: The hemispheric contrast in cloud microphysical properties constrains aerosol forcing, *Proc. Natl. Acad. Sci. U. S. A.*, 117(32), 18998–19006, doi:10.1073/pnas.1922502117, 2020.
- Menary, M. B., Robson, J., Allan, R. P., Booth, B. B. B., Cassou, C., Gastineau, G., Gregory, J., Hodson, D., Jones, C., Mignot, J., Ringer, M., Sutton, R., Wilcox, L. and Zhang, R.: Aerosol-Forced AMOC Changes in CMIP6 Historical Simulations, *Geophys. Res. Lett.*, 47(14), doi:10.1029/2020GL088166, 2020.
- Mueller, B. L., Gillett, N. P., Monahan, A. H. and Zwiers, F. W.: Attribution of Arctic sea ice decline from 1953 to 2012 to influences from natural, greenhouse gas, and anthropogenic aerosol forcing, *J. Clim.*, 31(19), 7771–7787, doi:10.1175/JCLI-D-17-0552.1, 2018.
- Mülmenstädt, J., Mülmenstädt, J., Nam, C., Salzmann, M., Kretzschmar, J., L'Ecuyer, T. S., Lohmann, U., Ma, P. L., Myhre, G., Neubauer, D., Stier, P., Suzuki, K., Wang, M. and Quaas, J.: Reducing the aerosol forcing uncertainty using observational constraints on warm rain processes, *Sci. Adv.*, 6(22), doi:10.1126/sciadv.aaz6433, 2020.
- Myhre, G., Shindell, D., Aamaas, B., Boucher, O., Dalsøren, S., Daniel, J., Forster, P., Granier, C., Haigh, J. and Hodnebrog, Ø.: Anthropogenic and natural radiative forcing, in *Climate Change 2013 the Physical Science Basis: Working Group I Contribution to the Fifth Assessment Report of the Intergovernmental Panel on Climate Change*, vol. 9781107057, pp. 659–740., 2013.
- Neubauer, D., Lohmann, U., Hoose, C. and Frontoso, M. G.: Impact of the representation of marine stratocumulus clouds on the anthropogenic aerosol effect, *Atmos. Chem. Phys.*, 14(21), 11997–12022, doi:10.5194/acp-14-11997-2014, 2014.
- Paulot, F., Paynter, D., Winton, M., Ginoux, P., Zhao, M. and Horowitz, L. W.: Revisiting the Impact of Sea Salt on Climate Sensitivity, *Geophys. Res. Lett.*, 47(3), e2019GL085601, doi:10.1029/2019GL085601, 2020.
- Peace, A. H., Carslaw, K. S., Lee, L. A., Regayre, L. A., Booth, B. B. B., Johnson, J. S. and Bernie, D.: Effect of aerosol radiative forcing uncertainty on projected exceedance year of a 1.5 °C global temperature rise, *Environ. Res. Lett.*, 15(9), 0940a6, doi:10.1088/1748-9326/aba20c, 2020.
- Pierce, J. R., Croft, B., Kodros, J. K., D'Andrea, S. D. and Martin, R. V.: The importance of

interstitial particle scavenging by cloud droplets in shaping the remote aerosol size distribution and global aerosol-climate effects, *Atmos. Chem. Phys.*, 15(11), 6147–6158, doi:10.5194/acp-15-6147-2015, 2015.

Possner, A., Eastman, R., Bender, F. and Glassmeier, F.: Deconvolution of boundary layer depth and aerosol constraints on cloud water path in subtropical stratocumulus decks, *Atmos. Chem. Phys.*, 20(6), 3609–3621, doi:10.5194/acp-20-3609-2020, 2020.

Quaas, J., Ming, Y., Menon, S., Takemura, T., Wang, M., Penner, J. E., Gettelman, A., Lohmann, U., Bellouin, N., Boucher, O., Sayer, A. M., Thomas, G. E., McComiskey, A., Feingold, G., Hoose, C., Kristjánsson, J. E., Liu, X., Balkanski, Y., Donner, L. J., Ginoux, P. A., Stier, P., Grandey, B., Feichter, J., Sednev, I., Bauer, S. E., Koch, D. and Grainger, R. G.: Aerosol indirect effects – general circulation model intercomparison and evaluation with satellite data, *Atmos. Chem. Phys.* *Atmos. Chem. Phys.*, 9, 8697–8717 [online] Available from: www.atmos-chem-phys.net/9/8697/2009/ (Accessed 15 March 2018), 2009.

Quaas, J., Stevens, B., Stier, P. and Lohmann, U.: Interpreting the cloud cover – aerosol optical depth relationship found in satellite data using a general circulation model, *Atmos. Chem. Phys.*, 10(13), 6129–6135, doi:10.5194/acp-10-6129-2010, 2010.

Randall, D., Artaxo, P., Bretherton, C., Feingold, G., Forster, P., Kerminen, V., Kondo, Y., Liao, H., Lohmann, U., Rasch, P., Satheesh, S., Sherwood, S., Stevens, B., Zhang, X., Qin, D., Plattner, G., Tignor, M., Allen, S., Boschung, J., Nauels, A., Xia, Y., Bex, V., Midgley, P., Boucher, O. and Randall, D.: Clouds and aerosols, in *Climate Change 2013 the Physical Science Basis: Working Group I Contribution to the Fifth Assessment Report of the Intergovernmental Panel on Climate Change*, vol. 9781107057, pp. 571–658., 2013.

Rao, S., Klimont, Z., Smith, S. J., Van Dingenen, R., Dentener, F., Bouwman, L., Riahi, K., Amann, M., Bodirsky, B. L., van Vuuren, D. P., Aleluia Reis, L., Calvin, K., Drouet, L., Fricko, O., Fujimori, S., Gernaat, D., Havlik, P., Harmsen, M., Hasegawa, T., Heyes, C., Hilaire, J., Luderer, G., Masui, T., Stehfest, E., Strefler, J., van der Sluis, S. and Tavoni, M.: Future air pollution in the Shared Socio-economic Pathways, *Glob. Environ. Chang.*, 42, 346–358, doi:10.1016/j.gloenvcha.2016.05.012, 2017.

Regayre, L. A., Pringle, K. J., Booth, B. B. B., Lee, L. A., Mann, G. W., Browse, J., Woodhouse, M. T., Rap, A., Reddington, C. L. and Carslaw, K. S.: Uncertainty in the magnitude of aerosol-cloud radiative forcing over recent decades, *Geophys. Res. Lett.*, 41(24), 9040–9049, doi:10.1002/2014GL062029, 2014.

Regayre, L. A., Pringle, K. J., Lee, L. A., Rap, A., Browse, J., Mann, G. W., Reddington, C. L., Carslaw, K. S., Booth, B. B. B. and Woodhouse, M. T.: The climatic importance of uncertainties in regional aerosol-cloud radiative forcings over recent decades, *J. Clim.*, 28(17), 6589–6607, doi:10.1175/JCLI-D-15-0127.1, 2015.

Regayre, L. A., Johnson, J. S., Yoshioka, M., Pringle, K. J., Sexton, D. M. H., Booth, B. B. B., Lee, L., Bellouin, N. and Carslaw, K.: Aerosol and physical atmosphere model parameters are both important sources of uncertainty in aerosol ERF, *Atmos. Chem. Phys.*, 18(13), 1–54, doi:10.5194/acp-2018-175, 2018.

Regayre, L. A., Schmale, J., Johnson, J. S., Tatzelt, C., Baccharini, A., Henning, S., Yoshioka, M., Stratmann, F., Gysel-Beer, M., Grosvenor, D. P. and Carslaw, K. S.: The value of remote marine aerosol measurements for constraining radiative forcing uncertainty, *Atmos. Chem. Phys.*, 20(16), 10063–10072, doi:10.5194/acp-20-10063-2020, 2020.

Riahi, K., van Vuuren, D. P., Kriegler, E., Edmonds, J., O'Neill, B. C., Fujimori, S., Bauer, N., Calvin, K., Dellink, R., Fricko, O., Lutz, W., Popp, A., Cuaresma, J. C., KC, S., Leimbach, M., Jiang, L., Kram, T., Rao, S., Emmerling, J., Ebi, K., Hasegawa, T., Havlik, P., Humpenöder, F., Da Silva, L. A., Smith, S., Stehfest, E., Bosetti, V., Eom, J., Gernaat, D., Masui, T., Rogelj, J., Strefler, J., Drouet, L., Krey, V., Luderer, G., Harmsen, M., Takahashi, K., Baumstark, L., Doelman, J. C., Kainuma, M., Klimont, Z., Marangoni, G., Lotze-Campen, H., Obersteiner, M., Tabeau, A. and Tavoni, M.: The Shared Socioeconomic Pathways and their energy, land use, and greenhouse gas emissions implications: An overview, *Glob. Environ. Chang.*, 42, 153–168, doi:10.1016/j.gloenvcha.2016.05.009, 2017.

Richardson, T. B., Forster, P. M., Andrews, T., Boucher, O., Faluvegi, G., Fläschner, D., Hodnebrog, K., Kassoar, M., Kirkevåg, A., Lamarque, J. F., Myhre, G., Olivié, D., Samset, B. H., Shawki, D., Shindell, D., Takemura, T. and Voulgarakis, A.: Drivers of precipitation change: An energetic understanding, *J. Clim.*, 31(23), 9641–9657, doi:10.1175/JCLI-D-17-0240.1, 2018.

- Ridley, H. E., Asmerom, Y., Baldini, J. U. L., Breitenbach, S. F. M., Aquino, V. V., Pruber, K. M., Culleton, B. J., Polyak, V., Lechleitner, F. A., Kennett, D. J., Zhang, M., Marwan, N., Macpherson, C. G., Baldini, L. M., Xiao, T., Peterkin, J. L., Awe, J. and Haug, G. H.: Aerosol forcing of the position of the intertropical convergence zone since ad 1550, *Nat. Geosci.*, 8(3), 195–200, doi:10.1038/ngeo2353, 2015.
- Rotstayn, L. D. and Lohmann, U.: Tropical Rainfall Trends and the Indirect Aerosol Effect, *J. Clim.*, 15(15), 2103–2116, doi:10.1175/1520-0442(2002)015<2103:TRTATI>2.0.CO;2, 2002.
- Rotstayn, L. D., Collier, M. A., Chrastansky, A., Jeffrey, S. J. and Luo, J. J.: Projected effects of declining aerosols in RCP4.5: Unmasking global warming?, *Atmos. Chem. Phys.*, 13(21), 10883–10905, doi:10.5194/acp-13-10883-2013, 2013.
- Rotstayn, L. D., Plymin, E. L., Collier, M. A., Boucher, O., Dufresne, J. L., Luo, J. J., Von Salzen, K., Jeffrey, S. J., Foujols, M. A., Ming, Y. and Horowitz, L. W.: Declining aerosols in CMIP5 projections: Effects on atmospheric temperature structure and midlatitude jets, *J. Clim.*, 27(18), 6960–6977, doi:10.1175/JCLI-D-14-00258.1, 2014.
- Rotstayn, L. D., Collier, M. A., Shindell, D. T. and Boucher, O.: Why does aerosol forcing control historical global-mean surface temperature change in CMIP5 models?, *J. Clim.*, 28(17), 6608–6625, doi:10.1175/JCLI-D-14-00712.1, 2015.
- Salzmann, M.: Global warming without global mean precipitation increase', *Sci. Adv.*, 2(6), doi:10.1126/sciadv.1501572, 2016.
- Samset, B. H., Sand, M., Smith, C. J., Bauer, S. E., Forster, P. M., Fuglestedt, J. S., Osprey, S. and Schleussner, C. F.: Climate Impacts From a Removal of Anthropogenic Aerosol Emissions, *Geophys. Res. Lett.*, 45(2), 1020–1029, doi:10.1002/2017GL076079, 2018a.
- Scott, C. E., Arnold, S. R., Monks, S. A., Asmi, A., Paasonen, P. and Spracklen, D. V.: Substantial large-scale feedbacks between natural aerosols and climate, *Nat. Geosci.*, 11(1), 44–48, doi:10.1038/s41561-017-0020-5, 2018.
- Seinfeld, J. H., Bretherton, C., Carslaw, K. S., Coe, H., DeMott, P. J., Dunlea, E. J., Feingold, G., Ghan, S., Guenther, A. B., Kahn, R., Kraucunas, I., Kreidenweis, S. M., Molina, M. J., Nenes, A., Penner, J. E., Prather, K. A., Ramanathan, V., Ramaswamy, V., Rasch, P. J., Ravishankara, A. R., Rosenfeld, D., Stephens, G. and Wood, R.: Improving our fundamental understanding of the role of aerosol–cloud interactions in the climate system, *Proc. Natl. Acad. Sci.*, 113(21), 5781–5790, doi:10.1073/pnas.1514043113, 2016.
- Seong, M. G., Min, S. K., Kim, Y. H., Zhang, X. and Sun, Y.: Anthropogenic greenhouse gas and aerosol contributions to extreme temperature changes during 1951–2015, *J. Clim.*, 34(3), 857–870, doi:10.1175/JCLI-D-19-1023.1, 2021.
- Shindell, D. T., Lamarque, J. F., Schulz, M., Flanner, M., Jiao, C., Chin, M., Young, P. J., Lee, Y. H., Rotstayn, L., Mahowald, N., Milly, G., Faluvegi, G., Balkanski, Y., Collins, W. J., Conley, A. J., Dalsoren, S., Easter, R., Ghan, S., Horowitz, L., Liu, X., Myhre, G., Nagashima, T., Naik, V., Rumbold, S. T., Skeie, R., Sudo, K., Szopa, S., Takemura, T., Voulgarakis, A., Yoon, J. H. and Lo, F.: Radiative forcing in the ACCMIP historical and future climate simulations, *Atmos. Chem. Phys.*, 13(6), 2939–2974, doi:10.5194/acp-13-2939-2013, 2013.
- Skeie, R. B., Berntsen, T. K., Myhre, G., Tanaka, K., Kvalevåg, M. M. and Hoyle, C. R.: Anthropogenic radiative forcing time series from pre-industrial times until 2010, *Atmos. Chem. Phys.*, 11(22), 11827–11857, doi:10.5194/acp-11-11827-2011, 2011.
- Smith, C. J., Forster, P. M., Allen, M., Leach, N., Millar, R. J., Passerello, G. A. and Regayre, L. A.: FAIR v1.3: A simple emissions-based impulse response and carbon cycle model, *Geosci. Model Dev.*, 11(6), 2273–2297, doi:10.5194/gmd-11-2273-2018, 2018.
- Smith, C. J., Kramer, R. J., Myhre, G., Alterskjær, K., Collins, W., Sima, A., Boucher, O., Dufresne, J. L., Nabat, P., Michou, M., Yukimoto, S., Cole, J., Paynter, D. J., Shiogama, H., O'Connor, F. M., Robertson, E., Wiltshire, A., Andrews, T., Hannay, C., Miller, R., Nazarenko, L., Kirkevåg, A., Olivie, D., Fiedler, S., Pincus, R. and Forster, P. M.: Effective radiative forcing and rapid adjustments in CMIP6 models, *Atmos. Chem. Phys. Discuss.* [online] Available from: <https://www.atmos-chem-phys-discuss.net/acp-2019-1212/> (Accessed 27 April 2020), 2020.
- Smith, C. J., Harris, G. R., Palmer, M. D., Bellouin, N., Collins, W., Myhre, G., Schulz, M., Golaz, J. C., Ringer, M., Storelvmo, T. and Forster, P. M.: Energy Budget Constraints on the Time History of Aerosol Forcing and Climate Sensitivity, *J. Geophys. Res. Atmos.*, 126(13),

e2020JD033622, doi:10.1029/2020JD033622, 2021.

Smith, D. M., Booth, B. B. B., Dunstone, N. J., Eade, R., Hermanson, L., Jones, G. S., Scaife, A. A., Sheen, K. L. and Thompson, V.: Role of volcanic and anthropogenic aerosols in the recent global surface warming slowdown, , doi:10.1038/NCLIMATE3058, 2016.

Smith, S. J., Van Aardenne, J., Klimont, Z., Andres, R. J., Volke, A. and Delgado Arias, S.: Anthropogenic sulfur dioxide emissions: 1850-2005, *Atmos. Chem. Phys.*, 11(3), 1101–1116, doi:10.5194/acp-11-1101-2011, 2011.

Soden, B., Chung, E.-S., Soden, B. and Chung, E.-S.: The Large-Scale Dynamical Response of Clouds to Aerosol Forcing, *J. Clim.*, 30(21), 8783–8794, doi:10.1175/JCLI-D-17-0050.1, 2017.

Stevens, B.: Rethinking the lower bound on aerosol radiative forcing, *J. Clim.*, 28(12), 4794–4819, doi:10.1175/JCLI-D-14-00656.1, 2015.

Stier, P., Schutgens, N. A. J., Bellouin, N., Bian, H., Boucher, O., Chin, M., Ghan, S., Huneeus, N., Kinne, S., Lin, G., Ma, X., Myhre, G., Penner, J. E., Randles, C. A., Samset, B., Schulz, M., Takemura, T., Yu, F., Yu, H. and Zhou, C.: Host model uncertainties in aerosol radiative forcing estimates: Results from the AeroCom Prescribed intercomparison study, *Atmos. Chem. Phys.*, 13(6), 3245–3270, doi:10.5194/acp-13-3245-2013, 2013.

Storelvmo, T., Lohmann, U. and Bennartz, R.: What governs the spread in shortwave forcings in the transient IPCC AR4 models?, *Geophys. Res. Lett.*, 36(1), L01806, doi:10.1029/2008GL036069, 2009.

Szopa, S., Balkanski, Y., Schulz, M., Bekki, S., Cugnet, D., Fortems-Cheiney, A., Turquety, S., Cozic, A., Déandréis, C., Hauglustaine, D., Idelkadi, A., Lathièrre, J., Lefevre, F., Marchand, M., Vuolo, R., Yan, N. and Dufresne, J. L.: Aerosol and ozone changes as forcing for climate evolution between 1850 and 2100, *Clim. Dyn.*, 40(9–10), 2223–2250, doi:10.1007/s00382-012-1408-y, 2013.

Textor, C., Schulz, M., Guibert, S., Kinne, S., Balkanski, Y., Bauer, S., Berntsen, T., Berglen, T., Boucher, O., Chin, M., Dentener, F., Diehl, T., Easter, R., Feichter, H., Fillmore, D., Ghan, S., Ginoux, P., Gong, S., Grini, A., Hendricks, J., Horowitz, L., Huang, P., Isaksen, I., Iversen, I., Kloster, S., Koch, D., Kirkevåg, A., Kristjansson, J. E., Krol, M., Lauer, A., Lamarque, J. F., Liu, X., Montanaro, V., Myhre, G., Penner, J., Pitari, G., Reddy, S., Seland, Ø., Stier, P., Takemura, T. and Tie, X.: Analysis and quantification of the diversities of aerosol life cycles within AeroCom, *Atmos. Chem. Phys.*, 6(7), 1777–1813, doi:10.5194/acp-6-1777-2006, 2006.

Textor, C., Schulz, M., Guibert, S., Kinne, S., Balkanski, Y., Bauer, S., Berntsen, T., Berglen, T., Boucher, O., Chin, M., Dentener, F., Diehl, T., Feichter, J., Fillmore, D., Ginoux, P., Gong, S., Grini, A., Hendricks, J., Horowitz, L., Huang, P., Isaksen, I. S. A., Iversen, T., Kloster, S., Koch, D., Kirkevåg, A., Kristjansson, J. E., Krol, M., Lauer, A., Lamarque, J. F., Liu, X., Montanaro, V., Myhre, G., Penner, J. E., Pitari, G., Reddy, M. S., Seland, Stier, P., Takemura, T. and Tie, X.: The effect of harmonized emissions on aerosol properties in global models - An AeroCom experiment, *Atmos. Chem. Phys.*, 7(17), 4489–4501, doi:10.5194/acp-7-4489-2007, 2007.

Thornhill, G., Collins, W., Olivie, D., B. Skeie, R., Archibald, A., Bauer, S., Checa-Garcia, R., Fiedler, S., Folberth, G., Gjernundsen, A., Horowitz, L., Lamarque, J. F., Michou, M., Mulcahy, J., Nabat, P., Naik, V., M. O'Connor, F., Paulot, F., Schulz, M., E. Scott, C., Séférian, R., Smith, C., Takemura, T., Tilmes, S., Tsigaridis, K. and Weber, J.: Climate-driven chemistry and aerosol feedbacks in CMIP6 Earth system models, *Atmos. Chem. Phys.*, 21(2), 1105–1126, doi:10.5194/acp-21-1105-2021, 2021.

Toll, V., Christensen, M., Quaas, J. and Bellouin, N.: Weak average liquid-cloud-water response to anthropogenic aerosols, *Nature*, 572(7767), 51–55, doi:10.1038/s41586-019-1423-9, 2019.

Tsutsui, J.: Minimal CMIP Emulator (MCE v1.2): a new simplified method for probabilistic climate projections, *Geosci. Model Dev.*, 15(3), 951–970, doi:10.5194/gmd-15-951-2022, 2022.

Turnock, S. T., Allen, R. J., Andrews, M., Bauer, S. E., Deushi, M., Emmons, L., Good, P., Horowitz, L., John, J. G., Michou, M., Nabat, P., Naik, V., Neubauer, D., O'Connor, F. M., Olivie, D., Oshima, N., Schulz, M., Sellar, A., Shim, S., Takemura, T., Tilmes, S., Tsigaridis, K., Wu, T. and Zhang, J.: Historical and future changes in air pollutants from CMIP6 models, *Atmos. Chem. Phys.*, 20(23), 14547–14579, doi:10.5194/acp-20-14547-2020, 2020.

Twomey, S.: Pollution and the planetary albedo, *Atmos. Environ.*, 8(12), 1251–1256, doi:10.1016/0004-6981(74)90004-3, 1974.

- Undorf, S., Bollasina, M. A., Booth, B. B. B. and Hegerl, G. C.: Contrasting the Effects of the 1850–1975 Increase in Sulphate Aerosols from North America and Europe on the Atlantic in the CESM, *Geophys. Res. Lett.*, 45(21), 11,930–11,940, doi:10.1029/2018GL079970, 2018.
- Verma, T., Saravanan, R., Chang, P. and Mahajan, S.: Tropical Pacific Ocean dynamical response to short-term sulfate aerosol forcing, *J. Clim.*, 32(23), 8205–8221, doi:10.1175/JCLI-D-19-0050.1, 2019.
- Villarini, G., Vecchi, G. A., Villarini, G. and Vecchi, G. A.: Projected Increases in North Atlantic Tropical Cyclone Intensity from CMIP5 Models, *J. Clim.*, 26(10), 3231–3240, doi:10.1175/JCLI-D-12-00441.1, 2013.
- van Vuuren, D. P., Edmonds, J., Kainuma, M., Riahi, K., Thomson, A., Hibbard, K., Hurtt, G. C., Kram, T., Krey, V., Lamarque, J.-F., Masui, T., Meinshausen, M., Nakicenovic, N., Smith, S. J. and Rose, S. K.: The representative concentration pathways: an overview, *Clim. Change*, 109(1–2), 5–31, doi:10.1007/s10584-011-0148-z, 2011.
- Wang, H. and Wen, Y. J.: Climate response to the spatial and temporal evolutions of anthropogenic aerosol forcing, *Clim. Dyn.*, 1–17, doi:10.1007/s00382-021-06059-2, 2021.
- Warren, S. G. and Wiscombe, W. J.: A model for the spectral albedo of snow. II: snow containing atmospheric aerosols., *J. Atmos. Sci.*, 37(12), 2734–2745, doi:10.1175/1520-0469(1980)037<2734:AMFTSA>2.0.CO;2, 1980.
- Westervelt, D. M., Horowitz, L. W., Naik, V., Golaz, J.-C. and Mauzerall, D. L.: Radiative forcing and climate response to projected 21st century aerosol decreases, *Atmos. Chem. Phys.*, 15(22), 12681–12703, doi:10.5194/acp-15-12681-2015, 2015.
- Westervelt, D. M., Conley, A. J., Fiore, A. M., Lamarque, J. F., Shindell, D. T., Previdi, M., Mascioli, N. R., Faluvegi, G., Correa, G. and Horowitz, L. W.: Connecting regional aerosol emissions reductions to local and remote precipitation responses, *Atmos. Chem. Phys.*, 18(16), 12461–12475, doi:10.5194/acp-18-12461-2018, 2018.
- Wilcox, L. J., Highwood, E. J., Booth, B. B. B. and Carslaw, K. S.: Quantifying sources of inter-model diversity in the cloud albedo effect, *Geophys. Res. Lett.*, doi:10.1002/2015GL063301, 2015.
- Wilcox, L. J., Liu, Z., Samset, B. H., Hawkins, E., Lund, M. T., Nordling, K., Undorf, S., Bollasina, M., Ekman, A. M. L., Krishnan, S., Merikanto, J. and Turner, A. G.: Accelerated increases in global and Asian summer monsoon precipitation from future aerosol reductions, *Atmos. Chem. Phys.*, 20(20), 11955–11977, doi:10.5194/acp-20-11955-2020, 2020.
- Zelinka, M. D., Andrews, T., Forster, P. M. and Taylor, K. E.: Quantifying components of aerosol-cloud-radiation interactions in climate models, *J. Geophys. Res. Atmos.*, 119(12), 7599–7615, doi:10.1002/2014JD021710, 2014.
- Zhang, S., Stier, P. and Watson-Parris, D.: On the contribution of fast and slow responses to precipitation changes caused by aerosol perturbations, *Atmos. Chem. Phys.*, 21(13), 10179–10197, doi:10.5194/acp-21-10179-2021, 2021.

Chapter 2 Effect of Aerosol Radiative Forcing Uncertainty on Projected Exceedance Year of a 1.5 °C Global Temperature Rise

A. H. Peace¹, K. S. Carslaw¹, L. A. Lee^{1,a}, L. A. Regayre¹, B. B. Booth²,
J. S. Johnson¹, D. Bernie²

¹ Institute for Climate and Atmospheric Science, University of Leeds, Leeds, UK

² Met Office Hadley Centre, Exeter, UK

^a now at: Department of Engineering and Mathematics, Sheffield Hallam University, Sheffield, UK

Abstract

Anthropogenic aerosol emissions are predicted to decline sharply throughout the 21st century, in line with climate change and air quality mitigation policies, causing a near-term warming of climate that will impact our trajectory towards 1.5 °C above pre-industrial temperatures. However, the persistent uncertainty in aerosol radiative forcing limits our understanding of how much the global mean temperature will respond to near-term reductions in anthropogenic aerosol emissions. We quantify the model and scenario uncertainty in global mean aerosol radiative forcing up to 2050 using statistical emulation of a perturbed parameter ensemble for emission reduction scenarios consistent with three Shared Socioeconomic Pathways. We then use a simple climate model to translate the uncertainty in aerosol radiative forcing into uncertainty in global mean temperature projections, accounting additionally for the potential correlation of aerosol radiative forcing and climate sensitivity. Near-term aerosol radiative forcing uncertainty alone causes an uncertainty window of around 5 years (2034-2039) on the projected year of exceeding a global temperature rise of 1.5 °C above pre-industrial temperatures for a middle of the road emissions scenario (SSP2-RCP4.5). A correlation between aerosol radiative forcing and climate sensitivity would increase the 1.5 °C exceedance window by many years. The results highlight the importance of quantifying aerosol radiative forcing and any relationship with climate sensitivity in climate models in order to reduce uncertainty in temperature projections.

2.1 Introduction

The Paris Agreement of the United Nations Framework Convention on Climate Change aims to restrict global mean temperature change since the pre-industrial era to well below 2 °C and pursue efforts to limit global mean temperature change to 1.5 °C (United Nations Convention on Climate Change, 2015). The year when a proportion of climate model realizations exceed a global mean temperature rise of 1.5 °C can be used to calculate the remaining carbon budgets at that point, and thereafter translate into guidance for climate change mitigation policies (Rogelj et al., 2016). However, there are many uncertainties associated with the projected exceedance year of a global mean temperature rise of 1.5 °C. These include definitional ambiguities such as the pre-industrial reference year used for calculating a temperature anomaly, whether all warming or only human-induced warming is included, the future emission scenarios, and how the climate will respond to changes in emissions (IPCC et al., 2018; Rogelj et al., 2017; Schurer et al., 2017). In particular, near-term projections of climate are sensitive to the emissions scenarios and climatic impacts of short lived climate forcers such as atmospheric aerosols, methane and tropospheric ozone (Bindoff et al., 2013b).

Atmospheric aerosols affect the radiative balance of the planet by scattering and absorbing incoming solar radiation, altering the microphysics of clouds, and subsequent rapid atmospheric adjustments. Anthropogenic aerosol emissions have caused a negative radiative forcing over the industrial period of between -1.9 to -0.1 W m⁻² (Randall et al., 2013), counteracting some of the warming of climate caused by greenhouse gases. Regionally, anthropogenic aerosol emissions have declined over Europe and North America since the 1980s (Granier et al., 2011; Hand et al., 2012; Vestreng et al., 2007), and more recently anthropogenic SO₂ emissions have declined over China (Li et al., 2017). Future emissions scenarios predict further global reductions in anthropogenic aerosol emissions to combat poor air quality and in line with climate change mitigation policies (Riahi et al., 2017; van Vuuren et al., 2011). The projected reductions in anthropogenic aerosols will lead to a warming of climate in the near-term that will add to the warming effect of greenhouse gases (Rotstayn et al., 2013; Westervelt et al., 2015). Due to the short lifetime of atmospheric aerosols relative to greenhouse gases, rapid reductions in anthropogenic aerosol emissions and other short lived climate forcers could be the main drivers of near-term climate

change (Chalmers et al., 2012). Consequently, changes in anthropogenic aerosol emissions will have a bearing on whether we exceed, and if so by how much, the target to limit global average temperature rise to 1.5 °C since the pre-industrial period as set by the Paris Agreement (Hienola et al., 2018; United Nations Convention on Climate Change, 2015).

Estimates of aerosol radiative forcing are highly uncertain (Myhre et al., 2013a), limiting how well we understand the drivers of historical climate change and how accurately we can predict future climate (Collins et al., 2012). Historical aerosol forcing uncertainty has been quantified using multi-model ensembles (Myhre et al., 2013b; Rotstayn et al., 2014; Shindell et al., 2013) and perturbed parameter ensembles (Carslaw et al., 2013; Regayre et al., 2014, 2015, 2018). Multi-model ensembles sample the spread in model output due to differing parameterizations and assumptions of physical processes in different models, known as model structural uncertainty. Perturbed parameter ensembles of models sample the spread in model output caused by the uncertainty in model parameters and process representations in an individual model, known as model parametric uncertainty. The spread in model output due to different emission scenarios, known as scenario uncertainty, causes an additional source of uncertainty in climate projections. Analyses of uncertainty in near-term aerosol forcing and climate impacts have so far been limited by the small range of aerosol emission pathways sampled by the Representative Concentration Pathways (RCPs) or by using a small number of models to assess model uncertainty (Bartlett et al., 2018; Chalmers et al., 2012; Fiedler et al., 2019; Lund et al., 2019; Rotstayn et al., 2014, 2015; Samset et al., 2018; Shindell et al., 2013; Szopa et al., 2013; Westervelt et al., 2015). Model parametric uncertainty in aerosol radiative forcing, can be as large as multi-model spread (Johnson et al., 2018), but has so far largely been neglected in near-term climate projections of aerosol radiative forcing and climate response.

In this work we quantify the uncertainty in near-term projections of aerosol radiative forcing due to parametric model uncertainty and scenario uncertainty for a single model, and examine what impact this uncertainty has on predicting the exceedance year of a mean climate 1.5 °C global temperature rise since pre-industrial levels. We use a perturbed parameter ensemble (PPE) of our aerosol-climate model (HadGEM3-UKCA) and statistical emulation to sample

aerosol radiative forcing uncertainty in near-term climate projections. We then use a simple climate model (FaIR v1.4) to translate our parametric uncertainty in near-term projections of aerosol radiative forcing to uncertainty in projected global temperature change. We highlight the importance of reducing aerosol radiative forcing uncertainty for improving predictions of the exceedance year of the 1.5 °C target set by the Paris Agreement.

2.2 Methods

2.2.1 Climate Model: HadGEM3-UKCA

The base model used in this work is the Met Office Hadley Centre Climate Model, HadGEM3 (Hewitt et al., 2011). HadGEM3 was run at a N96 resolution (1.25° in latitude, 1.875° in longitude), with 85 vertical levels up to 85 km above sea level. This model uses the 4th Global Atmosphere configuration (GA4) (Walters et al., 2014). The model was run in atmosphere-only mode with sea surface temperatures and sea ice prescribed using reanalysed monthly varying fields. Horizontal wind speeds and temperature fields were nudged between approximately 1 km and 60 km to Medium-Range Weather Forecast ERA-Interim reanalysis.

The model incorporates version 8.4 of the UK Chemistry and Aerosol (UKCA) model. UKCA is an atmospheric chemistry and aerosol model, which simulates the evolution of particle size distribution and size-resolved chemical composition of aerosol (O'Connor et al., 2014). The modal version of the GLObal Model of Aerosol Processes (GLOMAP-mode) is used to simulate new particle formation, gas-to-gas particle transfer, aerosol coagulation, cloud processing of aerosol, and aerosol deposition (Mann et al., 2010). In this model setup GLOMAP-mode resolves sulfate, organic carbon, black carbon, sea salt and dust in seven modes. The degree of atmospheric nudging in this model setup allows for the diagnosis of instantaneous effects of aerosol-radiation interactions and aerosol-cloud interactions (direct and first indirect aerosol radiative forcing).

2.2.2 A Perturbed Parameter Ensemble of HadGEM3-UKCA

A perturbed parameter ensemble (PPE) of the model setup described above was created to quantify and constrain uncertainty in model output due to uncertain aerosol parameters (Yoshioka et al., 2019). Twenty six uncertain parameters that

sample the uncertainty in aerosol emissions, processes, and removal were perturbed. Expert elicitation was used to define the probability distribution representing uncertainty in each parameter. The definition of the 26 parameters perturbed and their trapezoidal distribution are given in the supporting information (Table A.1).

Once the uncertain parameters were selected, Maximin Latin Hypercube sampling was used to design model simulations that span the 26-dimensional space of the parameter uncertainties, producing an ensemble of simulations that can be used for statistical techniques, such as emulation (O’Hagan, 2006). The PPE consists of a set of 235 single-year global model simulations with anthropogenic aerosol emissions prescribed for the year 2008. The pre-industrial to present day aerosol forcing in the PPE is stronger (more negative), but spans a similar range, to multi-model experiments, as shown by a visual comparison in Figure A.2. A more detailed methodology for the model and perturbed parameter set up used in this paper can be found in Yoshioka et al. (2019).

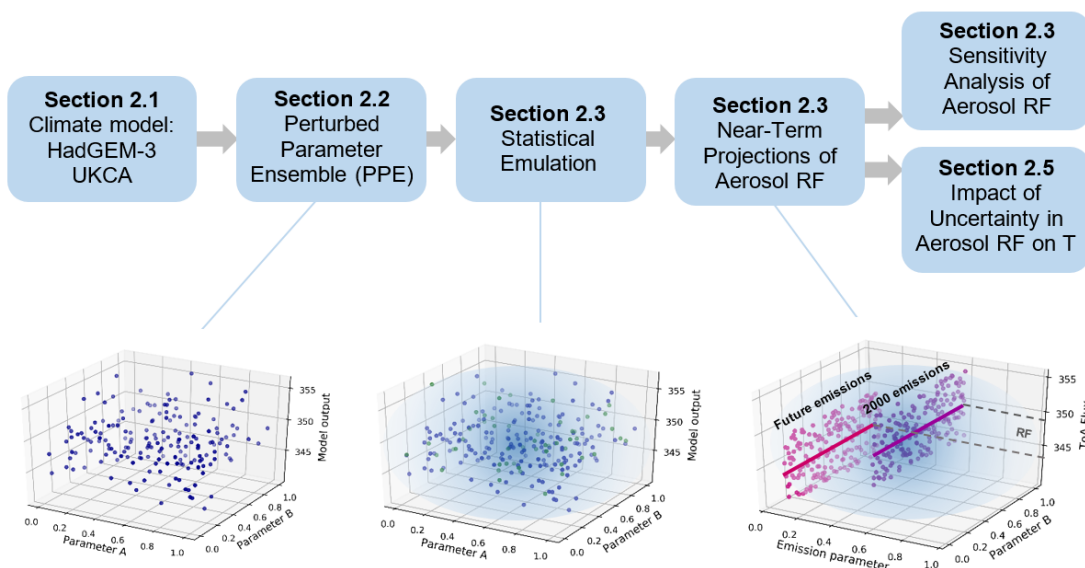


Figure 2.1 This schematic illustrates the steps used to quantify the uncertainty in near-term aerosol radiative forcing. The figure to the left shows a 2-dimensional example of a perturbed parameter ensemble. The middle figure illustrates a statistical emulator (blue cloud) trained from the perturbed parameter ensemble model output (blue dots), and validated against further model output (green dots). The figure to the right illustrates how by using the emulator, an anthropogenic emission scaling can be applied to predict a range of aerosol radiative forcing that represents the aerosol climate model uncertainty.

2.2.3 Using Statistical Emulation to Estimate Uncertainty in Future Aerosol Forcing

The design of the perturbed parameter ensemble allows for Gaussian process emulation (O'Hagan, 2006). Gaussian process emulation provides a statistical representation of model output across the multi-dimensional parameter space that enables model output to be predicted for any parameter combination within the ranges of the PPE. We used emulation, as described below, to estimate the uncertainty in near-term projections of aerosol radiative forcing for selected aerosol emission reduction scenarios consistent with the Shared Socioeconomic Pathways (SSPs).

Firstly, we built an emulator for global mean top of atmosphere flux (shortwave and longwave). The emulator is trained from 183 model simulations from the PPE described above, and then validated against a further 52 model simulations from the PPE to ensure the emulator can predict model output accurately.

The anthropogenic aerosol emissions parameters (anthropogenic SO₂, carbonaceous fossil fuel and carbonaceous biofuel) in the PPE were perturbed over a wide range of values above and below their 2008 values, with the lowest values mostly comparable to the aerosol emissions expected between 2035 and 2060 in the SSPs. We are therefore able to use our emulators of 2008 shortwave and longwave top of atmosphere flux to predict the top of atmosphere flux for future years that have lower anthropogenic aerosol emissions.

To predict top of atmosphere flux for future years, we scale global mean values of our three anthropogenic aerosol emission parameters to match global mean values in a particular year (2000, 2005, 2010, 2015, 2020, 2030, 2040, and 2050) of the Shared Socioeconomic Pathway emission scenarios (Figure 2.2). This approach effectively scales the 2008 emissions patterns of the PPE up or down. Then, for each scenario, we use the emulators of shortwave and longwave top of atmosphere flux to predict 270,000 values of top of atmosphere flux for each interval and corresponding emission scaling in our near-term future time series. In these 270,000 predictions of top of atmosphere flux, the values for the remaining 23 parameters in the PPE (related to aerosol processes and natural emissions) vary across their uncertainty range. We use 2000 as our baseline and calculate the difference in top of atmosphere flux between 2000 and each of the points in the future, giving us a time series of 270,000 predictions of aerosol

radiative forcing. The spread in these 270,000 predictions of aerosol radiative forcing accounts for the uncertainty in our model's aerosol process and removal parameters, which is our model uncertainty. The steps in this process are visualised in Figure 2.1.

The advantage of our approach is that we are able to estimate the model and scenario uncertainty in aerosol radiative forcing out to 2050 for emissions pathways consistent with the Shared Socioeconomic Pathways, without the computational expense of designing a new PPE that specifically samples the uncertainty in future aerosol radiative forcing. We acknowledge that there are limitations in our approach. For example, since we are applying a scaling to the existing pattern of 2008 aerosol emissions within our PPE, we can represent regions of future emissions reductions across most of the world, but not opposing regions of increasing emissions, for example in India (Figure 2.2). However, India has been shown to have a small global mean cooling response induced by its aerosol emissions (Persad and Caldeira, 2018). Nevertheless, we focus our analysis on global mean values, rather than at a regional level. Also, using this technique, we are limited to the minimum and maximum values of anthropogenic aerosol emission parameters covered by the PPE. For anthropogenic SO₂, the lower limit of the perturbation represents a 40% reduction in anthropogenic SO₂ relative to the original 2008 emissions. Therefore, scenarios such as SSP1-RCP2.6 that represent rapid near-term reductions in anthropogenic aerosol are outside of our perturbation boundary. In this case, we have used emission changes to extrapolate top of atmosphere radiative flux to give an impression of what aerosol radiative forcing might be, which is explained in more detail in the supporting information (Section A.5).

We identify the causes of aerosol radiative forcing uncertainty in our near-term projections using variance-based sensitivity analysis (Saltelli et al., 1999), as described in Lee et al. 2013 (Lee et al., 2013). The sensitivity analysis enables us to calculate the proportion of variance in aerosol forcing that could be explained if an uncertain parameter was known precisely.

2.2.4 Shared Socioeconomic Pathways (SSPs)

The Shared Socioeconomic Pathways (SSPs) are a range of emission, land use and energy projections based on five narratives describing how the future may unfold with differing socioeconomic developments. The five socioeconomic narratives of the SSPs are: SSP1 – sustainable development, SSP2 – middle of the road development, SSP3 – regional rivalry, SSP4 – inequality, and SSP5 – fossil-fuelled development (Riahi et al., 2017). Each SSP scenario combines with the Representative Concentration Pathways (RCPs). The RCPs describe emission and land-use scenarios that represent the net forcing of all anthropogenic forcing agents at the year 2100 (van Vuuren et al., 2011). The SSP pathways are designed to depict a wide range of future scenarios, and hence encompass a wide range of future air quality emission scenarios, in contrast to the RCPs which assume similar air pollution pathways (Rao et al., 2017). Within each SSP pathway, scenarios are produced for each RCP forcing level, and also a baseline scenario which assumes no future mitigation for climate change, giving the notation style SSPX-RCPX or SSPX-baseline. Each SSP pathway has an associated air pollution control strength. In this paper we have chosen three SSP scenarios selected from ScenarioMIP for CMIP6 (O'Neill et al., 2016). Our chosen scenarios: SSP1-RCP2.6, SSP2-RCP4.5, SSP4-RCP6.0 assume strong, medium and weak pollution controls respectively, and therefore sample a wide range of scenario uncertainty in anthropogenic aerosol emissions. We use global mean values from these three scenarios to scale our 2008 pattern of anthropogenic aerosol emissions. These three scenarios also have differing greenhouse gas (GHG) representations that are relevant for the temperature projections section of this paper, with SSP1-RCP2.6 having strong mitigation of GHG emissions, to SSP4-RCP6.0 having weaker mitigation of GHG emissions by mid-century. As our focus is on capturing scenario uncertainty associated with near-term aerosol reductions, we have not used a scenario that has the weakest mitigation of GHG emissions, such as SSP5-RCP8.5, that will have the largest increase in global mean temperature by the end of century (Meinshausen et al., 2019).

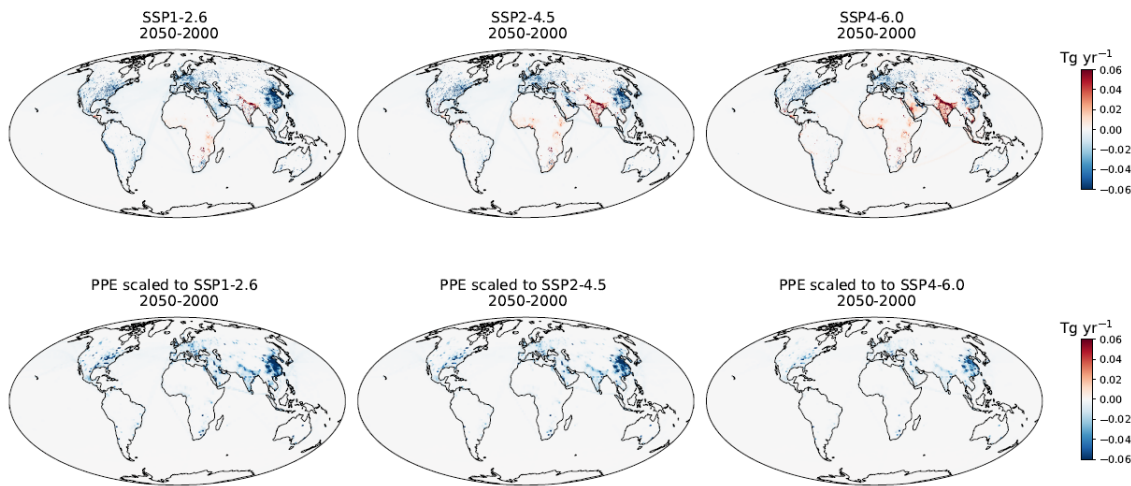


Figure 2.2 Changes in anthropogenic SO₂ emissions between 2000-2050 for the Shared Socioeconomic Pathways scenarios SSP1-RCP2.6, SSP2-RCP4.5 and SSP4-RCP6.0 used (top row), in comparison to the scalings applied to our 2008 emissions from the PPE simulations (bottom row).

2.2.5 Temperature Projection with a Simple Climate Model

Simple climate models represent the most important aspects of fully coupled climate models, and are commonly used to translate global radiative forcing or emissions scenario inputs into global temperature change. We use version 1.4 of the Finite Amplitude Impulse Response model (FaIR), to translate our uncertainty in aerosol radiative forcing in near-term projections into uncertainty in global temperature change (Millar et al., 2017; Smith et al., 2018). FaIR has been validated against carbon cycle and earth system models from AR5, and is used within IPCC SR1.5 to estimate the temperature impacts of differing emissions scenarios (Rogelj et al., 2018; Shindell and Smith, 2019; Smith et al., 2019). For aerosol-radiation interactions, FaIR assumes a linear relationship between global emissions and global aerosol forcing. For aerosol-cloud interactions, FaIR uses a logarithmic dependence of aerosol forcing as a function of sulfate and primary organic aerosol. FaIR then uses a forcing efficacy of 1 for all forcing agents apart from black carbon on snow, to convert global mean radiative forcings to temperature change. Shindell et al. (2014) suggest that the asymmetric pattern of aerosol forcing can lead to a larger temperature response to aerosols than that to greenhouse gases, and hence the temperature response of aerosols may be underestimated in simple climate models that do not take the spatial pattern of aerosol forcing into account (Shindell, 2014). The use of a single model could introduce biases in the projected temperature change, due to differing climate responses to emission changes across simple climate models, based on the

assumptions and parameterizations used in each model. Schwarber et al. (2019) explored the temperature response to concentration impulse tests amongst simple climate models, and showed FalR v1.0 had a weaker response to a CO₂ impulse than other simple climate models (Schwarber et al., 2019). Furthermore, FalR has been shown to have a weaker near-term warming trend than the simple climate model MAGICC (Rogelj et al., 2018). On this basis we might expect the years of exceedance of 1.5 °C to shift if the conversion of aerosol forcing to temperature was treated differently, or if a different simple climate model was used.

Firstly, we run FalR with its default settings that include constrained estimates of equilibrium climate sensitivity (ECS) and transient climate response (TCR) of 2.75 K and 1.6 K respectively to calculate a forcing time series from emissions prescribed by the SSP scenarios. To isolate the impact of our parametric uncertainty in near-term aerosol radiative forcing on the exceedance year of 1.5 °C, we substitute in our calculated aerosol radiative forcing from 2000 onwards, and run FalR in forcing driven mode to obtain the temperature projections that account for near-term aerosol forcing uncertainty. At 2000 we also normalize the temperature projections from FalR to the observed global mean temperature from the HadCRUT4 data set, to account for any deviations in global mean temperature that may have arisen through the historical period (Morice et al., 2012).

Previous studies have shown a statistical relationship between historical aerosol forcing and equilibrium climate sensitivity emerges in generations of climate models up to CMIP5 when ensembles of simulations are constrained by the historical temperature record, and also such relationship exists between historical aerosol forcing and transient climate response in FalR v1.3 (Andreae et al., 2005; Smith et al., 2018; Tanaka and Raddatz, 2011). Hence, we illustrate the effect of a statistical relationship between aerosol forcing and climate sensitivity on projecting the exceedance year of a 1.5 °C by combining our weak, mean, and strong aerosol radiative forcing with a relevant ECS and TCR from the IPCC AR5 likely range (Bindoff et al., 2013a). For example, from 2000, we combine the strong aerosol radiative projection with a higher value of ECS of 4.5 K and TCR of 2.5 K. The values for ECS and TCR that are selected for each projection strand are shown in Figure 2.4 and Table A.3. We note that this is an illustrative

approach to show the potential implications of a statistical relationship between climate sensitivity and aerosol forcing based on historical assumptions. We do not address the implications of any physical relationships between forcing and feedback, as described in Gettelman et al. 2016 (Gettelman et al., 2016), that may alter climate sensitivity. For both the approaches described in this section we calculate the mean climate temperature anomaly relative to an 1850-1900 baseline, in line with the definition of a 1.5 °C temperature rise adopted in the IPCC SR1.5 (IPCC et al., 2018).

2.3 Results

2.3.1 Quantifying Uncertainty in Near-Term Aerosol Radiative Forcing

Here we examine the spread in aerosol radiative forcing in near-term climate projections caused by the effect of uncertain aerosol parameters within our aerosol-climate model (HadGEM3-UKCA). We focus on three Shared Socioeconomic Pathways: SSP1-RCP2.6, SSP2-RCP4.5 and SSP4-RCP6.0 that span different socio-economic narratives and air quality policies. The use of multiple scenarios allows us to compare the scenario uncertainty to parametric model uncertainty in aerosol radiative forcing. Figure 2.3 shows predictions of global mean aerosol radiative forcing relative to the year 2000. The spread of predictions in a single scenario (shaded regions) represents the parametric model uncertainty from 270,000 combinations of uncertain aerosol parameters.

Initially the aerosol radiative forcing is negative relative to 2000 as global historical anthropogenic aerosol emissions continue to increase within the SSPs. As anthropogenic aerosol emissions decline from 2010 onwards within the SSP pathways, we see a positive radiative forcing relative to 2000. Reductions in anthropogenic SO₂ are the main driver of positive radiative forcing (Figure A.9). The implementation of strong air quality policies in SSP1-RCP2.6 and therefore the rapid reductions in anthropogenic aerosols lead to a more positive radiative forcing than in SSP4-RCP6.0 which assumes weak air quality policies. The three scenarios SSP1-RCP2.6, SSP2-RCP4.5 and SSP4-RCP6.0 cause a mean global aerosol radiative forcing by 2050 relative to 2000 of 1.12, 0.78 and 0.30 W m⁻² respectively. The spread in the forcing of 0.82 W m⁻² between the scenarios reflects the scenario uncertainty.

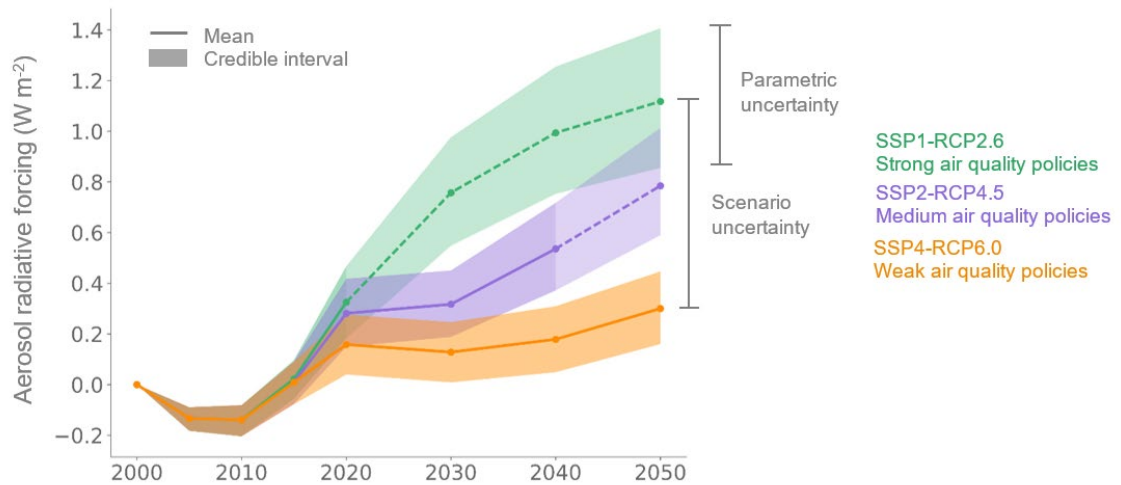


Figure 2.3 Global mean radiative forcing relative to the year 2000 for anthropogenic aerosol emission (anthropogenic SO₂, carbonaceous fossil fuel, carbonaceous biofuel) reductions scaled to match three SSP emission scenarios. The solid line represents the mean of radiative forcing predictions, with the shaded area representing the 95% credible interval that represents the parametric uncertainty within the aerosol-climate model. The dashed line and lighter shaded areas represent where aerosol radiative forcing has been extrapolated.

In the middle of the road scenario (SSP2-RCP4.5), the mean radiative forcing by 2050 is 0.78 W m⁻², with a 95% credible interval of 0.59-1.01 W m⁻² that represents the parametric model uncertainty. Overall, by mid-century the scenario uncertainty is larger than parametric model uncertainty in near-term aerosol radiative forcing projections. However, the model uncertainty in this single scenario (SSP2-RCP4.5), is equivalent to 52% of the scenario uncertainty. The model uncertainty increases with the magnitude of radiative forcing as the model is being perturbed further away from its baseline state (radiative forcing in 2000) where we have assumed no uncertainty, and therefore the parametric model uncertainty in a single scenario increases from 35% to 67% of the scenario uncertainty between SSP4-RCP6.0 to SSP1-RCP2.6 which has increasingly stringent pollution controls. When accounting for both model and scenario uncertainty, the combined uncertainty is larger with a spread of 1.35 W m⁻², in comparison to 0.82 W m⁻² when scenario uncertainty is considered alone. Hence, the parametric model uncertainty contributes an important component of the overall uncertainty in near-term aerosol forcing.

It is difficult to compare our single model spread in near-term aerosol radiative forcing to multi-model spread because previous multi-model ensembles calculated aerosol radiative forcing at 2100 relative to the present day or pre-

industrial. Zelinka et al. (2014) report a pre-industrial to present day aerosol radiative forcing of $-1.40 \pm 0.56 \text{ W m}^{-2}$ (standard deviation) that represents the spread in the current generations of climate models (Zelinka et al., 2014). In comparison, the pre-industrial to present day aerosol radiative forcing within our PPE is $-2.12 \pm 1.29 \text{ W m}^{-2}$ (90% credible interval) (Yoshioka et al., 2019). Industrial era aerosol forcing in our PPE is stronger and the spread larger than current multi-model ensembles. Therefore, we expect our aerosol radiative forcing in near-term projections to be stronger, and the spread larger than what would be diagnosed in a similar experiment using a multi-model ensemble. Further detail on the aerosol radiative forcing in our PPE in context of multi-model studies is provided in the supporting information (Section A.2). Given the perturbed parameters in our climate model have analogues in most other climate models, we expect, but cannot confirm, that other models would have similarly large parametric uncertainty.

2.3.2 Sources of Uncertainty in Near-Term Aerosol Radiative Forcing

In order to reduce the uncertainty in the aerosol radiative forcing, it is first useful to understand which parameters within the PPE are the main causes of spread in the aerosol radiative forcing uncertainty. Sensitivity analysis allows us to decompose the variance in aerosol radiative forcing predictions into individual contributions from the uncertain aerosol parameters within our aerosol-climate model.

The sensitivity analysis for global mean radiative forcing over the period 2010-2040 for SSP2-RCP4.5 is shown in Figure A.10. The sea spray emission flux (Sea_Spray) accounts for 60% of the variance in our near-term projections of aerosol radiative forcing, with the standard deviation of updraft velocities (Sig_W) causing a further 17% of the variance.

The sea spray emission flux parameter within our PPE is a scaling factor for sea spray aerosol emissions. Sea spray aerosol emissions greatly influence background aerosol concentrations over marine regions. When sea spray emissions are higher, radiative forcing (particularly indirect radiative forcing) has a lower sensitivity to changes in anthropogenic aerosol emissions, as the background aerosol concentration is higher (Carslaw et al., 2013). Therefore, natural aerosol emission parameters such as sea spray will become increasingly

important contributors to aerosol forcing uncertainty as anthropogenic aerosol concentrations return to a more natural baseline state. Furthermore, there may be feedbacks between the changing climate and natural aerosols emissions, although we do not account for such feedbacks in this study (Tegen and Schepanski, 2018).

The standard deviation of updraft velocities (Sig_W), is the second most important parameter in causing variance in our aerosol radiative forcing projections, and controls the width of the distributions of sub-grid updraft velocities that are used to calculate the activation of aerosol into cloud droplets. A larger value of this parameter will widen the distribution of updraft velocities, allowing larger updraft velocities. Larger updraft velocities for a given supersaturation will cause a greater number of aerosol particles to activate to cloud droplets, increasing cloud droplets concentrations and cloud albedo, and thus strengthening indirect radiative forcing. Updraft velocity uncertainty is particularly important over polluted land regions where cloud droplet number concentrations are updraft-limited (Reutter et al., 2009). The remaining variance is caused by small contributions (<5%) from each of the other parameters (Figure A.10).

To reduce the uncertainty in uncertain parameters and aerosol radiative forcing, observational constraint is required. Recent observational constraint on our PPE has shown that ground and marine observations of aerosol properties can successfully constrain the probability distributions of some of the most uncertain parameters within the PPE, and reduce the confidence interval of pre-industrial to present-day radiative forcing from aerosol-cloud interactions by around 21% (Johnson et al., 2019; Regayre et al., 2019), and presumably an equivalent constraint would reduce our near-term aerosol radiative forcing uncertainty by a similar amount.

2.3.3 Impact of Uncertainty in Aerosol Radiative Forcing on Temperature Projection

Next we examine how aerosol radiative forcing uncertainty impacts our ability to predict temperature change. Specifically, we focus on how the projected exceedance year of the 1.5 °C target set by the Paris Agreement (United Nations Convention on Climate Change, 2015) is affected by taking the parametric

uncertainty in aerosol forcing into account. At short lead times, such as the timescales of predicting the exceedance year of 1.5 °C, it has been shown that model uncertainty represents the largest fractional source of uncertainty in global temperature projections (Hawkins and Sutton, 2011). Therefore, as in previous studies, we focus on mean temperature change and do not take into account fluctuations due to internal variability when calculating the year of exceedance of a 1.5 °C temperature rise. We use the simple climate model FaIR v1.4 (Millar et al., 2017; Smith et al., 2018) to translate our radiative forcing values into temperature change. Previous studies have shown a statistical relationship between aerosol forcing and equilibrium climate sensitivity (ECS) (Andreae et al., 2005; Tanaka and Raddatz, 2011), although emerging evidence suggests such relationship may not exist in the latest generation of models as configured in CMIP6 (Smith et al., 2020). We first isolate the effect of the uncertainty in near-term aerosol radiative forcing only on the exceedance year of a 1.5 °C temperature rise, and secondly, we show an illustrative effect of accounting for a relationship between aerosol forcing and climate sensitivity.

The results in this section focus on the SSP pathway SSP2-RCP4.5, which is a middle of the road scenario in terms of its socioeconomics and the underlying narrative, with moderate reductions in emissions of GHGs and aerosols to address climate change and air quality. Importantly, it is also the only scenario to be simulated by CMIP6 which has global emissions in 2030 consistent with the Nationally Determined Contributions (NDCs). The NDCs embody efforts by each country to reduce national emissions and are at the heart of the Paris Agreement and efforts to achieve long-term climate goals, yet the IPCC SR1.5 is clear that the current NDCs are insufficient to limiting warming to 1.5 °C or 2 °C (Rogelj et al., 2018). As such, until additional pledges on emissions in 2030 and beyond are in place, SSP2-RCP4.5 is the most relevant of the CMIP6 scenarios to the current status of international emission reduction agreement.

Figure 2.4 shows the mean climate global temperature change relative to the 1850-1900 average using our estimated range of aerosol forcings from 2000, with the temperature at 2000 normalized relative to the HadCRUT4 estimate (Morice et al., 2012). Taking into account the uncertainty in near-term aerosol radiative forcing only, the mean of our aerosol radiative forcings projects an exceedance of 1.5 °C in 2036, with the credible interval exceeding 1.5 °C between 2034 and

2039 for SSP2-RCP4.5. Additionally, if we take into account an illustrative correlation between aerosol radiative forcing and climate sensitivity then the window of exceedance extends from 2022 until after 2050 (assuming an ECS of 4.5 K, TCR of 2.5 K for the strong forcing and an ECS of 1.5 K, TCR of 1 K for weak forcing). If we take into account a smaller range of uncertainty in climate sensitivity, for example an ECS of 3-4.5 K (in line with the central estimate from CMIP6 models (Zelinka et al., 2020)), then the exceedance window of 1.5 °C for SSP2-4.5 narrows to between 2022 and 2036, as shown in Figure A.16. In our illustrative approach of taking the uncertainty in climate sensitivity and transient climate response into account, the rate of change in the temperature projection that follows a high climate sensitivity and strong aerosol forcing is higher than in observations over recent decades. Hence, although a high climate sensitivity and strong aerosol forcing may represent a combination that is plausible in some models, based on the statistical relationship obtained with historical temperature constraint, it does not necessarily represent a plausible combination in all models over the recent decades, nor into the future. A probabilistic analysis of ECS and aerosol forcing may result in a narrower plausible exceedance range.

These results show that the exceedance year window due to the uncertainty in near-term aerosol radiative forcing uncertainty alone is comparable or larger than that induced from uncertainties in processes related to inter-annual variability, such as the phase of the Pacific Decadal Modulation (Henley and King, 2017). However, as natural variability may lead to transient exceedances of 1.5 °C, uncertainty in aerosol radiative forcing will affect the mean climate projections, and is therefore more relevant to mitigation policy decisions, such as calculating remaining carbon budgets by using a threshold exceedance approach. When the collective uncertainty in climate sensitivity and near-term aerosol radiative forcing uncertainty is taken into account, the uncertainty in exceedance year of 1.5 °C is far greater. Thus, these results show that in order to reduce the uncertainty in exceedance year of 1.5 °C we need to quantify and reduce the uncertainty in aerosol radiative forcing, and quantify any corresponding relationship between aerosol forcing and climate sensitivity.

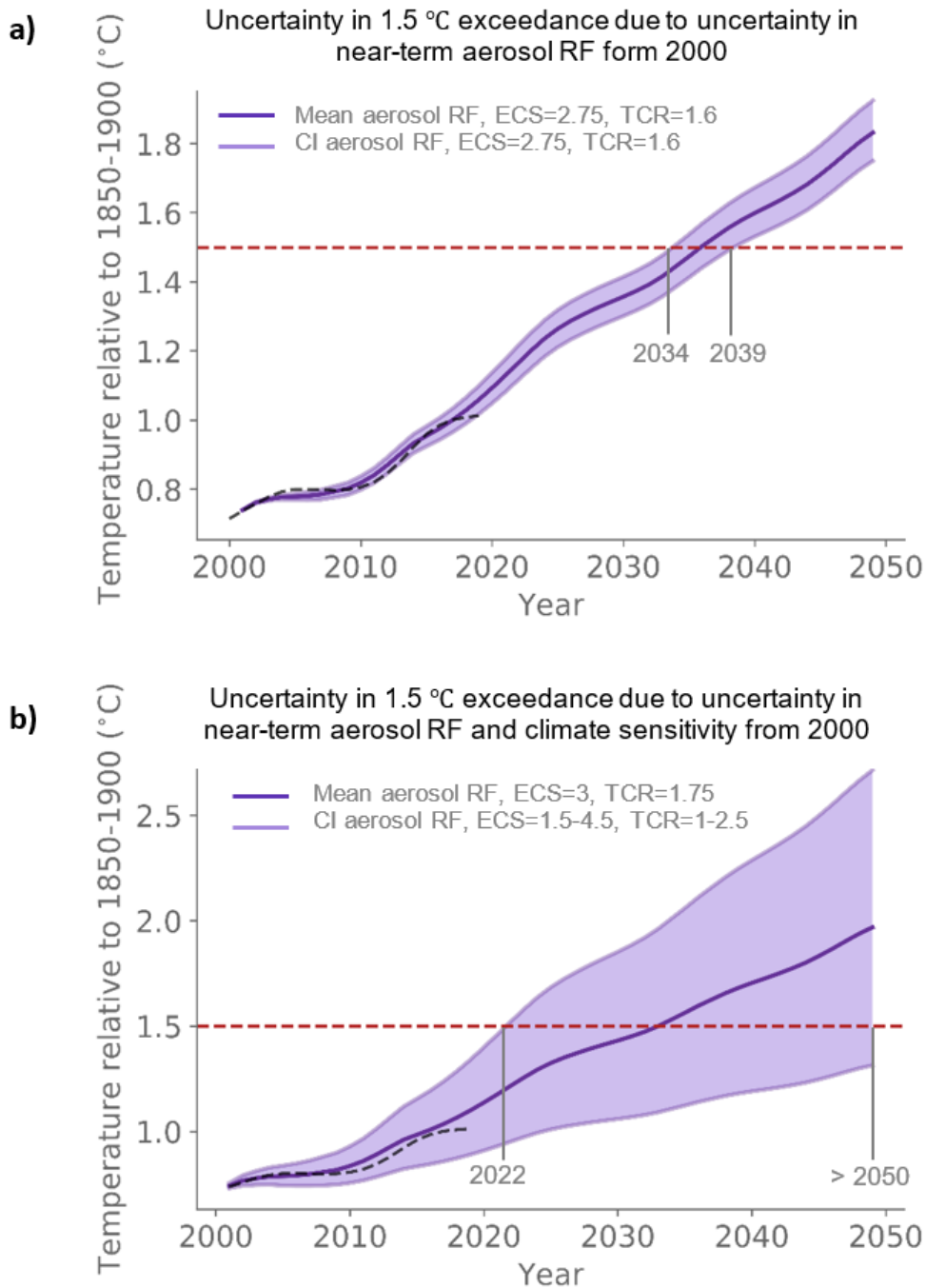


Figure 2.4 Global mean temperature change relative to 1850-1900 for SSP2-RCP4.5. We prescribe our aerosol radiative forcing (RF) from 2000 for anthropogenic aerosol emissions changes. All other forcings are calculated by FaIR v1.4 from SSP2-RCP4.5 prescribed emissions. The top figure (a) shows the impact of model uncertainty in aerosol radiative forcing from 2000, with the darker shaded line representing our mean radiative forcing value translated to temperature and the shaded region representing the 95% credible interval (CI) for aerosol radiative forcing, with the black dashed line representing observations from HadCRUT4. The bottom figure (b) displays an illustrative range in exceedance year of 1.5 °C if a statistical relationship between uncertainty in aerosol radiative forcing and climate sensitivity is accounted for from 2000, for example if stronger values of our aerosol forcing range are paired with higher values of ECS and TCR, and weaker values of our aerosol forcing range are paired with lower values of ECS and TCR. The range of values selected for ECS and TCR in each projection is displayed in the figure legend.

2.4 Discussion and Conclusion

The persistent uncertainty in aerosol radiative forcing limits our understanding of how the climate will respond to future reductions in anthropogenic aerosol emissions, and therefore it is important we acknowledge how single and multi-model uncertainty in aerosol radiative forcing affects near-term climate projections. We have used statistical emulation of a perturbed parameter ensemble of climate model simulations to sample the uncertainty due to aerosol emissions and processes in near-term (up to 2050) projections of aerosol radiative forcing. Then, using a simple climate model, FaIR v1.4, we have translated our aerosol radiative forcing uncertainty into projections of global mean temperature change.

Our results show a global mean positive radiative forcing in the near-term future due to reductions in anthropogenic aerosol emissions. The magnitude of aerosol radiative forcing is dependent on the air pollution controls assumed in each SSP pathway. Within the three SSP pathways used (SSP1-RCP2.6, SSP2-RCP4.5, SSP4-RCP6.0) that sample strong, medium and weak implementations of air quality policies there is a global mean aerosol radiative forcing of 0.30-1.12 W m⁻² by 2050 relative to 2000, representing a large scenario uncertainty. This uncertainty increases to 0.16-1.41 W m⁻² when the parametric model uncertainty is included. The uncertainty in aerosol radiative forcing due to our parameters in a single scenario is 35% to 67% of the uncertainty due to the differing emission scenarios. We note that the pre-industrial to present-day aerosol radiative forcing in our PPE is stronger than in multi-model studies. Therefore, we assume the magnitude of near-term aerosol radiative forcing in our ensemble is likely stronger than other models, but we expect the uncertainty range would be similar in models that represent the same uncertain processes that we have perturbed in our ensemble. Although scenario uncertainty is the dominant driver of uncertainty in our near-term aerosol radiative forcing projections, it cannot be reduced until strategic actions by multiple influential nations have been taken, and due to recent reductions in emissions from China for example, there may already be deviations from the emission inventories used for scenarios (Zheng et al., 2018). Therefore parametric model uncertainty in aerosol radiative forcing is large enough (as a component of the overall uncertainty) to warrant efforts to better understand its causes so that it can be

reduced. Recent work using the PPE used in this study has shown it is possible to constrain the probability distributions of the uncertain parameters by using multiple point observations of aerosol properties, which can reduce the number of 1,000,000 model variants by up to 98%. However due to model equifinality, where multiple model variants can combine in ways to produce the same value of model output, the resultant constraint on radiative forcing due to aerosol-cloud interactions is more modest, at around 21% (Johnson et al., 2019; Regayre et al., 2019).

Current emission reduction commitments suggest a global mean temperature rise of 1.5 °C since pre-industrial times will likely happen during the next two decades (Rogelj et al., 2018). This gives little time to put in place mitigation measures that will limit global mean temperature rise, and as such, uncertainties in climate modelling that alter the projected exceedance year of a 1.5 °C temperature rise are important factors to consider. Hence, due to projected reductions in anthropogenic aerosols, the uncertainty in aerosol radiative forcing has relevance in predicting near-term human induced temperature change and thus the year of exceedance of a global mean temperature rise of 1.5 °C since the pre-industrial era. Our results show that for a scenario with moderate reductions in anthropogenic aerosol and greenhouse gases, SSP2-RCP4.5, the parametric model uncertainty in near-term aerosol radiative forcing alone can alter the predicted year of exceedance of 1.5 °C by 5 years (2034 to 2039). Furthermore, when taking an illustrative approach where the uncertainty in aerosol forcing and climate sensitivity are assumed to be correlated the exceedance window of 1.5 °C increases greatly (2022 to > 2050). However, in accordance with the observed global mean temperature rise between 2000 and 2019, the outer limits of our climate sensitivity and aerosol forcing couplings are likely to be an out of bounds example. Over the historical period aerosol cooling and greenhouse gas warming have had counteracting effects on temperature change, and therefore a strong aerosol radiative forcing coupled with a high climate sensitivity has a similar projected global mean temperature change to a weak aerosol radiative forcing coupled with a low climate sensitivity. Yet when such relationship is considered in the near-term future, when projected reductions in anthropogenic aerosols may cause a warming of climate, temperature projections with a combination of strong aerosol radiative forcing and high climate

sensitivity diverge from those with a weak aerosol radiative forcing and low climate sensitivity, and hence accounting for the uncertainty in climate sensitivity greatly increases the exceedance window of 1.5 °C (Tanaka and Raddatz, 2011). Therefore, if the uncertainty range of climate sensitivity were smaller, as may be the case in a probabilistic analysis, the exceedance window of 1.5 °C would narrow accordingly.

This study has shown aerosol radiative forcing uncertainty, and in particular the collective impact of aerosol forcing uncertainty and any relationship with climate sensitivity on projecting exceedance year of 1.5 °C, illustrates the need for the continued effort in reducing aerosol radiative forcing uncertainty and quantifying the relationship between climate sensitivity and aerosol forcing, in order for successful implementation of climate change mitigation policies.

References

- Andreae, M. O., Jones, C. D. and Cox, P. M.: Strong present-day aerosol cooling implies a hot future, *Nature*, 435(7046), 1187–1190, doi:10.1038/nature03671, 2005.
- Bartlett, R. E., Bollasina, M. A., Booth, B. B. B., Dunstone, N. J., Marengo, F., Messori, G. and Bernie, D. J.: Do differences in future sulfate emission pathways matter for near-term climate? A case study for the Asian monsoon, *Clim. Dyn.*, 50(5–6), 1863–1880, doi:10.1007/s00382-017-3726-6, 2018.
- Bindoff, N. L., Stott, P. A., AchutaRao, K. M., Allen, M. R., Gillett, N., Gutzler, D., Hansingo, K., Hegerl, G., Hu, Y., Jain, S. and Mokhov, I. I.: Detection and Attribution of Climate Change: from Global to Regional, in *Climate Change 2013 the Physical Science Basis: Working Group I Contribution to the Fifth Assessment Report of the Intergovernmental Panel on Climate Change.*, 2013a.
- Bindoff, N. L., Durack, P. J., Slater, A., Cameron-Smith, P., Chikamoto, Y., Clifton, O., Ginoux, P., Holland, M., Holmes, C., Infanti, J., Jacob, D., John, J., Knutson, T., Lawrence, D., Lu, J., Murphy, D., Naik, V., Robock, A., Vavrus, S., Ishii, M., Corti, S., Fichefet, T., García-Serrano, J., Guemas, V., Rodrigues, L., Gray, L., Hawkins, E., Smith, D., Stevenson, D. S., Voulgarakis, A., Weisheimer, A., Wild, O., Woollings, T., Young, P., Krinner, G., Klimont, Z., Sedláček, J., van den Hurk, B. and van Noije, T.: Near-term climate change: Projections and predictability, in *Climate Change 2013 the Physical Science Basis: Working Group I Contribution to the Fifth Assessment Report of the Intergovernmental Panel on Climate Change*, vol. 9781107057, pp. 953–1028., 2013b.
- Carslaw, K. S., Lee, L. A., Reddington, C. L., Pringle, K. J., Rap, A., Forster, P. M., Mann, G. W., Spracklen, D. V., Woodhouse, M. T., Regayre, L. A. and Pierce, J. R.: Large contribution of natural aerosols to uncertainty in indirect forcing, *Nature*, 503(7474), 67–71, doi:10.1038/nature12674, 2013.
- Chalmers, N., Highwood, E. J., Hawkins, E., Sutton, R. and Wilcox, L. J.: Aerosol contribution to the rapid warming of near-term climate under RCP 2.6, *Geophys. Res. Lett.*, 39(18), doi:10.1029/2012GL052848, 2012.
- Collins, M., Chandler, R. E., Cox, P. M., Huthnance, J. M., Rougier, J. and Stephenson, D. B.: Quantifying future climate change, *Nat. Clim. Chang.*, 2(6), 403–409, doi:10.1038/nclimate1414, 2012.
- Fiedler, S., Stevens, B., Gidden, M., Smith, S. J., Riahi, K. and van Vuuren, D.: First forcing estimates from the future CMIP6 scenarios of anthropogenic aerosol optical properties and an associated Twomey effect, *Geosci. Model Dev.*, 12(3), 989–1007, doi:10.5194/gmd-12-989-2019, 2019.
- Gottelman, A., Lin, L., Medeiros, B. and Olson, J.: Climate feedback variance and the interaction of aerosol forcing and feedbacks, *J. Clim.*, 29(18), 6659–6675, doi:10.1175/JCLI-D-16-0151.1, 2016.
- Granier, C., Bessagnet, B., Bond, T., D'Angiola, A., Denier van der Gon, H., Frost, G. J., Heil, A., Kaiser, J. W., Kinne, S., Klimont, Z., Kloster, S., Lamarque, J.-F., Lioussé, C., Masui, T., Meleux, F., Mieville, A., Ohara, T., Raut, J.-C., Riahi, K., Schultz, M. G., Smith, S. J., Thompson, A., van Aardenne, J., van der Werf, G. R. and van Vuuren, D. P.: Evolution of anthropogenic and biomass burning emissions of air pollutants at global and regional scales during the 1980–2010 period, *Clim. Change*, 109(1–2), 163–190, doi:10.1007/s10584-011-0154-1, 2011.
- Hand, J. L., Schichtel, B. A., Malm, W. C. and Pitchford, M. L.: Particulate sulfate ion concentration and SO₂ emission trends in the United States from the early 1990s through 2010, *Atmos. Chem. Phys.*, 12(21), 10353–10365, doi:10.5194/acp-12-10353-2012, 2012.
- Hawkins, E. and Sutton, R.: The potential to narrow uncertainty in projections of regional precipitation change, *Clim. Dyn.*, 37(1), 407–418, doi:10.1007/s00382-010-0810-6, 2011.
- Henley, B. J. and King, A. D.: Trajectories toward the 1.5°C Paris target: Modulation by the Interdecadal Pacific Oscillation, *Geophys. Res. Lett.*, 44(9), 4256–4262, doi:10.1002/2017GL073480, 2017.
- Hewitt, H. T., Copley, D., Culverwell, I. D., Harris, C. M., Hill, R. S. R., Keen, A. B., McLaren, A. J. and Hunke, E. C.: Design and implementation of the infrastructure of HadGEM3: The next-

- generation Met Office climate modelling system, *Geosci. Model Dev.*, 4(2), 223–253, doi:10.5194/gmd-4-223-2011, 2011.
- Hienola, A., Partanen, A. I., Pietikainen, J. P., O'Donnell, D., Korhonen, H., Matthews, H. D. and Laaksonen, A.: The impact of aerosol emissions on the 1.5 °C pathways, *Environ. Res. Lett.*, 13(4), 044011, doi:10.1088/1748-9326/aab1b2, 2018.
- IPCC, Allen, M. ., Dube, O. P., Solecki, W., Aragón-Durand, F., Cramer, W., Humphreys, S., Kainuma, M., Kala, J., Mahowald, N., Mulugetta, Y., Perez, R., Wairiu, M. and Zichfeld, K.: Framing and Context, in *Global Warming of 1.5°C. An IPCC Special Report on the impacts of global warming of 1.5°C above pre-industrial levels and related global greenhouse gas emission pathways, in the context of strengthening the global response to the threat of climate change*, pp. 51–91. [online] Available from: https://www.ipcc.ch/site/assets/uploads/sites/2/2019/02/SR15_Chapter1_Low_Res.pdf, 2018.
- Johnson, J., Regayre, L., Yoshioka, M., Pringle, K., Turnock, S., Browse, J., Sexton, D. M., Rostron, J., Schutgens, N. A., Partridge, D., Liu, D., Allan, J., Coe, H., Ding, A., Cohen, D., Atanacio, A., Vakkari, V., Asmi, E. and Carslaw, K.: Robust observational constraint of uncertain aerosol processes and emissions in a climate model and the effect on aerosol radiative forcing, *Atmos. Chem. Phys. Discuss.*, 1–51, doi:10.5194/acp-2019-834, 2019.
- Johnson, J. S., Regayre, L. A., Yoshioka, M., Pringle, K. J., Lee, L. A., Sexton, D., Rostron, J., Booth, B. B. B. and Carslaw, K. S.: The importance of comprehensive parameter sampling and multiple observations for robust constraint of aerosol radiative forcing, *Atmos. Chem. Phys.*, 18(17), 13031–13053, doi:10.5194/acp-2018-174, 2018.
- Lee, L. A., Pringle, K. J., Reddington, C. L., Mann, G. W., Stier, P., Spracklen, D. V., Pierce, J. R. and Carslaw, K. S.: The magnitude and causes of uncertainty in global model simulations of cloud condensation nuclei, *Atmos. Chem. Phys.*, 13(17), 8879–8914, doi:10.5194/acp-13-8879-2013, 2013.
- Li, C., McLinden, C., Fioletov, V., Krotkov, N., Carn, S., Joiner, J., Streets, D., He, H., Ren, X., Li, Z. and Dickerson, R. R.: India Is Overtaking China as the World's Largest Emitter of Anthropogenic Sulfur Dioxide, *Sci. Rep.*, 7(1), 1–7, doi:10.1038/s41598-017-14639-8, 2017.
- Lund, M. T., Myhre, G. and Samset, B. H.: Anthropogenic aerosol forcing under the Shared Socioeconomic Pathways, *Atmos. Chem. Phys.*, 19(22), 13827–13839, doi:10.5194/acp-2019-606, 2019.
- Mann, G. W., Carslaw, K. S., Spracklen, D. V., Ridley, D. A., Manktelow, P. T., Chipperfield, M. P., Pickering, S. J. and Johnson, C. E.: Geoscientific Model Development Description and evaluation of GLOMAP-mode: a modal global aerosol microphysics model for the UKCA composition-climate model, *Geosci. Model Dev.*, 3, 519–551, doi:10.5194/gmd-3-519-2010, 2010.
- Meinshausen, M., Nicholls, Z., Lewis, J., Gidden, M., Vogel, E., Freund, M., Beyerle, U., Gessner, C., Nauels, A., Bauer, N., Canadell, J., Daniel, J., John, A., Krummel, P., Luderer, G., Meinshausen, N., Montzka, S., Rayner, P., Reimann, S., Smith, S., van den Berg, M., Velders, G., Vollmer, M. and Wang, H. J.: The SSP greenhouse gas concentrations and their extensions to 2500, *Geosci. Model Dev. Discuss.*, 1–77, doi:10.5194/gmd-2019-222, 2019.
- Millar, J. R., Nicholls, Z. R., Friedlingstein, P. and Allen, M. R.: A modified impulse-response representation of the global near-surface air temperature and atmospheric concentration response to carbon dioxide emissions, *Atmos. Chem. Phys.*, 17(11), 7213–7228, doi:10.5194/acp-17-7213-2017, 2017.
- Morice, C. P., Kennedy, J. J., Rayner, N. A. and Jones, P. D.: Quantifying uncertainties in global and regional temperature change using an ensemble of observational estimates: The HadCRUT4 data set, *J. Geophys. Res. Atmos.*, 117(8), n/a-n/a, doi:10.1029/2011JD017187, 2012.
- Myhre, G., Shindell, D., Aamaas, B., Boucher, O., Dalsøren, S., Daniel, J., Forster, P., Granier, C., Haigh, J. and Hodnebrog, Ø.: Anthropogenic and natural radiative forcing, in *Climate Change 2013 the Physical Science Basis: Working Group I Contribution to the Fifth Assessment Report of the Intergovernmental Panel on Climate Change*, vol. 9781107057, pp. 659–740., 2013a.
- Myhre, G., Samset, B. H., Schulz, M., Balkanski, Y., Bauer, S., Berntsen, T. K., Bian, H., Bellouin, N., Chin, M., Diehl, T., Easter, R. C., Feichter, J., Ghan, S. J., Hauglustaine, D., Iversen, T., Kinne, S., Kirkevåg, A., Lamarque, J. F., Lin, G., Liu, X., Lund, M. T., Luo, G., Ma, X., Van Noije, T., Penner, J. E., Rasch, P. J., Ruiz, A., Seland, Skeie, R. B., Stier, P., Takemura, T., Tsigaridis, K.,

- Wang, P., Wang, Z., Xu, L., Yu, H., Yu, F., Yoon, J. H., Zhang, K., Zhang, H. and Zhou, C.: Radiative forcing of the direct aerosol effect from AeroCom Phase II simulations, *Atmos. Chem. Phys.*, 13(4), 1853–1877, doi:10.5194/acp-13-1853-2013, 2013b.
- O'Connor, F. M., Johnson, C. E., Morgenstern, O., Abraham, N. L., Braesicke, P., Dalvi, M., Folberth, G. A., Sanderson, M. G., Telford, P. J., Voulgarakis, A., Young, P. J., Zeng, G., Collins, W. J. and Pyle, J. A.: Evaluation of the new UKCA climate-composition model – Part 2: The Troposphere, *Geosci. Model Dev.*, 7(1), 41–91, doi:10.5194/gmd-7-41-2014, 2014.
- O'Hagan, A.: Bayesian analysis of computer code outputs: A tutorial, *Reliab. Eng. Syst. Saf.*, 91(10–11), 1290–1300, doi:10.1016/j.ress.2005.11.025, 2006.
- O'Neill, B. C., Tebaldi, C., Van Vuuren, D. P., Eyring, V., Friedlingstein, P., Hurtt, G., Knutti, R., Kriegler, E., Lamarque, J. F., Lowe, J., Meehl, G. A., Moss, R., Riahi, K. and Sanderson, B. M.: The Scenario Model Intercomparison Project (ScenarioMIP) for CMIP6, *Geosci. Model Dev.*, 9(9), 3461–3482, doi:10.5194/gmd-9-3461-2016, 2016.
- Persad, G. G. and Caldeira, K.: Divergent global-scale temperature effects from identical aerosols emitted in different regions., *Nat. Commun.*, 9(1), 3289, doi:10.1038/s41467-018-05838-6, 2018.
- Randall, D., Artaxo, P., Bretherton, C., Feingold, G., Forster, P., Kerminen, V., Kondo, Y., Liao, H., Lohmann, U., Rasch, P., Satheesh, S., Sherwood, S., Stevens, B., Zhang, X., Qin, D., Plattner, G., Tignor, M., Allen, S., Boschung, J., Nauels, A., Xia, Y., Bex, V., Midgley, P., Boucher, O. and Randall, D.: Clouds and aerosols, in *Climate Change 2013 the Physical Science Basis: Working Group I Contribution to the Fifth Assessment Report of the Intergovernmental Panel on Climate Change*, vol. 9781107057, pp. 571–658., 2013.
- Rao, S., Klimont, Z., Smith, S. J., Van Dingenen, R., Dentener, F., Bouwman, L., Riahi, K., Amann, M., Bodirsky, B. L., van Vuuren, D. P., Aleluia Reis, L., Calvin, K., Drouet, L., Fricko, O., Fujimori, S., Gernaat, D., Havlik, P., Harmsen, M., Hasegawa, T., Heyes, C., Hilaire, J., Luderer, G., Masui, T., Stehfest, E., Strefler, J., van der Sluis, S. and Tavoni, M.: Future air pollution in the Shared Socio-economic Pathways, *Glob. Environ. Chang.*, 42, 346–358, doi:10.1016/j.gloenvcha.2016.05.012, 2017.
- Regayre, L., Schmale, J., Johnson, J., Tatzelt, C., Baccarini, A., Henning, S., Yoshioka, M., Stratmann, F., Gysel-Beer, M. and Carslaw, K.: The value of remote marine aerosol measurements for constraining radiative forcing uncertainty, *Atmos. Chem. Phys. Discuss.*, 1–11, doi:10.5194/acp-2019-1085, 2019.
- Regayre, L. A., Pringle, K. J., Booth, B. B. B., Lee, L. A., Mann, G. W., Browse, J., Woodhouse, M. T., Rap, A., Reddington, C. L. and Carslaw, K. S.: Uncertainty in the magnitude of aerosol-cloud radiative forcing over recent decades, *Geophys. Res. Lett.*, 41(24), 9040–9049, doi:10.1002/2014GL062029, 2014.
- Regayre, L. A., Pringle, K. J., Lee, L. A., Rap, A., Browse, J., Mann, G. W., Reddington, C. L., Carslaw, K. S., Booth, B. B. B. and Woodhouse, M. T.: The climatic importance of uncertainties in regional aerosol-cloud radiative forcings over recent decades, *J. Clim.*, 28(17), 6589–6607, doi:10.1175/JCLI-D-15-0127.1, 2015.
- Regayre, L. A., Johnson, J. S., Yoshioka, M., Pringle, K. J., Sexton, D. M. H., Booth, B. B. B., Lee, L., Bellouin, N. and Carslaw, K.: Aerosol and physical atmosphere model parameters are both important sources of uncertainty in aerosol ERF, *Atmos. Chem. Phys.*, 18(13), 1–54, doi:10.5194/acp-2018-175, 2018.
- Reutter, P., Su, H., Trentmann, J., Simmel, M., Rose, D., Gunthe, S. S., Wernli, H., Andreae, M. O. and Pöschl, U.: Aerosol- and updraft-limited regimes of cloud droplet formation: Influence of particle number, size and hygroscopicity on the activation of cloud condensation nuclei (CCN), *Atmos. Chem. Phys.*, 9(18), 7067–7080, doi:10.5194/acp-9-7067-2009, 2009.
- Riahi, K., van Vuuren, D. P., Kriegler, E., Edmonds, J., O'Neill, B. C., Fujimori, S., Bauer, N., Calvin, K., Dellink, R., Fricko, O., Lutz, W., Popp, A., Cuaresma, J. C., KC, S., Leimbach, M., Jiang, L., Kram, T., Rao, S., Emmerling, J., Ebi, K., Hasegawa, T., Havlik, P., Humpenöder, F., Da Silva, L. A., Smith, S., Stehfest, E., Bosetti, V., Eom, J., Gernaat, D., Masui, T., Rogelj, J., Strefler, J., Drouet, L., Krey, V., Luderer, G., Harmsen, M., Takahashi, K., Baumstark, L., Doelman, J. C., Kainuma, M., Klimont, Z., Marangoni, G., Lotze-Campen, H., Obersteiner, M., Tabeau, A. and Tavoni, M.: The Shared Socioeconomic Pathways and their energy, land use, and greenhouse gas emissions implications: An overview, *Glob. Environ. Chang.*, 42, 153–168, doi:10.1016/j.gloenvcha.2016.05.009, 2017.

- Rogelj, J., Schaeffer, M., Friedlingstein, P., Gillett, N. P., Van Vuuren, D. P., Riahi, K., Allen, M. and Knutti, R.: Differences between carbon budget estimates unravelled, *Nat. Clim. Chang.*, 6(3), 245–252, doi:10.1038/nclimate2868, 2016.
- Rogelj, J., Schleussner, C. F. and Hare, W.: Getting It Right Matters: Temperature Goal Interpretations in Geoscience Research, *Geophys. Res. Lett.*, 44(20), 10,662–10,665, doi:10.1002/2017GL075612, 2017.
- Rogelj, J., Shindell, D., Jiang, K., Fifita, S., Forster, P., Ginzburg, V., Handa, C., Kheshgi, H., Kobayashi, S., Kriegler, E., Mundaca, L., Seferian, R. and Vilarino, M. V.: Mitigation Pathways Compatible With 1.5°C in the Context of Sustainable Development, in Global warming of 1.5°C. An IPCC Special Report [...], p. 82pp. [online] Available from: https://www.ipcc.ch/site/assets/uploads/sites/2/2019/02/SR15_Chapter2_Low_Res.pdf, 2018.
- Rotstayn, L. D., Collier, M. A., Chrastansky, A., Jeffrey, S. J. and Luo, J. J.: Projected effects of declining aerosols in RCP4.5: Unmasking global warming?, *Atmos. Chem. Phys.*, 13(21), 10883–10905, doi:10.5194/acp-13-10883-2013, 2013.
- Rotstayn, L. D., Plymin, E. L., Collier, M. A., Boucher, O., Dufresne, J. L., Luo, J. J., Von Salzen, K., Jeffrey, S. J., Foujols, M. A., Ming, Y. and Horowitz, L. W.: Declining aerosols in CMIP5 projections: Effects on atmospheric temperature structure and midlatitude jets, *J. Clim.*, 27(18), 6960–6977, doi:10.1175/JCLI-D-14-00258.1, 2014.
- Rotstayn, L. D., Collier, M. A. and Luo, J.-J.: Effects of declining aerosols on projections of zonally averaged tropical precipitation, *Environ. Res. Lett.*, 10(4), 044018, doi:10.1088/1748-9326/10/4/044018, 2015.
- Saltelli, A., Tarantola, S. and Chan, K. P.-S.: A Quantitative Model-Independent Method for Global Sensitivity Analysis of Model Output, *Technometrics*, 41(1), 39–56, doi:10.1080/00401706.1999.10485594, 1999.
- Samset, B. H., Sand, M., Smith, C. J., Bauer, S. E., Forster, P. M., Fuglestedt, J. S., Osprey, S. and Schleussner, C. F.: Climate Impacts From a Removal of Anthropogenic Aerosol Emissions, *Geophys. Res. Lett.*, 45(2), 1020–1029, doi:10.1002/2017GL076079, 2018.
- Schurer, A. P., Mann, M. E., Hawkins, E., Tett, S. F. B. and Hegerl, G. C.: Importance of the pre-industrial baseline for likelihood of exceeding Paris goals, *Nat. Clim. Chang.*, 7(8), 563–567, doi:10.1038/NCLIMATE3345, 2017.
- Schwarber, A. K., Smith, S. J., Hartin, C. A., Aaron Vega-Westhoff, B. and Sriver, R.: Evaluating climate emulation: Fundamental impulse testing of simple climate models, *Earth Syst. Dyn.*, 10(4), 729–739, doi:10.5194/esd-10-729-2019, 2019.
- Shindell, D. and Smith, C. J.: Climate and air-quality benefits of a realistic phase-out of fossil fuels, *Nature*, 573(7774), 408–411, doi:10.1038/s41586-019-1554-z, 2019.
- Shindell, D. T.: Inhomogeneous forcing and transient climate sensitivity, *Nat. Clim. Chang.*, 4(4), 274–277, doi:10.1038/nclimate2136, 2014.
- Shindell, D. T., Lamarque, J. F., Schulz, M., Flanner, M., Jiao, C., Chin, M., Young, P. J., Lee, Y. H., Rotstayn, L., Mahowald, N., Milly, G., Faluvegi, G., Balkanski, Y., Collins, W. J., Conley, A. J., Dalsoren, S., Easter, R., Ghan, S., Horowitz, L., Liu, X., Myhre, G., Nagashima, T., Naik, V., Rumbold, S. T., Skeie, R., Sudo, K., Szopa, S., Takemura, T., Voulgarakis, A., Yoon, J. H. and Lo, F.: Radiative forcing in the ACCMIP historical and future climate simulations, *Atmos. Chem. Phys.*, 13(6), 2939–2974, doi:10.5194/acp-13-2939-2013, 2013.
- Smith, C. J., Forster, P. M., Allen, M., Leach, N., Millar, R. J., Passerello, G. A. and Regayre, L. A.: FAIR v1.3: A simple emissions-based impulse response and carbon cycle model, *Geosci. Model Dev.*, 11(6), 2273–2297, doi:10.5194/gmd-11-2273-2018, 2018.
- Smith, C. J., Forster, P. M., Allen, M., Fuglestedt, J., Millar, R. J., Rogelj, J. and Zickfeld, K.: Current fossil fuel infrastructure does not yet commit us to 1.5 °C warming, *Nat. Commun.*, 10(1), 101, doi:10.1038/s41467-018-07999-w, 2019.
- Smith, C. J., Kramer, R. J., Myhre, G., Alterskjær, K., Collins, W., Sima, A., Boucher, O., Dufresne, J. L., Nabat, P., Michou, M., Yukimoto, S., Cole, J., Paynter, D. J., Shiogama, H., O'Connor, F. M., Robertson, E., Wiltshire, A., Andrews, T., Hannay, C., Miller, R., Nazarenko, L., Kirkevåg, A., Olivie, D., Fiedler, S., Pincus, R. and Forster, P. M.: Effective radiative forcing and rapid

adjustments in CMIP6 models, *Atmos. Chem. Phys. Discuss.* [online] Available from: <https://www.atmos-chem-phys-discuss.net/acp-2019-1212/> (Accessed 27 April 2020), 2020.

Szopa, S., Balkanski, Y., Schulz, M., Bekki, S., Cugnet, D., Fortems-Cheiney, A., Turquety, S., Cozic, A., Déandres, C., Hauglustaine, D., Idelkadi, A., Lathière, J., Lefevre, F., Marchand, M., Vuolo, R., Yan, N. and Dufresne, J. L.: Aerosol and ozone changes as forcing for climate evolution between 1850 and 2100, *Clim. Dyn.*, 40(9–10), 2223–2250, doi:10.1007/s00382-012-1408-y, 2013.

Tanaka, K. and Raddatz, T.: Correlation between climate sensitivity and aerosol forcing and its implication for the “climate trap,” *Clim. Change*, 109(3–4), 815–825, doi:10.1007/s10584-011-0323-2, 2011.

Tegen, I. and Schepanski, K.: Climate Feedback on Aerosol Emission and Atmospheric Concentrations, *Curr. Clim. Chang. Reports*, 4(1), 1–10, doi:10.1007/s40641-018-0086-1, 2018.

United Nations Convention on Climate Change: Paris Agreement., 2015.

Vestreng, V., Myhre, G., Fagerli, H., Reis, S. and Tarrasón, L.: Twenty-five years of continuous sulphur dioxide emission reduction in Europe, *Atmos. Chem. Phys.*, 7(13), 3663–3681, doi:10.5194/acp-7-3663-2007, 2007.

van Vuuren, D. P., Edmonds, J., Kainuma, M., Riahi, K., Thomson, A., Hibbard, K., Hurtt, G. C., Kram, T., Krey, V., Lamarque, J.-F., Masui, T., Meinshausen, M., Nakicenovic, N., Smith, S. J. and Rose, S. K.: The representative concentration pathways: an overview, *Clim. Change*, 109(1–2), 5–31, doi:10.1007/s10584-011-0148-z, 2011.

Walters, D. N., Williams, K. D., Boutle, I. A., Bushell, A. C., Edwards, J. M., Field, P. R., Lock, A. P., Morcrette, C. J., Stratton, R. A., Wilkinson, J. M., Willett, M. R., Bellouin, N., Bodas-Salcedo, A., Brooks, M. E., Cosey, D., Earnshaw, P. D., Hardiman, S. C., Harris, C. M., Levine, R. C., Maclachlan, C., Manners, J. C., Martin, G. M., Milton, S. F., Palmer, M. D., Roberts, M. J., Rodríguez, J. M., Tennant, W. J. and Vidale, P. L.: The Met Office Unified Model Global Atmosphere 4.0 and JULES Global Land 4.0 configurations, *Geosci. Model Dev.*, 7(1), 361–386, doi:10.5194/gmd-7-361-2014, 2014.

Westervelt, D. M., Horowitz, L. W., Naik, V., Golaz, J.-C. and Mauzerall, D. L.: Radiative forcing and climate response to projected 21st century aerosol decreases, *Atmos. Chem. Phys.*, 15(22), 12681–12703, doi:10.5194/acp-15-12681-2015, 2015.

Yoshioka, M., Regayre, L. A., Pringle, K. J., Johnson, J. S., Mann, G. W., Partridge, D. G., Sexton, D. M. H., Lister, G. M. S., Schutgens, N., Stier, P., Kipling, Z., Bellouin, N., Browse, J., Booth, B. B., Johnson, C. E., Johnson, B., Mollard, J. D. P., Lee, L. and Carslaw, K. S.: Ensembles of Global Climate Model Variants Designed for the Quantification and Constraint of Uncertainty in Aerosols and their Radiative Forcing, *J. Adv. Model. Earth Syst.*, 11(11), 3728–3754, doi:10.1029/2019ms001628, 2019.

Zelinka, M. D., Andrews, T., Forster, P. M. and Taylor, K. E.: Quantifying components of aerosol-cloud-radiation interactions in climate models, *J. Geophys. Res. Atmos.*, 119(12), 7599–7615, doi:10.1002/2014JD021710, 2014.

Zelinka, M. D., Myers, T. A., McCoy, D. T., Po-Chedley, S., Caldwell, P. M., Ceppi, P., Klein, S. A. and Taylor, K. E.: Causes of Higher Climate Sensitivity in CMIP6 Models, *Geophys. Res. Lett.*, 47(1), doi:10.1029/2019GL085782, 2020.

Zheng, B., Tong, D., Li, M., Liu, F., Hong, C., Geng, G., Li, H., Li, X., Peng, L., Qi, J., Yan, L., Zhang, Y., Zhao, H., Zheng, Y., He, K. and Zhang, Q.: Trends in China’s anthropogenic emissions since 2010 as the consequence of clean air actions, *Atmos. Chem. Phys. Discuss.*, 18, 1–27, doi:10.5194/acp-2018-374, 2018.

Chapter 3 Evaluating Uncertainty in Aerosol Forcing of Tropical Precipitation Shifts

Amy H. Peace¹, Ben B. B. Booth², Leighton A. Regayre¹, Ken S. Carslaw¹, David M. H. Sexton², Céline J. W. Bonfils³, John W. Rostron²

¹Institute for Climate and Atmospheric Science, University of Leeds, Leeds, UK

²Met Office Hadley Centre, Exeter, UK

³Lawrence Livermore National Laboratory, Livermore, CA, USA

Abstract

An observed southward shift in tropical rainfall over land between 1950 and 1985, followed by a weaker recovery post 1985, has been attributed to anthropogenic aerosol radiative forcing and cooling of the Northern Hemisphere relative to the Southern Hemisphere. We might therefore expect models that have a strong historic hemispheric contrast in aerosol forcing to simulate a further northward tropical rainfall shift in the near-term future when anthropogenic aerosol emission reductions will predominantly warm the Northern Hemisphere. We investigate this paradigm using a perturbed parameter ensemble (PPE) of transient coupled ocean-atmosphere climate simulations that span a range of aerosol radiative forcing comparable to multi-model studies. In the 20th century, in our single-model ensemble, we find no relationship between the magnitude of pre-industrial to 1975 inter-hemispheric anthropogenic aerosol radiative forcing and tropical precipitation shifts. Instead, tropical precipitation shifts are associated with major volcanic eruptions and are strongly affected by internal variability. However, we do find a relationship between the magnitude of pre-industrial to 2005 inter-hemispheric anthropogenic aerosol radiative forcing and future tropical precipitation shifts over 2006 to 2060 under scenario RCP8.5. Our results suggest that projections of tropical precipitation shifts will be improved by reducing aerosol radiative forcing uncertainty, but predictive gains may be offset by temporary shifts in tropical precipitation caused by future major volcanic eruptions.

3.1 Introduction

The interaction of atmospheric aerosols with clouds and radiation is the largest cause of uncertainty in the radiative forcing of the Earth system over the industrial period (e.g. Bellouin et al., 2020; Myhre et al., 2013). Atmospheric aerosols have short residence times of days to weeks, therefore the strongest radiative effects of aerosols occur relatively close to emission sources. The increase in anthropogenic aerosol emissions over the industrial era has therefore caused a negative radiative forcing mainly in the Northern Hemisphere. This hemispheric nature of anthropogenic aerosol radiative forcing has been linked to observed shifts in tropical precipitation and understood using idealised and transient climate model simulations (Allen et al., 2015; Bonfils et al., 2020; Chang et al., 2011; Chemke and Dagan, 2018; Evans et al., 2020; Hwang et al., 2013; Rotstayn et al., 2000; Rotstayn and Lohmann, 2002; Williams et al., 2001). Most notably, anthropogenic aerosol emissions that increased rapidly across Europe and North America up to the 1980s (Lamarque et al., 2010) have been linked to an observed southward shift in tropical precipitation, which was associated with widespread drying of the Sahel between the 1950s and 1980s (Ackerley et al., 2011; Allen et al., 2015; Biasutti and Giannini, 2006; Booth et al., 2012; Dong et al., 2014; Herman et al., 2020; Hirasawa et al., 2020; Kang et al., 2021). Over recent decades there has been a partial northward return of tropical precipitation alongside a modest recovery of rainfall over the Sahel (Giannini and Kaplan, 2019) and India, but increased drought in the Northeast Brazilian region (Utida et al., 2019). Natural aerosols from major volcanic eruption can also cause a negative radiative forcing primarily in one hemisphere, dependent on the latitude of the eruption (Haywood et al., 2013).

Latitudinal shifts of tropical precipitation are intertwined with perturbations to the Hadley Circulation and movement of the Intertropical Convergence Zone (ITCZ). The theoretical energetic framework links the position of the ITCZ to the inter-hemispheric energy balance. As such, a perturbation to the inter-hemispheric energy balance, particularly in the extra tropics, can trigger a shift in the position of the ITCZ and associated tropical precipitation (Kang et al., 2008, 2009, 2018). From an atmospheric perspective, the Hadley Cell would adjust to transport more energy northwards in response to the anomalous inter-hemispheric energy balance imposed by a cooling of the Northern Hemisphere, for example, by

anthropogenic aerosol forcing (Hwang et al., 2013). From the perspective of a dynamical ocean, wind-driven shallow overturning cells also act to transport energy in the same direction as the atmosphere (Green and Marshall, 2017; Kang, 2020). Hence, in a framework where a dynamical ocean is taken into account, the atmospheric response of the ITCZ to an inter-hemispheric energy imbalance is partially dampened. In addition to aerosol radiative forcing, other forcing agents such as changes in high-latitude ice cover and ocean circulation can alter the inter-hemispheric energy balance (Broccoli et al., 2006; Chiang and Bitz, 2005; Chiang and Friedman, 2012). Migrations in tropical precipitation over the 20th century have also been linked to variability in the difference in sea surface temperature between the Northern and Southern Hemispheres (Chiang and Friedman, 2012; Thompson et al., 2010). Because there are multiple drivers, there remains debate over whether the shifts in tropical precipitation observed over the 20th century can be attributed to anthropogenic aerosols, other forced responses, natural climate variability, or a combination of these.

Anthropogenic aerosol emissions are projected to decline in the future in response to increasingly stringent air quality and climate change mitigation policies (Rao et al., 2017; van Vuuren et al., 2011b). Reductions in anthropogenic aerosol emissions will lead to a warming of climate relative to present day that will primarily affect the Northern Hemisphere, and could lead to a northward shift in tropical precipitation (Allen, 2015; Rotstayn et al., 2015). However, identifying the drivers of future tropical precipitation shifts is complex for a number of reasons. Warming of Northern Hemisphere landmasses caused by greenhouse gases could too lead to a northward shift in tropical precipitation (Friedman et al., 2013; Frierson and Hwang, 2012). If so, the relative warming from anthropogenic aerosol reductions and warming from increasing greenhouse gases could have an additive effect on any northward tropical precipitation shift, rather than acting in opposing directions as seen over the 20th century, making attribution to a particular forcing agent even harder to disentangle (Friedman et al., 2013). Throughout the 21st century, the climate response to warming also adds a layer of complexity to the attribution of tropical precipitation changes. Climate feedbacks, such as sea-ice feedbacks or changes in Atlantic Meridional Overturning Circulation (AMOC) strength can modulate the position of the ITCZ, leading to a tug-of-war between different forcing and feedback components

(Mamalakis et al., 2021; McFarlane and Frierson, 2017). Changes in large-scale circulation associated with warming (e.g. wet-gets-wetter paradigm) can also affect the tropical precipitation distribution and could mask an identifiable signal for latitudinal tropical precipitation shifts (Friedman et al., 2013).

Large uncertainty in anthropogenic aerosol radiative forcing limits our understanding of historical changes in climate and the drivers of tropical precipitation and ITCZ migrations. Multi-model studies show the strength of the hemispheric difference in aerosol radiative forcing correlates with the magnitude of tropical precipitation shifts in the 20th century. Coupled Model Inter-comparison Project 5 (CMIP5) models with relatively detailed representations of aerosol-cloud interactions simulate a further southward migration of tropical precipitation over 1950 to 1985 (Allen et al., 2015) and better reproduce decadal drivers of Indian rainfall (Choudhury et al., 2021). However, multi-model ensembles do not sample process parameter uncertainty, so cannot inform our understanding of which model processes influence the strength of the relationship between aerosol radiative forcing and tropical precipitation shifts. Whether or not aerosol reductions will be a main driver of tropical precipitation shifts in the future remains unclear, yet it is likely the large uncertainty in aerosol forcing will cause uncertainty in projected tropical precipitation shifts (Byrne et al., 2018).

Here, we use a perturbed parameter ensemble (PPE) of the coupled ocean-atmosphere model HadGEM3-GC3.05 to assess the relationship between anthropogenic aerosol radiative forcing and tropical precipitation shifts over the 20th and the 21st centuries. The PPE consists of 13 transient climate simulations with 47 parameters perturbed across a range of model schemes (Sexton et al., 2021; Yamazaki et al., 2021). By design, this ensemble spans a range of anthropogenic aerosol radiative forcing and we expect it to span a range of aerosol-driven climate responses. We compare the results from our PPE with those of earlier multi-model studies. For the 21st century, we compare the PPE simulations over high (RCP8.5) and low (RCP2.6) anthropogenic emission scenarios.

3.2 Methods

3.2.1 Perturbed Parameter Ensemble of HadGEM3-GC3.05

The base model used in this work is version 3.05 of the UK Hadley Centre Unified Model (HadGEM3-GC3.05), which is a global coupled ocean-atmosphere model. HadGEM3-GC3.05 includes many of the main improvements that were made to GC3.0 to create GC3.1 that was submitted to CMIP6 (Walters et al., 2019; Williams et al., 2018). The atmospheric component is HadGEM3-GA7.05 (Williams et al., 2018). The atmospheric and land components are configured at 'N216' resolution (approximately 60 km horizontal spacing of grid boxes at mid-latitudes), with 85 vertical atmospheric levels. HadGEM3-GC3.05 incorporates the modal version of the GLObal Version of Aerosol Processes (GLOMAP-mode) which simulates new particle formation, gas-to-gas particle transfer, aerosol coagulation, cloud processing of aerosol and aerosol deposition of sulphate, sea salt, dust, black carbon and particulate organic species (Mann et al., 2010). The ocean and sea-ice model components are NEMO and CICE respectively (Hewitt et al., 2011). The ocean component is eddy permitting with a resolution of $\frac{1}{4}^\circ$ and finer. Ocean components of Global Climate Models (GCMs) that are higher resolution and resolve eddies (such as this model version) can affect the mean state of the ocean, climate variability and climate response, in comparison to lower resolution ocean components (Hewitt et al., 2020).

A perturbed parameter ensemble of the above model set up was designed for UK Climate Projections 2018 (UKCP18) to sample the uncertainty in future climate changes for a given emission scenarios (Murphy et al., 2018; Yamazaki et al., 2021). This PPE samples the uncertainty in 47 model parameters from the model schemes representing convection, boundary layer, gravity wave drag, cloud radiative and microphysical properties, aerosol and land surface. The selection process for these schemes and parameters is described in detail in Sexton et al., (2021). Comprehensive filtering of the ensemble's 'parameter space' was undertaken to identify a plausible and diverse set of model variants for generating our PPE of transient climate simulations. The filtering process first involved assessing the performance of ensemble members against observed climate variables in an atmosphere-only set up using five-day weather hind-casts and five-year simulations (Sexton et al., 2021). The model variants considered

plausible after these stages were then assessed for diversity using the following idealized experiments that are similar to those used in CMIP5 protocol: aerosol effective radiative forcing (ERF) between 1860 and 2005 to 2009, ERF due to a quadrupling of CO₂, and sea surface temperature (SSTs) patterns prescribed for a global warming of 4 °C. Diversity was assessed using a combination of metrics from these idealized experiments, and transient coupled ocean-atmosphere simulations were created for the 25 most diverse, plausible model variants. Lastly, the transient PPE simulations were filtered based on their performance over 1900 to 2005, as described in Yamazaki et al. (2021). This multi-stage process left 15 (out of an initial 2800) remaining model variants that sample known model uncertainties and hence provide, for a given emissions scenario, a range of climate responses. We use 13 of these ensemble members in this study, excluding a further two members on the basis that these members show steady weakening of the AMOC (Sexton et al., 2020).

Historical emissions were prescribed in the ensemble members up to 2005, then forking into the Representative Concentration Pathway (RCP) scenarios RCP8.5 and RCP2.6 to 2100. The RCPs provide a range of greenhouse gas (GHG) concentrations and emission pathways that span a range of total radiative forcing at 2100. RCP8.5 is a high emissions scenario, with GHG emissions assumed to rise substantially out to 2100 (Riahi et al., 2011). In contrast, RCP2.6 assumes aggressive measures to substantially reduce future GHG emissions (van Vuuren et al., 2011a). The RCP scenarios assume successful implementation of air quality legislation, but RCP2.6 has approximately double the reduction of air pollutant emissions by 2030 compared to RCP8.5 (Riahi et al., 2011).

To supplement our analysis, we also use the small initial condition ensemble of four historical and SSP5-8.5 simulations performed with the HadGEM3-GC3.1-LL model that were submitted to the CMIP6 archive. These simulations provide different sequences of internal variability noise for the particular emissions scenarios, and thus can be used to estimate the range of internal variability superimposed to the forced signal.

3.2.2 Quantifying Shifts in Tropical Precipitation

We define the latitudinal position of the ITCZ and tropical precipitation, Φ_{ITCZ} (degrees), as the median of annual mean precipitation (mm day⁻¹) over area-

weighted regional means between 20 °S and 20 °N. Several studies have used this definition to quantify changes in the position of the ITCZ and tropical precipitation (Atwood et al., 2020; Donohoe et al., 2013; Evans et al., 2020; Frierson and Hwang, 2012; Green et al., 2017; Green and Marshall, 2017; Moreno-Chamarro et al., 2020). We calculate the linear trend of the 5-year rolling mean value of Φ_{ITCZ} over multi-decadal periods in the 20th and 21st century over three regions – Global, Atlantic and Pacific, where the Atlantic is defined as 75 °W to 30 °E, and the Pacific as 150 °E to 75 °W.

3.2.3 Inter-Hemispheric Temperature and Radiative Forcing

To study the drivers of the ITCZ shifts, we calculate the Spearman’s rank correlation coefficient of the decadal trend in Φ_{ITCZ} with variables related to the inter-hemispheric energy balance. These variables include the trend in the inter-hemispheric difference in surface air temperature and implied total radiative forcing, plus the inter-hemispheric difference in historical anthropogenic aerosol ERF. We also evaluate the role of cloud and non-cloud shortwave radiative responses and AOD. The inter-hemispheric difference is calculated as the difference between area-weighted Northern Hemisphere (0 °N to 60 °N) and Southern Hemisphere (0 °S to 60 °S) means, and referred to as ‘inter-hemispheric’ herein. The inter-hemispheric variables are calculated over both land and ocean, unless specified. Linear trends of the inter-hemispheric variables are calculated from a 5-year rolling mean. We focus on 0 to 60 ° as extratropical forcing has been shown to be a prime driver of ITCZ shifts (e.g. Kang et al. 2008, 2009, Frierson and Hwang 2012). Our main results of the study are not sensitive to calculating inter-hemispheric variables over 0 to 90 ° instead (Figure B.6 and Figure B.7)

The implied total radiative forcing for the transient PPE was estimated at each grid box using the formula derived from Gregory and Forster, 2008:

$$(1) \quad \Delta F_{Im} = \Delta F_{TOA} - \lambda \Delta T$$

Where ΔF_{Im} is the implied radiative forcing of interest, ΔF_{TOA} is the change in annual mean net top of atmosphere flux relative to a reference period, ΔT is the change in global annual mean surface air temperature relative to a reference period, and λ is the climate feedback parameter. In this convention, positive feedback components are represented by a positive contribution to λ . In the PPE

case, the value for λ was estimated using the approach in Gregory and Forster (2008), where for an abrupt 4 x CO₂ experiment, λ is the regression slope between radiative forcing and global temperature change, taking account of model drifts in the control runs. In the case of the small HadGEM3-GC3.1 initial condition ensemble, we estimate ΔF_{Im} using a 1850 to 1870 reference period and a feedback parameter value of $-0.86 \text{ W m}^{-2} \text{ K}^{-1}$ (following Andrews et al., 2019).

For PPE members, shortwave cloud and non-cloud radiative responses were estimated using the approximate partial radiative perturbation (APRP) method (Taylor et al., 2007). The APRP method uses a single-layer radiative transfer model to decompose climate model output into three components: the change in shortwave radiation due to cloud, the change in shortwave radiation due to non-cloud atmospheric scattering and absorption, and the change in shortwave radiation due to surface albedo. Under this method, changes in the cloud component are solely due to changes in cloud properties, whereas changes in the non-cloud component are due to changes in aerosols, ozone and water vapour (Zelinka et al., 2014).

The idealized simulations that were used to assess the diversity of PPE members for UK Climate Projections (Section 2.1; Sexton et al., (2021)), provide estimates of anthropogenic aerosol ERF between 1860 to 2005 for each PPE member in the transient coupled ocean-atmosphere simulations that we use to analyse tropical precipitation shifts. To better align with the historical time period, we completed additional simulations to provide estimates of anthropogenic aerosol ERF between 1860 and 1975 for the 13 PPE members used in this study. ERF was quantified as the change in radiative fluxes caused by changes in anthropogenic aerosol emissions between 1860 and 2005, plus 1860 and 1975, with SSTs, sea-ice extent and greenhouse gas concentrations held constant at 2005 to 2009 values (rather than pre-industrial values as in CMIP studies; Taylor et al., 2012).

Aerosol and physical atmosphere parameters are both important sources of uncertainty in aerosol ERF (Regayre et al., 2018). In our PPE, we perturb a total of 8 aerosol emission and process parameters in combination with multiple physical atmosphere parameters that, amongst other responses, affect aerosol forcing. Our 13 ensemble members span a range of global mean 1860 to 2005 aerosol ERF of -2.0 to -0.9 W m^{-2} , which is larger and more negative, than the

spread in 1850 to 2014 aerosol radiative forcing across 17 CMIP6 models (-1.37 to -0.63 W m^{-2}) (Smith et al., 2020), and similar to the estimated 1750 to 2014 aerosol ERF range from AR6 (-2.0 to -0.6 W m^{-2} ; medium confidence) (Forster et al., 2021).

We use the inter-hemispheric 1860 to 1975 aerosol ERF when analysing tropical precipitation shifts in the 20th century, and the inter-hemispheric 1860 to 2005 aerosol ERF when analysing the 21st century. Aerosol ERF values are shown in Figure B.1-2. We do not have simulations from which to quantify the aerosol ERF in the near-term future. Hence, our analyses rely on the assumption that ensemble members with strong or weak near-present day aerosol radiative forcing will also have a strong or weak response to changes in aerosol emissions over the near-term future time periods as anthropogenic aerosol emissions decline.

3.3 Results and Discussion

3.3.1 Tropical Precipitation Shifts over the 20th Century

We begin by examining the latitudinal shift of tropical precipitation (Φ_{ITCZ}) over the 20th century in our PPE. Figure 3.1 shows the 5-year rolling mean evolution of Φ_{ITCZ} over the historical period in the global, Atlantic and Pacific regional means. The PPE mean Φ_{ITCZ} migrates southwards over the 1940 to 1985 period (around $0.01 \text{ }^\circ\text{latitude year}^{-1}$ globally). This southward migration of tropical precipitation agrees with multi-model studies (CMIP3, CMIP5) and observations of tropical precipitation over land that show tropical precipitation shifted southward in the second half of the 20th century (Allen et al., 2015; Bonfils et al., 2020; Chung and Soden, 2017; Hwang et al., 2013).

There are brief shifts in Φ_{ITCZ} in the years following major volcanic eruptions in the 20th century. The Φ_{ITCZ} time series without the 5-year smoothing applied is shown in Figure B.3 to more precisely illustrate this effect. There is a northward shift in Φ_{ITCZ} following the Southern Hemisphere eruption of Mt Agung in 1963 and a southward shift following the Northern Hemisphere eruption of El Chichón in 1982. Hence, our ensemble mean time series of Φ_{ITCZ} agrees with the literature (Bonfils et al., 2020; Colose et al., 2016; Haywood et al., 2013; Iles et al., 2013) showing the position of the ITCZ and tropical precipitation responds to volcanic eruptions and shifts away from the hemisphere with the maximum stratospheric

aerosol loadings. After 1985 (the period after which pollution controls are enforced in Europe and North America), there is a northward migration of Φ_{ITCZ} to the end of the 20th century. In the time series, individual members display greater inter-annual variability in the Pacific, which could be due to different sequences of internal variability and/or different spatial-temporal evolution of the forced signal in the Atlantic and Pacific regions (e.g. Diao et al., 2021).

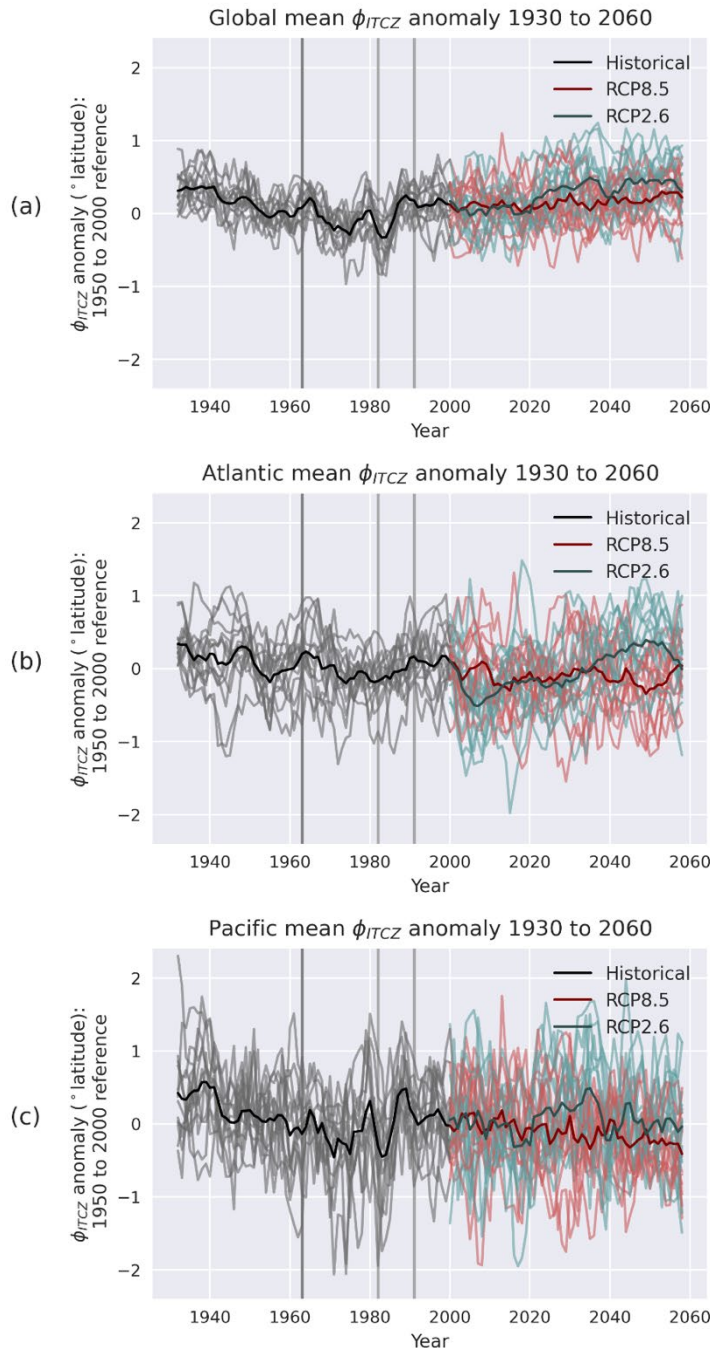


Figure 3.1 Time series of 5-year rolling mean Φ_{ITCZ} anomaly relative to the 1950 to 2000 reference period for (a) global, (b) Atlantic and (c) Pacific regional means. The ensemble mean time series is shown by the darker line, and the individual ensemble members in the lighter lines. Major volcanic eruptions are marked with grey vertical lines with maximum aerosol loading in the NH (El Chichón (1982, Mexico, 17.21° N) and Pinatubo (1991, Philippines, 15.08° N)) and in the SH (Mt. Agung (1963, Indonesia, 8.20° S)).

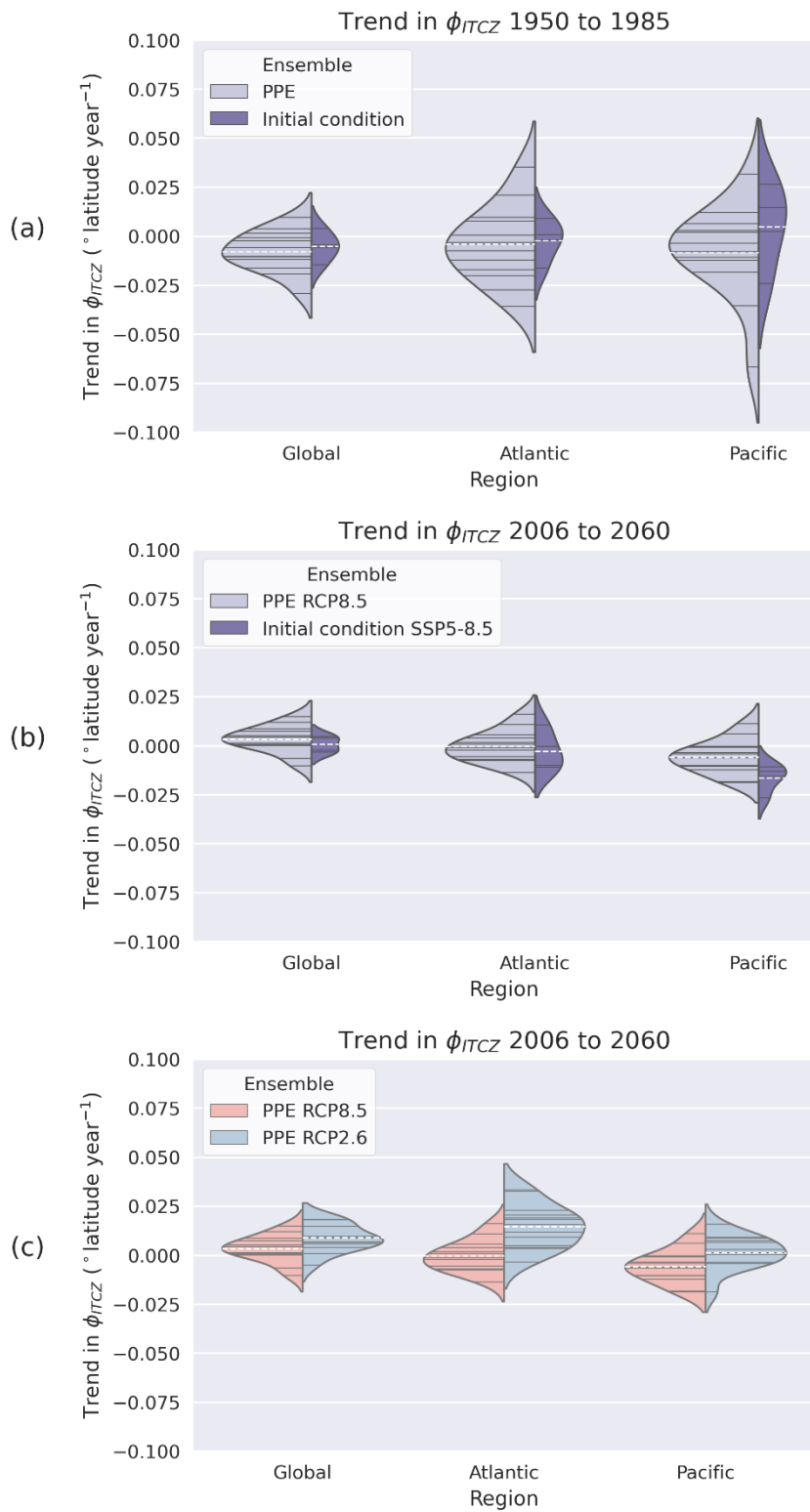


Figure 3.2 Trend in 5-year rolling mean ϕ_{ITCZ} for (a) 1950 to 1985 and (b,c) 2006 to 2060 for global (left), Atlantic (middle) and Pacific (right) regional means. The violin plots in light purple (in b) and red (in c) are equivalent. The black lines within the violin plots show individual ensemble members (13 in the PPE, 4 in the initial condition ensemble) and the white dashed line shows the ensemble mean.

Figure 3.2 shows the Φ_{ITCZ} trend over 1950 to 1985 in individual ensemble members and as a density function across the PPE and initial condition ensemble. The PPE mean shows a small southward shift in the Φ_{ITCZ} throughout this time period in each region. However, across the PPE, there are both southward and northward shifts (-0.03 to 0.01 °latitude year⁻¹ globally). The spread in tropical precipitation shifts over 1950 to 1985 across our single-model ensemble is comparable to that over the same period from CMIP5 (see Text B.1 and Figure B.14) which also displayed both south and northward migrations in tropical precipitation (Allen et al., 2015). We do not have an initial condition ensemble for each PPE member so cannot remove the effects of internal variability from each ensemble member as is common in multi-model studies. For example, in Allen et al. (2015) models that had aerosol radiative forcing experiments also had 3 to 10 ensemble members in the transient all forcing runs that were averaged to obtain the tropical precipitation shift for that model. We use the initial condition ensemble for HadGEM3-GC3.1 (a similar model version submitted to CMIP6; Andrews et al., 2020; Murphy et al., 2018) to estimate the spread in the Φ_{ITCZ} trend due to internal variability.

In the 1950 to 1985 global mean, the initial condition ensemble spread covers close to half (48%) of the spread in our PPE which suggests that a large fraction of our PPE spread is caused by natural variability, but there is still a considerable influence from perturbed parameters. Internal variability alone has been shown not to generate migrations in tropical precipitation consistent with observations over the 20th century (Allen et al., 2015; Chang et al., 2011). Whereas radiative forcing caused by anthropogenic aerosol, which predominantly cooled the Northern Hemisphere, peaking in the 1980s, has been implicated as a main driver of the migration of tropical precipitation southward up to the 1980s, followed by a northward recovery to the end of the 20th century. We note here that models incorporating both aerosol direct and indirect effects tend to better reproduce the historical changes in temperature (Booth et al., 2012; Chung and Soden, 2017) and ITCZ location (Allen et al., 2015; Bonfils et al., 2020; Friedman et al., 2013). Our single model PPE spans a range in aerosol forcing and tropical precipitation shifts comparable to multi-model studies. Therefore, we investigate the relationship between the uncertainty in the inter-hemispheric difference in aerosol forcing and tropical precipitation shifts in our PPE framework.

Figure 3.3 shows the relationships between Φ_{ITCZ} trend over 1950 to 1985 and the trend in inter-hemispheric (over 60 °S to 60 °N) surface air temperature (panel a), implied total radiative forcing (panel b) and 1860 to 1975 anthropogenic aerosol ERF (panel c). Figure B.8 shows the corresponding plot but with inter-hemispheric variables calculated only over the ocean. There is a strong statistical relationship ($r=0.91$ for global mean, $r = 0.66$ for regional means) between the trend in inter-hemispheric surface air temperature and the Φ_{ITCZ} trend over 1950 to 1985 (with an intercept near 0). As expected, the statistical relationship between the Φ_{ITCZ} trend and the trend in inter-hemispheric implied total forcing is also strong ($r \geq 0.63$). An energetics framework explains how the ITCZ and corresponding latitudinal position of tropical precipitation shifts in response to changes in the inter-hemispheric distribution of energy (Kang et al., 2008, 2009, 2018b). The perturbed cross-equatorial Hadley circulation rebalances the energy asymmetry by transporting energy towards the cooler (energy deficient) hemisphere, and consequently moisture towards the warmer hemisphere. Figure 3.3 shows that ensemble members that have greater cooling in the Northern Hemisphere and a larger difference in inter-hemispheric implied total radiative forcing over 1950 to 1985 simulate stronger southward shifts in tropical precipitation. This behaviour is in line with the energetics theory of a southward migration of the ITCZ due to an energy deficient Northern hemisphere. In CMIP5, models that had a stronger inter-hemispheric aerosol radiative forcing simulated further southward shifts in tropical precipitation over 1950 to 1985, with a correlation coefficient of $r \Rightarrow 0.71$ across 13 models (Allen et al., 2015). Despite these relationships, we do not see a strong relationship between the strength of inter-hemispheric aerosol ERF estimated from the atmosphere-only runs and the degree of southward shift in tropical precipitation over 1950 to 1985 in our PPE. In the paragraphs below we evaluate several hypotheses for this weaker than expected relationship.

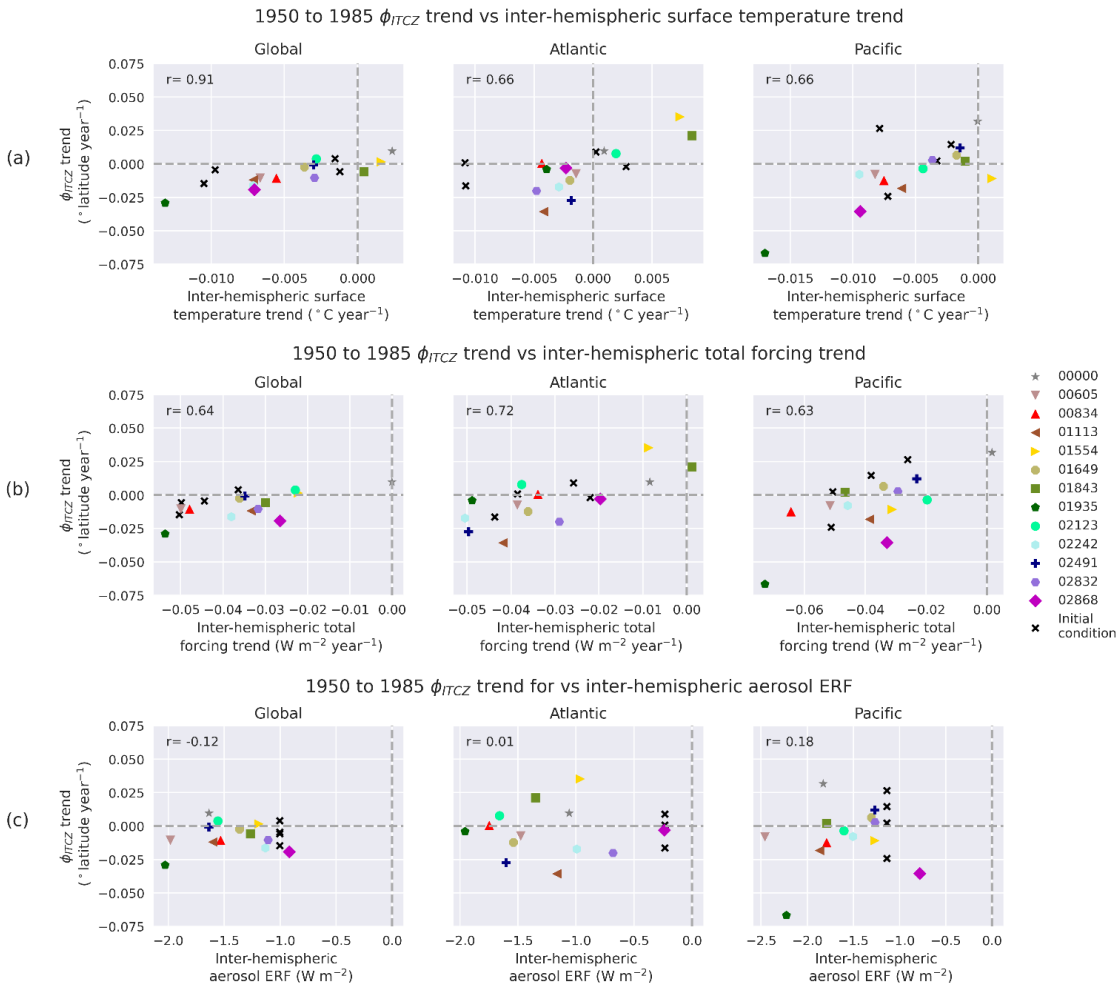


Figure 3.3 Scatter plot of the 1950 to 1985 trend in 5-year rolling mean Φ_{ITCZ} against the 1950 to 1985 trend in inter-hemispheric (over 60°S to 60°N) surface air temperature (a), implied total radiative forcing (b) and anthropogenic aerosol ERF (c) for global (left), Atlantic (middle) and Pacific (right) regional means. Anthropogenic aerosol ERF is calculated over 1860 to 1975 for the PPE, and 1850 to 2014 for the initial condition ensemble. The Spearman's rank correlation coefficient between variables is shown at top left of each plot.

3.3.1.1 Potential factors obscuring a relationship between tropical precipitation shifts and anthropogenic aerosol ERF in our PPE

The bottom panel of Figure 3.3 shows that for the initial condition ensemble of HadGEM3-GC3.1, where model realizations have the same pre-industrial to present-day aerosol forcing, a large spread in tropical precipitation shifts is possible in transient climate simulations due to internal variability. Although the spread in tropical precipitation shifts in our ensemble due to perturbed model parameters is larger than internal variability, this figure suggests the relationship between pre-industrial to present-day aerosol ERF and tropical precipitation shifts being obscured by internal variability in our PPE. In addition, the HadGEM3-GC3.1 initial condition ensemble explores a large fraction of the trend in the inter-

hemispheric difference in temperature, which may be the reason why there is also only a weak relationship between the trend in the inter-hemispheric difference in temperature during the 20th century and 1860 to 1975 anthropogenic aerosol ERF (Figure B.9). If we had an initial condition ensemble for each PPE member or a larger sample size, the expected relationships may have emerged more strongly. The effect of internal variability is therefore likely one of the main reasons why there is not a relationship between inter-hemispheric aerosol forcing and tropical precipitation shifts over the 20th century in our ensemble.

The strength of relationships between the Φ_{ITCZ} trend and inter-hemispheric variables are also sensitive to the time period chosen, as shown in Table 3.1. The 1950 to 1985 time period which has the strongest relationship between tropical precipitation shifts and both inter-hemispheric temperature and implied total forcing trends encapsulates two major volcanic eruptions. There is a weaker correlation in the longer time series or the time series excluding El Chichón. These results may indicate that volcanic rather than anthropogenic aerosol changes drive much of the coherent changes in inter-hemispheric temperature trends, implied total forcing trend, and tropical precipitation shifts during 1950 to 1985. However, the lack of a strong relationship between tropical precipitation shifts and historical anthropogenic aerosol ERF is unlikely to be related to the choice of analysis period as there is little evidence of stronger correlations with anthropogenic aerosol ERF estimates on other 20th century timescales.

The anthropogenic aerosol ERF is quantified as the radiative change between two periods (1860 to 1975) using atmosphere-only simulations with SSTs and other climate forcings prescribed for 2005 to 2009. As such, the anthropogenic aerosol ERF might not be representative of the aerosol radiative forcing time evolution in the transient climate simulations, due to the differences in time period, mediation of aerosol radiative effects by the coupling of ocean processes and evolution of other climate forcings, and/or internal variability (Voigt et al., 2017). To investigate further we examined the relationship between Φ_{ITCZ} trend and time evolving variables related to aerosol radiative effects, as shown in Table 3.2. Over 1950 to 1985, there is no clear relationship between the trend in Φ_{ITCZ} and the trend in the inter-hemispheric difference of either outgoing shortwave radiation at TOA (Figure B.10) or total AOD (Figure B.11). There is some suggestion of a relationship between tropical precipitation shifts and the trend in

the inter-hemispheric difference of both shortwave non-cloud radiative effect (Figure B.10) and dust AOD (Figure B.12), although these variables can also be affected by internal variability. Overall, the results with these time-evolving variables do not clarify how coupling of the atmosphere to the ocean affects the relationship between tropical precipitation shifts and the inter-hemispheric difference in anthropogenic aerosol ERF, nor explain the difference between our results and those from a multi-model ensemble (Allen et al. 2015).

Our 13 PPE members included the combined effects of perturbations to 8 aerosol and 39 non-aerosol parameters. So in our PPE, any relationship between anthropogenic aerosol radiative forcing and tropical precipitation might be masked by the effect of perturbations to physical atmosphere parameters. The strongest correlations between the Φ_{ITCZ} trend over 1950 to 1985 and individual perturbed parameters in our PPE are shown in Figure B.13. Some of these relationships may be indicative of important atmospheric parameter effects on tropical precipitation shifts. For example, Kang et al. (2008, 2009) showed how tuning a convective parameter related to entrainment can alter cloud radiative properties and cause a range in magnitude of ITCZ shifts for a given inter-hemispheric thermal forcing. In our PPE, the parameter that controls shallow convective core radiative effects (`cca_sh_knob`) and the parameter that controls the sensitivity of mid-level convection to relative humidity and entrainment (`ent_fac_md`) have a relationship with the Φ_{ITCZ} trend over some regions. Hence, both these parameters could modulate the sensitivity of ITCZ shifts through altering cloud radiative feedbacks. In the global and Atlantic means, the scaling of natural dimethyl sulphide emissions flux (`ps_natl_dms_emiss`), which could alter the hemispheric contrast of aerosol forcing, has a relationship with the Φ_{ITCZ} trend. Parameters from the land surface (related to soil moisture thresholds; `psm`, and altering the temperature dependence of photosynthesis; `tupp_io`) and the cloud microphysics (aspect ratio of ice particles; `ar`) scheme also have a relationship with Φ_{ITCZ} trend over some regions. These results are at best indications of possible parameter effects, since our correlations are calculated using only 13 ensemble members that conflate the uncertainty in 47 model parameters. So, further simulations would be needed to clarify parametric effects on tropical precipitation shifts.

Overall, our analysis of 20th century latitudinal shifts in tropical precipitation shows that any relationship between these shifts and the hemispheric contrast in 1860 to 1975 anthropogenic aerosol ERF is difficult to detect when accounting for the effect of single-model uncertainty and internal variability. The latitudinal shift of tropical precipitation over 1950 to 1985 is, however, associated with the trend in inter-hemispheric surface temperature and implied total radiative forcing. It is also clear that major volcanic eruptions in the 20th century induced relatively short-lived shifts in tropical precipitation, and contribute to a time-period dependence of the strength of these relationships.

Time period	Correlation with the trend in inter-hemispheric surface air temperature ($^{\circ}\text{C year}^{-1}$)	Correlation with the trend in inter-hemispheric implied total forcing ($\text{W m}^{-2} \text{ year}^{-1}$)	Correlation with inter-hemispheric 1860 to 1975 anthropogenic aerosol ERF (W m^{-2})
1950 to 1985 (shown)	$r = 0.91$	$r = 0.64$	$r = -0.12$
1950 to 1980	$r = 0.56$	$r = 0.65$	$r = -0.04$
1940 to 1985	$r = 0.29$	$r = 0.48$	$r = -0.12$
1940 to 1980	$r = -0.01$	$r = 0.57$	$r = -0.07$
1940 to 1975	$r = 0.19$	$r = 0.77$	$r = -0.30$

Table 3.1 Table of Spearman's rank correlation coefficients for the trend in global mean 5-year rolling mean Φ_{ITCZ} and global inter-hemispheric (60°S to 60°N) variables shown in Figure 3.3 with values for alternate time periods.

Variable	Correlation with Φ_{ITCZ} trend ($^{\circ}$ latitude year $^{-1}$)
Trend in inter-hemispheric total AOD (year $^{-1}$)	$r = -0.23$
Trend in inter-hemispheric dust AOD (year $^{-1}$)	$r = -0.54$
Trend in inter-hemispheric shortwave non-cloud radiative effect (W m $^{-2}$ year $^{-1}$)	$r = 0.54$
Trend in inter-hemispheric shortwave cloud radiative effect (W m $^{-2}$ year $^{-1}$)	$r = -0.34$
Trend in inter-hemispheric top of atmosphere outgoing shortwave flux (W m $^{-2}$ year $^{-1}$)	$r = -0.34$

Table 3.2 Table of Spearman's rank correlation coefficients for the 1950 to 1985 trend in global mean 5-year rolling mean Φ_{ITCZ} and additional global inter-hemispheric (60 $^{\circ}$ S to 60 $^{\circ}$ N) variables.

3.3.2 Tropical Precipitation Shifts Up To Mid-21st Century

Here, we examine the relationship between the Φ_{ITCZ} trend and our inter-hemispheric variables over 2006 to 2060 under emission scenarios RCP8.5 and RCP2.6. The reductions in anthropogenic aerosol emissions and consequential warming of the northern hemisphere in the 21st century have been projected to cause a northward shift in the position of ITCZ and tropical precipitation (Allen, 2015; Hwang et al., 2013). Although the warming caused by increasing CO₂ emissions is more homogeneous, it can also lead to a migration in the position of the ITCZ and tropical precipitation. For example, climate responses to GHG-induced warming such as ice-albedo feedbacks, the land-dominated Northern Hemisphere warming, cloud and ocean heat content changes may lead to a northward shift in the ITCZ, whereas responses such as AMOC weakening and enhanced longwave cooling may lead to a southward shift (McFarlane and Frierson, 2017). These drivers of tropical precipitation shifts in the 21st century will also act on different timescales. Results from multi-model studies have mixed conclusions on how zonal mean tropical precipitation will migrate in the future.

Figure 3.1 shows the 5-year rolling mean evolution of Φ_{ITCZ} up to 2060 across our PPE. For scenario RCP8.5, the ensemble mean Φ_{ITCZ} remains steady

globally and in the Atlantic up to mid-century, with a slight southward migration in the Pacific. For RCP2.6, there is a northward migration of Φ_{ITCZ} up to mid-century globally and in the Atlantic, followed by a southward migration from 2050 to 2060. Yet in the Pacific, the northward migration ends in around 2035 and is followed by a strong, but brief southward migration. The Φ_{ITCZ} exhibits greater variability in scenario RCP2.6, which is most pronounced in the Pacific.

Figure 3.2 shows the Φ_{ITCZ} trend over 2006 to 2060 across individual members in our PPE and as a density function. The middle panel of Figure 3.2 also shows an estimate of the impact of internal variability (superimposed on a forced signal) over the same period using the initial condition ensemble of HadGEM3-GC3.1 under emission scenario SSP5-RCP8.5. Under RCP8.5, the PPE mean shows only a small change in Φ_{ITCZ} , with both north and southward migrations in Φ_{ITCZ} across the ensemble. Hence, we find no robust evidence of tropical precipitation shifts under RCP8.5 by mid-21st century, which is in agreement with the conclusions based on end-of-century ITCZ shifts in Byrne et al. (2018). The spread in Φ_{ITCZ} trend due to internal variability under SSP5-RCP8.5 in the initial condition ensemble is smaller than under RCP8.5 in our PPE globally and in the Pacific, but comparable in the Atlantic region. The bottom panel of Figure 3.2 contrasts the Φ_{ITCZ} trend over 2006 to 2060 between RCP8.5 and RCP2.6 scenarios. By mid-century, tropical precipitation shifts further northward in RCP2.6, compared to RCP8.5. This northward migration in tropical precipitation for RCP2.6 is in line with Allen (2015), prior to the then southward shift between mid and end of the 21st century. The largest difference in tropical precipitation shift between emission scenarios is in the Atlantic, which may be related to scenario dependence of AMOC strength. The AMOC is projected to weaken under warming (Collins et al., 2019; Schleussner et al., 2014), and as AMOC weakening is likely to reduce a northward ITCZ shift (McFarlane and Frierson, 2017), the effect would be more dominant in RCP8.5 than RCP2.6 due to the greater warming from increasing GHG emissions combined with warming from anthropogenic aerosol emission reductions. The strength of the AMOC over the 20th century has been linked to the strength of aerosol forcing and thus aerosol forcing may also affect future projections (Menary et al., 2020). Hence, the further northward migration of tropical precipitation up to 2060 in RCP2.6 in our ensemble is likely due to a combination of greater anthropogenic aerosol

emission reductions in RCP2.6 compared to RCP8.5, and a greater dominance of processes in RCP8.5 that pull tropical precipitation southwards. We note here that in both emission scenarios, the spread in Φ_{ITCZ} trend across the near-term future ensembles is smaller than over the historical period, due to the trend being calculated over a longer time period. A shorter future time period induces a larger spread in the Φ_{ITCZ} trend across the PPE (Figure B.16), which is comparable the spread in the historical period.

Figure 3.4 shows the relationship between our inter-hemispheric variables and the Φ_{ITCZ} trend over 2006 to 2060 in RCP2.6 and RCP8.5. Figure B.15 shows a corresponding figure with inter-hemispheric variables calculated only over the ocean. The top panel of Figure 3.4 shows that there is a relationship between the Φ_{ITCZ} trend and the trend in inter-hemispheric surface temperature in each of the RCP ensembles. For each of the RCP scenario ensembles the relationship between the global Φ_{ITCZ} trend and the trend in inter-hemispheric surface temperature is stronger than we found in the longer historical trends (Table 3.1), but weaker than those beginning in 1950 which were most affected by volcanic eruptions (Figure 3.3). Contrary to the historical period, we identify a relationship between the Φ_{ITCZ} trend over 2006 to 2060 and inter-hemispheric 1860 to 2005 aerosol ERF in the Pacific under RCP8.5 ($r=-0.69$). Emission reductions in Asia will dominate future global reductions in anthropogenic aerosol emissions (Lund et al., 2019), and align with our results that there is a strong relationship between the magnitude of inter-hemispheric aerosol ERF and tropical precipitation shifts, particularly in the Pacific region. However, the lower latitude of emission reductions over Asia, in comparison to Europe or North America, may affect the sensitivity of the ITCZ shift. There is no relationship in the Atlantic, and consequently the global mean response ($r= -0.47$) is weaker than the Pacific. Figure B.9 shows there is also a suggestion of a relationship between the inter-hemispheric temperature trend and 1860 to 2005 aerosol ERF in the Pacific, which is slightly stronger over the ocean (not shown). These results show that in our PPE, ensemble members that have a stronger difference in inter-hemispheric aerosol ERF over the industrial period, and more warming in the Northern hemisphere in the near-term future under scenario RCP8.5, simulate further northward migrations in tropical precipitation, particularly in the Pacific region. It is surprising, however, that there is no clear relationship between the Φ_{ITCZ} trend

and inter-hemispheric aerosol ERF in RCP2.6, where we expected faster aerosol emission reductions to yield a clearer tropical precipitation response. Possible causes of a stronger relationship between tropical precipitation shifts and aerosol radiative forcing under RCP8.5 could be due to feedbacks between warming and aerosol radiative forcing. For example, aerosol residence times and associated net radiative effects may increase in a warmer climate (Bellouin et al., 2011; Takemura, 2020) which may amplify the effect of anthropogenic aerosol forcing on ITCZ position in RCP8.5 compared to RCP2.6.

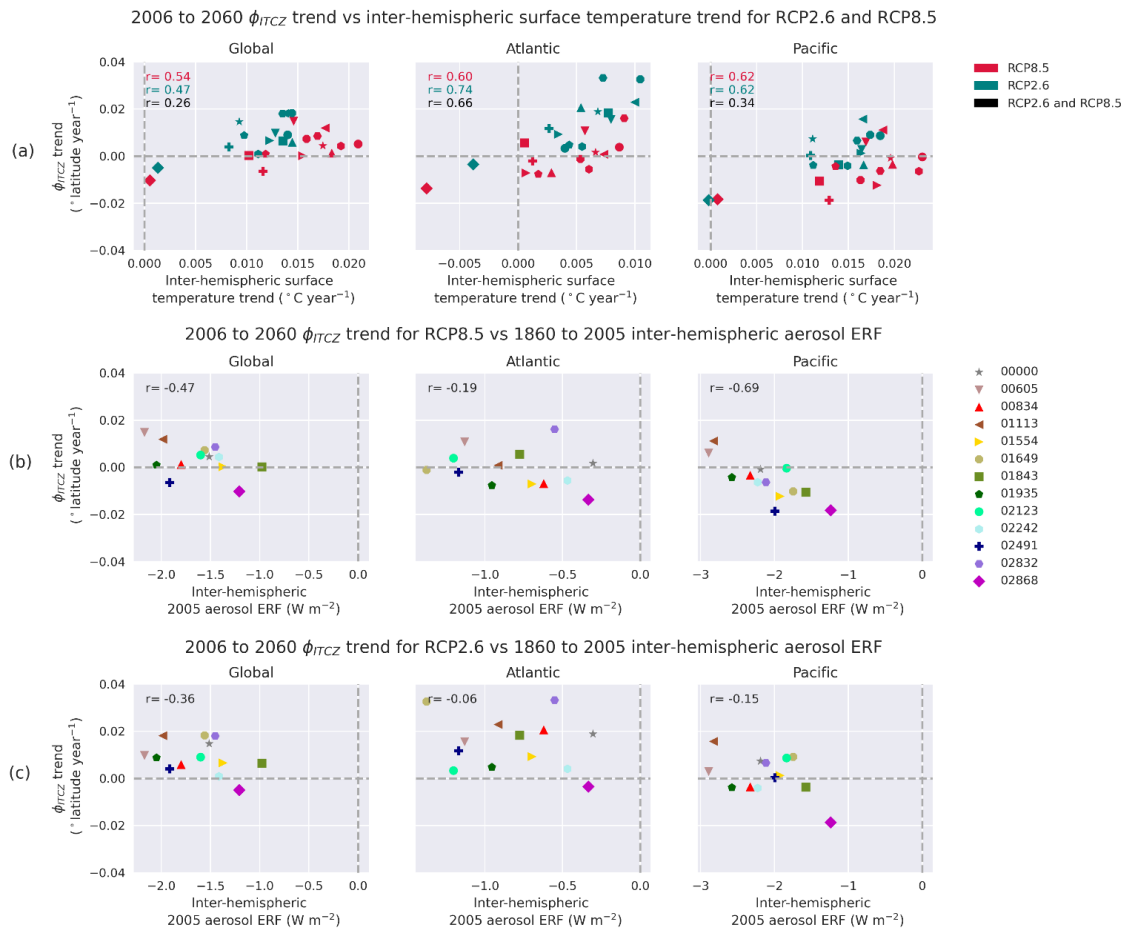


Figure 3.4 Scatter plot of trend in 5-year rolling mean Φ_{ITCZ} in 2006 to 2060 against the trend in inter-hemispheric (60°S-60°N) surface air temperature (a), and 1860 to 2005 anthropogenic aerosol ERF (b, c) for global (left), Atlantic (middle) and Pacific regional means (right). The Spearman's rank correlation coefficient is shown at top left of each plot.

Our analysis of 21st century tropical precipitation shifts suggests that the uncertainty in the inter-hemispheric difference in aerosol ERF contributes to the spread of projected tropical precipitation shifts across our ensemble in the near-term future under RCP8.5. This is especially the case in the Pacific regional mean, as near-term future aerosol reduction will be driven by reductions from

Asia. Our analysis of the historical period showed that the position of tropical precipitation can be strongly modulated by major volcanic eruptions that lead to inter-hemispheric differences in temperature. Hence, any predictive skill for future shifts in tropical precipitation will also be limited by the effect of any future major volcanic eruptions that induce differences in hemispheric energy balance.

3.4 Conclusion

The inter-hemispheric nature of anthropogenic aerosol radiative forcing associated with evolving anthropogenic aerosol emissions has been linked to driving tropical precipitation shifts during the latter half of the 20th century and over the 21st century (Allen, 2015; Allen et al., 2015; Chang et al., 2011; Chemke and Dagan, 2018; Hwang et al., 2013; Rotstayn et al., 2015). In the CMIP5 multi-model ensemble there is a strong correlation between the strength of pre-industrial to present-day inter-hemispheric aerosol forcing and the latitudinal shift in tropical precipitation over 1950 to 1985 (Allen et al., 2015). We have used a perturbed parameter ensemble of the HadGEM3-GC3.05 climate model that spans a range of aerosol forcing comparable to current generation climate models to further investigate the relationship between anthropogenic aerosol forcing and tropical precipitation shifts.

In the 20th century as anthropogenic aerosol emissions increased, our PPE mean shows a long-term southward migration in the latitudinal position of tropical precipitation globally and in the Atlantic and Pacific up to around 1985 (e.g. 0.01 °latitude year⁻¹ globally over 1940 to 1985). Over the 20th century there are also brief shifts in tropical precipitation in response to major volcanic eruptions. Of the time periods we analysed, the 1950 to 1985 time period which encapsulates two major volcanic eruptions, had the strongest relationship between tropical precipitation shifts and the hemispheric contrast in temperature and implied total radiative forcing over the same period (i.e. ensemble members with more cooling in the Northern Hemisphere simulated a further southward shift of the ITCZ). Both the long-term trends and the rapid response to volcanic eruptions are in-line with the theoretical energetic framework and modelling studies that have shown the zonal mean position of the ITCZ and corresponding tropical precipitation migrates in response to an anomalous inter-hemispheric energy balance (Kang et al., 2018).

Despite a contemporaneous relationship between tropical precipitation shifts and the trend in the inter-hemispheric difference in temperature and implied total forcing, we find no statistically significant relationship between the strength of inter-hemispheric 1860 to 1975 anthropogenic aerosol ERF and the magnitude of tropical precipitation shifts in the PPE over the 20th century, which contradicts results from CMIP5 (Allen et al., 2015). We propose multiple hypotheses for this different result. Overall, our results suggest that being unable to isolate forced changes from those due to internal variability (due to an absence of initial condition ensembles of our PPE members) and accounting for single-model uncertainty obscure the role of anthropogenic aerosol forced responses in our ensemble over the 20th century.

Drivers of future tropical precipitation shifts are harder to disentangle, as both forced responses and climate feedbacks due to warming will have a bearing on the direction and magnitude of ITCZ shifts over the 21st century (McFarlane and Frierson, 2017). In the near-term future (up to 2060) globally our ensemble mean shows a negligible migration in tropical precipitation in RCP8.5, and a further northward migration in tropical precipitation in RCP2.6. The further northward migration in RCP2.6 compared to RCP8.5 is likely due to a combination of a faster reduction of anthropogenic aerosol emissions, in combination with warming-induced feedbacks (such as AMOC weakening) having a greater modulation of the regional ITCZ position in RCP8.5. We do find ensemble members that have a stronger positive trend in inter-hemispheric temperature and forcing (i.e. due to more warming in the Northern Hemisphere) simulate further northward migrations in tropical precipitation.

In contrast to the historical time period, we find a relationship between the strength of inter-hemispheric 1860 to 2005 anthropogenic aerosol ERF (which we use as a proxy of present-day aerosol influence) and future tropical precipitation shifts under RCP8.5, but not RCP2.6. This relationship is strongest in the Pacific where Asian anthropogenic aerosols have a strong historical and future influence. On the premise that present-day anthropogenic aerosol influence is informative about future anthropogenic aerosol influence, this indicates ensemble members with a large hemispheric difference in historical aerosol radiative forcing, will have a further northward tropical precipitation shift in response to future aerosol reductions. Faster anthropogenic aerosol emission reductions is likely one of the

factors why RCP2.6 has a further northward shift in tropical precipitation by mid-21st century than RCP8.5. Yet, it is surprising that this logic does not follow through to there being a relationship between tropical precipitation shifts and aerosol forcing in RCP2.6, suggesting climate feedbacks due to warming can influence the sensitivity of the climate response to aerosol forcing (Nazarenko et al., 2017; Takemura, 2020).

Overall, our study suggests the persistent uncertainty in aerosol ERF plays a role in how accurately we can project zonal mean tropical precipitation shifts in the near-term future under RCP8.5. However, any predictive skill for future tropical precipitation shifts will also be limited by the effect of future major volcanic eruptions that can temporarily shift tropical precipitation. Our study presents open questions on the role of anthropogenic aerosol radiative forcing in modulating tropical precipitation shifts over the historical and future periods in climate models, which we cannot definitively answer here because our experiment is designed to sample single-model uncertainty and thus has a relatively small sample size and neglects the effects of internal variability. Additional experiments that clarify the role of aerosols on near-term future tropical precipitation shifts are also needed. In a broader analysis involving multi-model and other single-model ensembles we could further develop our understanding of the relationship between feedbacks due to warming, future aerosol forcing and tropical precipitation shifts up to mid-21st century across multiple emission scenarios. Hence, we suggest future work investigating the role between aerosol forcing and tropical precipitation shifts in the CMIP6 multi-model ensemble and other single-model ensembles that span a range of aerosol radiative forcing values.

References

- Ackerley, D., Booth, B. B. B., Knight, S. H. E., Highwood, E. J., Frame, D. J., Allen, M. R. and Rowell, D. P.: Sensitivity of Twentieth-Century Sahel Rainfall to Sulfate Aerosol and CO₂ Forcing, *J. Clim.*, 24(19), 4999–5014, doi:10.1175/JCLI-D-11-00019.1, 2011.
- Allen, R. J.: A 21st century northward tropical precipitation shift caused by future anthropogenic aerosol reductions, *J. Geophys. Res.*, 120(18), 9087–9102, doi:10.1002/2015JD023623, 2015.
- Allen, R. J., Evan, A. T. and Booth, B. B. B.: Interhemispheric aerosol radiative forcing and tropical precipitation shifts during the late Twentieth Century, *J. Clim.*, 28(20), 8219–8246, doi:10.1175/JCLI-D-15-0148.1, 2015.
- Andrews, M. B., Ridley, J. K., Wood, R. A., Andrews, T., Blockley, E. W., Booth, B., Burke, E., Dittus, A. J., Florek, P., Gray, L. J., Haddad, S., Hardiman, S. C., Hermanson, L., Hodson, D., Hogan, E., Jones, G. S., Knight, J. R., Kuhlbrodt, T., Misios, S., Mizielinski, M. S., Ringer, M. A., Robson, J. and Sutton, R. T.: Historical Simulations With HadGEM3-GC3.1 for CMIP6, *J. Adv. Model. Earth Syst.*, 12(6), e2019MS001995, doi:10.1029/2019MS001995, 2020.
- Andrews, T., Andrews, M. B., Bodas-Salcedo, A., Jones, G. S., Kuhlbrodt, T., Manners, J., Menary, M. B., Ridley, J., Ringer, M. A., Sellar, A. A., Senior, C. A. and Tang, Y.: Forcings, Feedbacks, and Climate Sensitivity in HadGEM3-GC3.1 and UKESM1, *J. Adv. Model. Earth Syst.*, 11(12), 4377–4394, doi:10.1029/2019MS001866, 2019.
- Atwood, A. R., Donohoe, A., Battisti, D. S., Liu, X. and Pausata, F. S. R.: Robust Longitudinally Variable Responses of the ITCZ to a Myriad of Climate Forcings, *Geophys. Res. Lett.*, 47(17), e2020GL088833, doi:https://doi.org/10.1029/2020GL088833, 2020.
- Bellouin, N., Rae, J., Jones, A., Johnson, C., Haywood, J. and Boucher, O.: Aerosol forcing in the Climate Model Intercomparison Project (CMIP5) simulations by HadGEM2-ES and the role of ammonium nitrate, *J. Geophys. Res.*, 116(D20), D20206, doi:10.1029/2011JD016074, 2011.
- Bellouin, N., Quaas, J., Gryspeerdt, E., Kinne, S., Stier, P., Watson-Parris, D., Boucher, O., Carslaw, K. S., Christensen, M., Daniau, A. L., Dufresne, J. L., Feingold, G., Fiedler, S., Forster, P., Gettelman, A., Haywood, J. M., Lohmann, U., Malavelle, F., Mauritsen, T., McCoy, D. T., Myhre, G., Mülmenstädt, J., Neubauer, D., Possner, A., Rugenstein, M., Sato, Y., Schulz, M., Schwartz, S. E., Sourdeval, O., Storelvmo, T., Toll, V., Winker, D. and Stevens, B.: Bounding Global Aerosol Radiative Forcing of Climate Change, *Rev. Geophys.*, 58(1), doi:10.1029/2019RG000660, 2020.
- Biasutti, M. and Giannini, A.: Robust Sahel drying in response to late 20th century forcings, *Geophys. Res. Lett.*, 33(11), doi:https://doi.org/10.1029/2006GL026067, 2006.
- Bonfils, C. J. W., Santer, B. D., Fyfe, J. C., Marvel, K., Phillips, T. J. and Zimmerman, S. R. H.: Human influence on joint changes in temperature, rainfall and continental aridity, *Nat. Clim. Chang.*, 1–6, doi:10.1038/s41558-020-0821-1, 2020.
- Booth, B. B. B., Dunstone, N. J., Halloran, P. R., Andrews, T. and Bellouin, N.: Aerosols implicated as a prime driver of twentieth-century North Atlantic climate variability, *Nature*, 484(7393), 228–232, doi:10.1038/nature10946, 2012.
- Broccoli, A. J., Dahl, K. A. and Stouffer, R. J.: Response of the ITCZ to Northern Hemisphere cooling, *Geophys. Res. Lett.*, 33(1), doi:10.1029/2005GL024546, 2006.
- Byrne, M. P., Pendergrass, A. G., Rapp, A. D. and Wodzicki, K. R.: Response of the Intertropical Convergence Zone to Climate Change: Location, Width, and Strength, *Curr. Clim. Chang. Reports*, 4(4), 355–370, doi:10.1007/s40641-018-0110-5, 2018.
- Chang, C. Y., Chiang, J. C. H., Wehner, M. F., Friedman, A. R. and Ruedy, R.: Sulfate aerosol control of tropical atlantic climate over the twentieth century, *J. Clim.*, 24(10), 2540–2555, doi:10.1175/2010JCLI4065.1, 2011.
- Chemke, R. and Dagan, G.: The effects of the spatial distribution of direct anthropogenic aerosols radiative forcing on atmospheric circulation, *J. Clim.*, 31(17), 7129–7145, doi:10.1175/JCLI-D-17-0694.1, 2018.
- Chiang, J. C. H. and Bitz, C. M.: Influence of high latitude ice cover on the marine Intertropical Convergence Zone, *Clim. Dyn.*, 25(5), 477–496, doi:10.1007/s00382-005-0040-5, 2005.

- Chiang, J. C. H. and Friedman, A. R.: Extratropical cooling, interhemispheric thermal gradients, and tropical climate change, *Annu. Rev. Earth Planet. Sci.*, 40, 383–412, doi:10.1146/annurev-earth-042711-105545, 2012.
- Choudhury, B. A., Rajesh, P. V., Zahan, Y. and Goswami, B. N.: Evolution of the Indian summer monsoon rainfall simulations from CMIP3 to CMIP6 models, *Clim. Dyn.*, 1–26, doi:10.1007/s00382-021-06023-0, 2021.
- Chung, E. S. and Soden, B. J.: Hemispheric climate shifts driven by anthropogenic aerosol-cloud interactions, *Nat. Geosci.*, doi:10.1038/NGEO2988, 2017.
- Collins, M., Sutherland, M., Bouwer, L., Cheong, S.-M., Frölicher, T., Combes, H. J. Des, Roxy, M. K., Losada, I., McInnes, K., Ratter, B., Rivera-Arriaga, E., Susanto, R. D., Swingedouw, D. and Tibig, L.: Extremes, Abrupt Changes and Managing Risk. In: IPCC Special Report on the Ocean and Cryosphere in a Changing Climate., 2019.
- Colose, C. M., LeGrande, A. N. and Vuille, M.: The influence of volcanic eruptions on the climate of tropical South America during the last millennium in an isotope-enabled general circulation model, *Clim. Past*, 12(4), 961–979, doi:10.5194/cp-12-961-2016, 2016.
- Diao, C., Xu, Y. and Xie, S.-P.: Anthropogenic aerosol effects on tropospheric circulation and sea surface temperature (1980–2020): separating the role of zonally asymmetric forcings, *Atmos. Chem. Phys.*, 21(24), 18499–18518, doi:10.5194/acp-21-18499-2021, 2021.
- Dong, B., Sutton, R. T., Highwood, E. and Wilcox, L.: The impacts of European and Asian anthropogenic sulfur dioxide emissions on Sahel rainfall, *J. Clim.*, 27(18), 7000–7017, doi:10.1175/JCLI-D-13-00769.1, 2014.
- Donohoe, A., Marshall, J., Ferreira, D. and Mcgee, D.: The relationship between ITCZ location and cross-equatorial atmospheric heat transport: From the seasonal cycle to the last glacial maximum, *J. Clim.*, 26(11), 3597–3618, doi:10.1175/JCLI-D-12-00467.1, 2013.
- Evans, S., Dawson, E. and Ginoux, P.: Linear Relation Between Shifting ITCZ and Dust Hemispheric Asymmetry, *Geophys. Res. Lett.*, 47(22), e2020GL090499, doi:https://doi.org/10.1029/2020GL090499, 2020.
- Forster, P., Storelvmo, T., Armour, K., Collins, W., Dufresne, J.-L., Frame, D., Lunt, D. J., Mauritsen, T., Palmer, M. D., Watanabe, M., Wild, M. and Zhang, H.: The Earth's Energy Budget, Climate Feedbacks, and Climate Sensitivity. In *Climate Change 2021: The Physical Science Basis. Contribution of Working Group I to the Sixth Assessment Report of the Intergovernmental Panel on Climate Change*, (In Press), 2021.
- Friedman, A. R., Hwang, Y.-T., Chiang, J. C. H. and Frierson, D. M. W.: Interhemispheric Temperature Asymmetry over the Twentieth Century and in Future Projections, *J. Clim.*, 26(15), 5419–5433, doi:10.1175/JCLI-D-12-00525.1, 2013.
- Frierson, D. M. W. and Hwang, Y. T.: Extratropical influence on ITCZ shifts in slab ocean simulations of global warming, *J. Clim.*, 25(2), 720–733, doi:10.1175/JCLI-D-11-00116.1, 2012.
- Giannini, A. and Kaplan, A.: The role of aerosols and greenhouse gases in Sahel drought and recovery, *Clim. Change*, 152(3–4), 449–466, doi:10.1007/s10584-018-2341-9, 2019.
- Green, B. and Marshall, J.: Coupling of Trade Winds with Ocean Circulation Damps ITCZ Shifts, *J. Clim.*, 30(12), 4395–4411, doi:10.1175/JCLI-D-16-0818.1, 2017.
- Green, B., Marshall, J. and Donohoe, A.: Twentieth century correlations between extratropical SST variability and ITCZ shifts, *Geophys. Res. Lett.*, 44(17), 9039–9047, doi:https://doi.org/10.1002/2017GL075044, 2017.
- Gregory, J. M. and Forster, P. M.: Transient climate response estimated from radiative forcing and observed temperature change, *J. Geophys. Res. Atmos.*, 113(23), D23105, doi:10.1029/2008JD010405, 2008.
- Haywood, J. M., Jones, A., Bellouin, N. and Stephenson, D.: Asymmetric forcing from stratospheric aerosols impacts Sahelian rainfall, *Nat. Clim. Chang.*, 3(7), 660–665, doi:10.1038/nclimate1857, 2013.
- Herman, R. J., Giannini, A., Biasutti, M. and Kushnir, Y.: The effects of anthropogenic and volcanic aerosols and greenhouse gases on twentieth century Sahel precipitation, *Sci. Rep.*, 10(1), 12203, doi:10.1038/s41598-020-68356-w, 2020.

- Hewitt, H. T., Copsey, D., Culverwell, I. D., Harris, C. M., Hill, R. S. R., Keen, A. B., McLaren, A. J. and Hunke, E. C.: Design and implementation of the infrastructure of HadGEM3: The next-generation Met Office climate modelling system, *Geosci. Model Dev.*, 4(2), 223–253, doi:10.5194/gmd-4-223-2011, 2011.
- Hewitt, H. T., Roberts, M., Mathiot, P., Biastoch, A., Blockley, E., Chassignet, E. P., Fox-Kemper, B., Hyder, P., Marshall, D. P., Popova, E., Treguier, A. M., Zanna, L., Yool, A., Yu, Y., Beadling, R., Bell, M., Kuhlbrodt, T., Arsouze, T., Bellucci, A., Castruccio, F., Gan, B., Putrasahan, D., Roberts, C. D., Van Roekel, L. and Zhang, Q.: Resolving and Parameterising the Ocean Mesoscale in Earth System Models, *Curr. Clim. Chang. Reports*, 6(4), 137–152, doi:10.1007/s40641-020-00164-w, 2020.
- Hirasawa, H., Kushner, P. J., Sigmond, M., Fye, J. and Deser, C.: Anthropogenic aerosols dominate forced multidecadal sahel precipitation change through distinct atmospheric and oceanic drivers, *J. Clim.*, 33(23), 10187–10204, doi:10.1175/JCLI-D-19-0829.1, 2020.
- Hwang, Y. T., Frierson, D. M. W. and Kang, S. M.: Anthropogenic sulfate aerosol and the southward shift of tropical precipitation in the late 20th century, *Geophys. Res. Lett.*, 40(11), 2845–2850, doi:10.1002/grl.50502, 2013.
- Iles, C. E., Hegerl, G. C., Schurer, A. P. and Zhang, X.: The effect of volcanic eruptions on global precipitation, *J. Geophys. Res. Atmos.*, 118(16), 8770–8786, doi:10.1002/jgrd.50678, 2013.
- Kang, S. M.: Extratropical Influence on the Tropical Rainfall Distribution, *Curr. Clim. Chang. Reports*, 6(1), 24–36, doi:10.1007/s40641-020-00154-y, 2020.
- Kang, S. M., Held, I. M., Frierson, D. M. W. and Zhao, M.: The response of the ITCZ to extratropical thermal forcing: Idealized slab-ocean experiments with a GCM, *J. Clim.*, 21(14), 3521–3532, doi:10.1175/2007JCLI2146.1, 2008.
- Kang, S. M., Frierson, D. M. W. and Held, I. M.: The Tropical Response to Extratropical Thermal Forcing in an Idealized GCM: The Importance of Radiative Feedbacks and Convective Parameterization, *J. Atmos. Sci.*, 66(9), 2812–2827, doi:10.1175/2009JAS2924.1, 2009.
- Kang, S. M., Shin, Y. and Xie, S.-P.: Extratropical forcing and tropical rainfall distribution: energetics framework and ocean Ekman advection, *npj Clim. Atmos. Sci.*, 1(1), 1–10, doi:10.1038/s41612-017-0004-6, 2018.
- Kang, S. M., Xie, S. P., Deser, C. and Xiang, B.: Zonal mean and shift modes of historical climate response to evolving aerosol distribution, *Sci. Bull.*, 66(23), 2405–2411, doi:10.1016/j.scib.2021.07.013, 2021.
- Lamarque, J. F., Bond, T. C., Eyring, V., Granier, C., Heil, A., Klimont, Z., Lee, D., Liousse, C., Mieville, A., Owen, B., Schultz, M. G., Shindell, D., Smith, S. J., Stehfest, E., Van Aardenne, J., Cooper, O. R., Kainuma, M., Mahowald, N., McConnell, J. R., Naik, V., Riahi, K. and Van Vuuren, D. P.: Historical (1850–2000) gridded anthropogenic and biomass burning emissions of reactive gases and aerosols: Methodology and application, *Atmos. Chem. Phys.*, 10(15), 7017–7039, doi:10.5194/acp-10-7017-2010, 2010.
- Lund, M. T., Myhre, G. and Samset, B. H.: Anthropogenic aerosol forcing under the Shared Socioeconomic Pathways, *Atmos. Chem. Phys.*, 19(22), 13827–13839, doi:10.5194/acp-2019-606, 2019.
- Mamalakis, A., Randerson, J. T., Yu, J. Y., Pritchard, M. S., Magnúsdóttir, G., Smyth, P., Levine, P. A., Yu, S. and Fofoula-Georgiou, E.: Zonally contrasting shifts of the tropical rain belt in response to climate change, *Nat. Clim. Chang.*, 11(2), 143–151, doi:10.1038/s41558-020-00963-x, 2021.
- Mann, G. W., Carslaw, K. S., Spracklen, D. V., Ridley, D. A., Manktelow, P. T., Chipperfield, M. P., Pickering, S. J. and Johnson, C. E.: Description and evaluation of GLOMAP-mode: a modal global aerosol microphysics model for the UKCA composition-climate model, *Geosci. Model Dev.*, 3(2), 519–551, doi:10.5194/gmd-3-519-2010, 2010.
- McFarlane, A. A. and Frierson, D. M. W.: The role of ocean fluxes and radiative forcings in determining tropical rainfall shifts in RCP8.5 simulations, *Geophys. Res. Lett.*, 44(16), 8656–8664, doi:10.1002/2017GL074473, 2017.
- Menary, M. B., Robson, J., Allan, R. P., Booth, B. B. B., Cassou, C., Gastineau, G., Gregory, J., Hodson, D., Jones, C., Mignot, J., Ringer, M., Sutton, R., Wilcox, L. and Zhang, R.: Aerosol-

- Forced AMOC Changes in CMIP6 Historical Simulations, *Geophys. Res. Lett.*, 47(14), doi:10.1029/2020GL088166, 2020.
- Moreno-Chamarro, E., Marshall, J. and Delworth, T. L.: Linking ITCZ Migrations to the AMOC and North Atlantic/Pacific SST Decadal Variability, *J. Clim.*, 33(3), 893–905, doi:10.1175/JCLI-D-19-0258.1, 2020.
- Murphy, J. M., Harris, G. R., Sexton, D. M. H., Kendon, E. J., Bett, P. E., Clark, R. T., Eagle, K. E., Fosse, G., Fung, F., Lowe, J. A., McDonald, R. E., McInnes, R. N., McSweeney, C. F., Mitchell, J. F. B., Rostron, J. W., Thornton, H. E., Tucker, S. and Yamazaki, K.: UKCP18: Land Projections Science Report., 2018.
- Myhre, G., Shindell, D., Aamaas, B., Boucher, O., Dalsøren, S., Daniel, J., Forster, P., Granier, C., Haigh, J. and Hodnebrog, Ø.: Anthropogenic and natural radiative forcing, in *Climate Change 2013 the Physical Science Basis: Working Group I Contribution to the Fifth Assessment Report of the Intergovernmental Panel on Climate Change*, vol. 9781107057, pp. 659–740., 2013.
- Nazarenko, L., Rind, D., Tsigaridis, K., Del Genio, A. D., Kelley, M. and Tausnev, N.: Interactive nature of climate change and aerosol forcing, *J. Geophys. Res. Atmos.*, 122(6), 3457–3480, doi:10.1002/2016JD025809, 2017.
- Rao, S., Klimont, Z., Smith, S. J., Van Dingenen, R., Dentener, F., Bouwman, L., Riahi, K., Amann, M., Bodirsky, B. L., van Vuuren, D. P., Aleluia Reis, L., Calvin, K., Drouet, L., Fricko, O., Fujimori, S., Gernaat, D., Havlik, P., Harmsen, M., Hasegawa, T., Heyes, C., Hilaire, J., Luderer, G., Masui, T., Stehfest, E., Strefler, J., van der Sluis, S. and Tavoni, M.: Future air pollution in the Shared Socio-economic Pathways, *Glob. Environ. Chang.*, 42, 346–358, doi:10.1016/j.gloenvcha.2016.05.012, 2017.
- Regayre, L. A., Johnson, J. S., Yoshioka, M., Pringle, K. J., Sexton, D. M. H., Booth, B. B. B., Lee, L., Bellouin, N. and Carslaw, K.: Aerosol and physical atmosphere model parameters are both important sources of uncertainty in aerosol ERF, *Atmos. Chem. Phys.*, 18(13), 1–54, doi:10.5194/acp-2018-175, 2018.
- Riahi, K., Rao, S., Krey, V., Cho, C., Chirkov, V., Fischer, G., Kindermann, G., Nakicenovic, N. and Rafaj, P.: RCP 8.5-A scenario of comparatively high greenhouse gas emissions, *Clim. Change*, 109(1), 33–57, doi:10.1007/s10584-011-0149-y, 2011.
- Rotstayn, L. D. and Lohmann, U.: Tropical Rainfall Trends and the Indirect Aerosol Effect, *J. Clim.*, 15(15), 2103–2116, doi:10.1175/1520-0442(2002)015<2103:TRTATI>2.0.CO;2, 2002.
- Rotstayn, L. D., Ryan, B. F. and Penner, J. E.: Precipitation changes in a GCM resulting from the indirect effects of anthropogenic aerosols, *Geophys. Res. Lett.*, 27(19), 3045–3048, doi:https://doi.org/10.1029/2000GL011737, 2000.
- Rotstayn, L. D., Collier, M. A. and Luo, J.-J.: Effects of declining aerosols on projections of zonally averaged tropical precipitation, *Environ. Res. Lett.*, 10(4), 044018, doi:10.1088/1748-9326/10/4/044018, 2015.
- Schleussner, C. F., Levermann, A. and Meinshausen, M.: Probabilistic projections of the Atlantic overturning, *Clim. Change*, 127(3–4), 579–586, doi:10.1007/s10584-014-1265-2, 2014.
- Sexton, D., Yamazaki, K., Murphy, J. and Rostron, J.: Assessment of drifts and internal variability in UKCP projections., 2020.
- Sexton, D. M. H., McSweeney, C. F., Rostron, J. W., Yamazaki, K., Booth, B. B. B., Johnson, J., Murphy, J. M. and Regayre, L.: A perturbed parameter ensemble of HadGEM3-GC3.05 coupled model projections: part 1: selecting the parameter combinations, *Clim Dyn* [online] Available from: https://doi.org/10.1007/s00382-021-05709-9, 2021.
- Smith, C. J., Kramer, R. J., Myhre, G., Alterskjær, K., Collins, W., Sima, A., Boucher, O., Dufresne, J. L., Nabat, P., Michou, M., Yukimoto, S., Cole, J., Paynter, D. J., Shiogama, H., O'Connor, F. M., Robertson, E., Wiltshire, A., Andrews, T., Hannay, C., Miller, R., Nazarenko, L., Kirkevåg, A., Olivé, D., Fiedler, S., Pincus, R. and Forster, P. M.: Effective radiative forcing and rapid adjustments in CMIP6 models, *Atmos. Chem. Phys. Discuss.* [online] Available from: https://www.atmos-chem-phys-discuss.net/acp-2019-1212/ (Accessed 27 April 2020), 2020.
- Takemura, T.: Return to different climate states by reducing sulphate aerosols under future CO₂ concentrations, *Sci. Rep.*, 10(1), 21748, doi:10.1038/s41598-020-78805-1, 2020.

- Taylor, K. E., Crucifix, M., Braconnot, P., Hewitt, C. D., Doutriaux, C., Broccoli, A. J., Mitchell, J. F. B. and Webb, M. J.: Estimating shortwave radiative forcing and response in climate models, *J. Clim.*, 20(11), 2530–2543, doi:10.1175/JCLI4143.1, 2007.
- Taylor, K. E., Stouffer, R. J. and Meehl, G. A.: An overview of CMIP5 and the experiment design, *Bull. Am. Meteorol. Soc.*, 93(4), 485–498, doi:10.1175/BAMS-D-11-00094.1, 2012.
- Thompson, D. W. J., Wallace, J. M., Kennedy, J. J. and Jones, P. D.: An abrupt drop in Northern Hemisphere sea surface temperature around 1970, *Nature*, 467(7314), 444–447, doi:10.1038/nature09394, 2010.
- Utida, G., Cruz, F. W., Etourneau, J., Bouloubassi, I., Schefuß, E., Vuille, M., Novello, V. F., Prado, L. F., Sifeddine, A., Klein, V., Zular, A., Viana, J. C. C. and Turcq, B.: Tropical South Atlantic influence on Northeastern Brazil precipitation and ITCZ displacement during the past 2300 years, *Sci. Rep.*, 9(1), 1–8, doi:10.1038/s41598-018-38003-6, 2019.
- Voigt, A., Pincus, R., Stevens, B., Bony, S., Boucher, O., Bellouin, N., Lewinschal, A., Medeiros, B., Wang, Z. and Zhang, H.: Fast and slow shifts of the zonal-mean intertropical convergence zone in response to an idealized anthropogenic aerosol, *J. Adv. Model. Earth Syst.*, 9(2), 870–892, doi:10.1002/2016MS000902, 2017.
- van Vuuren, D. P., Stehfest, E., den Elzen, M. G. J., Kram, T., van Vliet, J., Deetman, S., Isaac, M., Goldewijk, K. K., Hof, A., Beltran, A. M., Oostenrijk, R. and van Ruijven, B.: RCP2.6: Exploring the possibility to keep global mean temperature increase below 2°C, *Clim. Change*, 109(1), 95–116, doi:10.1007/s10584-011-0152-3, 2011a.
- van Vuuren, D. P., Edmonds, J., Kainuma, M., Riahi, K., Thomson, A., Hibbard, K., Hurtt, G. C., Kram, T., Krey, V., Lamarque, J.-F., Masui, T., Meinshausen, M., Nakicenovic, N., Smith, S. J. and Rose, S. K.: The representative concentration pathways: an overview, *Clim. Change*, 109(1–2), 5–31, doi:10.1007/s10584-011-0148-z, 2011b.
- Walters, D., Baran, A. J., Boutle, I., Brooks, M., Earnshaw, P., Edwards, J., Furtado, K., Hill, P., Lock, A., Manners, J., Morcrette, C., Mulcahy, J., Sanchez, C., Smith, C., Stratton, R., Tennant, W., Tomassini, L., Van Weverberg, K., Vosper, S., Willett, M., Browse, J., Bushell, A., Carslaw, K., Dalvi, M., Essery, R., Gedney, N., Hardiman, S., Johnson, B., Johnson, C., Jones, A., Jones, C., Mann, G., Milton, S., Rumbold, H., Sellar, A., Ujiie, M., Whittall, M., Williams, K. and Zerroukat, M.: The Met Office Unified Model Global Atmosphere 7.0/7.1 and JULES Global Land 7.0 configurations, *Geosci. Model Dev.*, 12(5), 1909–1963, doi:10.5194/gmd-12-1909-2019, 2019.
- Williams, K. D., Jones, A., Roberts, D. L., Senior, C. A. and Woodage, M. J.: The response of the climate system to the indirect effects of anthropogenic sulfate aerosol, *Clim. Dyn.*, 17(11), 845–856, doi:10.1007/s003820100150, 2001.
- Williams, K. D., Copsey, D., Blockley, E. W., Bodas-Salcedo, A., Calvert, D., Comer, R., Davis, P., Graham, T., Hewitt, H. T., Hill, R., Hyder, P., Ineson, S., Johns, T. C., Keen, A. B., Lee, R. W., Megann, A., Milton, S. F., Rae, J. G. L., Roberts, M. J., Scaife, A. A., Schiemann, R., Storkey, D., Thorpe, L., Watterson, I. G., Walters, D. N., West, A., Wood, R. A., Woollings, T. and Xavier, P. K.: The Met Office Global Coupled Model 3.0 and 3.1 (GC3.0 and GC3.1) Configurations, *J. Adv. Model. Earth Syst.*, 10(2), 357–380, doi:10.1002/2017MS001115, 2018.
- Yamazaki, K., Sexton, D. M. H., Rostron, J. W., McSweeney, C. F., Murphy, J. M. and Harris, G. R.: A perturbed parameter ensemble of HadGEM3-GC3.05 coupled model projections: part 2: global performance and future changes, *Clim. Dyn.*, 56(11–12), 3437–3471, doi:10.1007/s00382-020-05608-5, 2021.
- Zelinka, M. D., Andrews, T., Forster, P. M. and Taylor, K. E.: Quantifying components of aerosol-cloud-radiation interactions in climate models, *J. Geophys. Res. Atmos.*, 119(12), 7599–7615, doi:10.1002/2014JD021710, 2014.

Chapter 4 Underestimating European Dimming, Overestimating European Brightening

Amy H. Peace¹, Ben B. Booth², Leighton A. Regayre¹, Ken S. Carslaw¹

¹Institute for Climate and Atmospheric Science, University of Leeds, Leeds, UK

²Met Office Hadley Centre, Exeter, UK

Abstract

Atmospheric aerosols interact with radiation and modify the properties of clouds. Solar radiation observed at the surface across Europe and North America decreased when anthropogenic aerosol emissions increased over the industrial period, and increased when emissions were later reduced. The observed multi-decadal trends in surface solar radiation have been proposed as a way of constraining the persistent uncertainty in anthropogenic aerosol radiative forcing. Yet, models tend to underestimate the magnitude of trends in surface solar radiation. Here, we evaluate surface solar radiation trends over Europe using a perturbed parameter ensemble (PPE) of HadGEM-GC3.05 that spans a range of aerosol radiative forcing. We show that the PPE underestimates the observed dimming trend during 1960 to 1980, but overestimates the brightening trend over 1985 to 2005. There is a clear role of aerosols driving the all-sky surface solar radiation trend in the brightening period. In the dimming period, the role of aerosols in driving the all-sky trend in our PPE is possibly obscured by internal variability and parametric effects related to clouds and atmospheric circulation. Our results suggest increasing the removal rates of aerosols and precursor gases can improve model skill at simulating the surface solar radiation trends over Europe. However, many factors may influence the simulated relationships between model parameters, aerosol forcing and surface solar radiation, including choice of time period, seasons, degree of atmosphere-ocean coupling and ensemble size. As a result, based on our small ensemble size, we think caution needs to be applied when using multi-decadal trends in surface solar radiation to infer a constraint on future climate projections.

4.1 Introduction

Atmospheric aerosols affect the radiative balance of the planet by scattering and absorbing incoming solar radiation and altering cloud properties. Globally, anthropogenic aerosol emissions increased throughout the industrial period, which caused a net negative radiative forcing at the top of atmosphere and reduced the amount of solar radiation reaching the surface, producing a net cooling effect on climate (Myhre et al. 2013; Bellouin et al. 2020). Over the coming decades anthropogenic aerosol emissions are projected to decline (Rao et al., 2017; Riahi et al., 2017). Relative to present-day, reductions in aerosol emissions will lead to a net positive radiative forcing at the top of atmosphere corresponding to an increase in the amount of solar radiation reaching the surface. Aerosol-driven surface warming will add to the warming caused by rising greenhouse gases emissions and could amplify large scale climatic effects (Chalmers et al., 2012; Hienola et al., 2018; Lund et al., 2019; Rotstajn et al., 2014, 2015; Samset et al., 2018; Westervelt et al., 2015). Yet, the radiative forcing caused by changing anthropogenic aerosol emissions is the largest cause of uncertainty in the radiative forcing of the Earth system over the industrial period (Myhre et al. 2013; Bellouin et al. 2020). Reducing this uncertainty in aerosol radiative forcing is therefore an important task to improve the accuracy of future climate projections (Andreae et al., 2005; Collins and Knutti, 2013; Eyring et al., 2021; Peace et al., 2020; Seinfeld et al., 2016). The uncertainty has remained difficult to reduce in part because there is a lack of observations over the industrial period that can be used to constrain climate model simulations of long-term changes in aerosol and cloud properties (Carslaw et al., 2013; Gryspeerdt et al., 2017).

The Global Energy Balance Archive (GEBA) contains surface solar radiation (SSR) measurements dating back to 1922 which may be a useful proxy for constraining the long-term radiative effects of evolving anthropogenic aerosol emissions (Cherian et al., 2014; Wild et al., 2017). Observations from GEBA show a decrease in Northern Hemisphere SSR between the 1950s to 1980s (“dimming”) that coincides with increasing global anthropogenic aerosol emissions. This dimming period is followed by a recovery in SSR at many locations (“brightening”) when anthropogenic aerosol emissions declined across Europe and North America (Granier et al., 2011; Hand et al., 2012; Sanchez-Lorenzo et al., 2015; Vestreng et al., 2007; Wild, 2009a, Wild et al., 2005).

Numerous studies have therefore attributed multi-decadal trends in SSR to evolving anthropogenic aerosol emissions (Allen et al., 2013; Kudo et al., 2012; Onsum Moseid et al., 2020; Storelvmo et al., 2018; Turnock et al., 2015; Wang et al., 2012). Some studies have suggested changes in cloud cover and radiative properties drive SSR trends (Augustine and Dutton, 2013; Liley, 2009; Long et al., 2009; Mateos et al., 2014; Padma Kumari and Goswami, 2010; Pfeifroth et al., 2018; Stjern et al., 2009). Relative humidity and variations in solar radiation can also affect SSR, but have not changed sufficiently enough over recent decades to drive the observed trends in SSR (Antón and Mateos, 2013; Aparicio et al., 2020; Mateos et al., 2013).

Current and previous generations of Earth System Models (ESMs) underestimate the magnitude of the observed trend in global SSR (Allen et al., 2013; Storelvmo et al., 2018; Wild, 2009b). Analysis of the CMIP6 ensemble suggests that observed SSR trends over Europe are well represented in many models, but trends over Asia are underestimated (Moseid et al., 2020). However, in Asia, some of the discrepancy between models and observations may be due to changes in observational equipment in China during the early 1990s (Yang et al., 2018). The CMIP5 ensemble and HadGEM3-UKCA have shown an underestimation of observed SSR trends over Europe (Allen et al., 2013; Turnock et al., 2015). The underestimation of modelled SSR trends has been hypothesized to be caused by discrepancies in aerosol emissions and model treatment of processes that relate aerosol emissions to radiative forcing (Allen et al., 2013; Moseid et al., 2020; Ruckstuhl and Norris, 2009a; Storelvmo et al., 2018; Wild, 2009a).

We use a perturbed parameter ensemble (PPE) of climate model simulations to investigate the influence of model parameters and processes on simulated SSR trends, and evaluate the usefulness of SSR trends as a constraint of aerosol effective radiative forcing. Our PPE samples the uncertainty in 47 model parameters across a range of model schemes (Murphy et al., 2018; Sexton et al., 2021; Yamazaki et al., 2021). Within the aerosol scheme, we perturb 8 parameters related to anthropogenic and natural aerosol emissions, processes and removal. The PPE consists of both transient (1900 to 2100) coupled ocean-atmosphere simulations and idealised time slice atmosphere-only experiments. The PPE therefore provides a unique and useful opportunity to evaluate the

effects of uncertainties associated with aerosol emissions and processes on SSR trends.

Our analysis focuses on Europe due to the high density of GEBA stations in this region. We first focus on SSR trends during the dimming and brightening periods, using 15 ensemble members from the coupled ocean-atmosphere PPE. We then explore the uncertainty in 2005 to 2009 average SSR, also using a much larger 518 member atmosphere-only PPE.

4.2 Methods

4.2.1 Perturbed Parameter Ensemble of HadGEM3-GC3.05

The base model of the perturbed parameter ensemble (PPE) is version 3.05 of the UK Hadley Centre Unified Model (HadGEM3-GC3.05), which is a global coupled ocean-atmosphere model with the atmospheric component HadGEM3-GA7.05 (Williams et al., 2018). HadGEM3-GC3.05 incorporates the modal version of the GLObal Model of Aerosol Processes (GLOMAP-mode) which simulates new particle formation, gas-to-gas particle transfer, aerosol coagulation, cloud processing of aerosol and aerosol deposition. GLOMAP-mode resolves sulfate, sea salt, dust, black carbon and organic aerosol species (Mann et al., 2010). The model version HadGEM3-GC3.05 incorporates many of the main improvements that were made to GC3.0 to create GC3.1, the model version submitted to CMIP6 (Walters et al., 2019; Williams et al., 2018). In this work, we also use a small HadGEM3-GC3.1 initial condition ensemble to quantify estimates of internal variability where appropriate.

A PPE of the above model setup was designed for UK Climate Projections 2018 (UKCP18; Murphy et al., 2018). In the PPE, 47 uncertain model parameters and processes are perturbed from the model schemes representing convection, boundary layer, gravity wave drag, cloud radiative and microphysical properties, aerosol and land surface. The selection process for these schemes and parameters is described in detail in Sexton et al. (2021). Comprehensive filtering of PPE members helped identify a subset of plausible and diverse model variants (parameter combinations) to produce the transient climate simulations.

The first stage of the performance filtering process used atmosphere-only 5-day weather hind-cast experiments to assess a 2800 member PPE for performance

against a range of observed climate variables. This filtering stage left 442 members that sample the full range of uncertainty for most parameters. An additional 115 model variants were created to supplement the 442 model variants by filling gaps in the multi-dimensional parameter space. In the next filtering stage, these 557 model variants were assessed for plausibility and diversity using 5-year atmosphere-only experiments, similar to those used in CMIP5: aerosol effective radiative forcing (ERF) between 1860 and 2005-9, ERF due to a quadrupling of CO₂, and SST patterns prescribed for a global warming of 4 °C. Of the 557 PPE members, 39 were ruled out due to model crashes, leaving 518 member atmosphere-only PPEs. The 25 most diverse (and plausible) variants of the 518 members were selected to create the industrial period transient coupled ocean-atmosphere experiments. Lastly, the transient PPE simulations were filtered based on their performance over 1900 to 2005 as described in Yamazaki et al. (2021). This multi-stage filtering process left 15 remaining model variants that sample known model uncertainties and hence provide, for a given emissions scenario, a range of climate responses.

In this study we use the 15 ensemble members from the transient coupled-ocean atmosphere PPE to quantify trends in SSR over the dimming and brightening periods. These 15 ensemble members have paired anthropogenic aerosol ERF experiments with (5-year average) time slices at 1860, 1975 and 2005. We compare the 2005 to 2009 average SSR from the 15 coupled ocean-atmosphere ensemble members to their atmosphere-only counterpart, and the larger 518-member PPE used in the filtering process.

We also use the 4-member initial condition ensembles of HadGEM3-GC3.1-LL (low resolution) and HadGEM3-GC3.1-MM (medium resolution; same as PPE) that are similar model versions to the PPE and were submitted to CMIP6 (Andrews et al. 2020) to provide an estimate of how internal variability alone can generate uncertainty in SSR trends.

4.2.2 Observations of Surface Solar Radiation

Ground-based observations of all-sky downward SSR were obtained from GEBA. GEBA contains monthly mean measurements of surface energy flux components for more than 2500 sites worldwide, with the longest observational record dating back to 1922 (Wild et al., 2017). Most of the SSR measurements within GEBA

were made with pyranometers which have a relative random measurement error estimated at 5% of the monthly mean and 2% of the annual mean (Gilgen et al., 1998). GEBA measurements that are suspected of being erroneous are also flagged in the quality control procedure (Gilgen and Ohmura, 1999).

Observations at some GEBA stations go back to the early 20th century, but more complete records start in the 1960s. We use a dataset of long-term SSR measurements over Europe that was created by Sanchez-Lorenzo et al. (2013). The dataset consists of 56 stations mostly over central Europe where the series start before 1971 and contain at least 30 years of data. Inhomogeneity of a time series, created for example by instrument change or relocation, has been shown to significantly affect SSR trends at individual stations (Manara et al., 2016; Yang et al., 2018). We therefore use the data from 39 of the 56 stations classified as homogenous. To gain additional information on the spatial-temporal evolution of SSR trends, we partitioned the 38 stations (Reykjavik is excluded) into 5 European regions as shown in Figure 4.1 below. The stations were assigned to the 5 regions based on the results of Sanchez-Lorenzon et al. (2015) where principal component analysis was used to cluster the stations into regions of similar spatial-temporal variability.

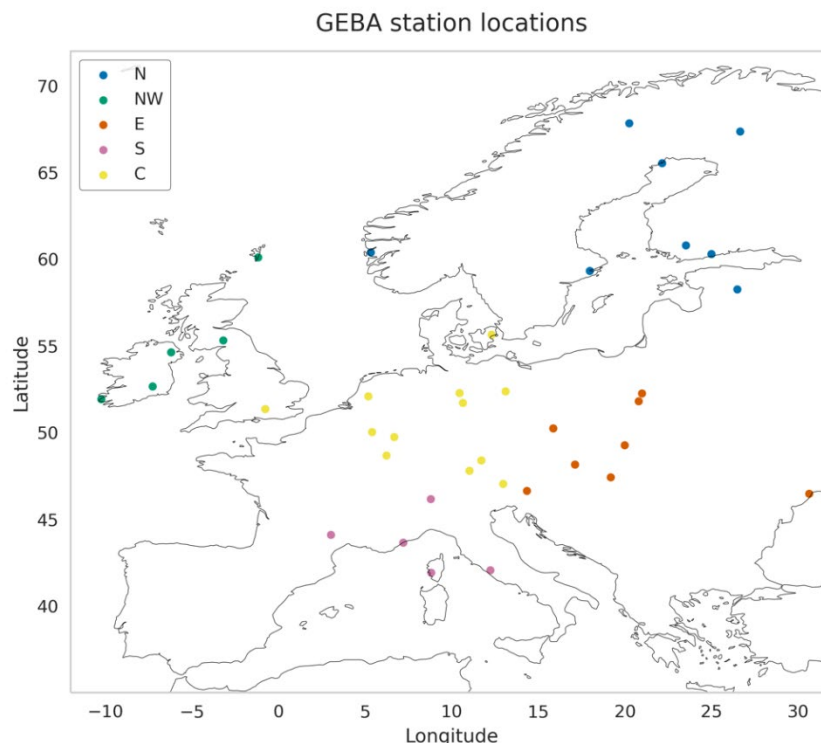


Figure 4.1 Location of the 39 GEBA stations used in this study. The stations are partitioned into 5 European regions: North (N), North-West (NW), East (E), South (S), and Central (C) based on principal component analysis performed in Sanchez-Lorenzo et al. (2015).

We first focus on the trend in all-sky SSR, comparing observations and simulations for 1960 to 1980 (dimming period) and 1985 to 2005 (brightening period). In the observations, the transition between dimming and brightening occurs in the mid-1980s (Sanchez-Lorenzo et al., 2015), but the simulated transition time can vary across models (Allen et al., 2013; Ruckstuhl and Norris, 2009b). We calculate annual anomalies over each time period. A common reference exacerbates model-observation differences in the dimming period (Figure C.2). We interpolate the SSR model data to the coordinates of the 39 GEBA stations using a ‘nearest neighbour’ approach (as used in Mosseid et al. (2020)). Our analysis therefore compares values from a model grid box to the pointwise location of a GEBA station. Previous studies have shown that there is generally a decrease in correlation between measurements that have increasing distance between, but that the representativeness improves for longer averaging periods (Hakuba et al., 2013; Li, 2005; Schwarz et al., 2017a). We focus on linear trends of annual and seasonal means. A 5-year rolling mean is applied prior to calculating linear trends to smooth the inter-annual variability of the data. We also calculate a multi-year average of SSR over 2005 to 2009. We do not use GEBA stations that contain missing values, so only use 35 stations to calculate the 2005 to 2009 regional average.

SSR from GEBA stations cannot be easily decomposed into clear- and cloudy-sky components. So, we compare model output to observations for all-sky SSR. Though, we use the clear-sky and cloudy-sky model components to inform our understanding. Simulated cloudy-sky SSR is calculated as the difference between all-sky and clear-sky SSR.

4.2.3 Model Evaluation Metrics and Parameter Relationships

We used the normalised root mean square error (nRMSE) to assess the performance of individual ensemble members in simulating the observed surface solar radiation trends or multi-year average across the European GEBA stations. The RMSE calculation is shown in the equation below, where Y_i is the observed value and \hat{Y}_i is the modelled value for each station. The RMSE value is normalised by the GEBA regional mean trend. Normalisation allows model performance to be compared between different variables (not shown). A larger nRMSE indicates larger deviation between model and observations. We use the nRMSE to identify if there are any ensemble members that consistently out-

perform other members, and to explore the relationships between perturbed parameters and model skill by calculating the Spearman's correlation coefficient between the nRMSE and parameter values across the ensemble. Since our PPE has a small sample size ($n=15$), there are too few degrees of freedom to perform robust statistical analyses, so parameter independence is assumed when calculating correlations between SSR and perturbed parameters.

$$(2) \quad RMSE = \sqrt{\frac{1}{n} \sum_{i=1}^n (Y_i - \hat{Y}_i)^2}$$

4.3 Results

4.3.1 Solar Dimming Period: 1960 to 1980

4.3.1.1 All-Sky SSR

There is consensus that SSR observations imply a dimming over Europe during the 1960 to 1980 period (e.g. Wild, 2009). Figure 4.2 shows the 1960 to 1980 trend in SSR over Europe in our PPE, with the trend at GEBA stations overlaid. Our PPE mean shows widespread dimming over central Europe during this time period when anthropogenic aerosol emissions were increasing (Hoesly et al., 2018). Our PPE mean also shows brightening across the United Kingdom and some coastal regions in Northern Europe, which is consistent with the GEBA observation trends and likely due to earlier emission reductions over this region (Folini and Wild, 2011). Table 4.1 shows that our PPE mean underestimates the European mean SSR trend at GEBA station locations. Regionally, GEBA observations shows the largest and statistically significant decreasing trend in SSR over East and Southern Europe. The PPE mean shows the largest underestimation of SSR trends over these two regions.

In our PPE members, there are large differences in the direction and magnitude of the 1960 to 1980 SSR trend across Europe. Local climatological and meteorological conditions (such as cloud properties, water vapour, aerosol loadings, topography and surface albedo) affect the spatial and temporal variation of SSR (Schwarz et al., 2017b). The spatial variation of SSR trends during the dimming period across Europe at both GEBA stations and in the PPE are therefore likely caused, at least in part, by local conditions. To obtain an idea of which of these variables have an effect on the spatial variability of SSR trends in the PPE, we calculated the spatial correlation between the SSR trend and trend in relevant simulated variables, as shown in Figure C.3. The spatial correlation analysis suggests the spatial variability in all-sky SSR trends across Europe in our PPE is more closely related to cloud properties, surface temperature and relative humidity, than with aerosol optical depth. The spatial variability in our PPE due to these variables could be caused by internal variability, parametric effects, or a combination of both. The 1960 to 1980 trend in the HadGEM3-GC3.1 initial condition ensembles, shown in Figure C.1, suggests internal variability plays an important role in causing spatial variability in SSR.

Trend in 1960 to 1980 all-sky SSR anomaly

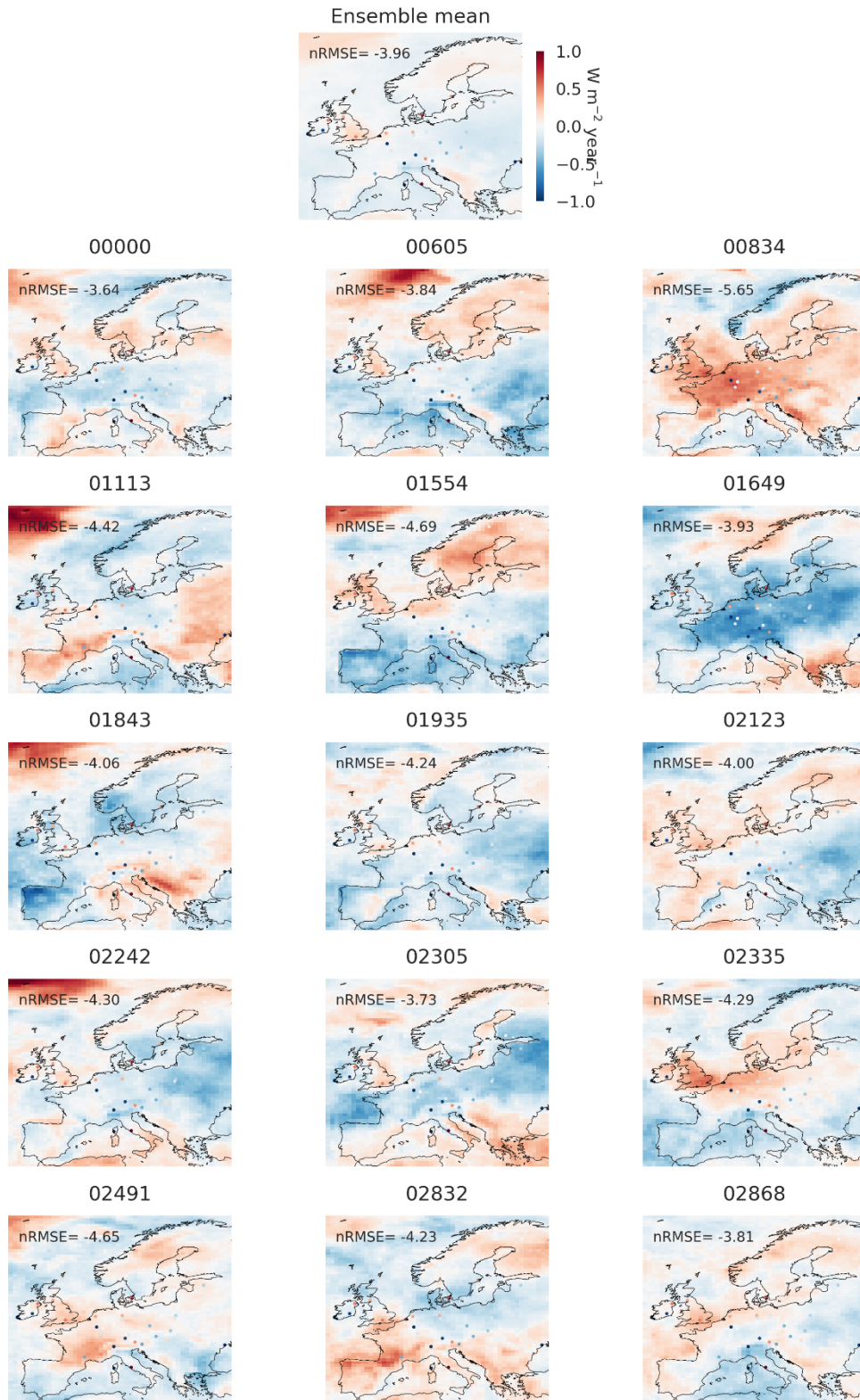


Figure 4.2 1960 to 1980 linear trend of the 5-year rolling mean annual anomaly (from the 1960 to 1980 mean) in all sky SSR ($W m^{-2} year^{-1}$) across Europe. GEBA observations are overlaid in circles. The ensemble mean is shown at the top, followed by the individual ensemble members. The normalised RMSE is shown in the top left of each plot.

	GEBA	PPE mean	Initial condition ensemble mean
Europe	-0.11 ± 0.04	-0.04 ± 0.02	-0.04 ± 0.01
North	0.03 ± 0.08	-0.02 ± 0.02	0.02 ± 0.02
North-west	0.12 ± 0.08	-0.02 ± 0.02	0.05 ± 0.01
East	-0.34 ± 0.04	-0.10 ± 0.03	-0.20 ± 0.02
South	-0.55 ± 0.12	-0.06 ± 0.04	-0.16 ± 0.02
Central	-0.08 ± 0.07	-0.02 ± 0.03	0.03 ± 0.02

Table 4.1 Regional mean 1960 to 1980 linear trend of the 5-year rolling mean annual anomaly in all-sky SSR ($W m^{-2} year^{-1}$) for GEBA, the PPE mean and initial condition ensemble mean when model data is interpolated to GEBA station locations. Linear trends in bold are statistically significant ($p < 0.05$) based on the Mann-Kendall test. The error is the standard error of the estimated trend. For the purpose of significance testing and error calculation, in the results shown in this table the regional mean for each year is calculated prior to trend calculation. In the other figures in this study, the regional mean is calculated following trend calculation.

We now focus on the performance of our PPE members in simulating the observed SSR dimming trend over Europe. Figure 4.3 shows density plots of the 1960 to 1980 SSR trend over European GEBA stations. The regional annual mean trend for GEBA observations is within the range of the PPE, but the majority (14) of PPE members underestimate the dimming trend, with some PPE members even simulating a brightening trend. Figure 4.3 also displays the average SSR trend across the whole European region (rather than just at GEBA stations). This shows that larger deviations of the PPE from the observed SSR trend at GEBA stations correspond to larger differences between the modelled trends averaged over European GEBA stations versus Europe as a whole. PPE members with a smaller divergence between these two averages generally have better model skill. The effects of internal variability and parameter perturbations on SSR spatial variability are conflated, as discussed in the previous paragraph. But, this result raises questions about how representative the SSR trends at a relatively small number of stations are for the whole of Europe.

We further analyse the roles of parameter perturbations and internal variability on the European average of the 1960 to 1980 trend across GEBA stations in Figure 4.4. The initial condition ensembles span 80% of the range of SSR trends in the PPE during the dimming period. This result suggests that the spread in the European mean SSR trend over GEBA stations could largely be due to the

sequence of internal variability simulated by model ensemble members. When averaged over the whole of Europe, both the PPE and initial condition ensembles span a smaller range of SSR trends (Figure C.4). However, both the PPE and initial condition ensemble mean underestimate the SSR trend over Europe (Table 4.1).

We also undertook a seasonal analysis to investigate if the underestimation of regional mean SSR trends was more evident during particular seasons (Figure C.5). In all seasons, the SSR trend is underestimated. The observed trends are always within the range of the PPE, but not within the initial condition ensemble range of HadGEM3-GC3.1-LL. The spread in SSR trends across the PPE is largest in Spring and Summer, when incoming solar radiation at the top of atmosphere is highest, with the largest spread in SSR trends in the initial condition ensemble in Spring.

1960 to 1980 trend in SSR across European GEBA stations

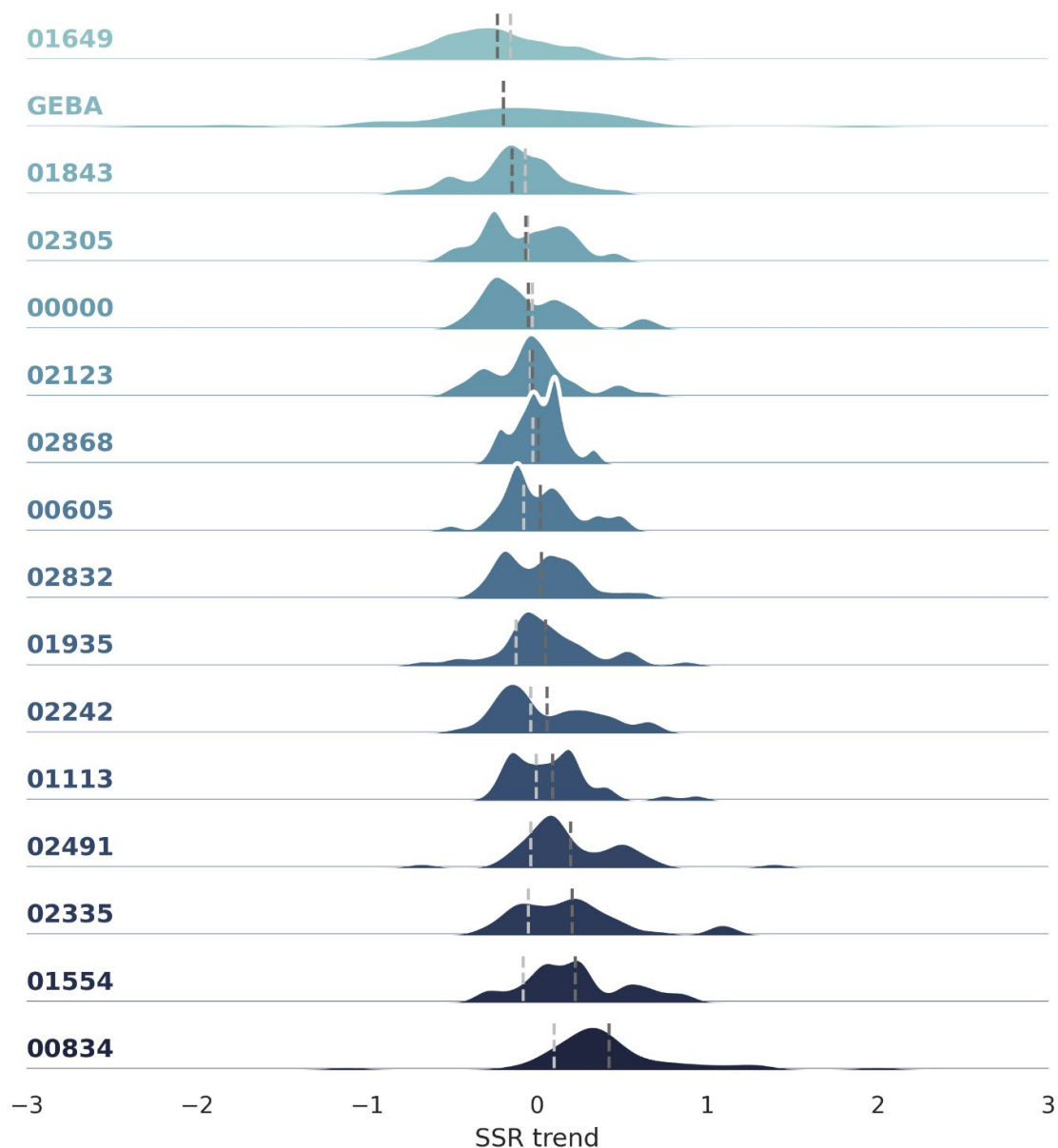


Figure 4.3 Density plots of the trend in the 5-year rolling mean SSR over 1960 to 1980 ($W m^{-2} year^{-1}$) at European GEBA stations. The rows of the plot labelled with numbers “0XXXX” represent PPE members where the model data has been interpolated to GEBA stations. The mean across the GEBA station locations is displayed by the dashed dark grey vertical line in each row, and the regional mean of PPE data over the whole of Europe is displayed with the light grey dashed line. Rows are ordered according to the magnitude of SSR trend at GEBA station locations.

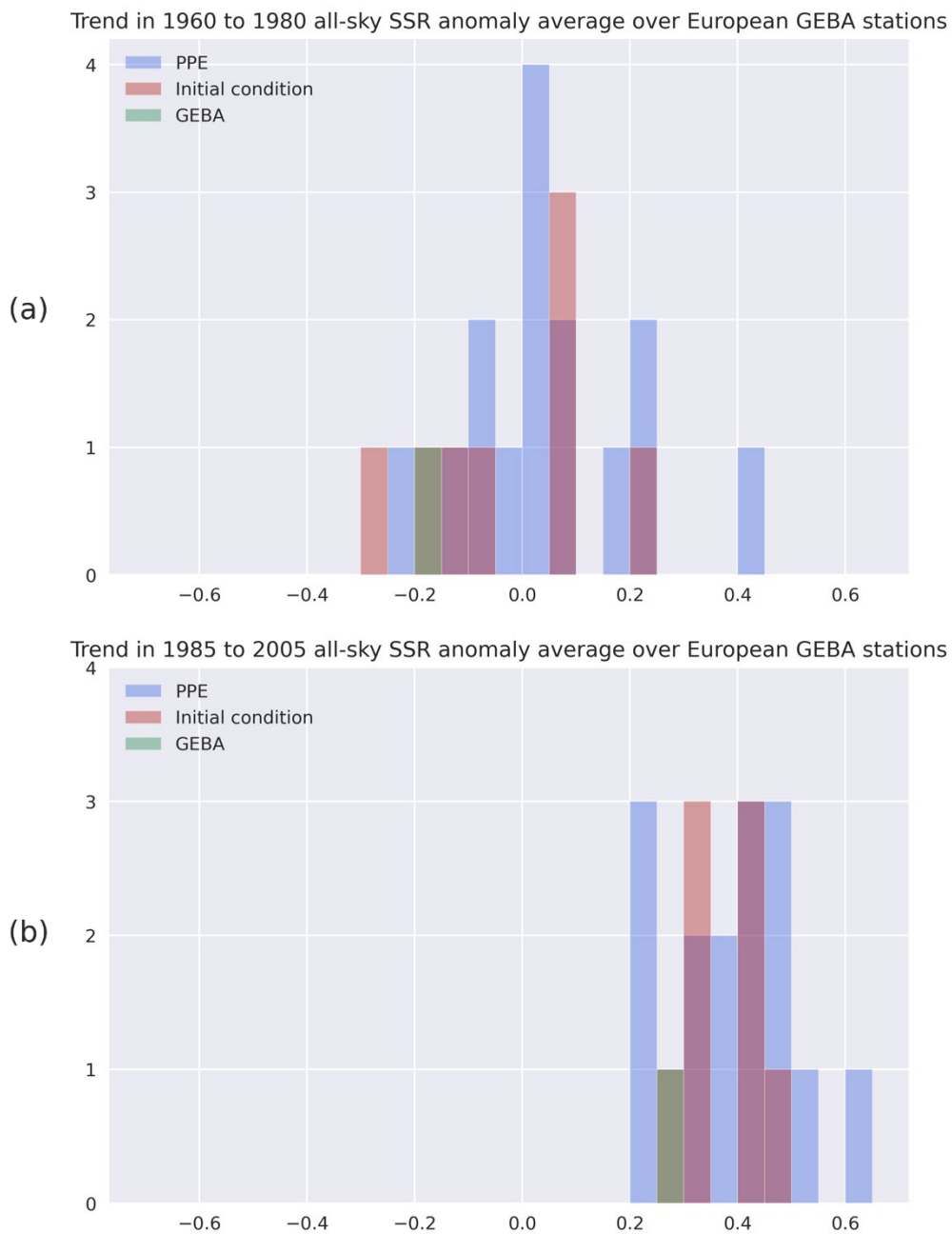


Figure 4.4 Histogram of the trend ($W m^{-2} year^{-1}$) in the five-year rolling mean time series of the annual anomaly in SSR for the average of the European GEBA stations over a) 1960 to 1980 and b) 1985 to 2005.

We next evaluate parametric effects on the performance of our PPE in simulating observed trends in SSR at European GEBA stations. The key model parameters affecting model skill at simulating SSR dimming (and brightening) trends are presented in Table 4.2. In the annual mean, model skill at simulating the dimming trend is correlated with the dry deposition rate of SO₂ (*ps_dry_depvel_so2*). Increasing the removal rate of SO₂ improves model skill. CCN concentrations and consequently aerosol forcing are most sensitive to changing aerosol concentrations when existing aerosol concentrations are low (Carslaw et al., 2013). Hence, aerosol forcing and SSR are likely to be most sensitive to changing the dry deposition rate of SO₂ at the beginning of the dimming period when sulphate burden is lower. Greater dry deposition of SO₂ could therefore weaken aerosol forcing at the beginning of the time period, which would amplify the SSR difference over 1960 to 1980, and improve model skill. Model skill in simulating the annual mean SSR trend is also correlated with parameters that modify the radiative properties of cloud (*dbsdtbs_turb_0*, *two_d_fsd_factor*). Higher values of *dbsdtbs_turb_0* are associated with more mixing of clear and cloudy air, which reduces cloud liquid water content and amount, plus modifies the lifetime of aerosols and precursor gases. A higher value of *dbsdtbs_turb_0* corresponds to reduced model skill here. *Two_d_fsd_factor* modifies the cloud-radiation balance and a higher value of the parameter reduces the outgoing SW radiation, and corresponds to improved model skill.

The parameters affecting model skill at simulating the SSR trend are seasonally dependent. In winter, model skill at simulating SSR changes during the dimming period is correlated with parameters in the convection scheme (*mparwtr*), gravity wave drag that affects wind speed and mean sea level pressure (*gwd_frc*), and land surface properties affecting snow, surface temperature and surface roughness (*rho_snow_fresh*, *dz0v_dh_io*). A parameter in the convection scheme (*ent_fac_dp*) and the cloud-radiation parameter (*two_d_fsd_factor*) are correlated with model skill in Spring, whereas parameters affecting the boundary layer stability (*g0_rp*, *ricrit_rp*) are correlated with model skill in Summer. In Autumn, a parameter in the gravity wave drag scheme (*fbcd*) and cloud microphysics scheme (*c_r_correl*) affect model skill. It is important to note that due to a small sample size these correlations are at best indicative of a parameter

effect on SSR and additional simulations would be needed to further clarify the parameter effects.

	Dimming (1960 to 1980)	Brightening (1985 to 2005)
Annual	dbstdtbs_turb_0= 0.75 two_d_fsd_factor= -0.67 ps_dry_depvel_so2= -0.70	ps_dry_depvel_so2= 0.62
DJF	mparwtr= -0.69 gwd_frc= 0.67 rho_snow_fresh= -0.60 dz0v_dh_io= 0.64	-
MAM	ent_fac_dp= -0.60 two_d_fsd_factor= -0.65	-
JJA	g0_rp= 0.61, ricrit_rp= -0.61	param_cloud_hplus= 0.66
SON	fbcd= 0.70 c_r_correl= 0.74	cca_md_knob, cca_dp_knob= 0.66

Table 4.2 Spearman’s rank correlation coefficient between the trend in all-sky SSR in the given time periods and the perturbed parameters. Only parameters that have $r \geq 0.6$ are shown. The sign of the relationships in the dimming period have been reversed, so that for example, a positive relationship corresponds to decreasing model skill with an increasing parameter value in both time periods (because nRMSE is negative in the dimming period). Parameter descriptions are shown in Table B.1.

4.3.1.2 Clear and Cloudy-Sky SSR

Here we study the clear and cloudy-sky components of all-sky forcing to further elucidate the role of aerosols and clouds in the all-sky SSR trends. The clear and cloudy-sky components of the SSR time series in our PPE is shown in Figure 4.7. In the dimming period, the ensemble mean clear-sky time series appears to closely follow that of all-sky. However, the standard deviation of SSR across the ensemble is much smaller for clear-sky than cloudy-sky. Clear-sky SSR observations are generally not available for GEBA so we have not compared observations across Europe to the model components here. Wild et al. (2021) inferred the time-series of clear-sky SSR for the GEBA station at Potsdam observatory in Germany, one of the GEBA station with longest record. Their study showed that at this observational site the cloud-free atmosphere played a major role in the explanation of the multi-decadal dimming trend. The study concluded that aerosols were likely the major factor in determining the decreasing SSR

trend, as also reasoned in modelling studies (Ruckstuhl and Norris, 2009a; Turnock et al., 2015). In our PPE, the large spread amongst ensemble member in all-sky and cloudy-sky, coupled with the influence of parameters relating to clouds and cloud radiation on model performance, emphasises the importance of cloud effects on SSR trends across Europe in the dimming period.

The 1960 to 1980 clear-sky SSR trend in the PPE (Figure C.7) shows a dipole-like pattern with dimming over most of Eastern and Central Europe, plus brightening over the British Isles. The regional clear-sky SSR trend is therefore in agreement with the all-sky GEBA observations that showed the largest dimming in the Eastern, Southern and Central European regions. Also, Folini and Wild (2011) divided Europe into nine regions and showed a stronger dimming trend in Eastern Europe than over the British Isles and mid-Europe, in line with our clear-sky results. Their analysis suggested that regional clear-sky SSR time series are likely driven by regional emissions. Hence, the dipole of clear-sky SSR trend in our PPE likely shows the aerosol-radiation interactions associated with anthropogenic aerosol emissions declining over regions of Western Europe whilst still increasing over Mainland and Eastern Europe. The clear emergence of these trends in the PPE in the clear-sky demonstrates how cloud and circulation variability associated with internal variability and parametric effects could mask an aerosol influence on all-sky SSR trends in individual ensemble members, leading to the underestimation of the regional all-sky SSR trends.

4.3.2 Solar Brightening Period: 1985 to 2005

4.3.2.1 All-Sky SSR

We now examine the SSR trends across Europe over the 1985 to 2005 brightening period when anthropogenic aerosol emissions were declining in Europe and North America. Figure 4.5 shows the trend in all-sky SSR over Europe across our PPE with GEBA observations overlaid. The PPE mean and individual ensemble members show widespread brightening over Europe during this time period, which is of larger magnitude than the dimming during 1960 to 1980. Spatially, there is less variation in the SSR trend across Europe during the brightening period than there was in the dimming period, though the magnitude of the trend differs between ensemble members by around $1 \text{ W m}^{-2} \text{ year}^{-1}$ over

large parts of the continent. Table 4.3 shows the PPE mean overestimates the observed brightening trend in most European regions.

Trend in 1985 to 2005 all-sky SSR anomaly

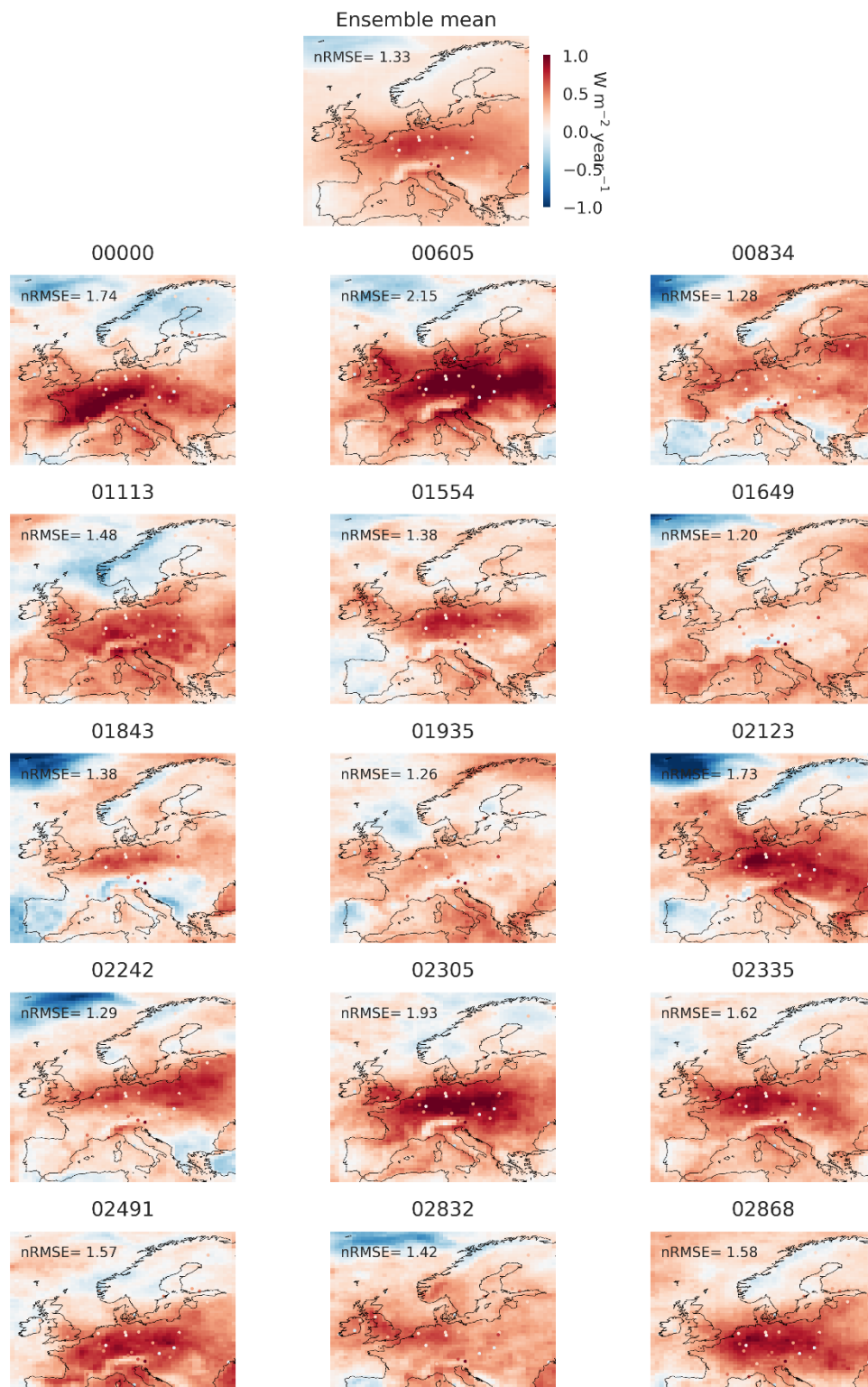


Figure 4.5 1985 to 2005 linear trend of the 5-year rolling mean annual anomaly (against a 1985 to 2005 base period) in all sky SSR ($W m^{-2} year^{-1}$) across Europe. GEBA observations are overlaid in circles. The ensemble mean is shown in top left of the plot, followed by the individual ensemble members. The normalised RMSE is shown in the top left of each plot.

Figure 4.6 shows density plots of the 1985 to 2005 SSR trend over European GEBA stations and each ensemble member in the PPE. As was the case in the dimming period, the trend over GEBA stations is within the range of the PPE. Compared to observations, three ensemble members simulate a weaker brightening trend, and twelve ensemble members simulate a stronger brightening trend for the European mean averaged over GEBA stations. Hence our PPE members tend to overestimate the brightening trend over Europe during 1985 to 2005. As PPE members simulate more brightening, there is a larger divergence between the European mean over GEBA stations and the European mean over the whole region, with the European mean over the whole region tending to be closer to the observed. This results shows that in both dimming and brightening periods, limited SSR station coverage could cause errors in evaluations of model performance.

The histogram in Figure 4.4 shows the SSR trend averaged over GEBA station locations in the PPE, initial condition ensemble and observations. The spread in SSR trend in the PPE during the brightening period is less than in the dimming period. The relative spread in SSR trends due to internal variability is also less, with the initial condition ensemble covering only 42% of the spread of the PPE. Hence, our perturbed parameters are likely having a substantial influence on the range of modelled SSR trends in the brightening period. The seasonal analysis shown in Figure C.6 also supports this conclusion. Although our PPE tends to overestimate the SSR trend in the brightening period, the absolute value of the nRMSE across the PPE is lower in the brightening period than in the dimming period. This suggests our model better simulates the increase in SSR trend due to reductions in anthropogenic aerosol emissions across Europe than the earlier SSR trend due to increases in anthropogenic aerosol emissions.

1985 to 2005 trend in SSR across European GEBA stations

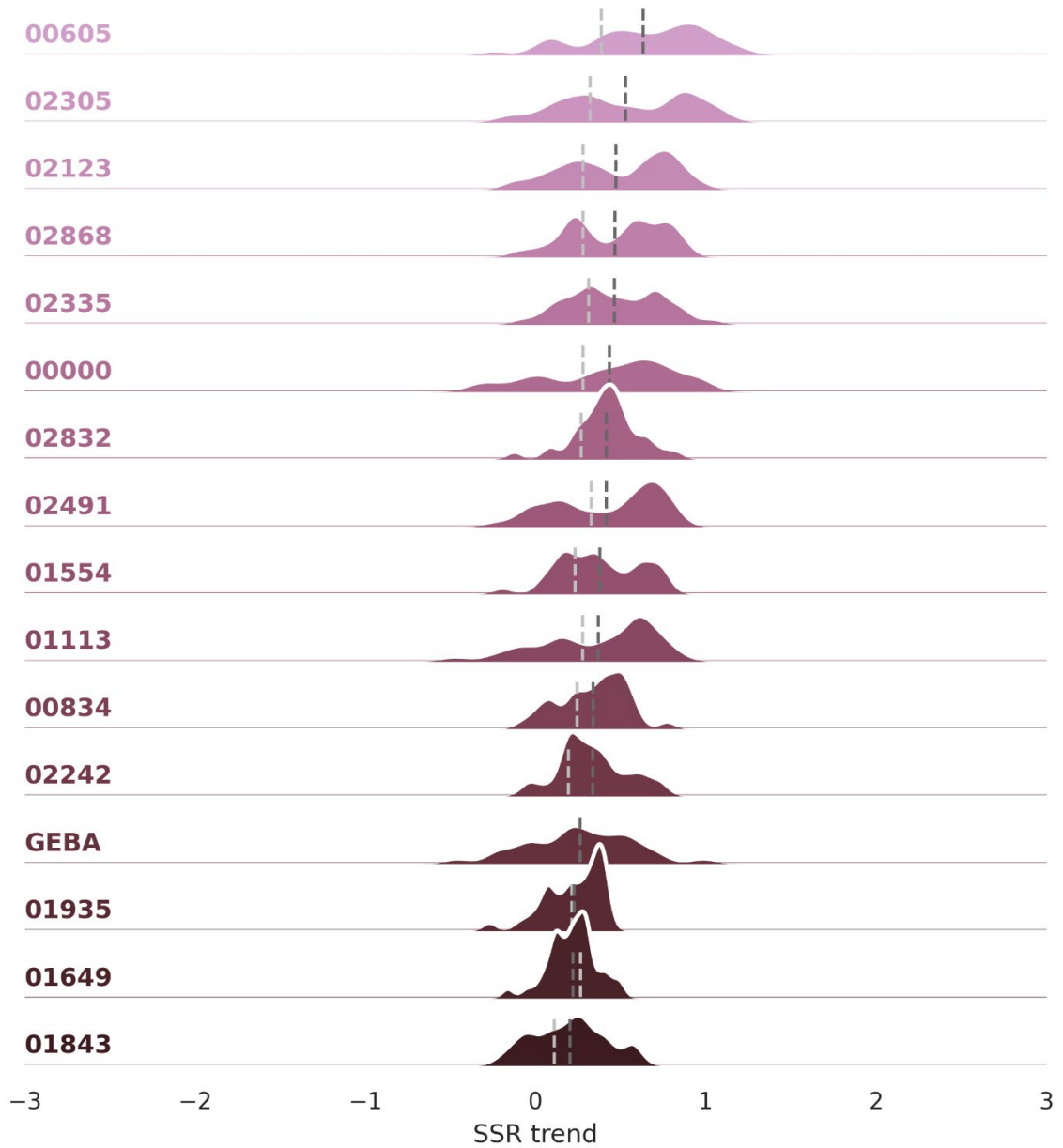


Figure 4.6 Density plots of the trend in the 5-year rolling mean SSR over 1960 to 1980 (W m^{-2}) at European GEBA stations. The rows of the plot labelled with numbers “0XXXX” represent PPE members where the model data has been interpolated to GEBA stations. The regional mean across the GEBA station locations is displayed by the dashed light grey vertical line in each row, and the regional mean of PPE data over the whole of Europe is displayed with the light grey dashed line. Rows are ordered according to the magnitude of SSR trend at GEBA station locations.

	GEBA	PPE mean	Initial condition ensemble mean
Europe	0.27 ± 0.03	0.40 ± 0.03	0.38 ± 0.02
North	0.31 ± 0.04	0.16 ± 0.02	0.20 ± 0.02
North-west	0.04 ± 0.07	0.24 ± 0.03	0.28 ± 0.02
East	0.33 ± 0.06	0.53 ± 0.04	0.50 ± 0.02
South	0.33 ± 0.04	0.34 ± 0.04	0.39 ± 0.04
Central	0.34 ± 0.07	0.58 ± 0.03	0.49 ± 0.01

Table 4.3 Regional mean 1985 to 2005 linear trend of the 5-year rolling mean annual anomaly in all-sky SSR ($W m^{-2} year^{-1}$) for GEBA, the PPE mean and initial condition ensemble mean when model data is interpolated to GEBA station locations. Trends in bold are statistically significant ($p < 0.05$) based on the Mann-Kendall test. The error is the standard error of the estimated trend. For the purpose of significance testing and error calculation, in the results shown in this table the regional mean for each year is calculated prior to trend calculation. In the other figures in this study, the regional mean is calculated following trend calculation.

We next investigate if any of the 47 perturbed parameters have a relationship with the model skill simulating SSR trends over Europe during 1985 to 2005. Table 4.2 shows the parameters that have a Spearman's correlation coefficient of ≥ 0.6 with the nRMSE for the SSR at GEBA stations over Europe. In the annual mean, the dry deposition of SO_2 (`ps_drydep_level`) once again is correlated with the model skill in simulating the brightening trend. Opposite to the dimming period, increasing the removal rate of SO_2 reduces model skill. The opposite relationship between time periods is because, through the mechanisms described in the Section 4.3.1 with regard to dimming, aerosol forcing will be more sensitive to dry deposition of SO_2 through its influence on aerosol concentrations in the period with lower emissions. Increasing the dry deposition of SO_2 would therefore have most effect towards 2005 in the brightening period, amplifying the SSR difference over 1985 to 2005, and reducing model skill since the model already overestimates the brightening trend. Whereas, in the dimming period the model underestimates SSR trends so amplifying the SSR difference between the start and end point of the time period improves model skill.

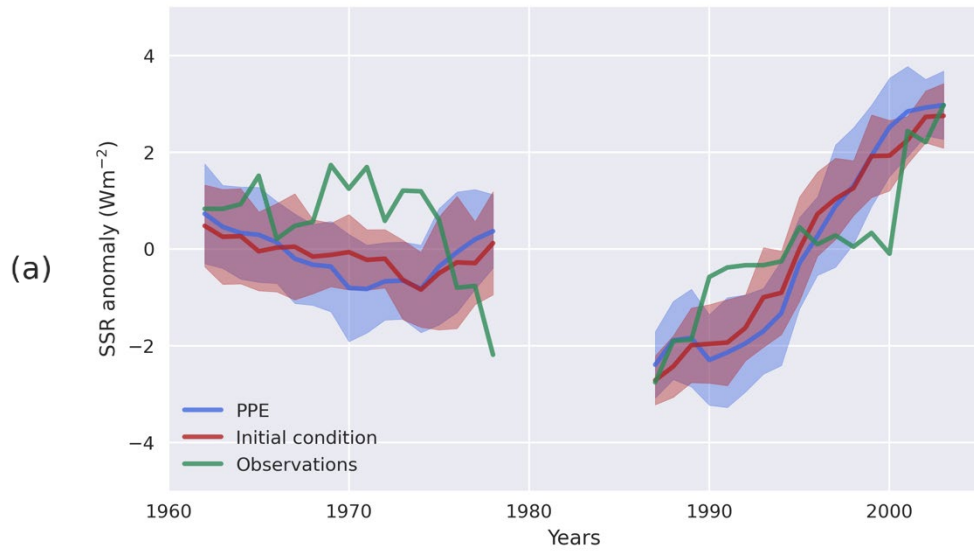
Seasonally, there are no parameters that have a strong correlation with the nRMSE in Winter or Spring. In Summer, there is a relationship with the pH of cloud droplets. In our PPE, ensemble members with higher pH are associated with better simulating the SSR brightening trend. Increasing pH leads to faster

SO₂ oxidation by ozone in cloud water and consequently more SO₄ production over polluted regions (Murphy et al., 2018; Turnock et al., 2019). In previous studies the pH of cloud droplets has a greater effect on aerosol concentrations in Northern Hemisphere winter due to larger SO₂ concentrations and more limited oxidants (Manktelow et al., 2007; Turnock et al., 2019) whereas in this study the pH of cloud droplets most clearly influences model skill in Summer. Yet, our result agrees with Turnock et al. (2019) who showed, a higher pH during the 2000s gave better agreement with observations over Europe. In Autumn there is a correlation between nRMSE and convective core radiative effects (cca_md_knob, cca_dp_knob). Perturbed parameters relating to cloud variability, radiation and atmospheric circulation have much less of an influence on model performance in the brightening period than in the dimming period. Again, these relationships are only indicative of our parametric effect and further simulations using a larger PPE of transient simulations would be needed to confirm the relative importance of these processes.

4.3.2.2 Clear and Cloudy-Sky SSR

Figure 4.7 shows the time series of clear, cloudy and all-sky components of the SSR trends for the mean of European GEBA stations, calculated using PPE data. It is clear that the brightening all-sky trend is mainly driven by increasing clear-sky SSR, with cloudy-sky SSR slightly declining over the same time period. In our PPE mean, there is also a decrease in cloud fraction over Europe during 1985 to 2005 (although some individual ensemble members show an increase; Figure C.10) which could increase sulphate residence time (Bellouin et al., 2011) and contribute to a stronger role of aerosol direct effects in the all-sky brightening trend (Folini and Wild, 2011). The dominance of the clear-sky SSR trend could be one of the reasons why there is less of an impact from internal variability in the form of cloud variability and parametric effects related to clouds in the brightening period, in comparison to the dimming period.

Ensemble mean all-sky SSR anomaly at European GEBA sites
(1960 to 2005, 1980 to 2000 base period, 5-year rolling mean)



Ensemble mean all-sky, clear-sky and cloudy-sky at European GEBA sites
(1960 to 80, 1985 to 2005 base period, 5-year rolling mean)

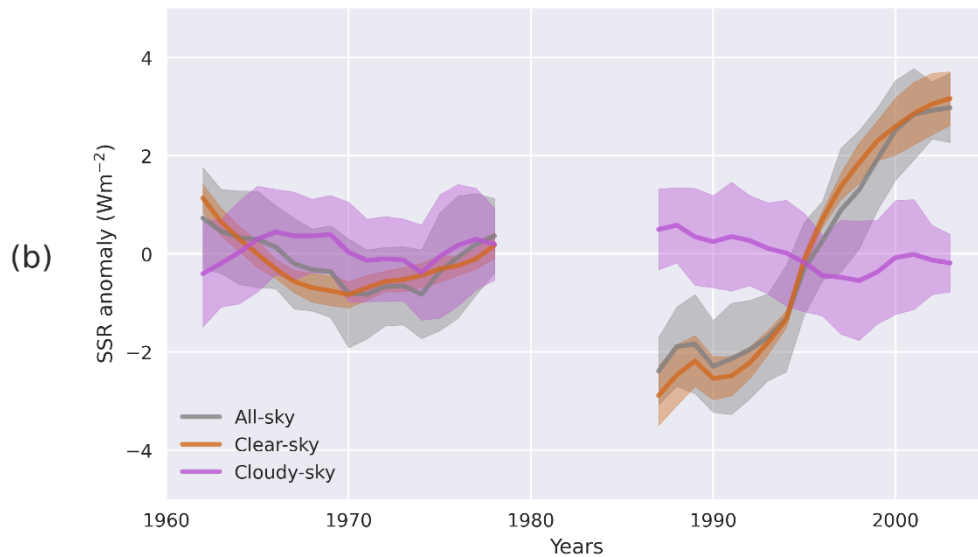


Figure 4.7 a): 5-year rolling mean time series of the annual anomaly (against 1960 to 1985 and 1985 to 2005 base period) in SSR ($W m^{-2}$) for the average of European GEBA stations (green), the nearest model grid boxes to stations in the PPE (blue), and nearest model grid boxes to stations from HadGEM3GC-3.1 initial condition ensemble (red). The shading around each time series shows the spread in the ensemble mean for \pm the ensemble standard deviation b): PPE mean 5-year rolling mean time series of the annual anomaly (against 1960 to 1985 and 1985 to 2005 base period) in SSR ($W m^{-2}$) for all-sky (blue), clear-sky (pink) and cloudy-sky (green) for the nearest model grid boxes to GEBA stations. The shading around each time series shows the ensemble mean \pm the ensemble standard deviation.

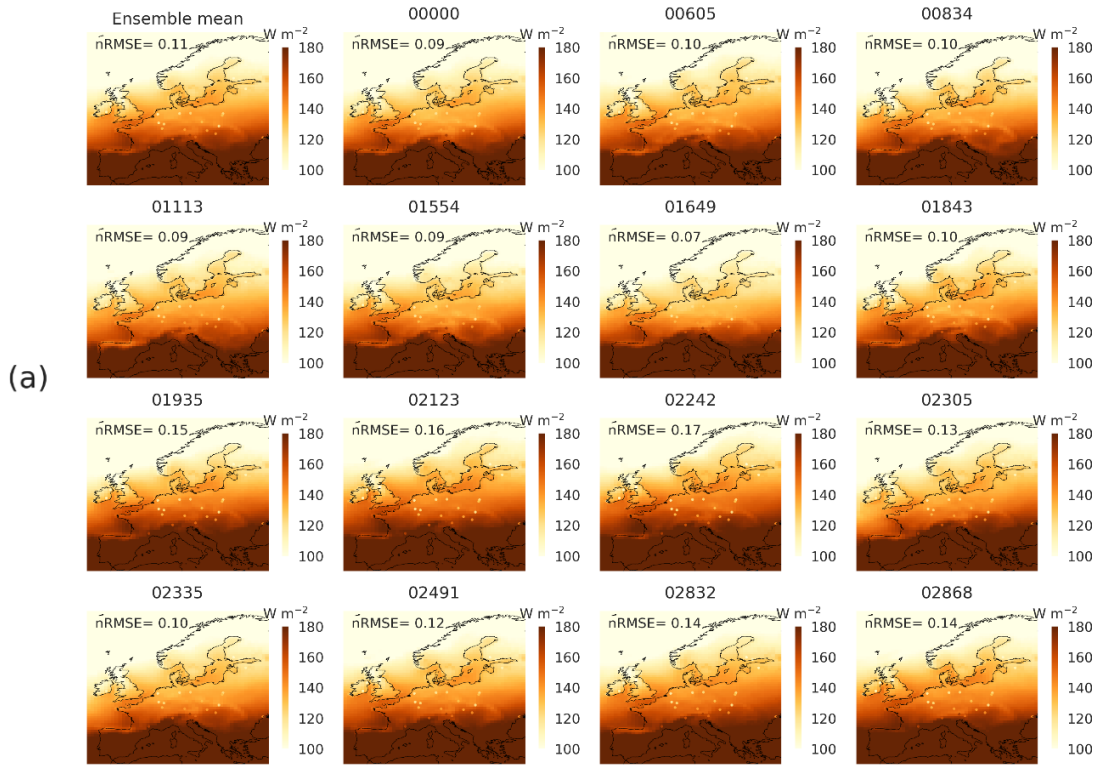
4.3.3 Multi-Year Average: 2005 to 2009

In this section we examine the multi-year SSR average over 2005 to 2009. Using this time period enables us to expand our analysis from the 15 transient coupled ocean-atmosphere simulations to the corresponding 15 atmosphere-only simulations, and a wider 518 atmosphere-only simulations that were used in filtering PPE members for diversity and plausibility. The use of multiple types of simulations allows us to explore the parametric effect on climatological SSR across sample sizes.

Figure 4.8 shows the multi-year average SSR for the coupled ocean-atmosphere simulations and their corresponding atmosphere-only simulations. The multi-year average SSR over Europe is visually similar between the experiment types and the ensemble members. Both simulation types slightly overestimate the 2005 to 2009 average SSR. However, the nRMSE is lower in the multi-year average than the multi-decadal time periods examined in this study, suggesting the PPE performs better in simulating climatological SSR rather than trends.

During 2005 to 2009 the 15-member coupled PPE has correlations between parameters and nRMSE seasonally but not in the annual mean. In Winter, there is a relationship between the model skill simulating SSR and parameters in the boundary layer (`dec_thresh_cld`, `dec_thresh_cloud2cu`, `forced_cub_fab`) and cloud microphysics model schemes (`ai`). Model skill in Spring appears to be most susceptible to parametric influence, being correlated with parameters in the convection (`ent_fac_md`), boundary layer (`ricrit_rp`, `par_mezcla`, `lambda_min`) and aerosol (`ps_anth_so2_emiss`) model schemes. In Autumn, parameters related to the boundary layer (`g0_rp`, `ricrit_rp`) are correlated with model skill. In comparison, the 15-member atmosphere-only PPE SSR model skill is only correlated in Spring with parameters related to entrainment (`ent_fac_dp`) and the density of snow (`rho_snow_fresh`). Most of these parametric effects on model skill simulating the 2005 to 2009 average SSR are related to physical atmosphere parameters, suggesting model performance in simulating climatological mean SSR over Europe is related to cloudy-sky SSR fluxes rather than clear-sky fluxes (which we would expect to have a greater influence from aerosol processes).

Coupled ocean-atmosphere 2005 to 2009 average all-sky SSR



Atmosphere-only 2005 to 2009 average all-sky SSR

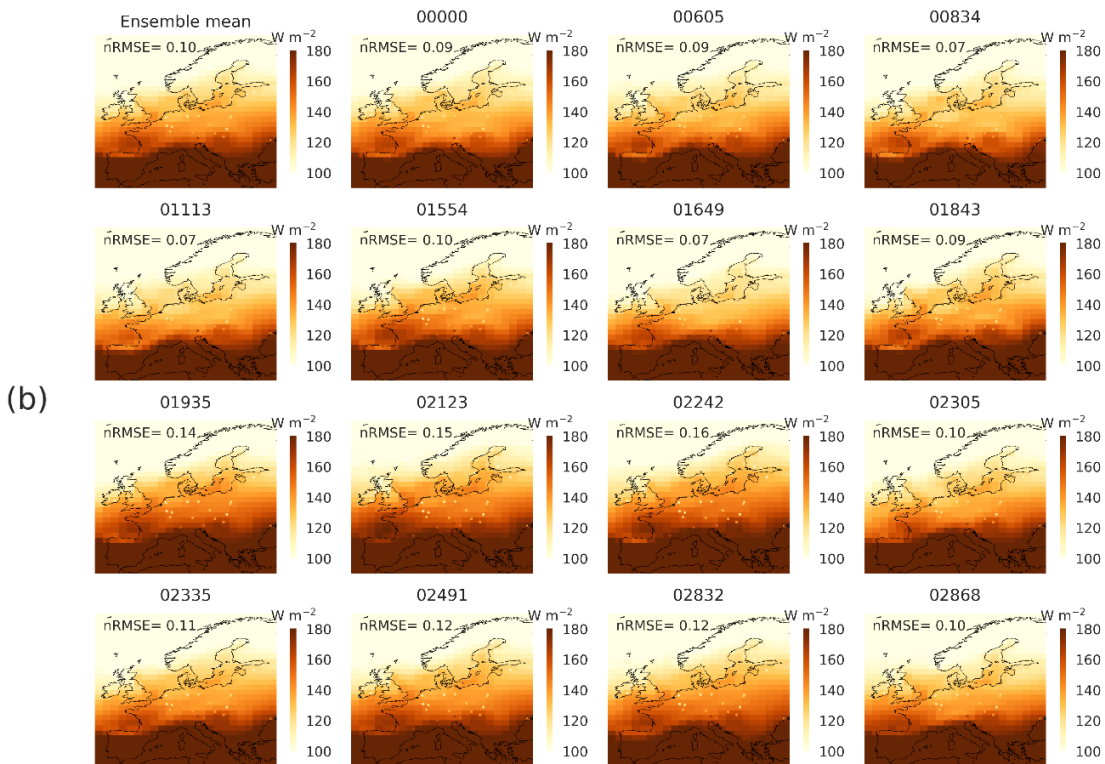


Figure 4.8 2005 to 2009 average in all sky SSR ($W m^{-2}$) across Europe for a) coupled ocean-atmosphere simulations and b) atmosphere-only simulations. 35 GEBA observations are overlaid in circles in circles. The ensemble mean is shown in top left of the plot, followed by the individual ensemble members. The normalised RMSE shown in the top left of each plot.

	Coupled ocean-atmosphere: 15 PPE members	Atmosphere-only: 15 PPE members	Atmosphere-only: 518 PPE members
Annual	-	-	-
DJF	dec_thres_cloud, dec_thresh_cu= 0.74 forced_cu_fac= 0.63 ai= 0.79	-	-
MAM	ent_fac_md= -0.66 ricrit_rp= 0.70 par_mezcla= -0.66 lambda_min_rp= -0.66 ps_anth_so2_emiss= -0.65	ent_fac_dp=-0.61 rho_snow_fresh= 0.68	-
JJA	-	-	-
SON	g0_rp= -0.77, ricrit_rp= 0.77	-	-

Table 4.4 Table shows Spearman's rank correlation coefficient between the 2005 to 2009 average in all-sky SSR in the given experiment types and the perturbed parameters. Only parameters that have $r \Rightarrow 0.6$ are shown. Parameter descriptions are shown in Table B.1.

Our results show differences in indications of the strength of parameter relationships in model skill simulating 5-year average SSR between our atmosphere-only simulations and coupled ocean-atmosphere simulations. The coupling of the atmosphere to the ocean appears to enhance the parametric effects on SSR. The parameter relationships in the 15-member atmosphere-only PPE do not exist in the 518-member atmosphere-only PPE, indicating the parameter relationship could be inflated by a small sample size, occur by chance, or be affected by the filtering processes that were used in selecting 15 diverse and plausible ensemble members from 518.

4.3.4 Surface Solar Radiation Trends as a Constraint on Anthropogenic Aerosol ERF

The trend in SSR over Europe has been proposed as an emergent constraint with potential to reduce the persistent uncertainty in aerosol ERF. Cherian et al. (2014) showed that increasing surface solar radiation over Europe during 1990 to 2005 scales well with regional and global mean pre-industrial to present-day anthropogenic aerosol ERF. Our PPE has time slice experiments for 1860, 1975 and 2005, designed so we can calculate aerosol ERF estimates for each PPE member in the transient coupled ocean-atmosphere simulations. We can therefore investigate if the relationship outlined in Cherian et al. (2014) holds within our PPE.

The 1860 to 1975 aerosol ERF is affected by increasing aerosol emissions over Europe, whereas the 1975 to 2005 aerosol ERF is affected by a decline in aerosol emissions over Europe. Gridded anthropogenic aerosol ERF for each of these time periods is shown in Figure C.11-C.12. To maintain consistency with the time periods of the anthropogenic aerosol ERF we first compare the trend in European mean SSR over 1945 to 1975 to the 1860 to 1975 European mean aerosol ERF. We also compare the SSR trend over 1975 to 2005 to the 1975 to 2005 European and global mean anthropogenic aerosol ERF. Then, to maintain consistency with the time periods used in Section 4.3.1 and 4.3.2, we compare the trend in European mean SSR over 1960 to 1980 to the 1860 to 1975 European mean aerosol ERF, and compare the SSR trend over 1985 to 2005 to the 1975 to 2005 anthropogenic aerosol ERF.

Over 1945 to 1975, ensemble members that have a stronger (more negative) anthropogenic aerosol ERF generally have a stronger dimming trend over Europe (Figure C.13). As the dimming trend was underestimated in our PPE by most ensemble members, this relationship indicates that aerosol ERF due to increasing emissions over Europe may also be underestimated by our PPE. Over 1975 to 2005, ensemble members that have a stronger aerosol ERF (more positive) generally simulate a greater brightening trend. Therefore, in contrast to the dimming period, this relationship indicates that aerosol ERF in response to emission reductions over Europe is overestimated in our PPE.

Calculating the European mean SSR trend over only GEBA stations weakens these relationships. There is no relationship between the European station mean

SSR trend and global mean anthropogenic aerosol ERF in our PPE. There is also no indication of a relationship between anthropogenic aerosol ERF and the SSR trend over 1960 to 1980 or 1985 to 2005 time periods (Figure C.14), which we examined in Section 4.3.1 and 4.3.2.

Our results therefore somewhat support those of Cherian et al. (2014) who showed surface brightening trends over Europe are related to European mean anthropogenic aerosol ERF in CMIP5 models. However, we find a time dependence of the relationship between European mean SSR trends and European mean aerosol ERF that was not explored in Cherian et al. (2014). In contrast to Cherian et al. (2014) we found no relationship between surface brightening trends over Europe and global mean anthropogenic aerosol ERF. The time dependence of the relationship between anthropogenic aerosol ERF and SSR trends does not seem to be due to the effect of internal variability being more evident when a trend is calculated over a short time frame as the relative spread in SSR trends due to internal variability is larger over 1975 to 2005 than 1985 to 2005. The time period dependence of the relationship is likely related to the representativeness of the aerosol ERF to other time periods, or because the 1945 to 1975 and 1975 to 2005 time periods align better to capture the evolving aerosol emissions and the transition between dimming and brightening in our PPE.

4.4 Discussion

Aerosol ERF is the largest source of uncertainty in the radiative forcing of the Earth system over the industrial period (Myhre et al. 2013; Bellouin et al. 2020). The uncertainty in historic forcing translates into uncertainty in climate projections. So, to improve climate projections the uncertainty in aerosol radiative forcing needs to be constrained. However, the uncertainty in aerosol radiative forcing over the industrial period remains difficult to reduce for multiple reasons. Firstly, it depends on a variety of physical processes, some of which are difficult to constrain using present-day measurements (Carslaw et al., 2013). Secondly, there is a temporal and spatial lack of measurements to compare model output to, so assumptions need to be made about the representativeness of sparse measurements (Christensen et al., 2022). Finally, causes of uncertainty can vary spatially and temporally (Gryspeerd et al., 2017; McCoy et al., 2017; Regayre et al., 2015), so reducing aerosol forcing uncertainty may require a combination of

regional constraints over multiple seasons and time periods. In this study we used observations from GEBA to evaluate the performance of a PPE of HadGEM3-GC3.05 in simulating long-term trends and climatological averages of SSR over Europe, and evaluate the usefulness of SSR trends as a constraint of aerosol ERF.

Our PPE members underestimate the 1960 to 1980 dimming trend over the European station mean in comparison to GEBA observations. CMIP5 models also show weak and statistically insignificant trends in SSR during the global dimming period in comparison to GEBA observations despite reproducing the temperature trend over the same period (Allen et al., 2013b; Storelvmo et al., 2018). More recent analysis using eight Earth System Models (ESMs) submitted to CMIP6 shows that globally the discrepancy between observed and modelled SSR trends persists in CMIP6, however whilst there is a large discrepancy between the observed and modelled trend in SSR over Asia, Europe is better represented (Onsum Moseid et al., 2020). Our PPE has better model skill simulating the brightening period than the dimming period, but many PPE members overestimate the 1985 to 2005 brightening over Europe. In contrast to our results, the CMIP5 ensemble mean underestimates the observed 1987 to 2007 trend in SSR, with just two models overestimating the brightening trend (Allen et al., 2013). Our study has investigated potential causes of the underestimation of dimming and overestimation of brightening in the PPE.

Spatially, there are differences in magnitude and direction of the 1960 to 1980 all-sky SSR trend across Europe. The GEBA observations show a large statistically significant all-sky dimming trend in Eastern, Southern and Central Europe which is underestimated by the PPE. Across the PPE, the spatial all-sky SSR dimming trend is correlated with cloud properties, water vapour and surface temperature. The clear-sky SSR trend over Europe exhibits a clear view of dimming over Central and Western Europe across the PPE, suggesting aerosol influence could be somewhat obscured by clouds in the all-sky SSR dimming trend. The spread in the regional mean all-sky SSR trend is much greater than in the clear-sky. Analysis focusing on smaller European regions using high-resolution PPE experiments would provide additional information about such regional evolution of aerosol radiative effects and cloudiness across Europe. In comparison, in the brightening period, there is less spatial variability across

Europe with both the observations and the PPE simulating statistically significantly brightening trends across most regions which are overestimated by the PPE. The all-sky SSR brightening trend is driven by the clear-sky SSR trend. Overall, these results suggest cloudiness and cloud adjustments influence SSR trends across Europe in the 1960 to 1980 period. Whereas there appears to be a greater dominance of an aerosol-driven all-sky SSR trend in the 1985 to 2005 period with less of an effect due to cloud variability. This is also likely a reason why the model has better skill at simulating SSR trends during the brightening time period. Analysis focusing on the smaller European regions using high-resolution PPE experiments would provide additional information about such regional evolution of aerosol radiative effects and cloudiness across Europe.

Our results in both dimming and brightening periods show that the European mean SSR trends are generally closer to the observed when averaged over the whole European region rather than over just GEBA stations. The CMIP5 analysis in Allen et al. (2013) used 38 European GEBA stations (similar to the number used in our analysis), whereas the CMIP6 analysis in Moseid et al. (2020) used a machine learning gap-filled dataset that enabled 503 European GEBA stations to be used. Therefore, some of the differences in the model-observation comparisons between generations of CMIP could also be due to differences in how the observations were used. Additional analysis looking into the differences in model-observation comparisons using the Sanchez-Lorenzo GEBA dataset as used in this study in comparison to the larger gap-filled dataset used in Moseid et al. (2020) and Storelvmo et al. (2018) would be informative to verify the effect of more observational data.

In the dimming period, a large proportion (~80%) of the range in European station mean all-sky SSR trends across the PPE is equivalent to the range due to internal variability alone, suggesting internal variability likely plays a large role in generating the spread in SSR trends across the PPE. The observed trend in the dimming period is within the range of both the PPE and initial condition ensemble members but underestimated by most ensemble members. In comparison, the range in European station mean SSR trends covered by the initial condition ensemble is smaller in the brightening period (~42% of the spread of the PPE) suggesting internal variability plays a smaller role and the perturbed parameters generate a larger proportion of the ensemble spread in the brightening period.

Of the possible reasons for model bias in simulating SSR trends over Europe discussed above, our PPE gives us an insight into which model parameters and processes may contribute towards the model skill in simulating SSR trends over Europe when 39 European GEBA stations are used. We identified which processes contribute to the underestimation of dimming and overestimation of brightening in our PPE. In both the dimming and brightening period, the dry deposition of SO₂ is strongly correlated with the model skill at simulating annual mean SSR trends over Europe. This result matches other studies that have suggested the underestimation of global dimming is due to the treatment of aerosol processes in the translation of aerosol emissions to forcing, including simulated SO₄ burdens (Moseid et al., 2020; Storelvmo et al., 2018). In our PPE, a higher dry deposition rate of SO₂ is associated with improved model skill at simulating the annual mean SSR trends in the dimming period, but worsened model skill in the brightening period. Aerosol radiative forcing is most sensitive to changing aerosol concentrations when background aerosol concentrations are lower (Carslaw et al., 2013). Therefore, aerosol forcing would be most sensitive to a reduction in sulphate burden through an increased dry deposition rate at the least polluted points in our analysis (towards 1960 or 2005). A weaker aerosol radiative flux at the start and end points of our time series would therefore amplify the SSR trend due to both aerosol emission increases and reductions. This SSR trend amplification translates to improved model skill in the dimming period (because the model underestimates dimming) but worsened model skill in the brightening period (because the model overestimated brightening).

The model skill at simulating the annual mean SSR trend in the dimming period is also correlated with a parameter controlling the radiative properties of clouds and a parameter affecting the cloud-radiation interactions, which is in line with our results that cloud properties have a greater influence on SSR trends over Europe in the dimming periods. Our analysis further suggests that the parameter influence on model skill simulating SSR trends over Europe is dependent on the time period, season, degree of ocean coupling and ensemble size.

We analysed the relationship between SSR trends and anthropogenic aerosol ERF in our PPE. During the 1960 to 1980 and 1985 to 2005 period, we found no relationship between the magnitude of aerosol ERF and SSR trends. However, if we use a time period for SSR trend calculation that is more closely aligned to the

aerosol ERF experiments (1945 to 1975 and 1975 to 2005), a relationship emerges with European mean aerosol ERF. PPE members with a stronger anthropogenic aerosol ERF (more negative for 1860 to 1975 and more positive with for 1975 to 2005) are associated with stronger all-sky SSR trends.

The model variants most consistent with observed SSR trends over the dimming period have stronger aerosol forcing over Europe when anthropogenic aerosol emissions were increasing. However, during 1960 to 2000, PPE members are at the cooler end of the CMIP5 temperature range, likely due to strong anthropogenic aerosol forcing (Murphy et al., 2018). In the brightening period, the overestimation of brightening is most prominent in model variants with stronger (more positive) aerosol ERF over Europe when anthropogenic aerosol emissions were declining. These results suggest the usefulness of SSR trends as an emergent constraint on anthropogenic aerosol ERF needs to be treated with caution. For example, the observed SSR trend could provide a constraint toward stronger (more negative) aerosol ERF values over Europe when anthropogenic aerosols were increasing, but weaker (less positive) aerosol ERF values for declining aerosol emissions. There could also be a spatial dependence of the relationship as there is no correlation between SSR trends over Europe and global mean anthropogenic aerosol ERF. More broadly, using a small sample size of models can inflate emergent relationships (e.g. Carslaw et al., 2018; Johnson et al., 2018) and finding a handful of ensemble members that correlate well with observations does not necessarily reduce the underlying causes of uncertainty, and thus would not improve climate projections (Ghan et al., 2016). Constraint using a large number of model variants (i.e. thousands that can be predicted using model emulation) to identify plausible parts of model parameter space or using observable relationships of underlying processes that affect aerosol ERF are approaches that could address the limitations of emergent constraints (e.g. Ghan et al., 2016; Johnson et al., 2018).

4.5 Conclusion

Our study shows the HadGEM-GC3.05 PPE underestimates the solar dimming trend over Europe during 1960 to 1980, but overestimates the brightening trend in 1985 to 2005. Our results support other studies that show the deviance of the model time evolution of SSR trends compared to the observed is due to the translation of aerosol emissions to aerosol radiative forcing, but there is also a

clear effect of clouds over Europe in the dimming period. The analysis suggests caution is needed when extrapolating parameter interactions or model constraints between time periods, trends versus climatological means, simulations with different degrees of atmosphere-ocean coupling, and sample size. This study is limited by the small sample size of the transient coupled ocean-atmosphere PPE that means robust statistical analyses to identify parametric effects on SSR trends cannot be performed. Hence, future studies to verify the conclusions discussed in this analysis are needed.

References

- Allen, R. J., Norris, J. R. and Wild, M.: Evaluation of multidecadal variability in CMIP5 surface solar radiation and inferred underestimation of aerosol direct effects over Europe, China, Japan, and India, *J. Geophys. Res. Atmos.*, 118(12), 6311–6336, doi:10.1002/jgrd.50426, 2013.
- Andreae, M. O., Jones, C. D. and Cox, P. M.: Strong present-day aerosol cooling implies a hot future, *Nature*, 435(7046), 1187–1190, doi:10.1038/nature03671, 2005.
- Andrews, M. B., Ridley, J. K., Wood, R. A., Andrews, T., Blockley, E. W., Booth, B., Burke, E., Dittus, A. J., Florek, P., Gray, L. J., Haddad, S., Hardiman, S. C., Hermanson, L., Hodson, D., Hogan, E., Jones, G. S., Knight, J. R., Kuhlbrodt, T., Misios, S., Mizielinski, M. S., Ringer, M. A., Robson, J., and Sutton, R. T.: Historical simulations with HadGEM3-GC3.1 for CMIP6, *J. Adv. Model. Earth Syst.*, 12, e2019MS001995, doi:10.1029/2019MS001995, 2020.
- Antón, M. and Mateos, D.: Shortwave radiative forcing due to long-term changes of total ozone column over the Iberian Peninsula, *Atmos. Environ.*, 81, 532–537, doi:10.1016/j.atmosenv.2013.09.047, 2013.
- Aparicio, A. J. P., Gallego, M. C., Antón, M. and Vaquero, J. M.: Relationship between solar activity and direct solar irradiance in Madrid (1910–1929), *Atmos. Res.*, 235, 104766, doi:10.1016/j.atmosres.2019.104766, 2020.
- Augustine, J. A. and Dutton, E. G.: Variability of the surface radiation budget over the United States from 1996 through 2011 from high-quality measurements, *J. Geophys. Res. Atmos.*, 118(1), 43–53, doi:10.1029/2012JD018551, 2013.
- Bellouin, N., Rae, J., Jones, A., Johnson, C., Haywood, J. and Boucher, O.: Aerosol forcing in the Climate Model Intercomparison Project (CMIP5) simulations by HadGEM2-ES and the role of ammonium nitrate, *J. Geophys. Res.*, 116(D20), D20206, doi:10.1029/2011JD016074, 2011.
- Carslaw, K., Lee, L., Regayre, L. and Johnson, J.: Climate Models Are Uncertain, but We Can Do Something About It, *Eos (Washington, DC)*, 99, doi:10.1029/2018EO093757, 2018.
- Carslaw, K. S., Lee, L. A., Reddington, C. L., Pringle, K. J., Rap, A., Forster, P. M., Mann, G. W., Spracklen, D. V., Woodhouse, M. T., Regayre, L. A. and Pierce, J. R.: Large contribution of natural aerosols to uncertainty in indirect forcing, *Nature*, 503(7474), 67–71, doi:10.1038/nature12674, 2013.
- Chalmers, N., Highwood, E. J., Hawkins, E., Sutton, R. and Wilcox, L. J.: Aerosol contribution to the rapid warming of near-term climate under RCP 2.6, *Geophys. Res. Lett.*, 39(18), doi:10.1029/2012GL052848, 2012.
- Cherian, R., Quaas, J., Salzmann, M. and Wild, M.: Pollution trends over Europe constrain global aerosol forcing as simulated by climate models, *Geophys. Res. Lett.*, 41(6), 2176–2181, doi:10.1002/2013GL058715, 2014.
- Christensen, M. W., Gettelman, A., Cermak, J., Dagan, G., Diamond, M., Douglas, A., Feingold, G., Glassmeier, F., Goren, T., Grosvenor, D. P., Gryspeerdt, E., Kahn, R., Li, Z., Ma, P.-L., Malavelle, F., McCoy, I. L., McCoy, D. T., McFarquhar, G., Mülmenstädt, J., Pal, S., Possner, A., Povey, A., Quaas, J., Rosenfeld, D., Schmidt, A., Schrödner, R., Sorooshian, A., Stier, P., Toll, V., Watson-Parris, D., Wood, R., Yang, M. and Yuan, T.: Opportunistic experiments to constrain aerosol effective radiative forcing, *Atmos. Chem. Phys.*, 22(1), 641–674, doi:10.5194/acp-22-641-2022, 2022.
- Collins, M. and Knutti, R.: Long-term climate change: Projections, commitments and irreversibility, in *Climate Change 2013 the Physical Science Basis: Working Group I Contribution to the Fifth Assessment Report of the Intergovernmental Panel on Climate Change*, vol. 9781107057, pp. 1029–1136., 2013.
- Eyring, V., Gillett, N. P., Achuta Rao, K. M., Barimalala, R., Barreiro Parrillo, M., Bellouin, N., Cassou, C., Durack, P. J., Kosaka, Y., McGregor, S., Min, S., Morgenstern, O. and Sun, Y.: Human Influence on the Climate System, *Clim. Chang. 2021 Phys. Sci. Basis. Contrib. Work. Gr. I to Sixth Assessment Rep. Intergov. Panel Clim. Chang.*, 2021.
- Folini, D. and Wild, M.: Aerosol emissions and dimming/brightening in Europe: Sensitivity studies with ECHAM5-HAM, *J. Geophys. Res. Atmos.*, 116(21), doi:10.1029/2011JD016227, 2011.

- Ghan, S., Wang, M., Zhang, S., Ferrachat, S., Gettelman, A., Griesfeller, J., Kipling, Z., Lohmann, U., Morrison, H., Neubauer, D., Partridge, D. G., Stier, P., Takemura, T., Wang, H. and Zhang, K.: Challenges in constraining anthropogenic aerosol effects on cloud radiative forcing using present-day spatiotemporal variability, *Proc. Natl. Acad. Sci.*, doi:10.1073/pnas.1514036113, 2016.
- Gilgen, H. and Ohmura, A.: The Global Energy Balance Archive, *Bull. Am. Meteorol. Soc.*, 80(5), 831–850, doi:10.1175/1520-0477(1999)080<0831:TGEBA>2.0.CO;2, 1999.
- Gilgen, H., Wild, M. and Ohmura, A.: Means and Trends of Shortwave Irradiance at the Surface Estimated from Global Energy Balance Archive Data, *J. Clim.*, 11(8), 2042–2061, doi:10.1175/1520-0442(1998)011<2042:matosi>2.0.co;2, 1998.
- Granier, C., Bessagnet, B., Bond, T., D'Angiola, A., Denier van der Gon, H., Frost, G. J., Heil, A., Kaiser, J. W., Kinne, S., Klimont, Z., Kloster, S., Lamarque, J.-F., Lioussé, C., Masui, T., Meleux, F., Mieville, A., Ohara, T., Raut, J.-C., Riahi, K., Schultz, M. G., Smith, S. J., Thompson, A., van Aardenne, J., van der Werf, G. R. and van Vuuren, D. P.: Evolution of anthropogenic and biomass burning emissions of air pollutants at global and regional scales during the 1980–2010 period, *Clim. Change*, 109(1–2), 163–190, doi:10.1007/s10584-011-0154-1, 2011.
- Gryspeerd, E., Quaas, J., Ferrachat, S., Gettelman, A., Ghan, S., Lohmann, U., Morrison, H., Neubauer, D., Partridge, D. G., Stier, P., Takemura, T., Wang, H., Wang, M. and Zhang, K.: Constraining the instantaneous aerosol influence on cloud albedo, *Proc. Natl. Acad. Sci.*, doi:10.1073/pnas.1617765114, 2017.
- Hakuba, M. Z., Folini, D., Sanchez-Lorenzo, A. and Wild, M.: Spatial representativeness of ground-based solar radiation measurements, *J. Geophys. Res. Atmos.*, 118(15), 8585–8597, doi:10.1002/jgrd.50673, 2013.
- Hand, J. L., Schichtel, B. A., Malm, W. C. and Pitchford, M. L.: Particulate sulfate ion concentration and SO₂ emission trends in the United States from the early 1990s through 2010, *Atmos. Chem. Phys.*, 12(21), 10353–10365, doi:10.5194/acp-12-10353-2012, 2012.
- Hienola, A., Partanen, A. I., Pietikainen, J. P., O'Donnell, D., Korhonen, H., Matthews, H. D. and Laaksonen, A.: The impact of aerosol emissions on the 1.5 °C pathways, *Environ. Res. Lett.*, 13(4), 044011, doi:10.1088/1748-9326/aab1b2, 2018.
- Hoesly, R. M., Smith, S. J., Feng, L., Klimont, Z., Janssens-Maenhout, G., Pitkanen, T., Seibert, J. J., Vu, L., Andres, R. J., Bolt, R. M., Bond, T. C., Dawidowski, L., Kholod, N., Kurokawa, J. I., Li, M., Liu, L., Lu, Z., Moura, M. C. P., O'Rourke, P. R. and Zhang, Q.: Historical (1750–2014) anthropogenic emissions of reactive gases and aerosols from the Community Emissions Data System (CEDS), *Geosci. Model Dev.*, 11(1), 369–408, doi:10.5194/gmd-11-369-2018, 2018.
- Johnson, J. S., Regayre, L. A., Yoshioka, M., Pringle, K. J., Lee, L. A., Sexton, D., Rostron, J., Booth, B. B. and Carslaw, K. S.: The importance of comprehensive parameter sampling and multiple observations for robust constraint of aerosol radiative forcing, *Atmos. Chem. Phys.*, 18(17), 13031–13053, doi:10.5194/acp-2018-174, 2018.
- Kudo, R., Uchiyama, A., Ijima, O., Ohkawara, N. and Ohta, S.: Aerosol impact on the brightening in Japan, *J. Geophys. Res. Atmos.*, 117(7), n/a-n/a, doi:10.1029/2011JD017158, 2012.
- Li, Z.: Natural variability and sampling errors in solar radiation measurements for model validation over the Atmospheric Radiation Measurement Southern Great Plains region, *J. Geophys. Res.*, 110(D15), D15S19, doi:10.1029/2004JD005028, 2005.
- Liley, J. B.: New Zealand dimming and brightening, *J. Geophys. Res. Atmos.*, 114(8), D00D10, doi:10.1029/2008JD011401, 2009.
- Long, C. N., Dutton, E. G., Augustine, J. A., Wiscombe, W., Wild, M., McFarlane, S. A. and Flynn, C. J.: Significant decadal brightening of downwelling shortwave in the continental United States, *J. Geophys. Res.*, 114(D10), doi:10.1029/2008jd011263, 2009.
- Lund, M. T., Myhre, G. and Samset, B. H.: Anthropogenic aerosol forcing under the Shared Socioeconomic Pathways, *Atmos. Chem. Phys.*, 19(22), 13827–13839, doi:10.5194/acp-2019-606, 2019.
- Manara, V., Brunetti, M., Celozzi, A., Maugeri, M., Sanchez-Lorenzo, A. and Wild, M.: Detection of dimming/brightening in Italy from homogenized all-sky and clear-sky surface solar radiation

- records and underlying causes (1959-2013), *Atmos. Chem. Phys.*, 16(17), 11145–11161, doi:10.5194/acp-16-11145-2016, 2016.
- Manktelow, P. T., Mann, G. W., Carslaw, K. S., Spracklen, D. V. and Chipperfield, M. P.: Regional and global trends in sulfate aerosol since the 1980s, *Geophys. Res. Lett.*, 34(14), L14803, doi:10.1029/2006GL028668, 2007.
- Mann, G. W., Carslaw, K. S., Spracklen, D. V, Ridley, D. A., Manktelow, P. T., Chipperfield, M. P., Pickering, S. J. and Johnson, C. E.: Geoscientific Model Development Description and evaluation of GLOMAP-mode: a modal global aerosol microphysics model for the UKCA composition-climate model, *Geosci. Model Dev*, 3, 519–551, doi:10.5194/gmd-3-519-2010, 2010.
- Mateos, D., Antón, M., Sanchez-Lorenzo, A., Calbó, J. and Wild, M.: Long-term changes in the radiative effects of aerosols and clouds in a mid-latitude region (1985-2010), *Glob. Planet. Change*, 111, 288–295, doi:10.1016/j.gloplacha.2013.10.004, 2013.
- Mateos, D., Sanchez-Lorenzo, A., Antón, M., Cachorro, V. E., Calbó, J., Costa, M. J., Torres, B. and Wild, M.: Quantifying the respective roles of aerosols and clouds in the strong brightening since the early 2000s over the Iberian Peninsula, *J. Geophys. Res. Atmos.*, 119(17), 10,382–10,393, doi:10.1002/2014JD022076, 2014.
- McCoy, D. T., Bender, F. A. -M., Mohrmann, J. K. C., Hartmann, D. L., Wood, R. and Grosvenor, D. P.: The global aerosol-cloud first indirect effect estimated using MODIS, MERRA, and AeroCom, *J. Geophys. Res.*, 122(3), 1779–1796, doi:10.1002/2016JD026141, 2017.
- Moseid, K. O., Schulz, M., Storelvmo, T., Julsrud, I. R., Olivie, D., Nabat, P., Wild, M., Cole, J. N. S. and Takemura, T.: Bias in CMIP6 models compared to observed regional dimming and brightening trends (1961–2014), *Atmos. Chem. Phys. Discuss.*, 2020, 1–20, doi:10.5194/acp-2019-1210, 2020.
- Murphy, J. M., Harris, G. R., Sexton, D. M. H., Kendon, E. J., Bett, P. E., Clark, R. T., Eagle, K. E., Fosser, G., Fung, F., Lowe, J. A., McDonald, R. E., McInnes, R. N., McSweeney, C. F., Mitchell, J. F. B., Rostron, J. W., Thornton, H. E., Tucker, S. and Yamazaki, K.: UKCP18: Land Projections Science Report., 2018.
- Padma Kumari, B. and Goswami, B. N.: Seminal role of clouds on solar dimming over the Indian monsoon region, *Geophys. Res. Lett.*, 37(6), n/a-n/a, doi:10.1029/2009GL042133, 2010.
- Peace, A. H., Carslaw, K. S., Lee, L. A., Regayre, L. A., Booth, B. B. B., Johnson, J. S. and Bernie, D.: Effect of aerosol radiative forcing uncertainty on projected exceedance year of a 1.5 °C global temperature rise, *Environ. Res. Lett.*, 15(9), 0940a6, doi:10.1088/1748-9326/aba20c, 2020.
- Pfeifroth, U., Sanchez-Lorenzo, A., Manara, V., Trentmann, J. and Hollmann, R.: Trends and Variability of Surface Solar Radiation in Europe Based On Surface- and Satellite-Based Data Records, *J. Geophys. Res. Atmos.*, 123(3), 1735–1754, doi:10.1002/2017JD027418, 2018.
- Rao, S., Klimont, Z., Smith, S. J., Van Dingenen, R., Dentener, F., Bouwman, L., Riahi, K., Amann, M., Bodirsky, B. L., van Vuuren, D. P., Aleluia Reis, L., Calvin, K., Drouet, L., Fricko, O., Fujimori, S., Gernaat, D., Havlik, P., Harmsen, M., Hasegawa, T., Heyes, C., Hilaire, J., Luderer, G., Masui, T., Stehfest, E., Strefler, J., van der Sluis, S. and Tavoni, M.: Future air pollution in the Shared Socio-economic Pathways, *Glob. Environ. Chang.*, 42, 346–358, doi:10.1016/j.gloenvcha.2016.05.012, 2017.
- Regayre, L. A., Pringle, K. J., Lee, L. A., Rap, A., Browse, J., Mann, G. W., Reddington, C. L., Carslaw, K. S., Booth, B. B. B. and Woodhouse, M. T.: The climatic importance of uncertainties in regional aerosol-cloud radiative forcings over recent decades, *J. Clim.*, 28(17), 6589–6607, doi:10.1175/JCLI-D-15-0127.1, 2015.
- Riahi, K., van Vuuren, D. P., Kriegler, E., Edmonds, J., O'Neill, B. C., Fujimori, S., Bauer, N., Calvin, K., Dellink, R., Fricko, O., Lutz, W., Popp, A., Cuaresma, J. C., KC, S., Leimbach, M., Jiang, L., Kram, T., Rao, S., Emmerling, J., Ebi, K., Hasegawa, T., Havlik, P., Humpenöder, F., Da Silva, L. A., Smith, S., Stehfest, E., Bosetti, V., Eom, J., Gernaat, D., Masui, T., Rogelj, J., Strefler, J., Drouet, L., Krey, V., Luderer, G., Harmsen, M., Takahashi, K., Baumstark, L., Doelman, J. C., Kainuma, M., Klimont, Z., Marangoni, G., Lotze-Campen, H., Obersteiner, M., Tabeau, A. and Tavoni, M.: The Shared Socioeconomic Pathways and their energy, land use, and greenhouse gas emissions implications: An overview, *Glob. Environ. Chang.*, 42, 153–168, doi:10.1016/j.gloenvcha.2016.05.009, 2017.

- Rotstayn, L. D., Plymin, E. L., Collier, M. A., Boucher, O., Dufresne, J. L., Luo, J. J., Von Salzen, K., Jeffrey, S. J., Foujols, M. A., Ming, Y. and Horowitz, L. W.: Declining aerosols in CMIP5 projections: Effects on atmospheric temperature structure and midlatitude jets, *J. Clim.*, 27(18), 6960–6977, doi:10.1175/JCLI-D-14-00258.1, 2014.
- Rotstayn, L. D., Collier, M. A. and Luo, J.-J.: Effects of declining aerosols on projections of zonally averaged tropical precipitation, *Environ. Res. Lett.*, 10(4), 044018, doi:10.1088/1748-9326/10/4/044018, 2015.
- Ruckstuhl, C. and Norris, J. R.: How do aerosol histories affect solar “dimming” and “brightening” over Europe?: IPCC-AR4 models versus observations, *J. Geophys. Res.*, 114(6), D00D04, doi:10.1029/2008JD011066, 2009a.
- Ruckstuhl, C. and Norris, J. R.: How do aerosol histories affect solar “dimming” and “brightening” over Europe?: IPCC-AR4 models versus observations, *J. Geophys. Res. Atmos.*, 114(D10), doi:10.1029/2008JD011066@10.1002/(ISSN)2169-8996.DIMBRIGHT1, 2009b.
- Samset, B. H., Sand, M., Smith, C. J., Bauer, S. E., Forster, P. M., Fuglestad, J. S., Osprey, S. and Schleussner, C. F.: Climate Impacts From a Removal of Anthropogenic Aerosol Emissions, *Geophys. Res. Lett.*, 45(2), 1020–1029, doi:10.1002/2017GL076079, 2018.
- Sanchez-Lorenzo, A., Wild, M., Brunetti, M., Gujjarro, J. A., Hakuba, M. Z., Calbó, J., Mystakidis, S. and Bartok, B.: Reassessment and update of long-term trends in downward surface shortwave radiation over Europe (1939-2012), *J. Geophys. Res.*, 120(18), 9555–9569, doi:10.1002/2015JD023321, 2015.
- Schwarz, M., Folini, D., Hakuba, M. Z. and Wild, M.: Spatial Representativeness of Surface-Measured Variations of Downward Solar Radiation, *J. Geophys. Res. Atmos.*, 122(24), 13,319–13,337, doi:10.1002/2017JD027261, 2017a.
- Schwarz, M., Folini, D., Hakuba, M. Z. and Wild, M.: Spatial Representativeness of Surface-Measured Variations of Downward Solar Radiation, *J. Geophys. Res. Atmos.*, 122(24), 13,319–13,337, doi:10.1002/2017JD027261, 2017b.
- Seinfeld, J. H., Bretherton, C., Carslaw, K. S., Coe, H., DeMott, P. J., Dunlea, E. J., Feingold, G., Ghan, S., Guenther, A. B., Kahn, R., Kraucunas, I., Kreidenweis, S. M., Molina, M. J., Nenes, A., Penner, J. E., Prather, K. A., Ramanathan, V., Ramaswamy, V., Rasch, P. J., Ravishankara, A. R., Rosenfeld, D., Stephens, G. and Wood, R.: Improving our fundamental understanding of the role of aerosol–cloud interactions in the climate system, *Proc. Natl. Acad. Sci.*, 113(21), 5781–5790, doi:10.1073/pnas.1514043113, 2016.
- Sexton, D. M. H., McSweeney, C. F., Rostron, J. W., Yamazaki, K., Booth, B. B. B., Johnson, J., Murphy, J. M. and Regayre, L.: A perturbed parameter ensemble of HadGEM3-GC3.05 coupled model projections: part 1: selecting the parameter combinations, *Clim Dyn* [online] Available from: <https://doi.org/10.1007/s00382-021-05709-9>, 2021.
- Stjern, C. W., Kristjánsson, J. E. and Hansen, A. W.: Global dimming and global brightening - An analysis of surface radiation and cloud cover data in northern Europe, *Int. J. Climatol.*, 29(5), 643–653, doi:10.1002/joc.1735, 2009.
- Storelvmo, T., Heede, U. K., Leirvik, T., Phillips, P. C. B., Arndt, P. and Wild, M.: Lethargic Response to Aerosol Emissions in Current Climate Models, *Geophys. Res. Lett.*, 45(18), 9814–9823, doi:10.1029/2018GL078298, 2018.
- Turnock, S. T., Spracklen, D. V., Carslaw, K. S., Mann, G. W., Woodhouse, M. T., Forster, P. M., Haywood, J., Johnson, C. E., Dalvi, M., Bellouin, N. and Sanchez-Lorenzo, A.: Modelled and observed changes in aerosols and surface solar radiation over Europe between 1960 and 2009, *Atmos. Chem. Phys.*, 15, 9477–9500, doi:10.5194/acp-15-9477-2015, 2015.
- Turnock, S. T., Mann, G. W., Woodhouse, M. T., Dalvi, M., O'Connor, F. M., Carslaw, K. S. and Spracklen, D. V.: The Impact of Changes in Cloud Water pH on Aerosol Radiative Forcing, *Geophys. Res. Lett.*, 46(7), 4039–4048, doi:10.1029/2019GL082067, 2019.
- Vestreng, V., Myhre, G., Fagerli, H., Reis, S. and Tarrasón, L.: Twenty-five years of continuous sulphur dioxide emission reduction in Europe, *Atmos. Chem. Phys.*, 7(13), 3663–3681, doi:10.5194/acp-7-3663-2007, 2007.
- Walters, D., Baran, A. J., Boutle, I., Brooks, M., Earnshaw, P., Edwards, J., Furtado, K., Hill, P., Lock, A., Manners, J., Morcrette, C., Mulcahy, J., Sanchez, C., Smith, C., Stratton, R., Tennant,

- W., Tomassini, L., Van Weverberg, K., Vosper, S., Willett, M., Browse, J., Bushell, A., Carslaw, K., Dalvi, M., Essery, R., Gedney, N., Hardiman, S., Johnson, B., Johnson, C., Jones, A., Jones, C., Mann, G., Milton, S., Rumbold, H., Sellar, A., Ujiie, M., Whittall, M., Williams, K. and Zerroukat, M.: The Met Office Unified Model Global Atmosphere 7.0/7.1 and JULES Global Land 7.0 configurations, *Geosci. Model Dev.*, 12(5), 1909–1963, doi:10.5194/gmd-12-1909-2019, 2019.
- Wang, K. C., Dickinson, R. E., Wild, M. and Liang, S.: Atmospheric impacts on climatic variability of surface incident solar radiation, *Atmos. Chem. Phys.*, 12(20), 9581–9592, doi:10.5194/acp-12-9581-2012, 2012.
- Westervelt, D. M., Horowitz, L. W., Naik, V., Golaz, J.-C. and Mauzerall, D. L.: Radiative forcing and climate response to projected 21st century aerosol decreases, *Atmos. Chem. Phys.*, 15(22), 12681–12703, doi:10.5194/acp-15-12681-2015, 2015.
- Wild, M.: Global dimming and brightening: A review, *J. Geophys. Res. Atmos.*, 114(12), doi:10.1029/2008JD011470, 2009a.
- Wild, M.: How well do IPCC-AR4/CMIP3 climate models simulate global dimming/brightening and twentieth-century daytime and nighttime warming?, *J. Geophys. Res.*, 114(9), D00D11, doi:10.1029/2008JD011372, 2009b.
- Wild, M., Gilgen, H., Roesch, A., Ohmura, A., Long, C. N., Dutton, E. G., Forgan, B., Kallis, A., Russak, V. and Tsvetkov, A.: From dimming to brightening: decadal changes in solar radiation at Earth's surface., *Science*, 308(5723), 847–50, doi:10.1126/science.1103215, 2005.
- Wild, M., Ohmura, A., Schär, C., Müller, G., Folini, D., Schwarz, M., Zyta Hakuba, M. and Sanchez-Lorenzo, A.: The Global Energy Balance Archive (GEBA) version 2017: A database for worldwide measured surface energy fluxes, *Earth Syst. Sci. Data*, 9(2), 601–613, doi:10.5194/essd-9-601-2017, 2017.
- Wild, M., Wacker, S., Yang, S. and Sanchez-Lorenzo, A.: Evidence for Clear-Sky Dimming and Brightening in Central Europe, *Geophys. Res. Lett.*, 48(6), e2020GL092216, doi:10.1029/2020GL092216, 2021.
- Williams, K. D., Copsey, D., Blockley, E. W., Bodas-Salcedo, A., Calvert, D., Comer, R., Davis, P., Graham, T., Hewitt, H. T., Hill, R., Hyder, P., Ineson, S., Johns, T. C., Keen, A. B., Lee, R. W., Megann, A., Milton, S. F., Rae, J. G. L., Roberts, M. J., Scaife, A. A., Schiemann, R., Storkey, D., Thorpe, L., Watterson, I. G., Walters, D. N., West, A., Wood, R. A., Woollings, T. and Xavier, P. K.: The Met Office Global Coupled Model 3.0 and 3.1 (GC3.0 and GC3.1) Configurations, *J. Adv. Model. Earth Syst.*, 10(2), 357–380, doi:10.1002/2017MS001115, 2018.
- Yamazaki, K., Sexton, D. M. H., Rostron, J. W., McSweeney, C. F., Murphy, J. M. and Harris, G. R.: A perturbed parameter ensemble of HadGEM3-GC3.05 coupled model projections: part 2: global performance and future changes, *Clim. Dyn.*, 56(11–12), 3437–3471, doi:10.1007/s00382-020-05608-5, 2021.
- Yang, S., Wang, X. L. and Wild, M.: Homogenization and trend analysis of the 1958-2016 in situ surface solar radiation records in China, *J. Clim.*, 31(11), 4529–4541, doi:10.1175/JCLI-D-17-0891.1, 2018.

Chapter 5 Thesis Conclusion

This thesis has used perturbed parameter ensembles (PPE) of a global climate model to quantify the effect that the uncertainty in aerosol radiative forcing has on projecting climate changes over the coming decades. This study is the first to quantify the parametric model uncertainty in future aerosol radiative forcing and identify which model parameters contribute to the uncertainty in aerosol radiative forcing projections. Additionally, this study evaluated model uncertainty in future aerosol-driven climate impacts, quantifying the uncertainty in projections of global mean temperature change and tropical precipitation shifts. Lastly, model skill in simulating surface solar radiation (SSR) trends was assessed, with the view to see whether this can point to which future changes in the PPE could be considered more plausible. The potential to use surface solar radiation trends as a constraint on aerosol radiative forcing was also evaluated. The following section summarises the major results of this thesis addressing questions in the order they were posed in Section 1.7 of the Introduction.

5.1 Summary of Main Results

5.1.1 Effect of Aerosol Radiative Forcing Uncertainty on Projected Exceedance Year of a 1.5 °C Global Temperature Rise

- The magnitude of global mean aerosol radiative forcing by 2050 (relative to 2000) varies from 0.30 W m⁻² for SSP4-RCP6.0 (weak air quality policies) to 0.78 W m⁻² for SSP2-RCP4.5 (medium) to 1.12 W m⁻² for SSP1-RCP2.6 (strong). Thus, the path we collectively choose for aerosol emissions will significantly alter the contribution of aerosol radiative forcing in the global energy balance over the coming decades.
- For the three emission scenarios we assessed, the parametric uncertainty in our single model is 35% to 67% of the scenario uncertainty. Accounting for model parametric uncertainty adds a considerable amount of uncertainty onto projections of aerosol radiative forcing that only account for scenario uncertainty.
- For SSP2-RCP4.5, sea spray emission flux and the standard deviation of updraft velocities are the most dominant causes of parametric model uncertainty in near-term aerosol radiative forcing. This result suggests that

the uncertainty in natural aerosol emissions will become increasingly important as anthropogenic aerosol emissions reduce to a lower baseline, whereas updraft velocity is important over polluted land regions. Observational constraints targeted at these parameters could therefore reduce the uncertainty in aerosol radiative forcing projections.

- Taking into account the uncertainty in near-term aerosol radiative forcing alone produces a 5-year window (2034 to 2039) in projecting the exceedance year of 1.5 °C global temperature rise for SSP2-RCP4.5. Accounting for an illustrative correlation between aerosol radiative forcing and climate sensitivity extends the exceedance window from 2022 until after 2050. Therefore, it is critical to reduce the uncertainty in aerosol radiative forcing to improve climate projections, particularly when a relationship between aerosol forcing and climate sensitivity is considered.

5.1.2 Evaluating Uncertainty in Aerosol Forcing of Tropical Precipitation Shifts

- Our PPE designed to sample the uncertainty in climate projections shows a southward shift in the PPE mean tropical precipitation from around 1940 to 1985, followed by a northward recovery to 2000. From 2000 to 2060, the PPE mean shows a further northward shift in tropical precipitation under scenario RCP2.6 compared to RCP8.5.
- The magnitude of the tropical precipitation shift correlates with the hemispheric contrast in surface temperature and total radiative forcing in the PPE (although the relationship varies depending on the time period), which is expected based on energetic arguments of the drivers of ITCZ and tropical precipitation shifts (e.g. Kang et al., 2018).
- However, in the PPE there is not a clear relationship between the magnitude of 20th century tropical precipitation shifts and the hemispheric contrast in industrial-era anthropogenic aerosol ERF, as expected based on analyses from CMIP5 (Allen et al., 2015; Chung and Soden, 2017). There is a clear influence of major volcanic eruptions of the 20th century temporarily shifting tropical precipitation away from the hemisphere with the greatest aerosol loading.
- Internal variability (which covers around half of the PPE spread in the 1950 to 1985 precipitation shift) and the effect of perturbed physical atmosphere

parameters likely confounds the relationship between aerosol radiative forcing and 20th century tropical precipitation shifts in the PPE.

- The further northward shift in tropical precipitation up to mid-21st century in RCP2.6 compared to RCP8.5 is likely due to faster anthropogenic aerosol emission reductions under RCP2.6 combined with a greater dominance of warming feedbacks in RCP8.5 that can pull tropical precipitation southwards (such as AMOC weakening).
- In contrast to the historical period, we find a relationship between the magnitude of the hemispheric contrast in aerosol radiative forcing and the tropical precipitation shift in the Pacific and global mean in RCP8.5, which is weaker in RCP2.6 (despite RCP2.6 having stronger near-term aerosol reductions). This result reinforces the message of Chapter 2 that it is critical to reduce parametric uncertainty in aerosol forcing to improve model skill at simulating climate projections.

5.1.3 Underestimating European Dimming, Overestimating European Brightening

- Our PPE shows an underestimation of observed European surface solar radiation dimming during 1960 to 1980 (increasing aerosol emissions), but an overestimation of European brightening over 1985 to 2005 (declining aerosol emissions). In comparison, most CMIP5 models underestimate surface solar radiation trends in both time periods (Allen et al., 2013), whereas many CMIP6 model better represent the observed trends over Europe (Moseid et al., 2020).
- The dry deposition rate of SO₂ is correlated with the model skill in simulating the surface solar radiation trends over Europe in both dimming and brightening periods and likely has the most influence when aerosol burden is lower. Our results provide support for previous studies which suggested the underestimation of surface solar radiation trends is due to the model treatment of translating aerosol emissions to radiative forcing (Moseid et al., 2020; Storelvmo et al., 2018).
- There is a clear aerosol influence on all-sky surface solar radiation trends in the brightening period. However, in the dimming period, changes in cloudiness and cloud radiation due to internal variability and parametric effects also affect model skill, and possibly obscure a distinct influence of

increasing aerosol emissions driving the declining surface solar radiation trend.

- The relationship between simulated surface solar radiation and model parameters and aerosol ERF is dependent on the time period examined, the season, degree of ocean-atmosphere coupling and ensemble size. As a result, it is not possible for us to robustly select a handful of well performing model members that would have the most plausible future projections. We therefore suggest caution in using trends in surface solar radiation as a constraint on climate projections, even in a region like Europe where the longest and most widespread surface solar radiation datasets exist.

5.2 Thesis Limitations

This thesis made use of existing PPEs that were designed to quantify the uncertainty in pre-industrial to present-day aerosol ERF (Chapter 2) and to sample uncertainty in climate changes for UK Climate Projections (Chapter 3, 4). Although rich in data, the PPEs were not designed specifically to answer the research questions of this thesis, which imposed some limitations on the interpretability of the results. Ideally, a new PPE targeted specifically for quantifying the uncertainty of future aerosol radiative forcing and aerosol-driven climate responses would have been created, but this would have been a computationally expensive task beyond the scope of a PhD thesis.

The statistical emulator used to create projections of future aerosol radiative forcing in Chapter 2 was trained and validated from a PPE of HadGEM3-UKCA model simulations of the year 2008. As such, the emission pathways as applied in the piece of work scaled up or down the existing spatial pattern of emissions for the year 2008. The analysis was therefore restricted to global mean changes, rather than the regional evolution of anthropogenic aerosol radiative forcing where discrepancies in the spatial evolution of emission would have a greater effect. In addition, global mean temperature projections could not be calculated from the present-day PPE so were created using a simple climate model. An illustrative approach to quantify the effect of a potential relationship between aerosol radiative forcing and climate sensitivity was adopted because the experimental design was not compatible with selecting an exact climate

sensitivity value corresponding to a future aerosol radiative forcing value. Since the experiment was not interactive in nature, the role of any potential feedbacks related to warming, aerosol radiative forcing and/or climate sensitivity were not quantified.

In Chapters 3 and 4, a perturbed parameter ensemble of HadGEM3-GC3.05 was used. The end-product of the PPE consisted of 15 transient coupled ocean-atmosphere simulations that sampled the uncertainty in 47 model parameters across a range of model schemes. In Chapter 3, only 13 ensemble members were used (a further 2 ensemble members were excluded due to ocean circulation model drifts that could affect tropical precipitation shifts). The coupled-ocean atmosphere PPE gave us the huge advantage of evaluating multi-decadal trends and aerosol-driven dynamical responses. However, the small sample size meant that robust statistical analysis, such as emulation and variance-based sensitivity analysis as used in Chapter 2 could not be completed with the transient PPE. In addition, ensemble members could have different evolutions, due to internal climate variability. The effect of a small sample size, evolving climate forcings, a large number of perturbed parameters, internal variability made the attribution of climate responses to variables or parameters a difficult task.

5.3 Directions for Future Work

In addition to the main results discussed above, this thesis has presented open challenges in our understanding of how aerosol radiative forcing uncertainty affects historical simulations and future projections.

In Chapter 3, we found that a relationship between aerosol radiative forcing and 20th century tropical precipitation shifts was potentially obscured by internal variability in our PPE. In multi-model studies, each model ensemble member would typically be an average of an initial condition ensemble, which is likely why the relationship emerges more clearly in a CMIP5 ensemble of a similar size (Allen et al., 2015; Chung and Soden, 2017). However, future work should focus on verifying if a relationship between aerosol radiative forcing and tropical precipitation shifts still exists in CMIP6. The range of climate responses due to parametric uncertainties in our single model highlight the value of exploring the parametric uncertainty in other simulations if we are to come to an idea of a more robust relationship between aerosol forcing and tropical precipitation shifts. For

transient PPEs with a small sample size like ours, a small initial condition ensemble for each PPE member would help isolate the climate response due to internal variability from the forced response and therefore be a useful addition for future work where (when) the computational expense allows. Furthermore, there may be feedbacks between aspects of internal variability and aerosol radiative forcing, which would be an interesting direction for further work to explore.

In contrast to the 20th century, our results in Chapter 3 showed a relationship between mid-century 21st century tropical precipitation shifts and pre-industrial to present-day aerosol ERF under the RCP8.5 emissions scenario that has rising GHGs in combination with anthropogenic aerosol emission reductions. Yet, in RCP2.6 where the reductions in anthropogenic aerosol emissions are more rapid, the relationship is weaker. Previous studies have suggested a sensitivity of natural aerosol emissions to warming that will impact aerosol radiative forcing (e.g. Carslaw et al., 2010; Thornhill et al., 2021). In addition, warming may increase the residence time of atmospheric aerosols, leading to a larger radiative forcing from anthropogenic aerosol emission reductions in scenarios such as RCP8.5 with higher GHG emissions (Ackerley et al., 2009; Allen et al., 2016; Bellouin et al., 2011; Takemura, 2020). Future research focused on feedbacks between GHG-induced warming and the magnitude of aerosol ERF and aerosol-driven climate responses for future emission scenarios would help us interpret the results of our analysis on future precipitation shifts. For example, there would be great benefit to analysing experiments of future aerosol radiative forcing time series or time slices that also account for uncertainties in evolving GHG emission scenarios and associated levels of warming.

In Chapter 5, we found our PPE underestimated European dimming and overestimated European brightening. The underestimation of the trend in surface solar radiation is in line with analysis of CMIP5 models that used a similar number of observational stations, but in analysis of CMIP6 models that used far more observation stations (Allen et al., 2013), the European trend in surface solar radiation is well represented (Moseid et al., 2020). There were differences in the results of our model-observation comparisons when the European average was calculated from only observation stations in comparison to the whole of Europe. Therefore, future research is needed to understand if, for a single PPE or MME, the interpretation of model performance simulating surface solar radiation trends

is dependent on the number of ground-based observational stations. Our analysis suggests that caution is needed when inferring relationships between model variables and perturbed parameters or aerosol forcing between time periods. As such, further research is needed to quantify the extent to which using observational constraints of a particular time period, season, model type extrapolates to reducing the uncertainty in aerosol-driven climate projections.

References

- Ackerley, D., Highwood, E. J., Frame, D. J. and Booth, B. B. B.: Changes in the global sulfate burden due to perturbations in global CO₂ concentrations, *J. Clim.*, 22(20), 5421–5432, doi:10.1175/2009JCLI2536.1, 2009.
- Allen, R. J., Norris, J. R. and Wild, M.: Evaluation of multidecadal variability in CMIP5 surface solar radiation and inferred underestimation of aerosol direct effects over Europe, China, Japan, and India, *J. Geophys. Res. Atmos.*, 118(12), 6311–6336, doi:10.1002/jgrd.50426, 2013.
- Allen, R. J., Evan, A. T. and Booth, B. B. B.: Interhemispheric aerosol radiative forcing and tropical precipitation shifts during the late Twentieth Century, *J. Clim.*, 28(20), 8219–8246, doi:10.1175/JCLI-D-15-0148.1, 2015.
- Allen, R. J., Landuyt, W. and Rumbold, S. T.: An increase in aerosol burden and radiative effects in a warmer world, *Nat. Clim. Chang.*, 6(3), 269–274, doi:10.1038/nclimate2827, 2016.
- Bellouin, N., Rae, J., Jones, A., Johnson, C., Haywood, J. and Boucher, O.: Aerosol forcing in the Climate Model Intercomparison Project (CMIP5) simulations by HadGEM2-ES and the role of ammonium nitrate, *J. Geophys. Res.*, 116(D20), D20206, doi:10.1029/2011JD016074, 2011.
- Carslaw, K. S., Boucher, O., Spracklen, D. V., Mann, G. W., Rae, J. G. L., Woodward, S. and Kulmala, M.: A review of natural aerosol interactions and feedbacks within the Earth system, *Atmos. Chem. Phys.*, doi:10.5194/acp-10-1701-2010, 2010.
- Chung, E. S. and Soden, B. J.: Hemispheric climate shifts driven by anthropogenic aerosol-cloud interactions, *Nat. Geosci.*, doi:10.1038/NGEO2988, 2017.
- Kang, S. M., Shin, Y. and Xie, S. P.: Extratropical forcing and tropical rainfall distribution: energetics framework and ocean Ekman advection, *npj Clim. Atmos. Sci.*, 1(1), 20172, doi:10.1038/s41612-017-0004-6, 2018.
- Moseid, K. O., Schulz, M., Storelvmo, T., Julsrud, I. R., Olivié, D., Nabat, P., Wild, M., Cole, J. N. S. and Takemura, T.: Bias in CMIP6 models compared to observed regional dimming and brightening trends (1961–2014), *Atmos. Chem. Phys. Discuss.*, 2020, 1–20, doi:10.5194/acp-2019-1210, 2020.
- Storelvmo, T., Heede, U. K., Leirvik, T., Phillips, P. C. B., Arndt, P. and Wild, M.: Lethargic Response to Aerosol Emissions in Current Climate Models, *Geophys. Res. Lett.*, 45(18), 9814–9823, doi:10.1029/2018GL078298, 2018.
- Takemura, T.: Return to different climate states by reducing sulphate aerosols under future CO₂ concentrations, *Sci. Rep.*, 10(1), 21748, doi:10.1038/s41598-020-78805-1, 2020.
- Thornhill, G., Collins, W., Olivié, D., B. Skeie, R., Archibald, A., Bauer, S., Checa-Garcia, R., Fiedler, S., Folberth, G., Gjermundsen, A., Horowitz, L., Lamarque, J. F., Michou, M., Mulcahy, J., Nabat, P., Naik, V., M. O'Connor, F., Paulot, F., Schulz, M., E. Scott, C., Séférian, R., Smith, C., Takemura, T., Tilmes, S., Tsigaridis, K. and Weber, J.: Climate-driven chemistry and aerosol feedbacks in CMIP6 Earth system models, *Atmos. Chem. Phys.*, 21(2), 1105–1126, doi:10.5194/acp-21-1105-2021, 2021.

Appendix A

A.1 Description and Distributions of Perturbed Parameters

A brief definition and the elicited distributions of the parameters perturbed in the PPE are shown below in Table A.1. Further detailed description on the parameters and the set-up of the PPE are explained in Yoshioka et al. (2019).

Perturbed Parameter	Parameter Description	min	mode 1	mode 2	max	n1	n3	alpha
BL_Nuc	Boundary layer nucleation rate	log10(0.1)	log10(0.2)	log10(5)	log10(10)	5	5	1
Ageing	Number of monolayers required for insoluble particle to age to become soluble	0.3	1	5	10	2	2	1
Acc_Width	Modal width of accumulation modes (nm)	1.2	1.35	1.65	1.8	2	2	1
Ait_Width	Modal width of Aitken modes (nm)	1.2	1.35	1.65	1.8	2	2	1
Cloud_pH	pH of cloud droplets	4.6	5.3	6.3	7	4	2	1
Carb_FF_Ems	Fossil fuel BC/OC mass emission flux	log10(0.5)	log10(0.625)	log10(1.6)	log10(4)	2	2	1
Carb_BB_Ems*	Biomass burning BC/OC mass emission rate	log10(0.25)	log10(0.76)	log10(2.3)	log10(4)	3.2	1.55	0.28
Carb_Res_Ems	Biofuel BC/OC mass emission rate	log10(0.25)	log10(0.5)	log10(3.2)	log10(4)	2	2	0.5
Carb_FF_Diam	Fossil fuel BC/OC emitted mode diameter (nm)	30	50.4	67.2	90	3	4.5	1
Carb_BB_Diam	Biomass burning BC/OC emitted mode diameter (nm)	90	160	240	300	2	2	1
Carb_Res_Diam	BC/OC emitted mode diameter (biofuel) (nm)	90	162	300	500	2	3.5	1
Prim_SO4_Frac	Mass fraction of SO ₂	log10(1 ⁻⁶)	log10(1 ⁻⁵)	log10(5 ⁻²)	log10(1 ⁻¹)	2	2	1

	converted to new sulfate particles in power plant plumes							
Prim_SO4_Diam	Mode diameter of new sub-grid sulfate particles (nm)	3	4	16	100	1.5	5	1
Sea_Spray	Sea spray mass flux (coarse/accumulation)	log10(0.125)	log10(0.6)	log10(3)	log10(8)	4	3	1
Anth_SO2*	Anthropogenic SO ₂ emission flux	log10(0.6)	log10(0.812)	log10(1.09)	log10(1.5)	2.2	1.75	0.722
Volc_SO2	Volcanic SO ₂ emission flux	log10(0.71)	log10(0.99)	log10(1.7)	log10(2.38)	4	1.1	1
BVOC_SOA*	Biogenic monoterpene production of SOA	log10(0.81)	log10(1.06)	log10(3.6)	log10(5.4)	3.8	2.6	0.28
DMS*	DMS emission flux	log10(0.5)	log10(1.28)	log10(1.82)	log10(2)	3	3	0.722
Dry_Dep_Ait	Dry deposition velocity of Aitken mode aerosol	log10(0.5)	log10(0.8)	log10(1.4)	log10(2)	2	2	1
Dry_Dep_Acc	Dry deposition velocity of accumulation mode aerosol	log10(0.1)	log10(0.32)	log10(3.16)	log10(10)	2	2	1
Dry_Dep_SO2	Dry deposition velocity of SO ₂	log10(0.2)	log10(0.56)	log10(1.78)	log10(5)	2	2	1
Kappa_OC	Hygroscopicity parameter κ for organic aerosols	0.1	0.14	0.25	0.6	4	4	1
Sig_W	Standard deviation of shallow-cloud updraft velocity	0.1	0.36	0.44	0.7	2	2	1

Dust	Dust emission flux scale factor	log10(0.5)	log10(0.7)	log10(1.4)	log10(2)	2	2	1
Rain_Frac	The fraction of the cloud covered area where rain forms	0.3	0.31	0.55	0.7	2	3	1
Cloud_Ice_Thresh	Threshold of cloud ice water fraction for scavenging	0.1	0.105	0.35	0.5	2	3	1

Table A.1 Elicited distributions of perturbed parameters in the ensemble used. Distributions refer to a trapezoidal distribution in the format (min, vertex 1, median, vertex 2, max, side, shapes). Values for parameters represent either absolute values for the applied perturbation or a log10 multiplicative scaling factor. Parameters with * were perturbed as a multiplicative scaling factor but are transformed onto log10 for emulation.

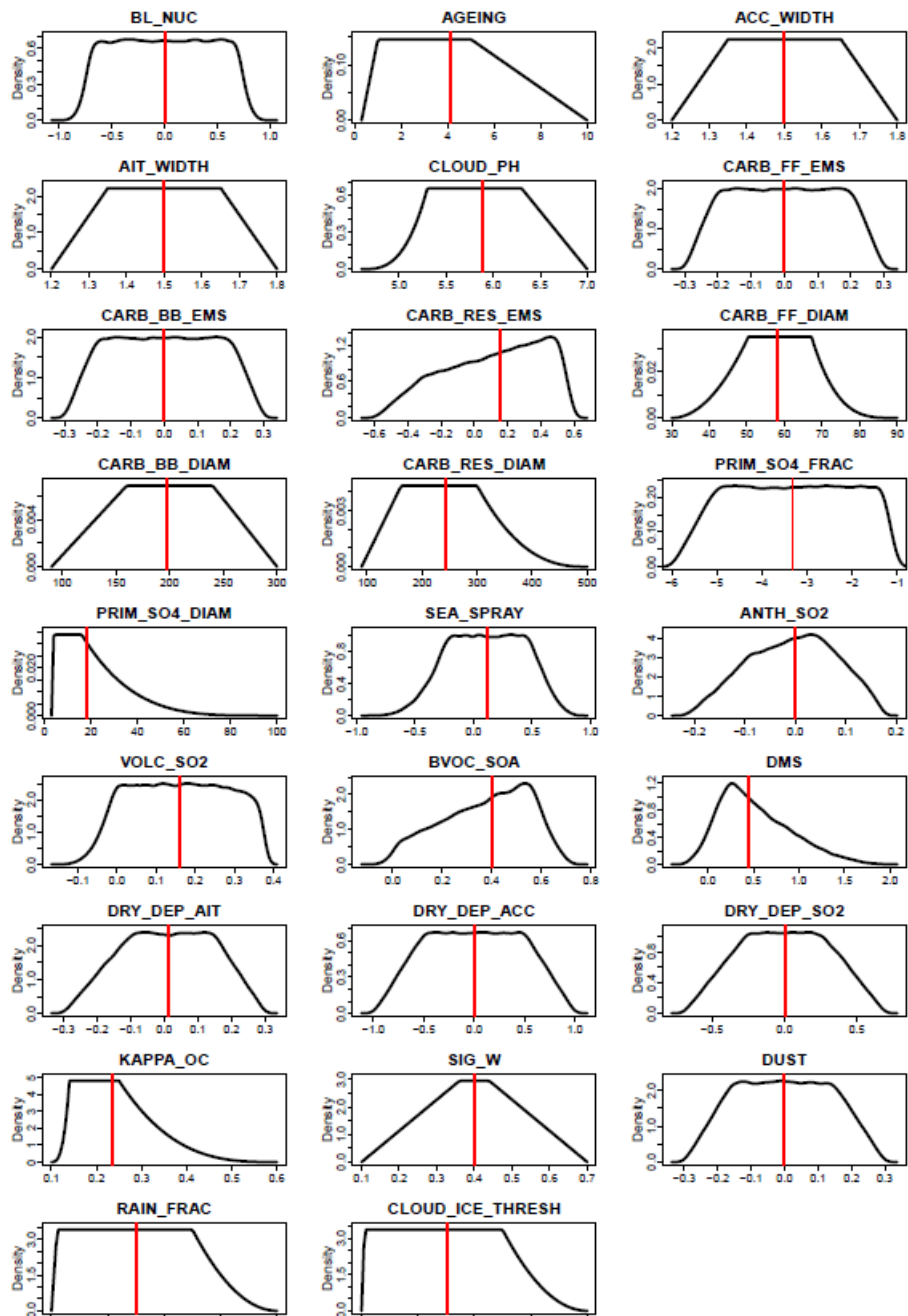


Figure A.1 Trapezoidal distribution shape of the 26 perturbed parameters according to the distribution specified in Table A.1.

A.2 Aerosol Radiative Forcing Range in the PPE: in Context

Figure A.2 from Yoshioka et al. (2019) compares the magnitude and range of pre-industrial to present day aerosol radiative forcing (RF) in the PPE (AER PPE) used in Chapter 2 with multi-model studies, and also another complementary PPE (AER-ATM PPE) in which physical atmosphere and aerosol parameters are perturbed using an updated version of the aerosol climate model HadGEM-UKCA (Yoshioka et al. 2019).

The pre-industrial to present day aerosol radiative forcing (RF) values in our PPE are stronger (more negative) than those in multi-model studies such as Forster et al. 2007 (Forster and Artaxo 2007). The range of direct aerosol radiative forcing is also more negative than multi-model studies (Myhre et al. 2013, Shindell et al. 2013, Forster and Artaxo 2007).

The nudging set up in AER-ATM PPE described in Yoshioka et al. (2019) diagnosed effective radiative forcing, and not radiative forcing as diagnosed in the AER PPE. The pre-industrial to present day aerosol ERF in the AER-ATM PPE is weaker than the aerosol RF in the AER PPE. The differences in aerosol forcing between the PPEs are partly due to the diagnosis of aerosol ERF from the AER-ATM PPE that includes rapid adjustments, in which atmospheric temperature, water and cloud cover react to the radiative effect of aerosols. In the IPCC AR5 rapid adjustments associated with aerosol-radiation interactions were given an uncertain forcing range of -0.3 to $+0.1$ W m^{-2} (Randall et al. 2013). However, the ERF associated with aerosol-cloud interactions that includes rapid adjustments in IPCC AR5 is weaker (less negative) than the RF associated with aerosol-cloud interactions without rapid adjustments in IPCC AR4 (Myhre et al. 2013). Due to the configuration of the radiation calls in these PPEs, it is not possible to isolate what contribution rapid adjustments make to aerosol ERF in the AER-ATM PPE. The differences in aerosol forcing in these PPEs are also due to modifications in the model set up, such as differences in emissions, meteorological wind fields and nudging methodology, which led to higher natural emissions and lower anthropogenic aerosol concentrations in the AER-ATM PPE, and resulted in differences in AOD and CCN between the PPEs.

Despite the magnitude of aerosol radiative forcing within our PPE being stronger than multi-model studies, the spread of values (90% confidence interval from each sample), is similar. The range of aerosol forcing across CMIP6 appears to be weaker in magnitude and narrower than previous multi-model studies (Smith et al. 2020). This suggests our model version (HadGEM3-UKCA) is more sensitive to changes in aerosols than the multi-model means in previous model comparison projects. On this basis, we expect, if our aerosol radiative forcing time series shown in Figure 2.3 was replicated in a multi-model experiment, the model uncertainty would span a similar or larger range, but the present day to future aerosol radiative forcing would be weaker, or less positive, as different models could have a weaker responses to reductions in aerosol emissions.

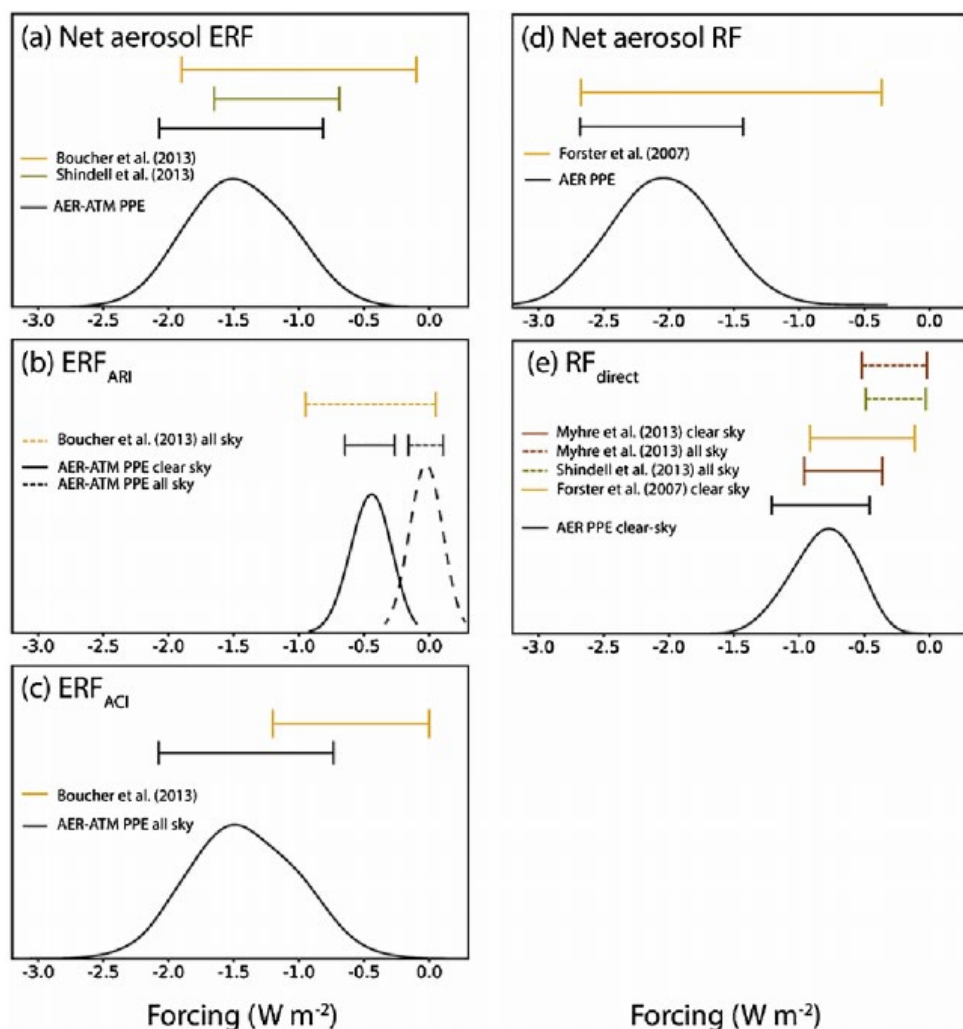


Figure A.2 The PPE used in our paper is annotated in the above figure as “AER PPE” and samples uncertainty in aerosol parameters. The “AER-ATM” PPE is another complementary PPE which samples the uncertainty in aerosol and physical atmosphere parameters and is able to diagnose aerosol ERF. The horizontal bars in (d) and (e) compare the credible interval (90%) of pre-industrial to present-day aerosol radiative forcing in the PPE to multi-model studies. This figure is from Yoshioka et al. (2019), and no changes have been made.

A.3 Emissions Scalings

In our PPE, there are three anthropogenic aerosol emission parameters, these are anthropogenic SO₂ (Anth_SO2), carbonaceous biofuel (Carb_BB_Ems) and carbonaceous fossil fuel burning (Carb_FF_Ems). The carbonaceous biofuel and fossil fuel emissions are composed of black and organic carbon emissions from specific sectors that correspond to how the emissions are inputted in our model version. The sectors included in the carbonaceous fossil fuel emission parameter are energy, industrial, transportation, waste and shipping, and the sectors included in the carbonaceous biofuel emission parameter are agriculture and residential. The distribution of these emission parameters in the PPE, including the minimum and maximum values, are displayed in Table A.1. The training data for the emulator uses a normalized range of the perturbed parameters. For example in the case of anthropogenic SO₂, the minimum value of this parameter is 60% of the 2008 value, and the maximum value is 150% of the 2008 value, but this is normalized to a 0 to 1 scale to train the emulator. Therefore, to scale our emissions to match the SSPs, we calculate what the global mean anthropogenic aerosol emissions are for the SSPs and then what the corresponding value of these emissions would be on our normalized scale. We then for each interval in the near-term future time series create a 270,000 member sample of our perturbed parameters, with the anthropogenic aerosol emission parameters fixed to the same value in each member, but with the other parameters varying to represent their uncertain range. Using this sample, we predict 270,000 values of top of atmosphere flux from our emulator, that take into account the uncertainty in 23 of the parameters in our aerosol-climate model. As we scale (fix) our anthropogenic aerosol emission parameters to a specific value to create the near-term projections of aerosol forcing, we effectively remove the uncertainty from these three parameters. Instead, to account for uncertainty in anthropogenic aerosol emissions, we look at scenario uncertainty. We do not scale open biomass burning emissions to match future predicted emission values. However, the uncertainty in present-day biomass burning emissions is sampled across the ensemble.

Our approach effectively scales up or down the 2008 emission patterns in our PPE. Figures A.3-A.5 show the gridded emission changes between 2000 and 2050 in the Shared Socioeconomic Pathways used in the paper (top row), in comparison to the representation of the anthropogenic aerosol emission scaling applied in our methods (bottom row).

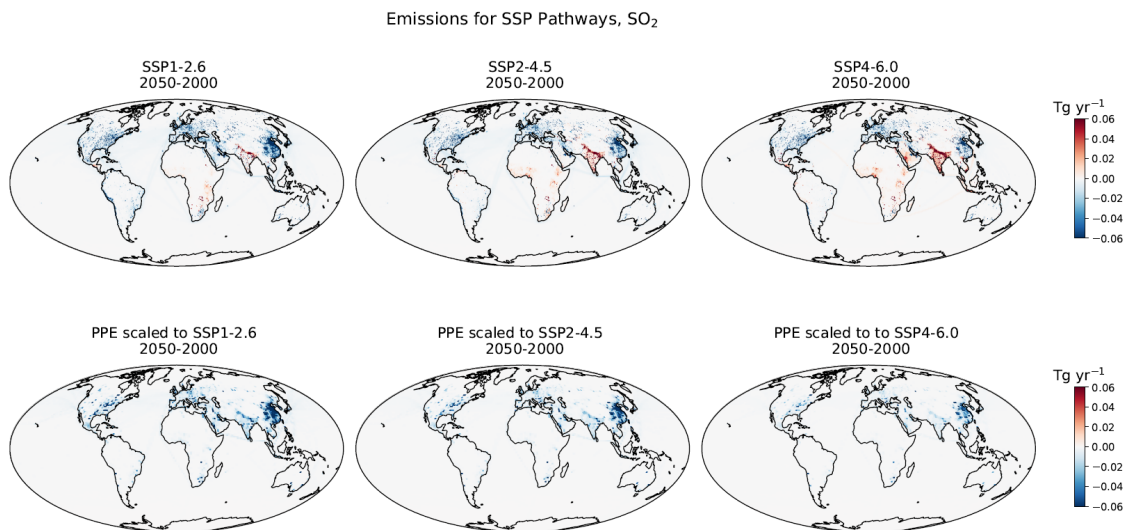


Figure A.3 Anthropogenic SO₂ emission changes in the Shared Socioeconomic Pathways (top row), in comparison to the emission scaling applied in our methods (bottom row).

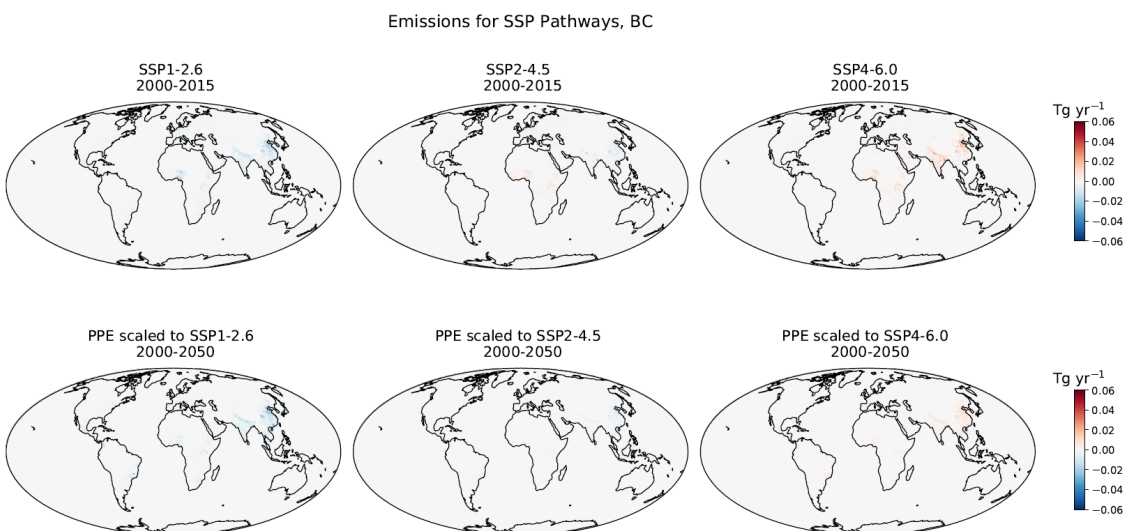


Figure A.4 Black carbon (BC) emission changes in the Shared Socioeconomic Pathways (top row), in comparison to the emission scaling applied in our methods (bottom row).

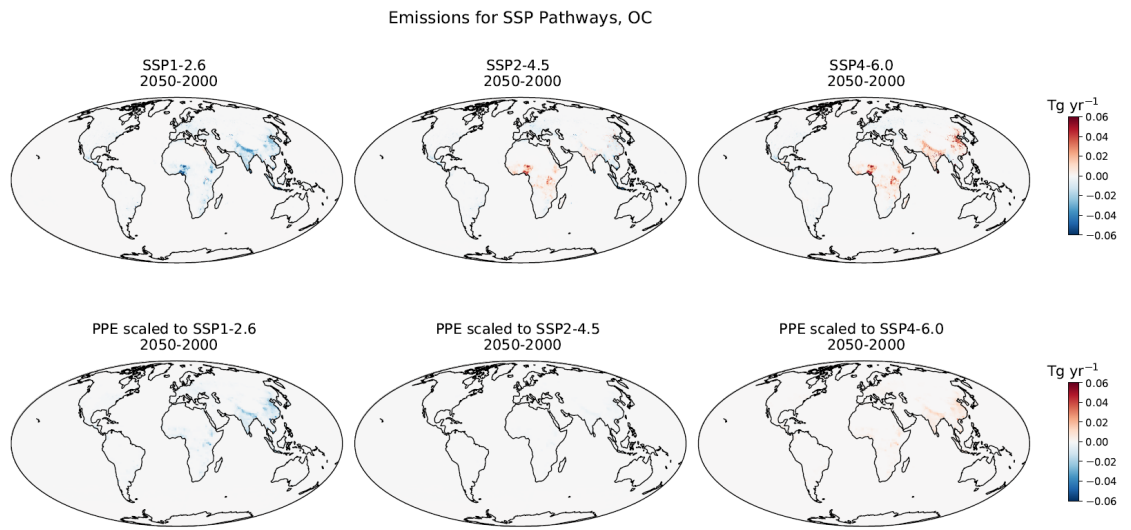


Figure A.5 Organic carbon (OC) emission changes in the Shared Socioeconomic Pathways (top row), in comparison to the emission scaling applied in our methods (bottom row).

A.4 Extrapolation of Aerosol Radiative Forcing

Scenarios with vast reductions of anthropogenic aerosol emissions are outside the ranges of anthropogenic emissions elicited in our PPE. In this case, we have extrapolated radiative forcing (mean, 2.5th percentile, 97.5th percentile and for shortwave + longwave top of atmosphere flux combined) using Python package 'scipy.interpolate, interp1d' against changes in each emission parameter to give an idea of aerosol radiative forcing. To test our extrapolation is accurate we have compared the extrapolation method to the emulator prediction of radiative forcing, both have good agreement as seen in Figure A.6.

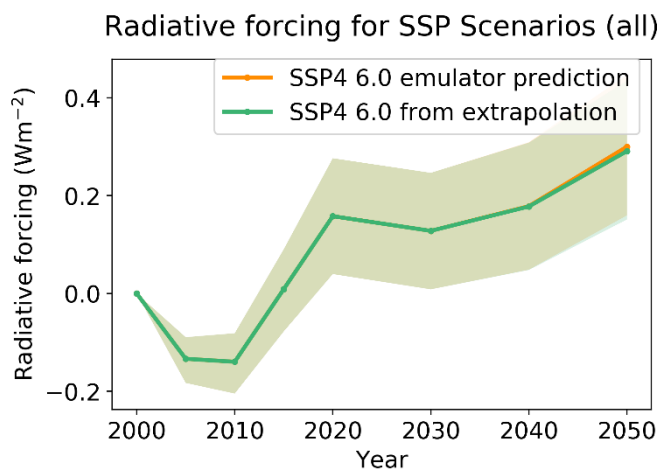


Figure A.6 Green shading indicates extrapolation of 2000-2030 radiative forcing to predict radiative forcing at 2040 and 2050, in comparison to the orange shading of emulator predicted radiative forcing. The comparison shows good agreement between emulator prediction and extrapolation.

A.5 Aerosol Radiative Forcing

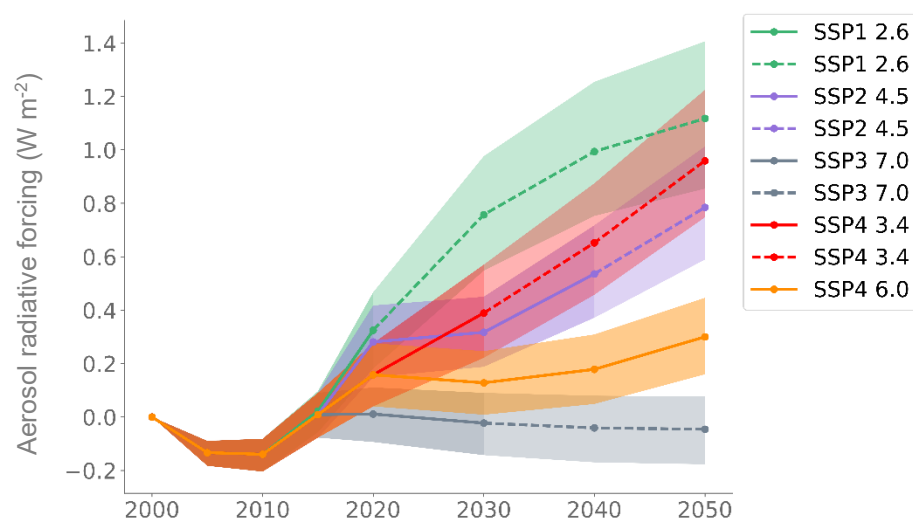


Figure A.7 Global mean aerosol radiative forcing relative to 2000 for selected SSP scenarios. Mean aerosol radiative forcing is represented by the line, and 2.5th and 97.5th percentiles in shaded regions.

	2005	2010	2015	2020	2030	2040	2050
SSP1-2.6	-0.13 (-0.18 to -0.09)	-0.14 (-0.20 to -0.08)	0.02 (-0.06 to 0.10)	0.32 (0.18 to 0.47)	0.75 (0.55 to 0.98)	0.99 (0.75 to 1.25)	1.12 (0.85 to 1.41)
SSP2-4.5	-0.13 (-0.18 to -0.09)	-0.14 (-0.20 to -0.08)	0.00 (-0.08 to 0.09)	0.28 (0.15 to 0.42)	0.32 (0.19 to 0.45)	0.54 (0.37 to 0.72)	0.78 (0.59 to 1.01)
SSP4-6.0	-0.13 (-0.18 to -0.09)	-0.14 (-0.20 to -0.08)	0.00 (-0.08 to 0.09)	0.16 (0.04 to 0.28)	0.13 (0.01 to 0.25)	0.18 (0.05 to 0.31)	0.30 (0.16 to 0.45)
SSP4-3.4	-0.13 (-0.18 to -0.09)	-0.14 (-0.20 to -0.08)	0.01 (-0.08 to 0.09)	0.16 (0.04 to 0.28)	0.39 (0.22 to 0.57)	0.65 (0.46 to 0.87)	0.96 (0.75 to 1.22)
SSP3-7.0	-0.13 (-0.18 to -0.09)	-0.14 (-0.30 to -0.08)	0.01 (-0.08 to 0.09)	0.01 (-0.09 to 0.11)	-0.02 (-0.14 to 0.09)	-0.04 (-0.17 to 0.08)	-0.06 (-0.18 to 0.08)

Table A.2 Global mean aerosol radiative forcing relative to 2000 for SSP scenarios at each time slice shown in main paper. Mean aerosol radiative forcing with 2.5th and 97.5th percentiles in brackets, italics represent where aerosol radiative forcing has been extrapolated.

Figure A.8 (left) shows the aerosol radiative forcing over the period 2010-2040 in each model grid box for emission pathway SSP2-RCP4.5 with anthropogenic SO₂, carbonaceous fossil fuel and carbonaceous biofuel emission scaling, and the associated standard deviation (right). Figure A.9 shows the aerosol radiative forcing for individual emission parameter scalings. Statistical emulators were built and sampled in each grid box to create these figures.

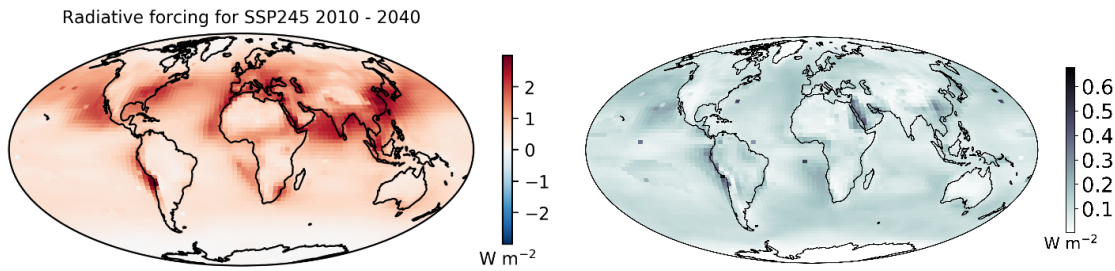


Figure A.8 Emulator mean prediction (left) and standard deviation (left) of 2010-2040 aerosol radiative forcing for anthropogenic aerosol emission scalings in SSP2-RCP4.5

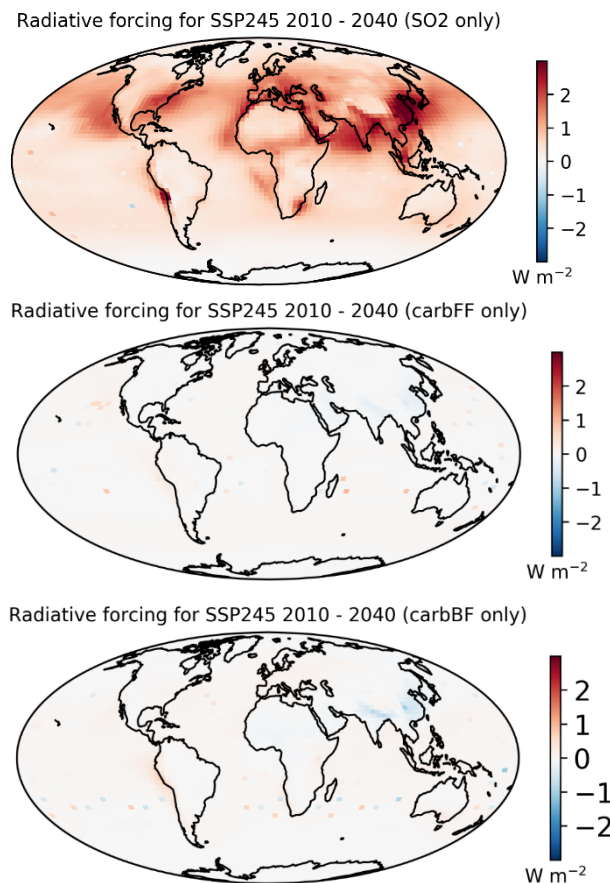


Figure A.9 Emulator mean prediction of 2010-2040 aerosol radiative forcing for individual anthropogenic aerosol emission scalings in SSP2-RCP4.5, anthropogenic SO₂ (top), carbonaceous fossil fuel (middle), and carbonaceous biofuel (bottom).

A.6 Sensitivity Analysis of Aerosol Radiative Forcing

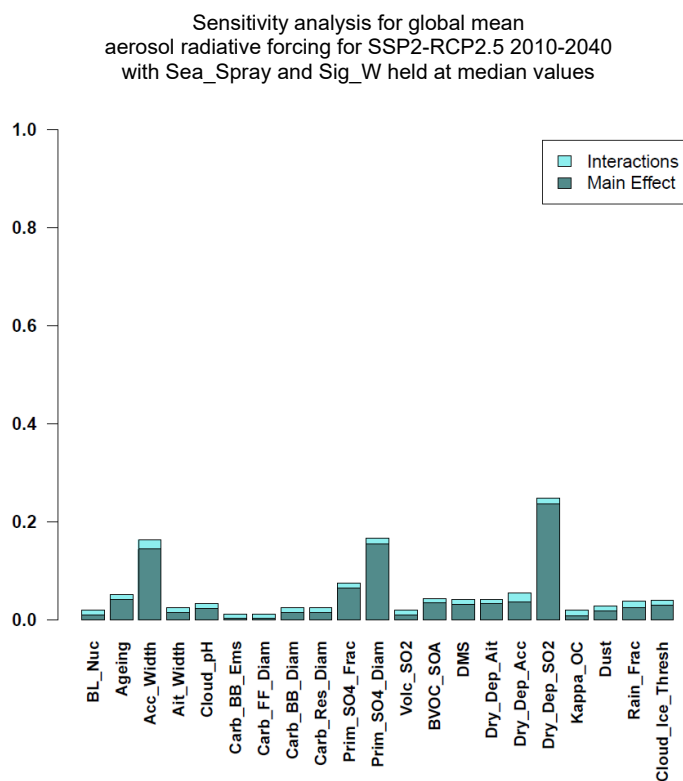
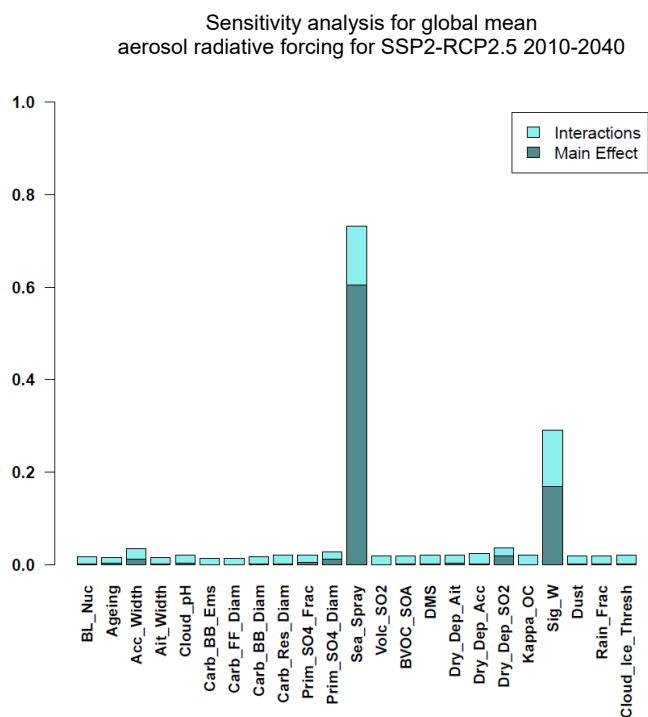


Figure A.10 Fourier Amplitude Sensitivity Analysis of global mean aerosol radiative forcing between 2010-2040 for SSP2-RCP4.5 (top), and with Sea_Spray and Sig_W held at the median values (bottom).

Sensitivity analysis of radiative forcing for SSP245 2010 - 2040

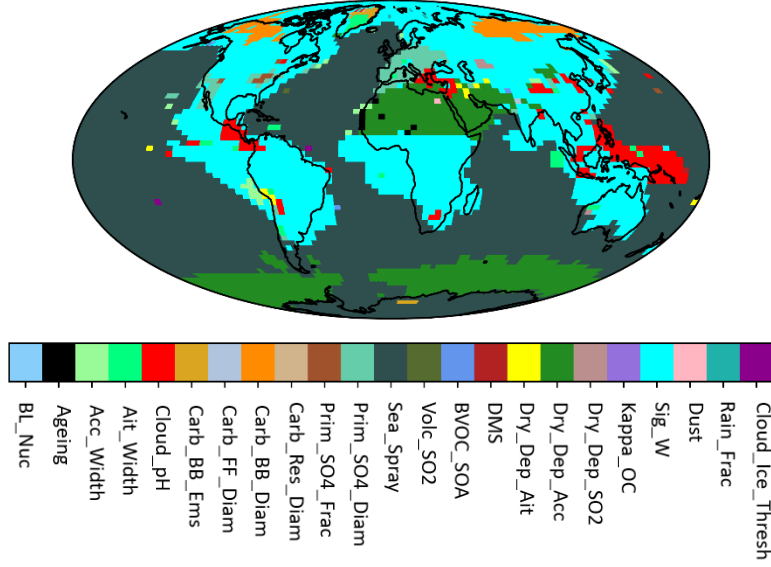


Figure A.11 Sensitivity analysis in each model grid box for aerosol radiative forcing between 2010-2040 for SSP2-RCP4.5.

A.7 Temperature Projections in a Simple Climate Model

A.7.1 Temperature Projections Taking into Account Near-term Aerosol Radiative Forcing Uncertainty

We use the simple climate model, FaIR v1.4, to translate our aerosol radiative forcing uncertainty from anthropogenic aerosol emission reductions into the impact on temperature projections. We use emissions specified by the Shared Socioeconomic Pathways (SSPs) to calculate the forcing of each forcing agent in FaIR throughout the historical and future time series. We then substitute our values for the lower credible interval, mean and upper credible interval of anthropogenic aerosol radiative forcing into FaIR from 2000 onwards, and run FaIR in forcing driven mode to give a range of exceedance years of a 1.5 °C global mean temperature rise due the uncertainty in near-term aerosol radiative forcing only. This approach does not take into account the historical aerosol radiative forcing uncertainty on temperature projections. We use FaIR's constrained estimate of ECS and TCR of 2.75 and 1.6 K respectively throughout the time series, and hence the spread in exceedance year of 1.5 °C is due to the parametric uncertainty in near-term aerosol radiative forcing alone.

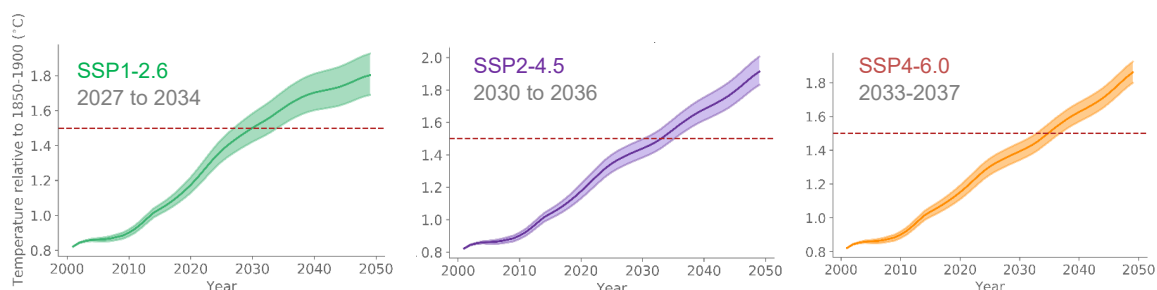


Figure A.12 Global mean temperature change relative to 1850-1900 for three SSP scenarios: SSP1-2.6 (left), SSP2-4.5 (middle) and SSP4-6.0 (right). The solid line represents our mean near-term aerosol radiative forcing, with the shaded area representing our lower to upper credible interval of near-term aerosol radiative forcing.

A.7.2 Temperature Projections Taking into Account Near-Term Aerosol Radiative Forcing Uncertainty, Normalized at a 2000 Baseline to HadCRUT4

To take into account deviation from observed temperatures that may have occurred in FaIR when ran from pre-industrial, we have used the decadal smoothed temperature time series from the HadCRUT4 dataset (Morice et al. 2012) and normalized our temperature projections to these observations at year 2000 when we insert our values for near-term aerosol radiative forcing. The results from this approach are shown in Figure A.13.

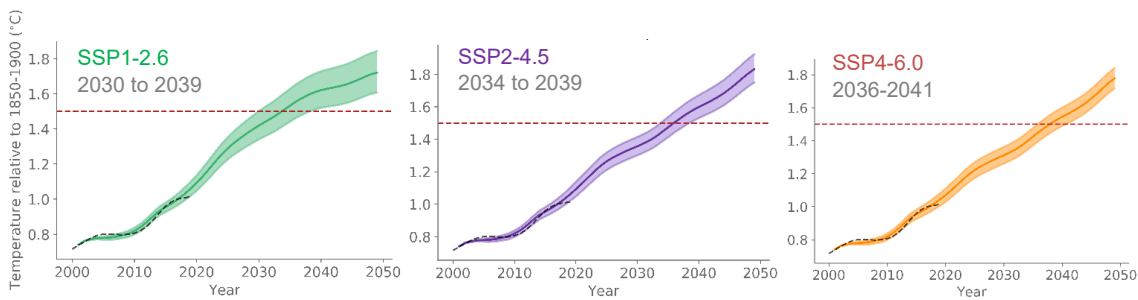


Figure A.13 Global mean temperature change relative to 1850-1900 for three SSP scenarios: SSP1-2.6 (left), SSP2-4.5 (middle) and SSP4-6.0 (right) normalized at 2000 to the HadCRUT4 observations. The solid line represents our mean near-term aerosol radiative forcing, with the shaded area representing our lower to upper credible interval of near-term aerosol radiative forcing, and the black dashed line representing global mean temperature from the HadCRUT4 dataset.

A.7.3 Temperature Projections Taking into Account Near-Term

Aerosol Radiative Forcing and Climate Sensitivity Uncertainty

To account for a statistical relationship between aerosol forcing and climate sensitivity that has been observed in some climate models (Andreae et al, 2005) up to and including the CMIP5 generation, we select values of equilibrium climate sensitivity (ECS) and through correlation transient climate response (TCR) (Smith et al 2018) that may be appropriate for our magnitude of aerosol radiative forcing. The IPCC AR5 gives a likely range of ECS of 1.5-4.5 K, and TCR of 1-2.5 K. Hence, we use an illustrative approach of combining this range of ECS and TCR, with our range of near-term aerosol radiative forcing to illustrate what the effect may look like if we account for the collective uncertainty in near-term aerosol radiative forcing, ECS and TCR. We run our temperature projections with the settings shown in Table A.3, so that the strong aerosol forcing projection also has a high ECS and TCR, whereas the weak aerosol forcing projection has a low ECS and TCR. The results for each scenario, for the mean, weak and strong credible interval of near-term aerosol radiative forcing and their corresponding ECS/TCR are shown below in Figure A.14 (no normalization) Figure A.15 (with normalization). We have also shown in Figure A.16 how the range in exceedance year of a 1.5 °C global mean temperature rise (with normalization) would narrow if the uncertainty in ECS and TCR was smaller.

Likewise to the method described in Section A7.1, we use our near-term aerosol radiative forcing from 2000 onwards, and also take use the relevant ECS/TCR for our aerosol radiative forcing from this point.

	ECS / K	TCR / K
Historical (default)	2.75	1.6
Weak near-term aerosol RF	1.5	1.0
Mean near-term aerosol RF	3.0	1.75
Strong near-term aerosol RF	4.5	2.5

Table A.3 The ECS and TCR values used to illustrative the collective uncertainty on exceedance year of 1.5 °C when the relationship between aerosol forcing and climate sensitivity is taken into account.

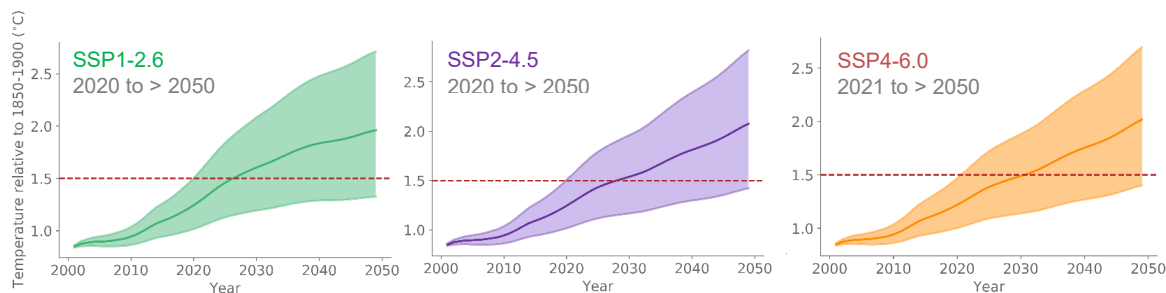


Figure A.14 Global mean temperature change relative to 1850-1900 for three SSP scenarios: SSP1-2.6 (left), SSP2-4.5 (middle) and SSP4-6.0 (right). The solid line represents our mean near-term aerosol radiative forcing and relevant ECS and TCR values, with the shaded area representing our lower to upper credible interval of near-term aerosol radiative forcing with the corresponding ECS and TCR as given in Table A.3.

A.7.4 Temperature Projections Taking into Account Near-Term Aerosol Radiative Forcing and Climate Sensitivity Uncertainty Normalized at a 2000 baseline to HadCRUT4

Figure A.15 shows the same approach as that described in Section A8.3, but the temperature at year 2000 is normalized to the value from HadCRUT4 observations.

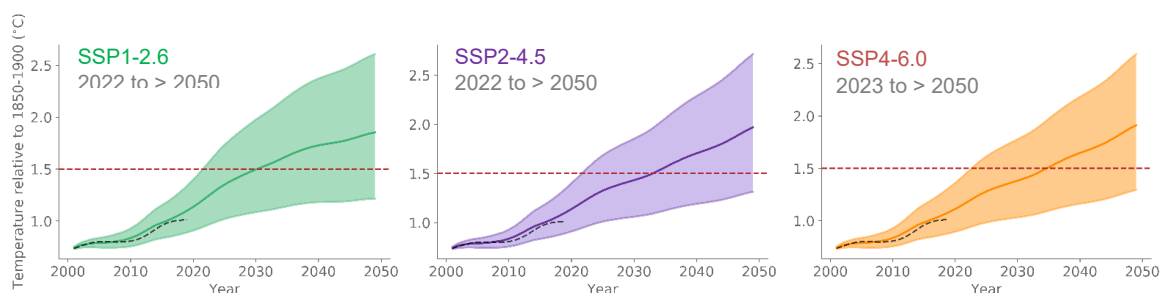


Figure A.15 Global mean temperature change relative to 1850-1900 for three SSP scenarios: SSP1-2.6 (left), SSP2-4.5 (middle) and SSP4-6.0 (right) normalized at 2000 to the HadCRUT4 observations. The solid line represents our mean near-term aerosol radiative forcing and relevant ECS and TCR values, with the shaded area representing our lower to upper credible interval of near-term aerosol radiative forcing with the corresponding ECS and TCR as given in Table A.3, the black dashed line represents global mean temperature from the HadCRUT4 dataset.

For illustrative purposes we have also used the same methodology as in Figure A.15 but paired our aerosol radiative forcing with a narrower upper range of ECS (3-4.5 K) and TCR (1.75-2.5 K) to show the effect of the uncertainty in aerosol radiative forcing and climate sensitivity on projected exceedance year of a 1.5 °C global mean temperature rise if the uncertainty in ECS and through correlation TCR was smaller.

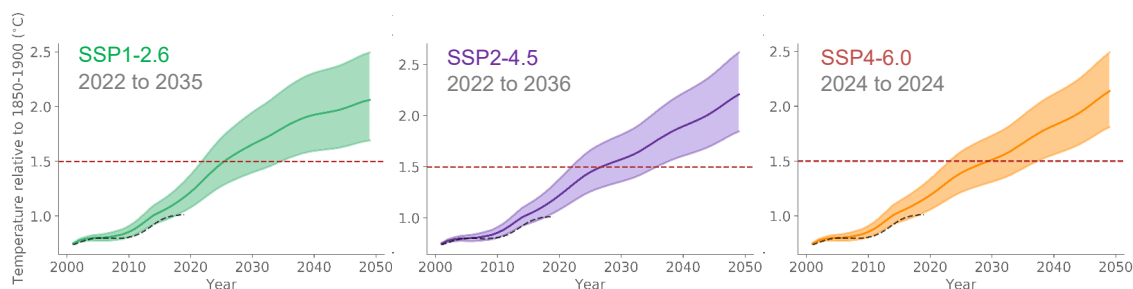


Figure A.16 Global mean temperature change relative to 1850-1900 for three SSP scenarios: SSP1-2.6 (left), SSP2-4.5 (middle) and SSP4-6.0 (right) normalized at 2000 to the HadCRUT4 observations. The solid line represents our mean near-term aerosol radiative forcing and an ECS of 3.75 K and TCR of 2.12 K, with the shaded area representing our lower to upper credible interval of near-term aerosol radiative forcing with a corresponding ECS of 3 and 4.5 K and TCR of 1.75 and 2.5 K, the black dashed line represents global mean temperature from the HadCRUT4 dataset.

A.7.5 Limitations and assumptions

FaIR uses effective radiative forcing (ERF) for its forcing agents where possible. In FaIR, ERF_{air} includes the direct radiative effect of aerosols, in addition to rapid adjustments due to changes in the atmospheric temperature, humidity and cloud profile, assuming a linear relationship between BC, OC, SO₂, NO_x, NH₃, and NMVOC emissions and forcing. We note this is different to the treatment of aerosols in our PPE, where due to the degree of nudging, rapid adjustments due to changes in temperature, humidity and cloud profile above 1200m will not be part of aerosol radiative forcing. For aerosol-cloud interactions, FaIR uses a logarithmic relationship between changes in SO₂, OC, BC emissions and aerosol forcing. Since FaIR is tuned on AR5 results, which are weaker than our pre-industrial to present-day aerosol forcing in the PPE, the default time series of aerosol forcing will be less negative. Therefore, we expect there to be a stronger temperature response to changing aerosol emissions when we use our near-term aerosol forcing values. From 2000 onwards we input our aerosol radiative forcing for BC, OC and SO₂, emission reductions, in addition to FaIR's calculated forcing for the other aerosol species (NO_x, NH₃, NMVOC).

References

- Andreae, M. O., Jones, C. D. and Cox, P. M.: Strong present-day aerosol cooling implies a hot future, *Nature*, 435(7046), 1187–1190, doi:10.1038/nature03671, 2005.
- Forster, P. and Artaxo, P.: Changes in Atmospheric Constituents and in Radiative Forcing. [online] Available from: <https://www.ipcc.ch/report/ar4/wg1/changes-in-atmospheric-constituents-and-radiative-forcing/> (Accessed 27 April 2020), 2005.
- Morice, C. P., Kennedy, J. J., Rayner, N. A. and Jones, P. D.: Quantifying uncertainties in global and regional temperature change using an ensemble of observational estimates: The HadCRUT4 data set, *J. Geophys. Res. Atmos.*, 117(8), n/a-n/a, doi:10.1029/2011JD017187, 2012.
- Myhre, G., Shindell, D., Aamaas, B., Boucher, O., Dalsøren, S., Daniel, J., Forster, P., Granier, C., Haigh, J. and Hodnebrog, Ø.: Anthropogenic and natural radiative forcing, in *Climate Change 2013 the Physical Science Basis: Working Group I Contribution to the Fifth Assessment Report of the Intergovernmental Panel on Climate Change*, vol. 9781107057, pp. 659–740., 2013a.
- Myhre, G., Samset, B. H., Schulz, M., Balkanski, Y., Bauer, S., Bernsten, T. K., Bian, H., Bellouin, N., Chin, M., Diehl, T., Easter, R. C., Feichter, J., Ghan, S. J., Hauglustaine, D., Iversen, T., Kinne, S., Kirkevåg, A., Lamarque, J. F., Lin, G., Liu, X., Lund, M. T., Luo, G., Ma, X., Van Noije, T., Penner, J. E., Rasch, P. J., Ruiz, A., Seland, Skeie, R. B., Stier, P., Takemura, T., Tsigaridis, K., Wang, P., Wang, Z., Xu, L., Yu, H., Yu, F., Yoon, J. H., Zhang, K., Zhang, H. and Zhou, C.: Radiative forcing of the direct aerosol effect from AeroCom Phase II simulations, *Atmos. Chem. Phys.*, 13(4), 1853–1877, doi:10.5194/acp-13-1853-2013, 2013b.
- Randall, D., Artaxo, P., Bretherton, C., Feingold, G., Forster, P., Kerminen, V., Kondo, Y., Liao, H., Lohmann, U., Rasch, P., Satheesh, S., Sherwood, S., Stevens, B., Zhang, X., Qin, D., Plattner, G., Tignor, M., Allen, S., Boschung, J., Nauels, A., Xia, Y., Bex, V., Midgley, P., Boucher, O. and Randall, D.: Clouds and aerosols, in *Climate Change 2013 the Physical Science Basis: Working Group I Contribution to the Fifth Assessment Report of the Intergovernmental Panel on Climate Change*, vol. 9781107057, pp. 571–658., 2013.
- Shindell, D. T., Lamarque, J. F., Schulz, M., Flanner, M., Jiao, C., Chin, M., Young, P. J., Lee, Y. H., Rotstajn, L., Mahowald, N., Milly, G., Faluvegi, G., Balkanski, Y., Collins, W. J., Conley, A. J., Dalsoren, S., Easter, R., Ghan, S., Horowitz, L., Liu, X., Myhre, G., Nagashima, T., Naik, V., Rumbold, S. T., Skeie, R., Sudo, K., Szopa, S., Takemura, T., Voulgarakis, A., Yoon, J. H. and Lo, F.: Radiative forcing in the ACCMIP historical and future climate simulations, *Atmos. Chem. Phys.*, 13(6), 2939–2974, doi:10.5194/acp-13-2939-2013, 2013.
- Smith, C. J., Forster, P. M., Allen, M., Leach, N., Millar, R. J., Passerello, G. A. and Regayre, L. A.: FAIR v1.3: A simple emissions-based impulse response and carbon cycle model, *Geosci. Model Dev.*, 11(6), 2273–2297, doi:10.5194/gmd-11-2273-2018, 2018.
- Smith, C. J., Kramer, R. J., Myhre, G., Alterskjær, K., Collins, W., Sima, A., Boucher, O., Dufresne, J. L., Nabat, P., Michou, M., Yukimoto, S., Cole, J., Paynter, D. J., Shiogama, H., O'Connor, F. M., Robertson, E., Wiltshire, A., Andrews, T., Hannay, C., Miller, R., Nazarenko, L., Kirkevåg, A., Olivie, D., Fiedler, S., Pincus, R. and Forster, P. M.: Effective radiative forcing and rapid adjustments in CMIP6 models, *Atmos. Chem. Phys. Discuss.* [online] Available from: <https://www.atmos-chem-phys-discuss.net/acp-2019-1212/> (Accessed 27 April 2020), 2020.
- Yoshioka, M., Regayre, L. A., Pringle, K. J., Johnson, J. S., Mann, G. W., Partridge, D. G., Sexton, D. M. H., Lister, G. M. S., Schutgens, N., Stier, P., Kipling, Z., Bellouin, N., Browse, J., Booth, B. B., Johnson, C. E., Johnson, B., Mollard, J. D. P., Lee, L. and Carslaw, K. S.: Ensembles of Global Climate Model Variants Designed for the Quantification and Constraint of Uncertainty in Aerosols and their Radiative Forcing, *J. Adv. Model. Earth Syst.*, 11(11), 3728–3754, doi:10.1029/2019ms001628, 2019.

Appendix B

Perturbed parameter	Name	Description
Convection		
ent_fac_dp	Deep entrainment amplitude	Controls the shape of the mass flux and sensitivity of deep convection to relative humidity to deep entrainment.
ent_fac_md	Mid entrainment amplitude	Controls the shape of the mass flux and the sensitivity of mid-level convection to relative humidity to mid-level entrainment.
amdet_fac	Mixing detrainment	Controls the rate of humidification of the atmosphere and the shape of the convective heating profile.
r_det	Coefficient for adaptive detrainment	Decrease of mass flux with height under decreasing parcel buoyancy.
cca_md_knob, cca_dp_knob	Convective core radiative effects	Controls how much deep and mid-level convective core gets seen by radiation.
cca_sh_knob	Shallow convection core radiative effects	Controls how much shallow convection gets seen by radiation.
mparwtr	Maximum condensate	The maximum condensate a convective parcel can hold before it is converted to precipitation.
qlmin	Minimum critical cloud condensate	The minimum value of the function that defines the maximum amount of condensate a convective parcel can hold before it is converted to precipitation.
Gravity wave drag		
gwd_frc	Critical Froude number	Determines the cut-off mountain height and the depth of the blocked flow layer around sub-grid mountains.
fbcd	Flow blocking drag coefficient	Determines the size of the low-level drag associated with flow blocking effects by sub-grid mountains.

gwd_fsat	Inverse critical Froude number for wave saturation	Determines the amplitude at which mountain waves generated by sub-grid orography will break, and exert a drag on the flow.
gsharp	Mountain wave amplitude	Determines the amplitude of the mountain waves generated by sub-grid orography.
orog_drag_param	Drag coefficient for turbulent form drag	Determines the size of the form drag exerted on flow by small-scale sub-grid hills.
nsigma	Scaling factor applied to the standard deviation of sub-grid mountain heights	Determines the local assumed sub-grid orography height which is used in the gravity wave drag scheme.
Boundary layer		
g0	Flux profile parameter	Used in the definition of stability functions.
ricrit = 10.0 / g0	Critical Richardson number	Value of Richardson number below which air becomes dynamically unstable and turbulent.
a_ent_1	Cloud-top entrainment rate.	Used in entrainment rate calculation.
g1	Cloud-top diffusion	Used in cloud-top diffusion calculation.
zhloc_depth_fac	Threshold fraction of the cloud layer depth	Fractional height into cloud layer for which Ri-based boundary layer depth can diagnose shear dominated layer.
par_mexcla	Neutral mixing length	Mixing length for fluid parcels under neutral stability conditions.
lambda_min	Minimum value of mixing length	
dec_thresh_cld, dec_thresh_cloud2cu	Decoupling threshold for cloud boundary layers.	
forced_cub_fac	Mixing factor applied to the in-cloud water content of forced cumulus clouds	Determines the fraction of diagnosed adiabatic water content of forced cumulus clouds which is allowed to remain.
Clouds and cloud radiation		
dbstdtbs_turb_0	Cloud erosion rate	Determines the rate which un-resolved sub-grid motions mix clear and cloudy air.

two_d_fsd_factor	Scaling to make sub-grid cloud condensate variance to cloud cover and convective activity to dimensional	Makes the cloud water variability around the grid box average a two dimensional relationship, based on 1-d empirical relationship.
dp_corr_strat	Decorrelation scale pressure	Determines the vertical overlap between clouds in the sub-column in the cloud generator used to calculate the radiative impact of clouds.
ice_width	Ice width	Determines the amount of ice water content that corresponds to a factor of two reduction in the width of the vapour distribution in the liquid-free part of the grid box.
Cloud microphysics		
c_r_correl	Cloud-rain correlation coefficient	Determines the sub-grid correlation between cloud and precipitation.
m_ci	Ice fall speed	Scaling factor for the ice fall speed.
ai	Precursor coefficient in the mass-diameter relationship for ice	Changing ai has the effect of changing the density of ice.
x1r		Controls the shape of the PSD for raindrops.
ar	Aspect ratio of ice particles	Used to calculate the depositional capacitance of ice crystals which affects how efficiently they grow by depleting water vapour.
mp_dz_scal	Vertical scale in mixed-phase turbulent production of supercooled liquid water	Vertical length scale over which the turbulence acts to produce supercooled water.
Aerosols		
ps_anth_so2_emiss	Anthropogenic SO ₂ emission flux	Direct scaling of anthropogenic SO ₂ emission flux.

ps_dry_so2_veloc	Dry deposition rate of SO ₂	Scaling factor for the dry deposition rate which removes SO ₂ from lowest levels through deposition according to land surface type and prevailing wind speed.
ps_sigma_updraught	Scaling of the standard deviation use to define the pdf of updraught velocity	Relates the activation of aerosols to cloud droplets to the standard deviation used to define the pdf of updraught velocity.
biom_aer_ems_scaling	Scaling of emission flux from biomass burning	Direct scaling of emission flux.
ps_natl_ss_emiss	Scaling of emission flux from sea spray	Direct scaling of emissions flux.
pd_natl_dms_emiss	Dimethyl-sulphide emission flux	Direct scaling of emissions flux.
ps_acc_cor_scav	Scavenging rate in the coarse and accumulation modes	Scaling of the scavenging rate calculated in the model.
ps_cloud-pH	pH of cloud drops	Controls the in-cloud SO ₄ production dependent on SO ₂ availability.
Land surface and snow		
u10_max_coare	Maximum wind speed used in the Coupled Ocean-Atmosphere Response Experiment (COARE) algorithm	This is the highest wind speed used in calculating the Charnock coefficient in the COARE algorithm.
r0	Grain size of fresh snow	The grain size of fresh snow is set to this value.
rho_snow_fresh	Fresh snow density	The density of fresh snow.
tupp_io	Upper value about 4K above the optimal value for photosynthesis	Temperatures above the optimal value for photosynthesis will drive a decline in photosynthesis.
f0_io	Maximum ratio of internal to external CO ₂	Controls the gradient of CO ₂ between plant stomata and the ambient air.

dz0v_dh_io	Rate of change of vegetation roughness length for momentum with height	Controls surface roughness which affects the surface exchange of momentum and therefore heat, water and trace gases.
nl0-io	Top leaf nitrogen concentration	Defines the top leaf ration of nitrogen to carbon. Plant photosynthesis is defined in the model to be proportional to the leaf nitrogen concentration.
rootd_ft_io	Root depth	Controls the depth to which soil moisture is available.
psm	Scaling factor for critical and saturation levels for soil moisture towards wilt level	This pair of parameters control the critical and saturated volumetric soil moisture thresholds. The critical threshold controls the level above which evapotranspiration is no longer soil moisture dependent.

Table B.1 Perturbed parameters (47 independent and 5 dependent) in the GC3.05-PPE. Descriptions are from, and more detail of parameters can be found in Murphy et al. 2018.

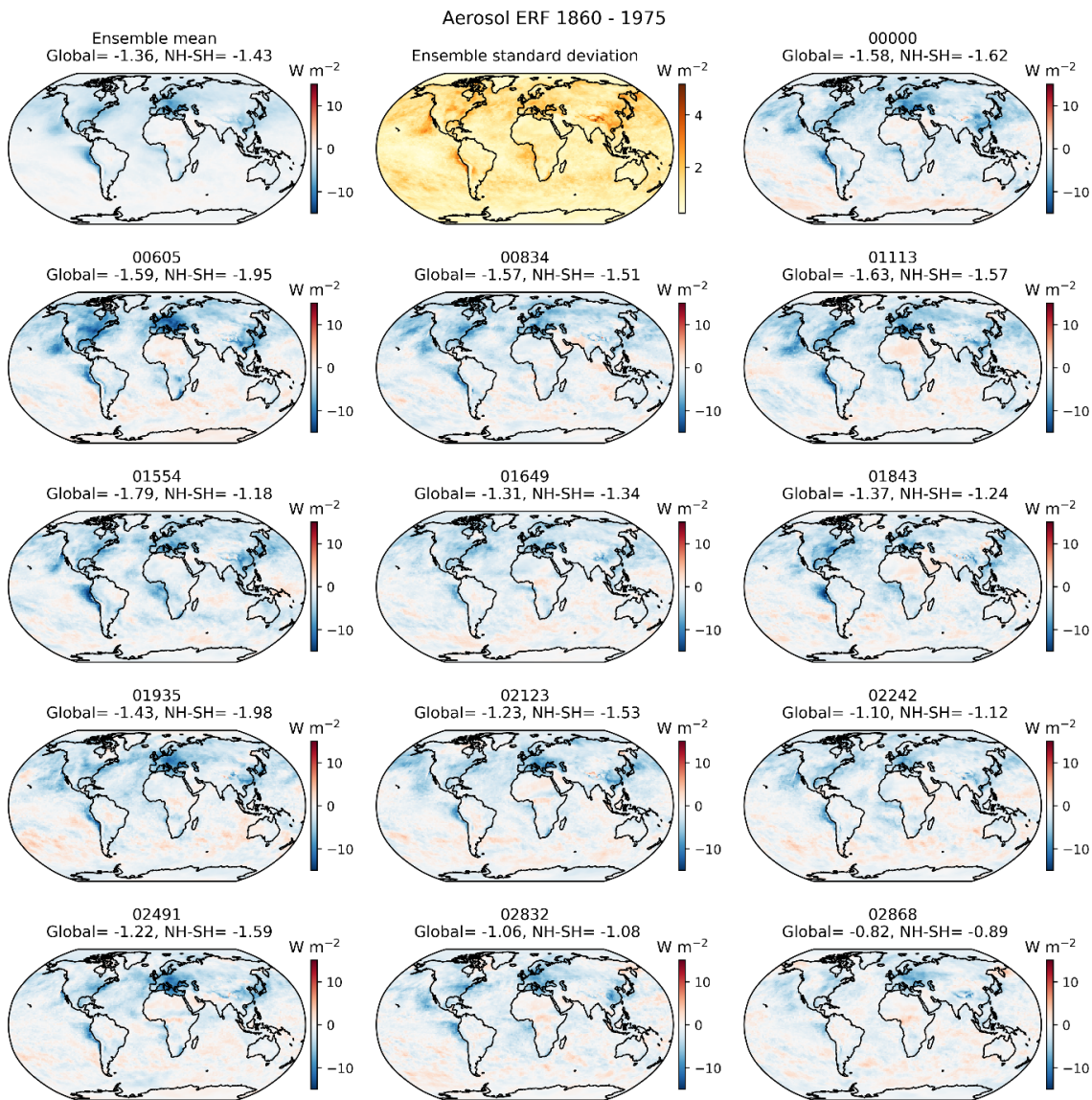


Figure B.1 1860 to 1975 aerosol ERF for individual ensemble members. Global mean aerosol ERF, and northern hemisphere (0 to 60 °N) – southern hemisphere (0 to 60 °S) are shown above each ensemble member. The ensemble mean and standard deviation are shown in the first two plots.

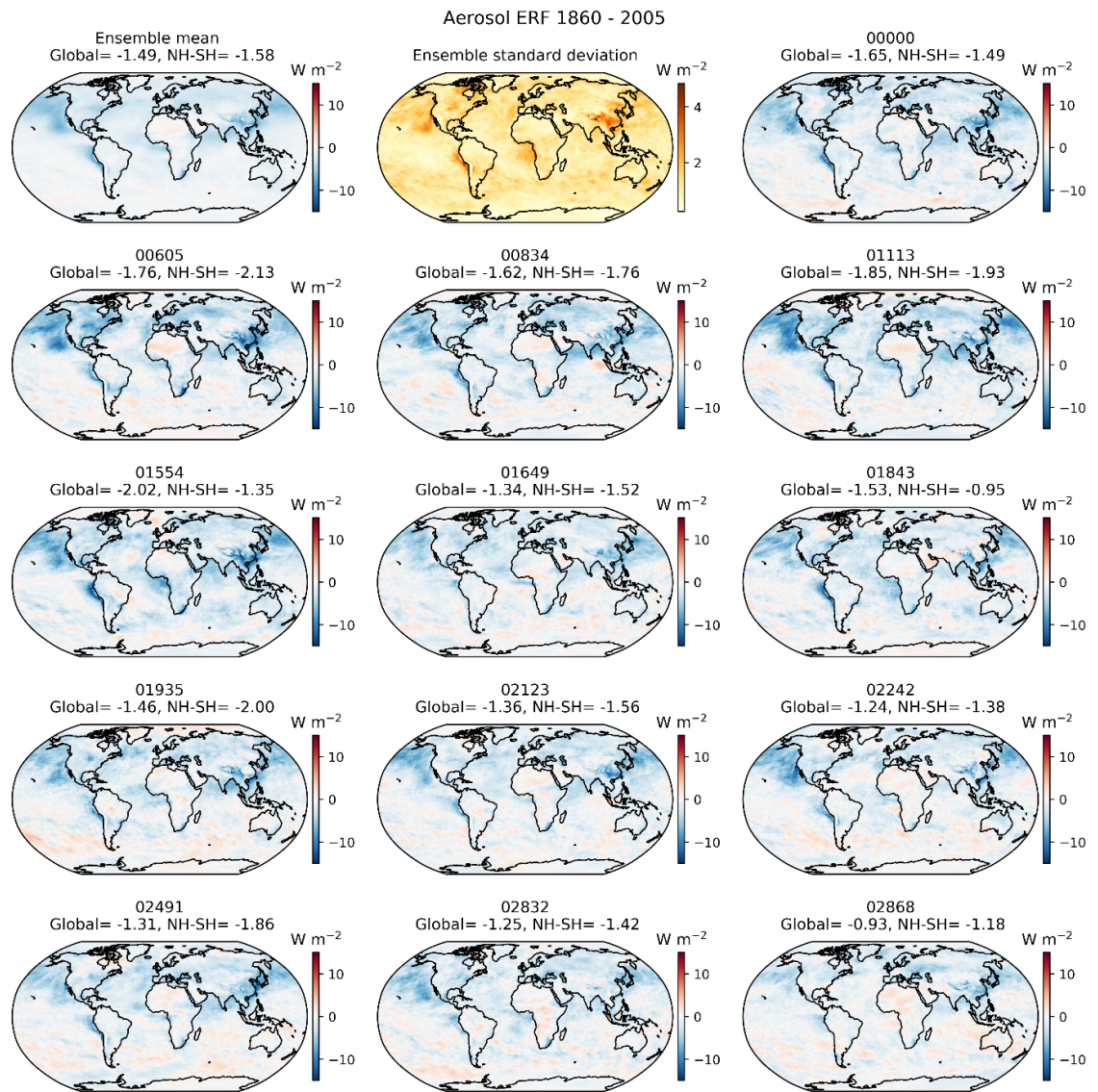


Figure B.2 1860 to 2005 aerosol ERF for individual ensemble members. Global mean aerosol ERF, and northern hemisphere (0 to 60 °N) – southern hemisphere (0 to 60 °S) are shown above each ensemble member. The ensemble mean and standard deviation are shown in the first two plots.

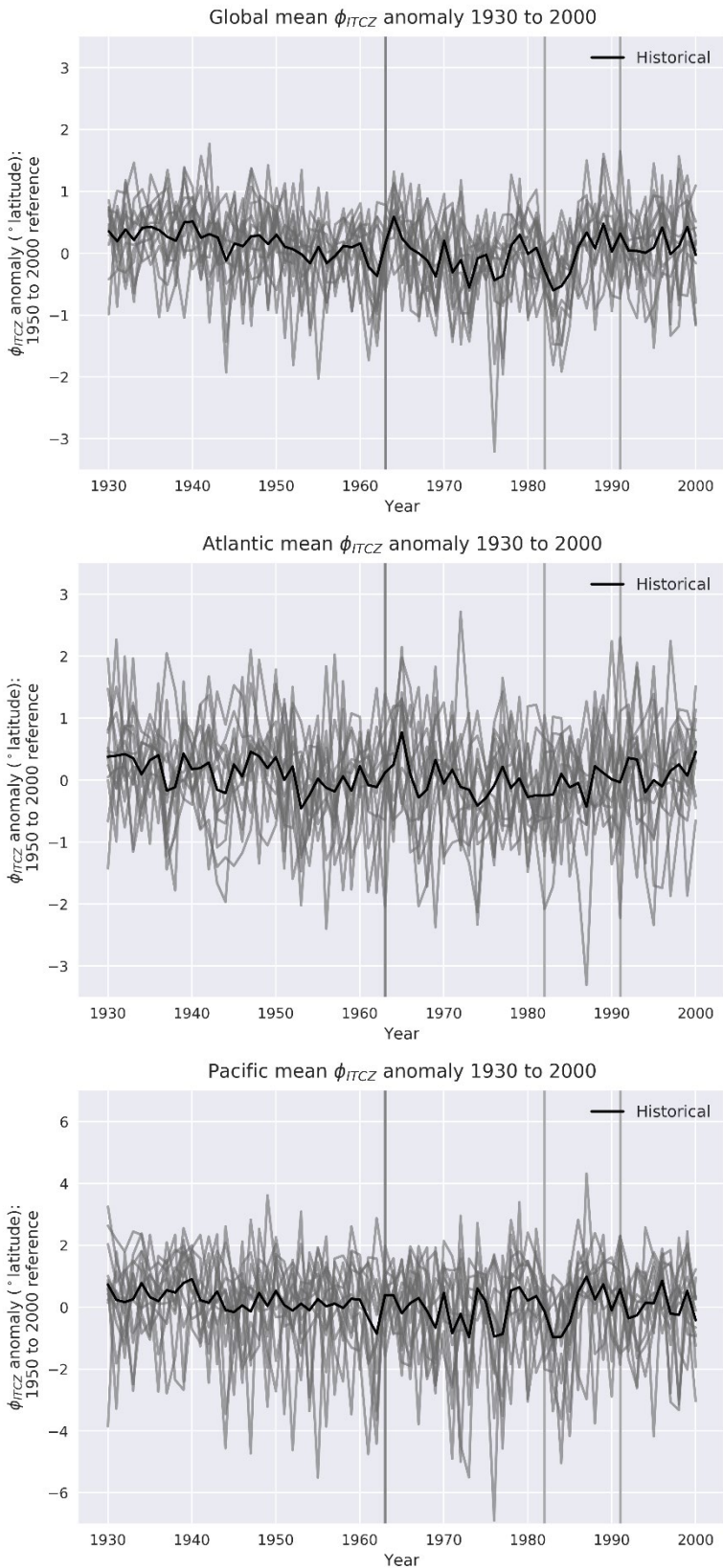


Figure B.3 Time series of ϕ_{ITCZ} anomaly against a 1950 to 2000 reference period with no rolling mean for global (top, 0 - 360 ° longitude), Atlantic (middle, -70 - 10 ° longitude) and Pacific regional means (150 - 285 ° longitude). Historical emissions are shown in black, RCP8.5 in red and RCP2.6 in blue. Major volcanic eruptions are marked with grey vertical lines. The ensemble mean is shown by the darker line, and the individual ensemble members in the lighter lines.

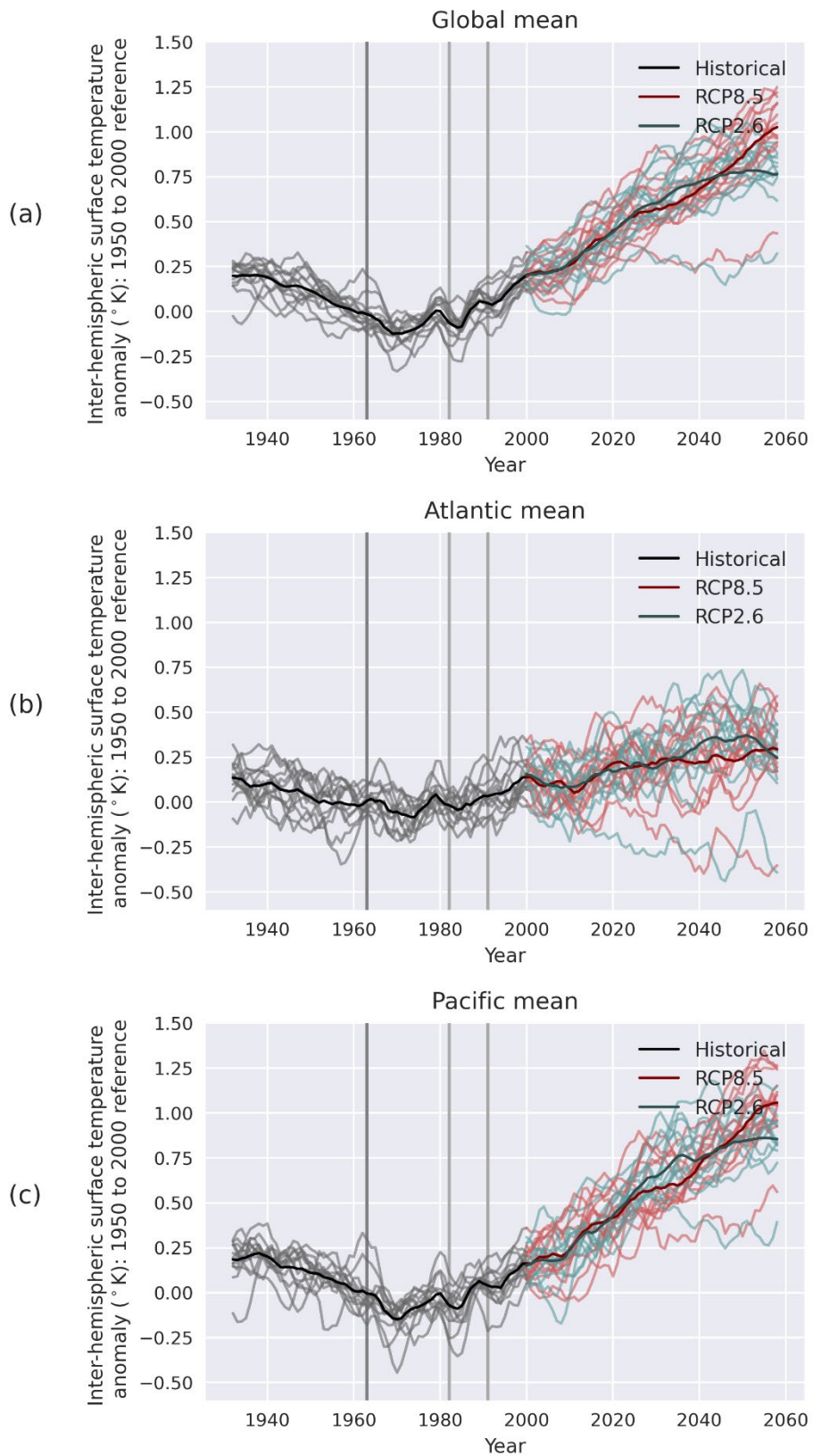


Figure B.4 Time series of the inter-hemispheric (60 °S to 60 °N, NH-SH) surface temperature anomaly against a 1950 to 2000 reference period with a 5-year rolling mean for global (top, 0 - 360 ° longitude), Atlantic (middle, -70 - 10 ° longitude) and Pacific regional means (150 - 285 ° longitude). Historical emissions are shown in black, RCP8.5 in red and RCP2.6 in blue. Major volcanic eruptions are marked with grey vertical lines. The ensemble mean is shown by the darker line, and the individual ensemble members in the lighter lines.

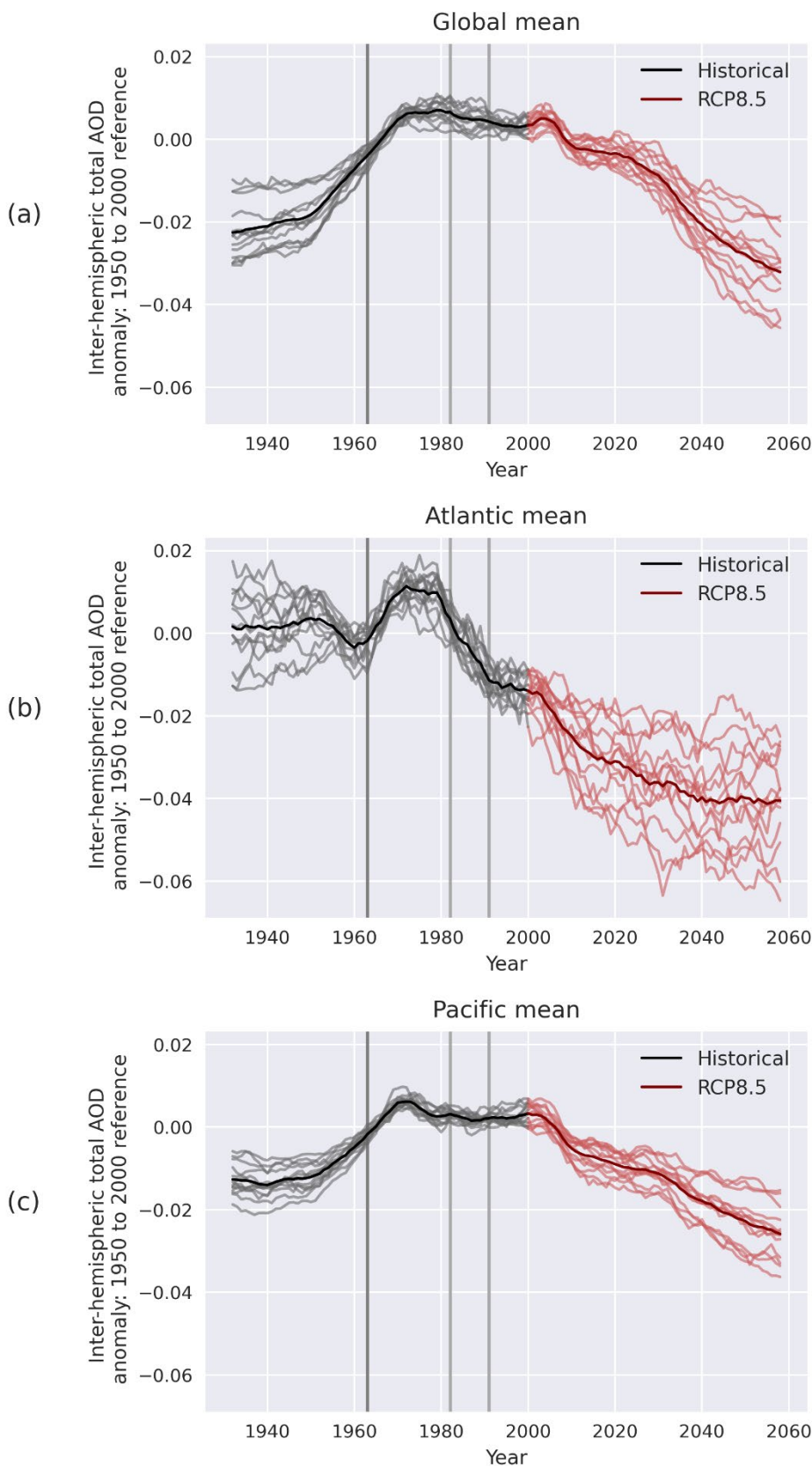


Figure B.5 Time series of the inter-hemispheric (60 °S to 60 °N, NH-SH) total AOD anomaly against a 1950 to 2000 reference period with a 5-year rolling mean for global (top, 0 - 360 ° longitude), Atlantic (middle, -70 - 10 ° longitude) and Pacific regional means (150 - 285 ° longitude). Historical emissions are shown in black and RCP8.5 in red. Major volcanic eruptions are marked with grey vertical lines. The ensemble mean is shown by the darker line, and the individual ensemble members in the lighter lines.

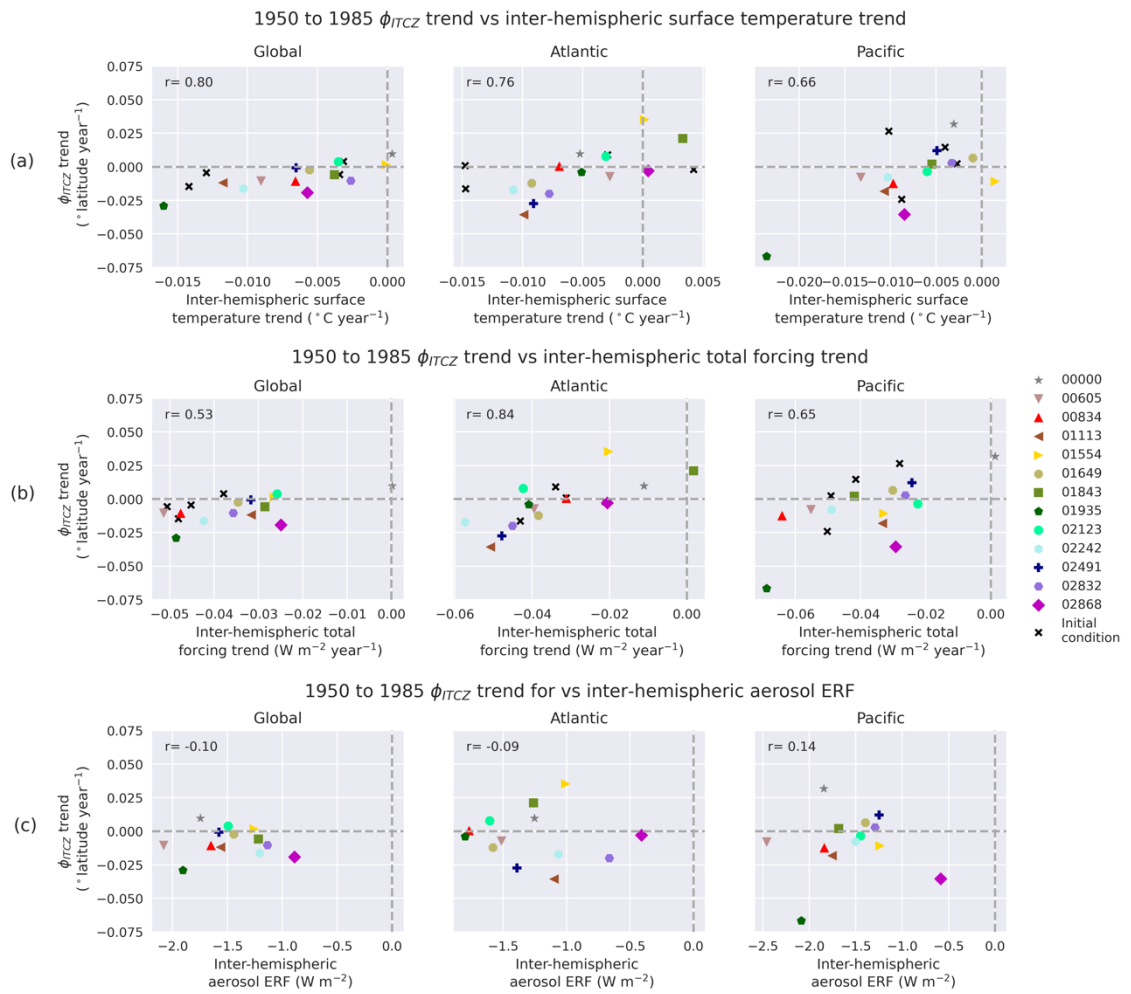
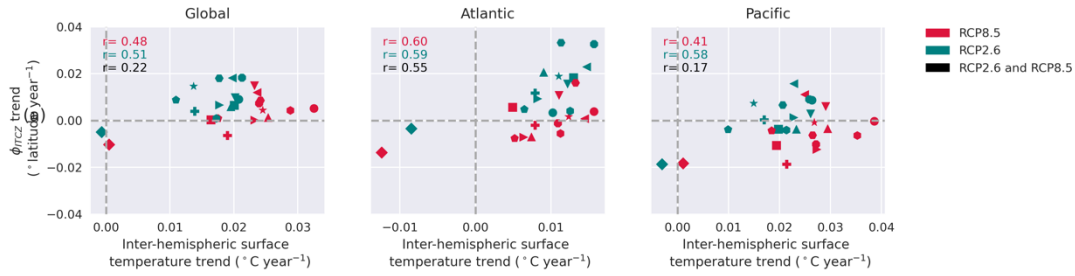
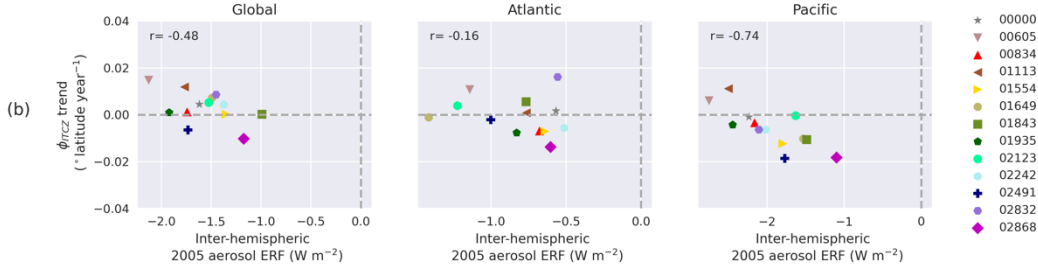


Figure B.6 Scatter plot of the 1950 to 1985 trend in 5-year rolling mean Φ_{ITCZ} against the 1950 to 1985 trend in inter-hemispheric (over 90° S to 90° N) surface air temperature (a), implied total radiative forcing (b) and anthropogenic aerosol ERF (c) for global (left), Atlantic (middle) and Pacific (right) regional means. Anthropogenic aerosol ERF is calculated over 1860 to 1975 for the PPE. The Spearman's rank correlation coefficient between variables is shown at top left of each plot.

2006 to 2060 ϕ_{ITCZ} trend vs inter-hemispheric surface temperature trend for RCP2.6 and RCP8.5



2006 to 2060 ϕ_{ITCZ} trend for RCP8.5 vs 1860 to 2005 inter-hemispheric aerosol ERF



2006 to 2060 ϕ_{ITCZ} trend for RCP2.6 vs 1860 to 2005 inter-hemispheric aerosol ERF

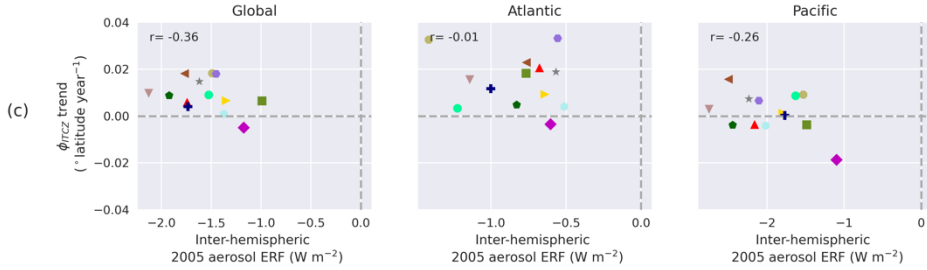


Figure B.7 Scatter plot of trend in 5-year rolling mean ϕ_{ITCZ} in 2006 to 2060 against the trend in inter-hemispheric (90 °S-90 °N) surface air temperature (a), and 1860 to 2005 anthropogenic aerosol ERF (b, c) for global (left), Atlantic (middle) and Pacific regional means (right). The Spearman's rank correlation coefficient is shown at top left of each plot.

ϕ_{ITCZ} trend for 1950 to 1985 vs ocean-only inter-hemispheric variables (60° S to 60° N)

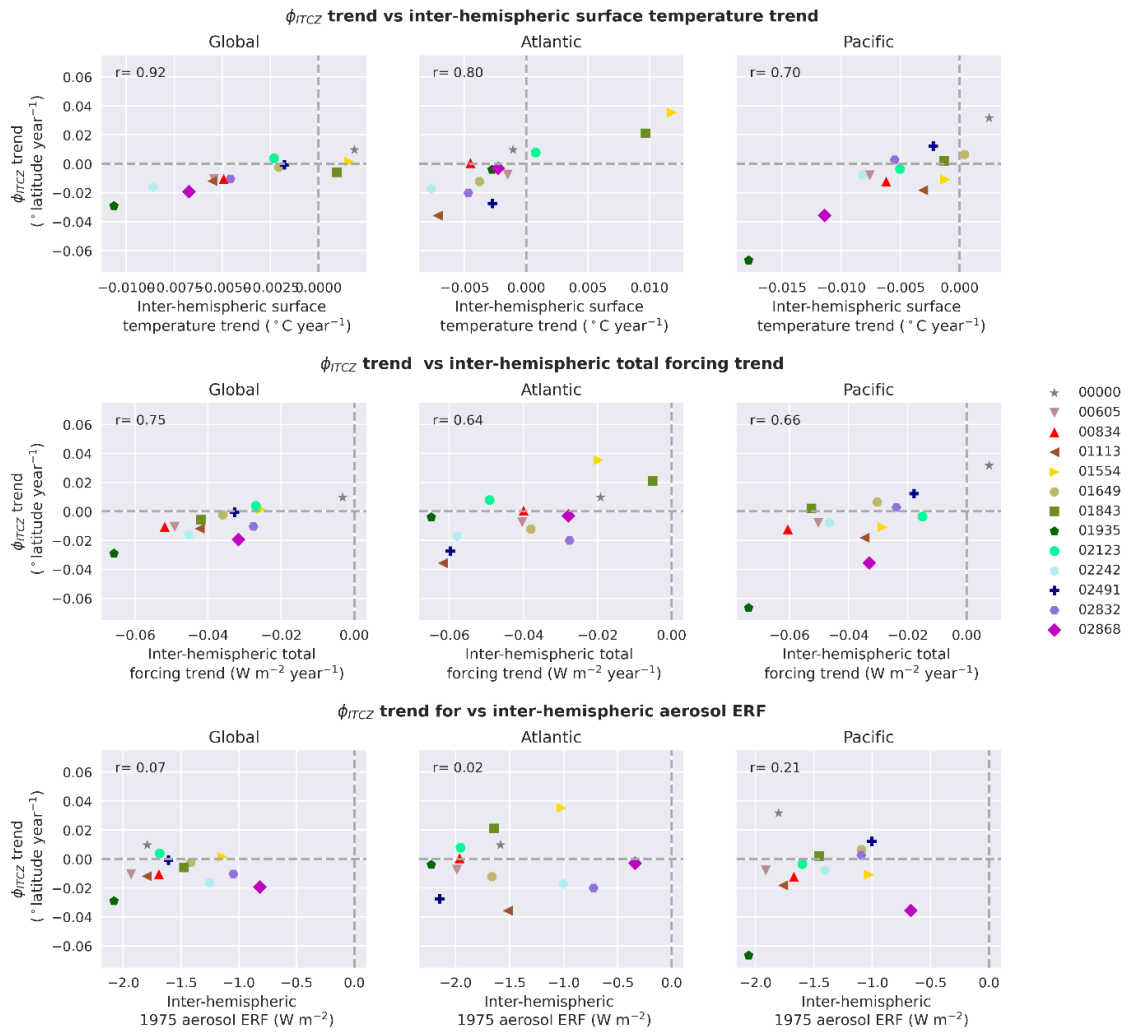


Figure B.8 Scatter plot of trend in 5-year rolling mean Φ_{ITCZ} in 1950 to 1985 (top) against ocean-only inter-hemispheric (60° S to 60° N) trend in surface air temperature (top), total implied radiative forcing (middle) and 1860 to 1975 aerosol ERF (bottom) for global (left), Atlantic (middle) and Pacific (right) regional means. Individual ensemble members are coloured according to legend. Spearman's rank correlation coefficient is shown at top left of each plot.

Time period	Correlation with the trend in inter-hemispheric surface air temperature ($^{\circ}\text{C year}^{-1}$)	Correlation with the trend in inter-hemispheric implied total forcing ($\text{W m}^{-2} \text{ year}^{-1}$)	Inter-hemispheric 1860 to 1975 aerosol ERF (W m^{-2})
1950 to 1985 (shown)	$r = 0.92$	$r = 0.75$	$r = 0.07$
1950 to 1980	$r = 0.69$	$r = 0.66$	$r = 0.14$
1940 to 1985	$r = 0.19$	$r = 0.55$	$r = -0.08$
1940 to 1980	$r = -0.03$	$r = 0.49$	$r = -0.10$
1940 to 1975	$r = 0.26$	$r = 0.63$	$r = -0.35$

Table B.2 Table of Spearman's rank correlation coefficients for the trend in global mean 5-year rolling mean Φ_{ITCZ} and ocean-only inter-hemispheric variables shown in Figure 3 for the time periods: 1950 to 1985, 1950 to 1980, 1940 to 1985, 1940 to 1980 and 1940 to 1975.

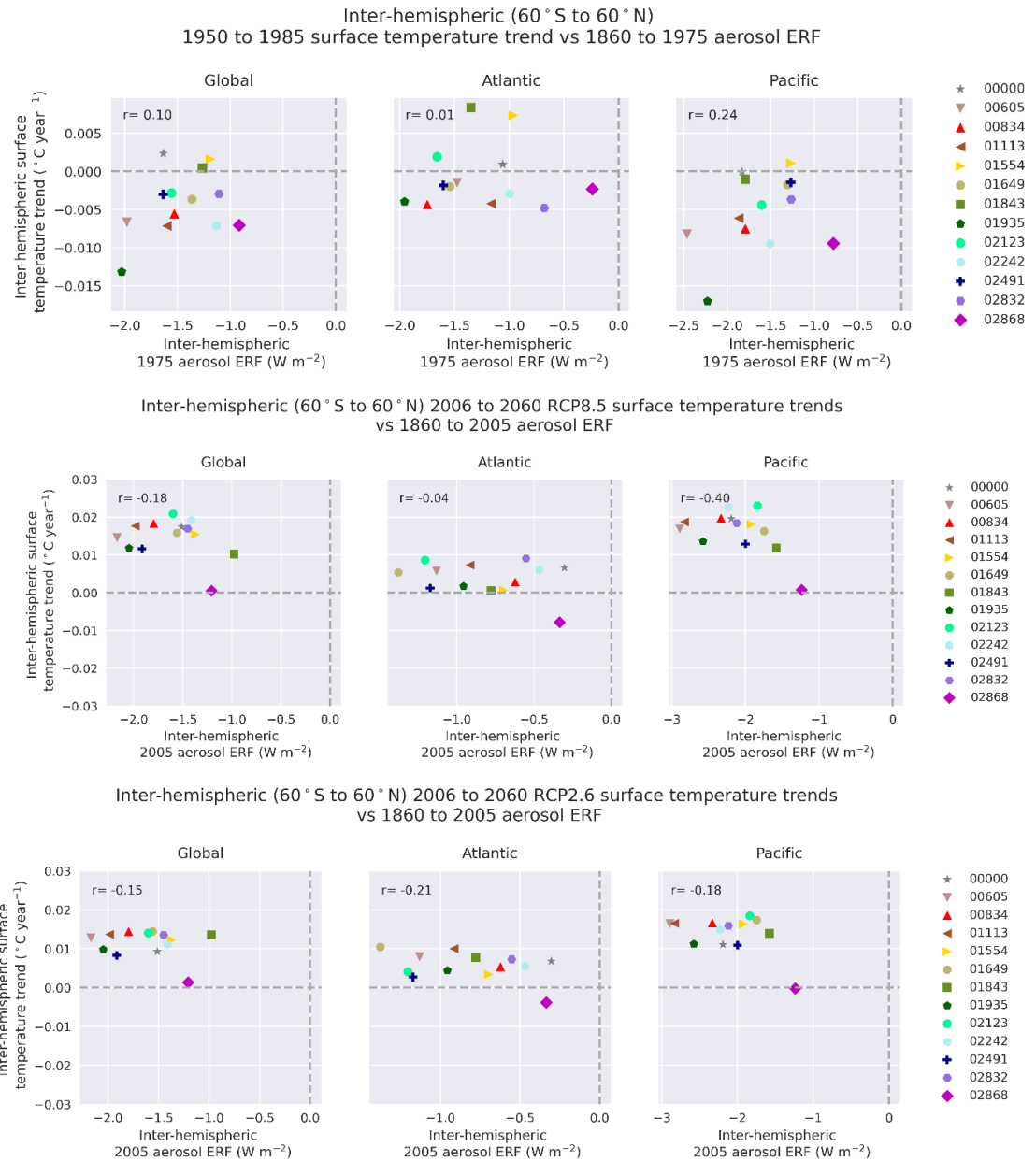


Figure B.9 Scatter plot of (top) 1950 to 1985 inter-hemispheric surface temperature trend against 1860 to 1975 aerosol ERF and (middle, bottom) 2006 to 2060 inter-hemispheric surface temperature trend against 1860 to 2005 aerosol ERF for global (left), Atlantic (middle) and Pacific (right) regional means. Individual ensemble members are coloured according to legend. Spearman's correlation coefficient is shown at top left of each plot.

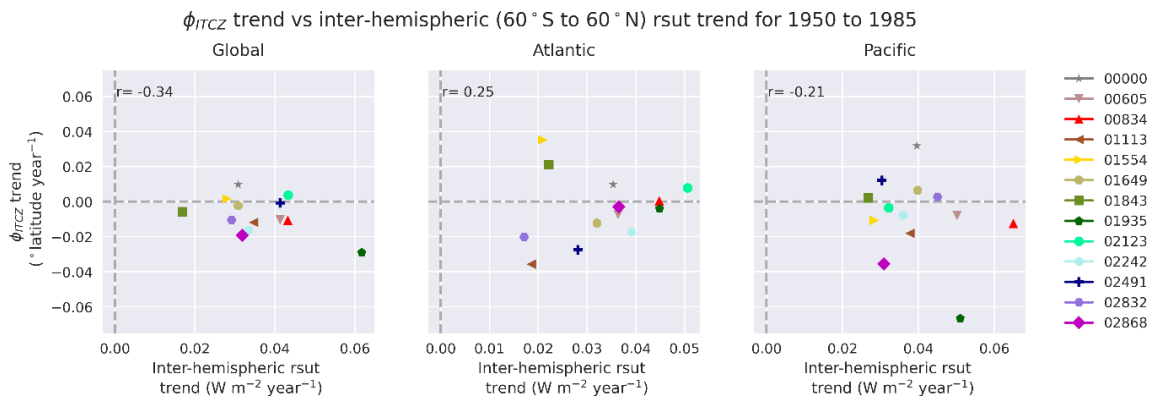


Figure B.10 Scatter plot of the 1950 to 1985 trend in 5-year rolling mean Φ_{ITCZ} against inter-hemispheric top of atmosphere outgoing shortwave flux (rsut) (0 to 60 $^{\circ}$ S and $^{\circ}$ N latitude) for global (left), Atlantic (middle) and Pacific (right) regional means. Individual ensemble members are coloured according to legend. Spearman's rank correlation coefficient is shown at top left of each plot.

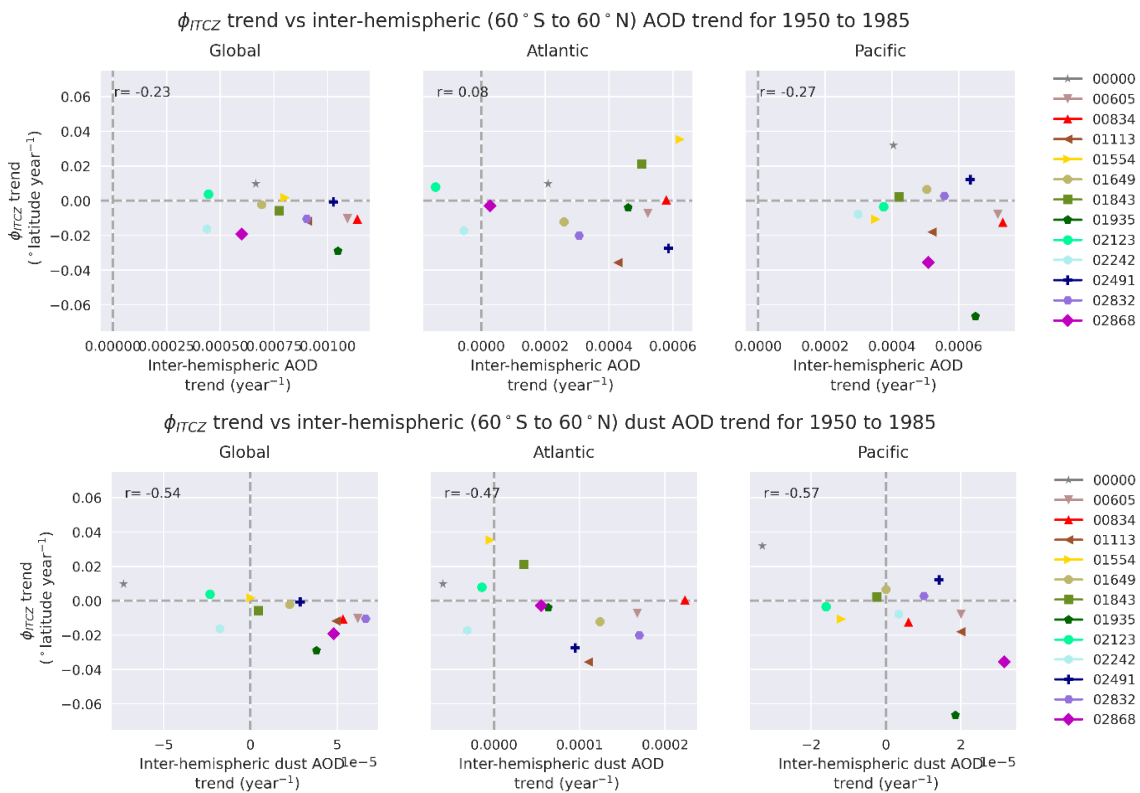


Figure B.11 Scatter plot of the 1950 to 1985 trend in 5-year rolling mean Φ_{ITCZ} against inter-hemispheric (0 to 60 $^{\circ}$ S and $^{\circ}$ N latitude) total AOD (top) and dust AOD (bottom) for global (left), Atlantic (middle) and Pacific (right) regional means. Individual ensemble members are coloured according to legend. Spearman's rank correlation coefficient is shown at top left of each plot.

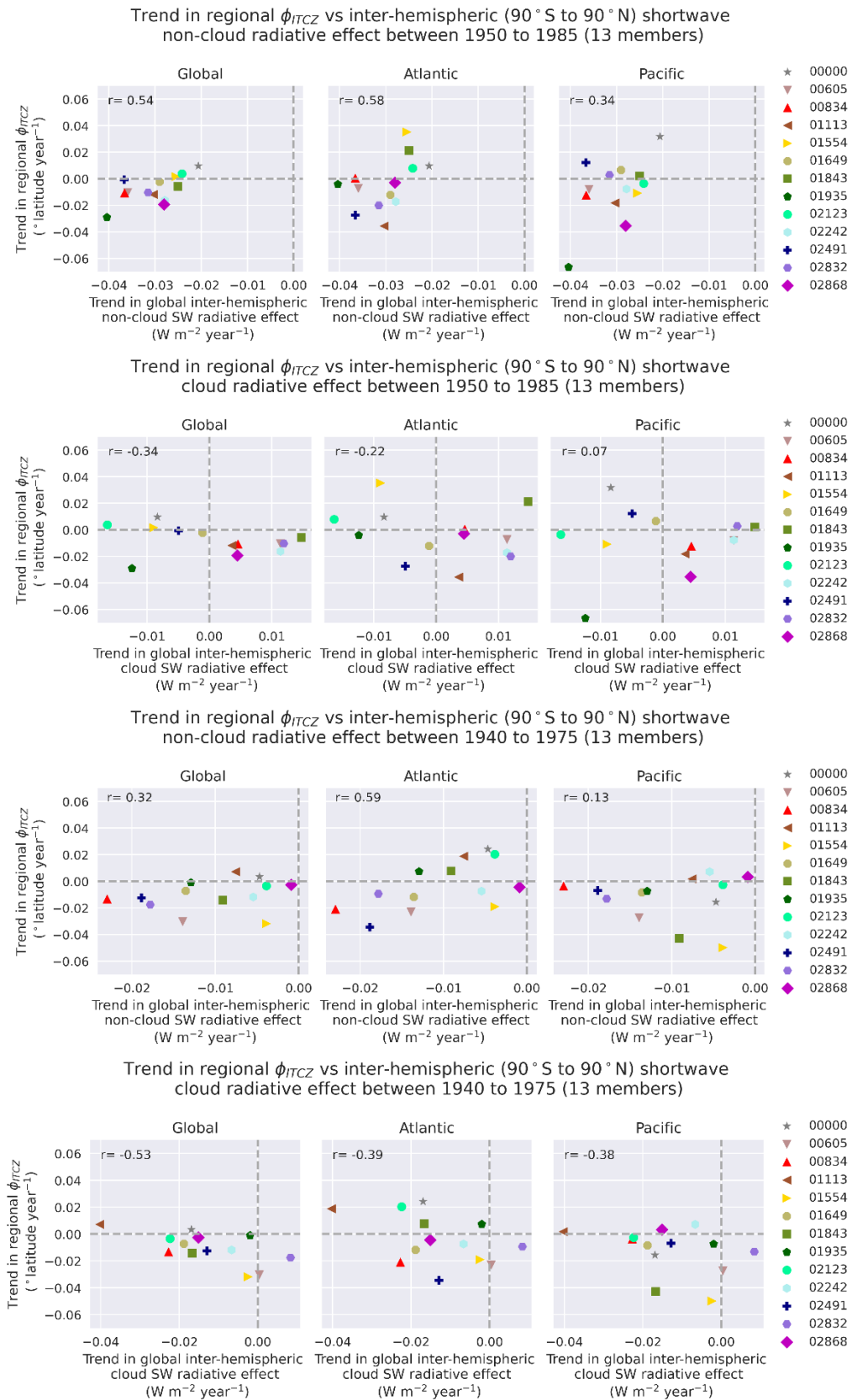


Figure B.12 Scatter plot of 1950 to 1985 and 1940 to 1975 trend in 5-year rolling mean Φ_{ITCZ} against trend in global inter-hemispheric (90° S to 90° N) implied forcing from shortwave non-cloud interactions and cloud interactions for global (left), Atlantic (middle) and Pacific (right) regional. Spearman's rank correlation coefficient is shown at top left of each plot.

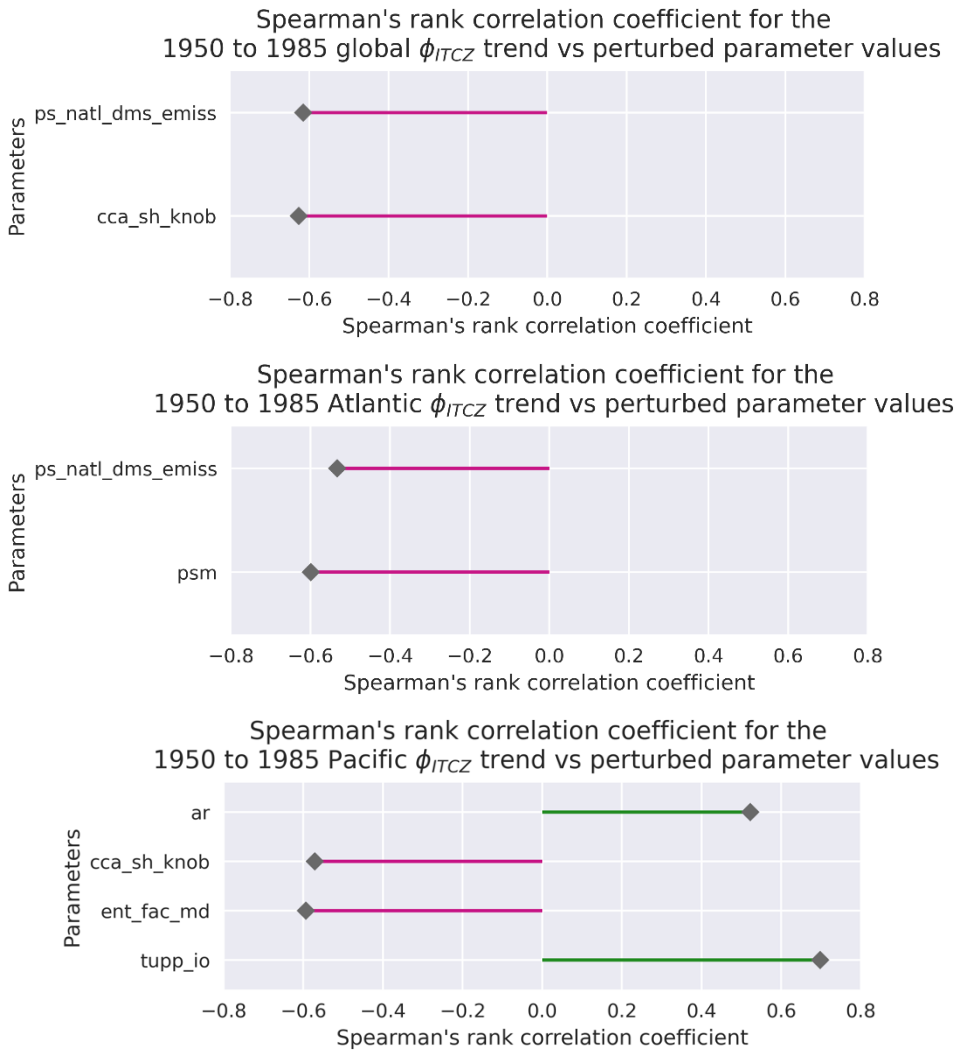


Figure B.13 Plots of the parameters that have a Spearman's rank correlation coefficient or $r > 0.5$ with the trend in 5-year rolling mean ϕ_{ITCZ} in 1950 to 1985 in global (top), Atlantic (middle) and Pacific (bottom) regional means. Individual ensemble members are coloured according to legend. Negative relationships are shown in pink and positive in green. Definitions of parameters are in Table B.1.

Text B.1. Tropical precipitation shifts were also calculated based on the methodology in Allen et al. 2015 in order to compare the spread in our single-model PPE to a multi-model ensemble. First, the annual precipitation anomaly is calculated against a 1961 – 1990 base period. This methodology then defines tropical precipitation shifts (mm decade⁻¹) as the difference between area-weighted northern hemisphere (0 – 20 °N) and southern hemispheric (0 – 20 °S) regional means over land and ocean. The Atlantic region is defined (75 °W – 30 °E) and the Pacific region as (30 °E – 75 °W). The trend over 1950 – 1985 is calculated from the 5-year rolling mean of this metric.

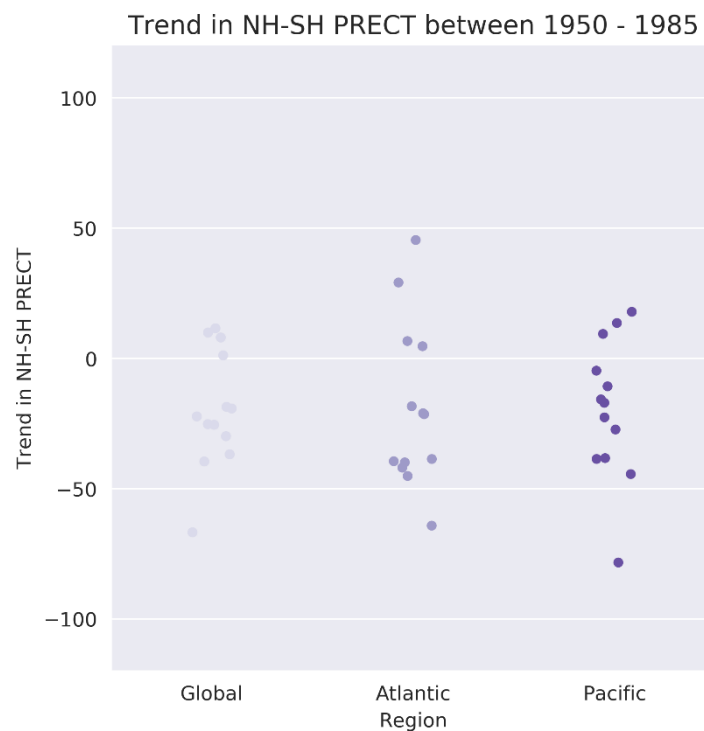


Figure B.14 The 1950 to 1985 trend in the tropical precipitation metric (NH-SH PRECT / mm decade⁻¹) defined in Text B.1 over land and ocean for the three regional means.

ϕ_{ITCZ} trend for 2006 to 2060 vs ocean-only inter-hemispheric variables (60° S to 60° N)

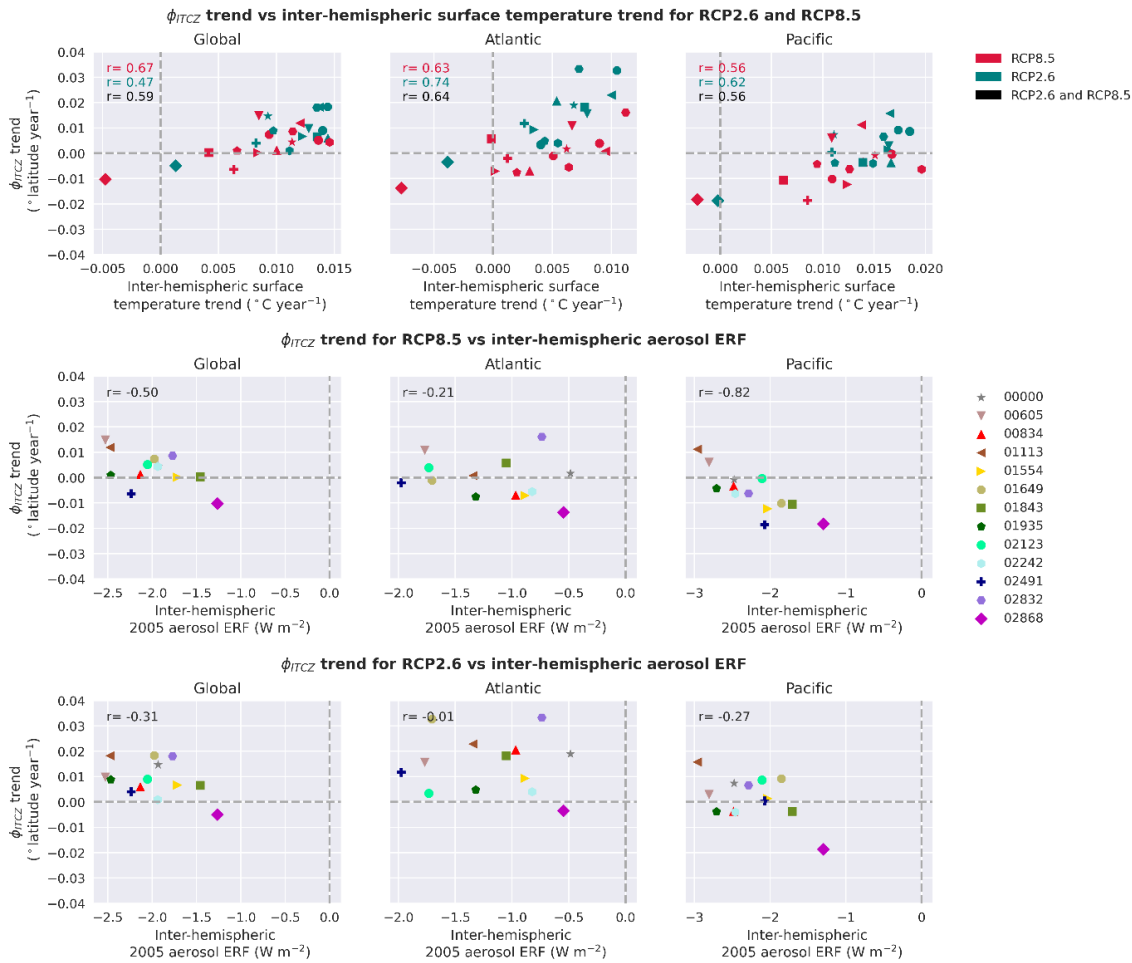


Figure B.15 Scatter plot of trend in 5-year rolling mean Φ_{ITCZ} in 2006 to 2060 (top) against ocean-only inter-hemispheric (60° S to 60° N) trend in surface air temperature (top), implied total forcing (middle) and 1860 to 1975 aerosol ERF (bottom) for global (left), Atlantic (middle) and Pacific (right) regional means. Individual ensemble members are coloured according to legend. The Spearman's rank correlation coefficient is shown at top left of each plot. For the top row, RCP8.5 is red, RCP2.6 is teal, and the scenarios combined is black.

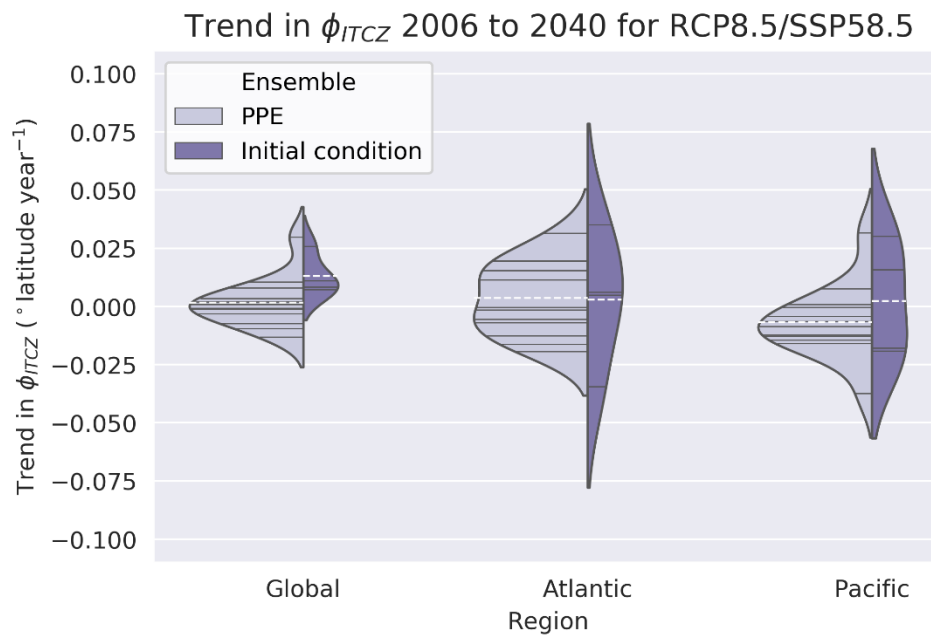


Figure B.16 Violin plot of trend in 5-year rolling mean Φ_{ITCZ} in 2006 to 2040 for RCP8.5, the internal variability is estimated from HadGEM3-GC3.1 (historical and SSP5-8.5) ensemble. This figure tests how the trend over a future time period of comparable size to the historical time period influences the range of trends in tropical precipitation across the ensemble.

References

Allen, R. J., Evan, A. T. and Booth, B. B. B.: Interhemispheric aerosol radiative forcing and tropical precipitation shifts during the late Twentieth Century, *J. Clim.*, 28(20), 8219–8246, doi:10.1175/JCLI-D-15-0148.1, 2015.

Murphy, J. M., Harris, G. R., Sexton, D. M. H., Kendon, E. J., Bett, P. E., Clark, R. T., Eagle, K. E., Fosse, G., Fung, F., Lowe, J. A., McDonald, R. E., McInnes, R. N., McSweeney, C. F., Mitchell, J. F. B., Rostron, J. W., Thornton, H. E., Tucker, S. and Yamazaki, K.: UKCP18: Land Projections Science Report., 2018.

Appendix C

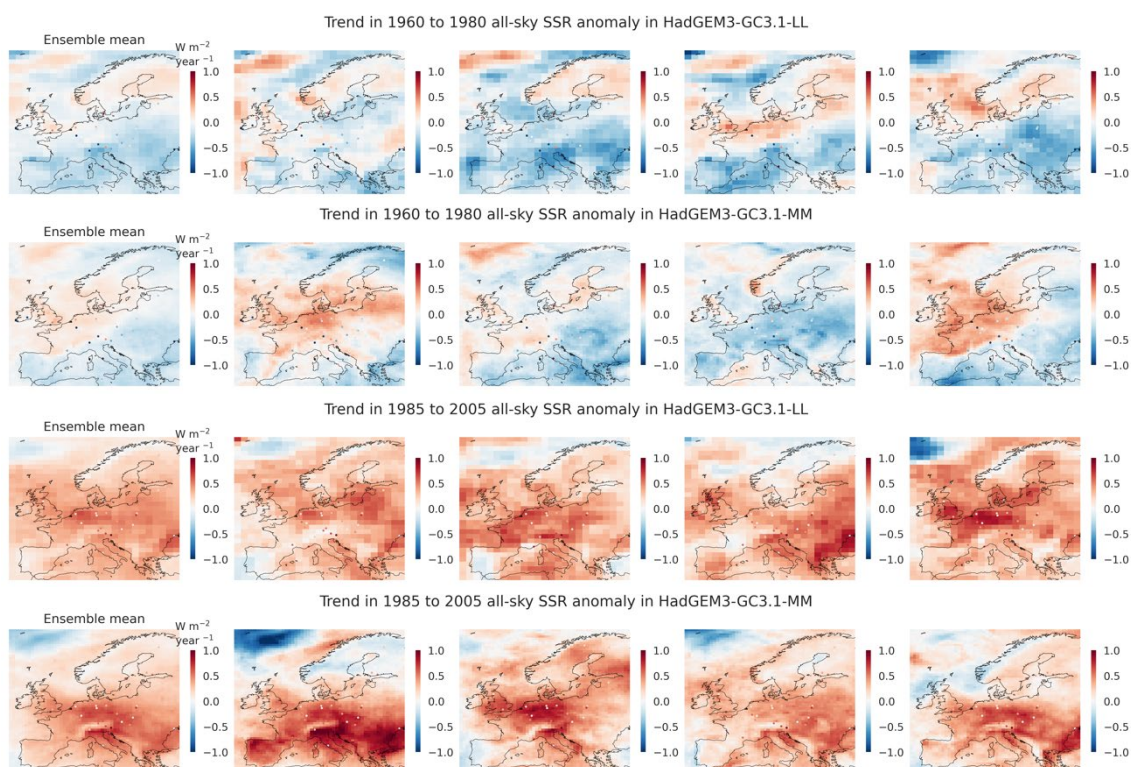


Figure C.1 (top rows) 1960 to 1980 linear trend of the five-year rolling mean annual anomaly (from the 1960 to 1980 mean) and (bottom rows) 1985 to 2005 linear trend of the five-year rolling mean annual anomaly (from the 1985 to 2005 base period) in all sky SSR ($\text{W m}^{-2} \text{ year}^{-1}$) across Europe. GEBA observations are overlaid in circles. The ensemble mean is shown at the left of the plot, followed by initial condition ensemble members.

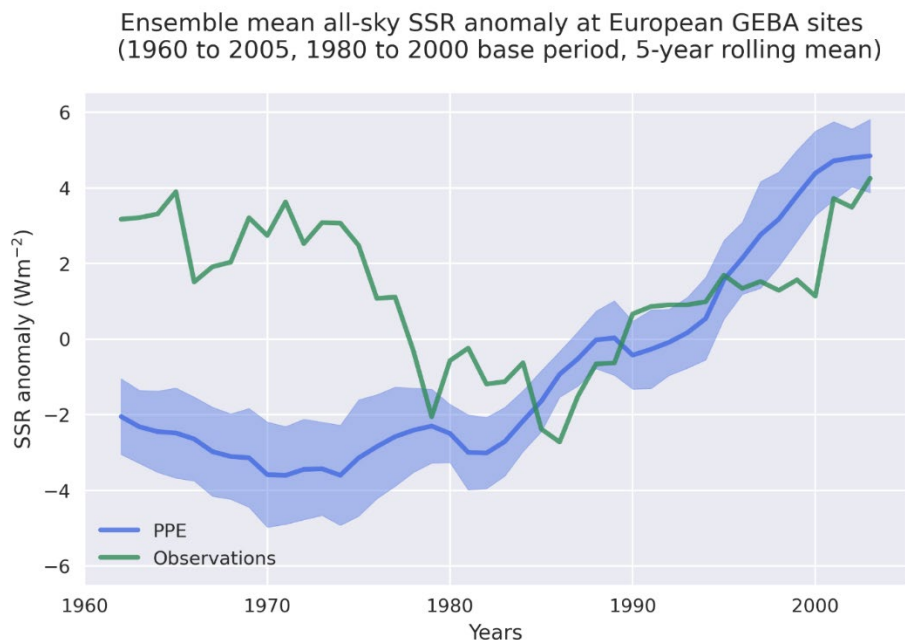
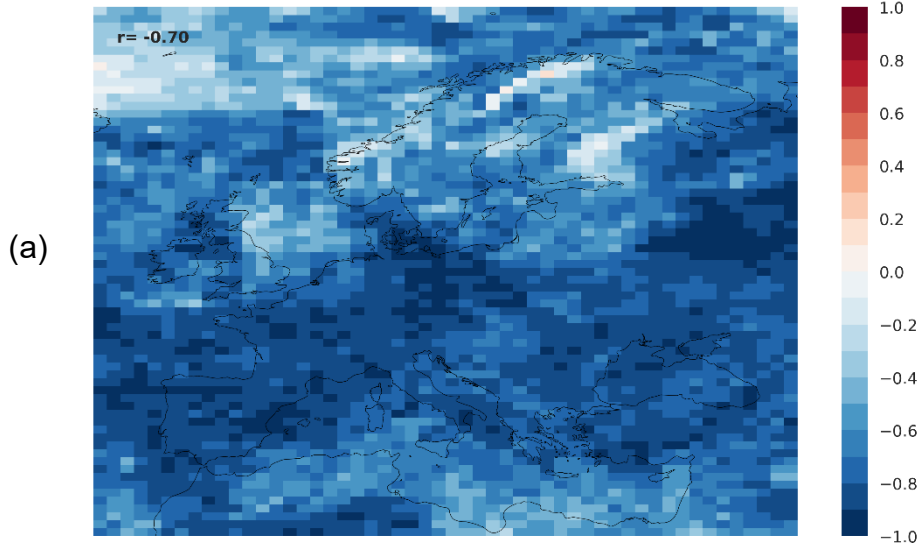
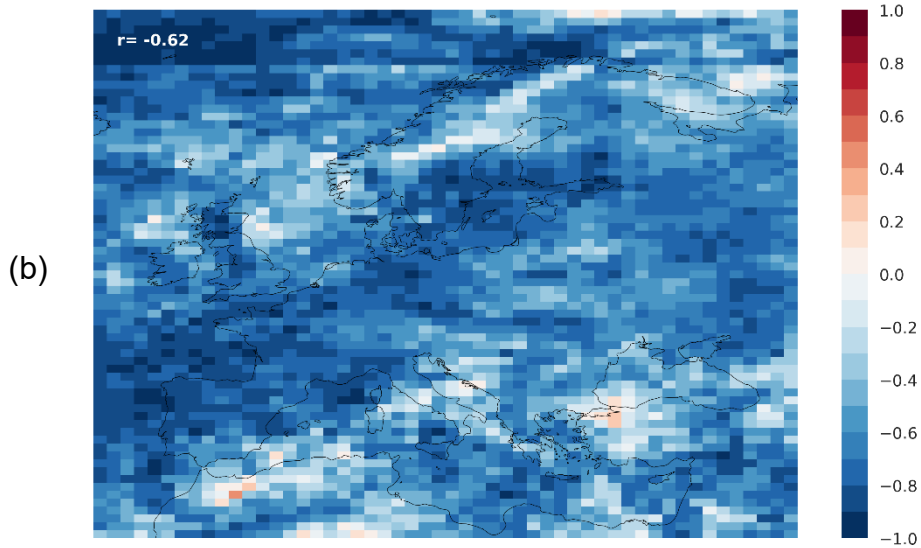


Figure C.2 Five year rolling mean time series of the annual anomaly (against 1980 to 2000 base period) in SSR (W m^{-2}) for the average over European GEBA stations (green), the nearest model grid boxes to stations in the PPE (blue). The shading around the PPE each time series shows the spread in the ensemble mean for \pm the ensemble standard.

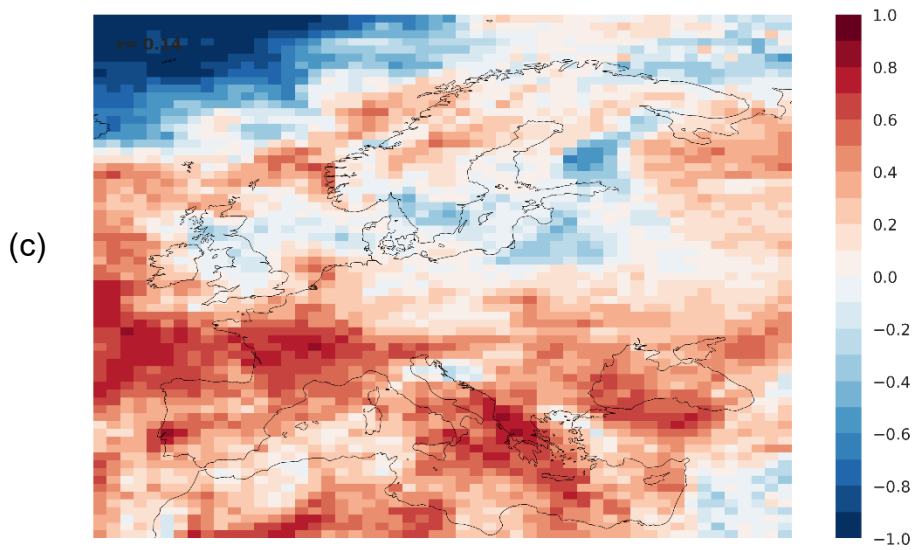
Spearman's correlation coefficient between
1960 to 1980 trend in annual rsds and cit



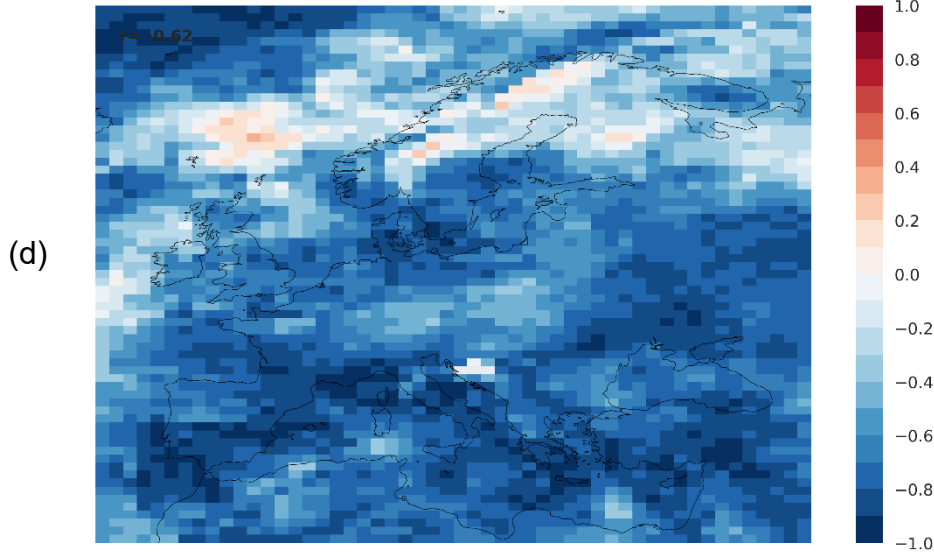
Spearman's correlation coefficient between
1960 to 1980 trend in annual rsds and isccp cloud albedo



Spearman's correlation coefficient between
1960 to 1980 trend in annual rsds and tas



Spearman's correlation coefficient between
1960 to 1980 trend in annual rds and hur @ 850 hPa



Spearman's correlation coefficient between
1960 to 1980 trend in annual rds and AOD

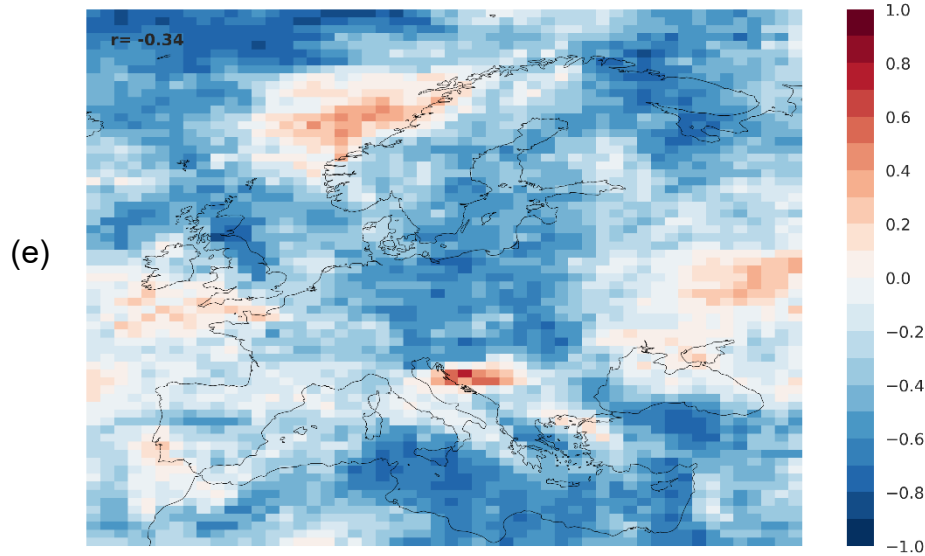


Figure C.3 Spearman's correlation coefficient for the 1960 to 1980 SSR against a) cloud fraction, b) cloud albedo weighted by cloud fraction, c) surface air temperature, d) relative humidity at pressure level 850 hPa, and e) aerosol optical depth.

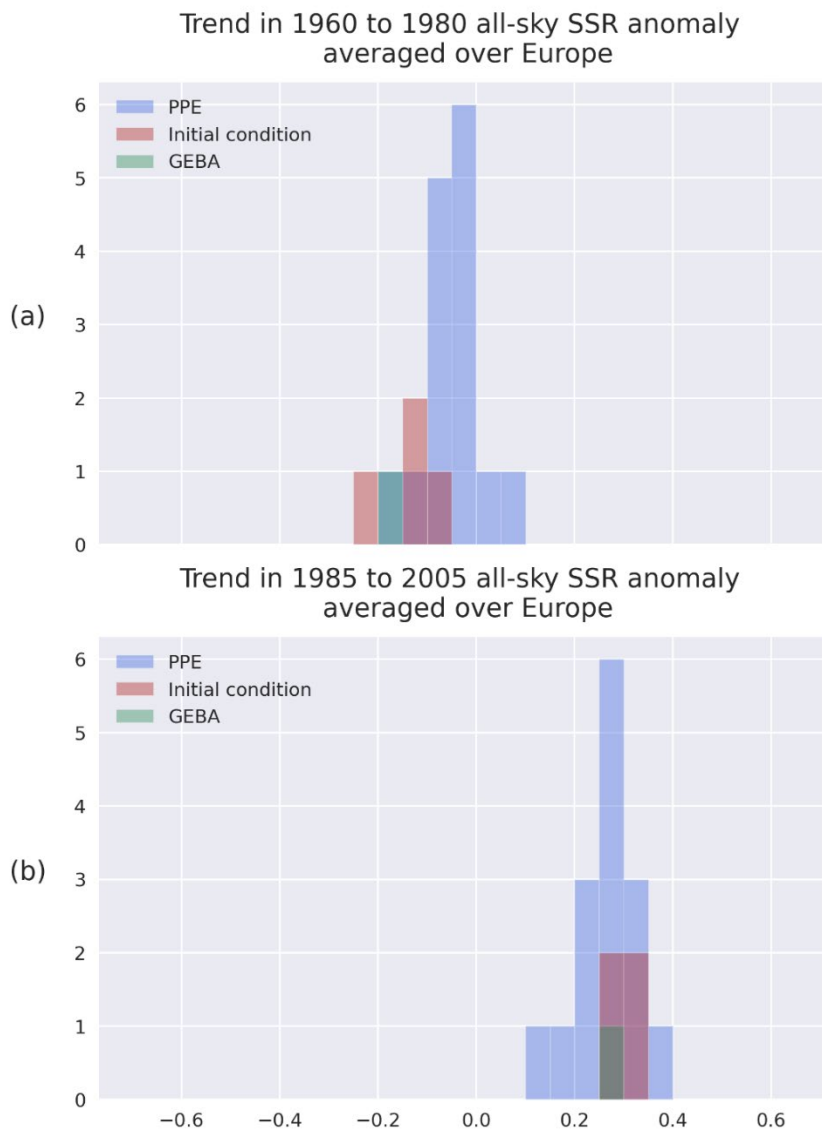


Figure C.4 Histogram of the trend ($W m^{-2} year^{-1}$) in the five-year rolling mean time series of the annual anomaly in SSR for the whole European average of modelled data and for the average over European GEBA station over a) 1960 to 1980 and b) 1985 to 2005. Initial condition ensemble is HadGEM3-GC3.1-LL.

Trend in 1960 to 1980 seasonal all-sky SSR anomaly
averaged over European GEBA stations

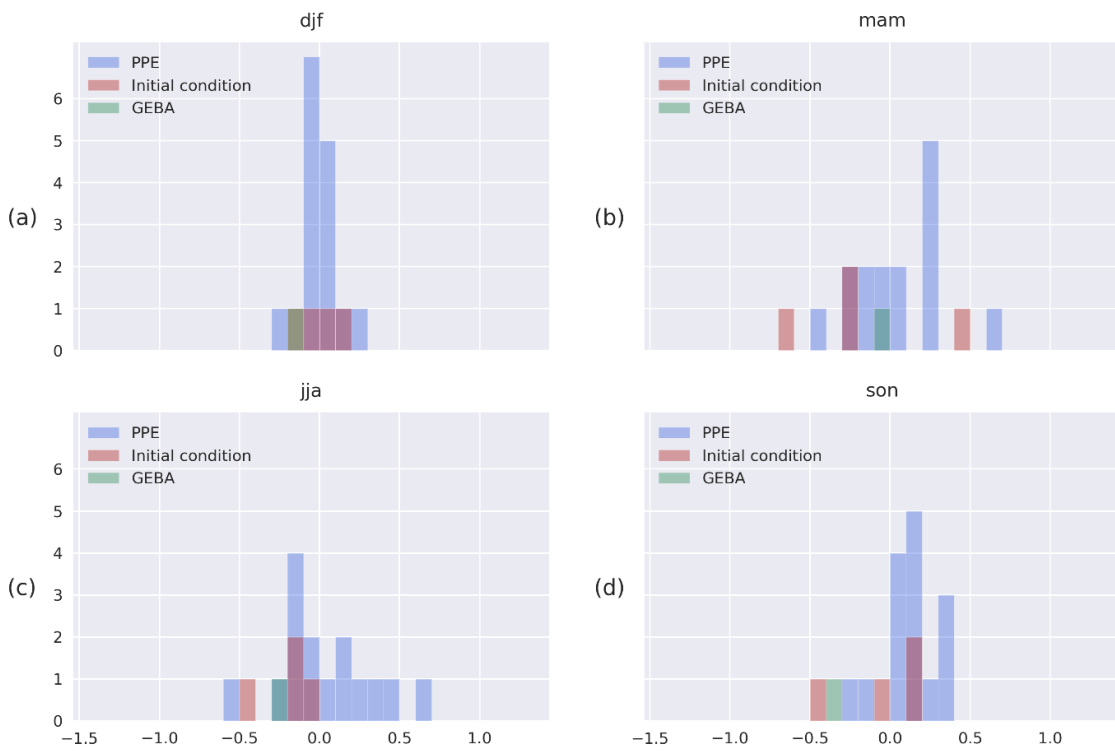


Figure C.5 Histogram of the 1960 to 1980 trend ($W m^{-2} year^{-1}$) in the 5-year rolling mean time series of the anomaly in SSR for the average over European GEBA station in a) DJF*, b) MAM, c) JJA and d) SON. *GEBA seasonal mean is calculated over January and February only. Initial condition ensemble is HadGEM3-GC3.1-LL.

Trend in 1985 to 2005 seasonal all-sky SSR anomaly
averaged over European GEBA stations

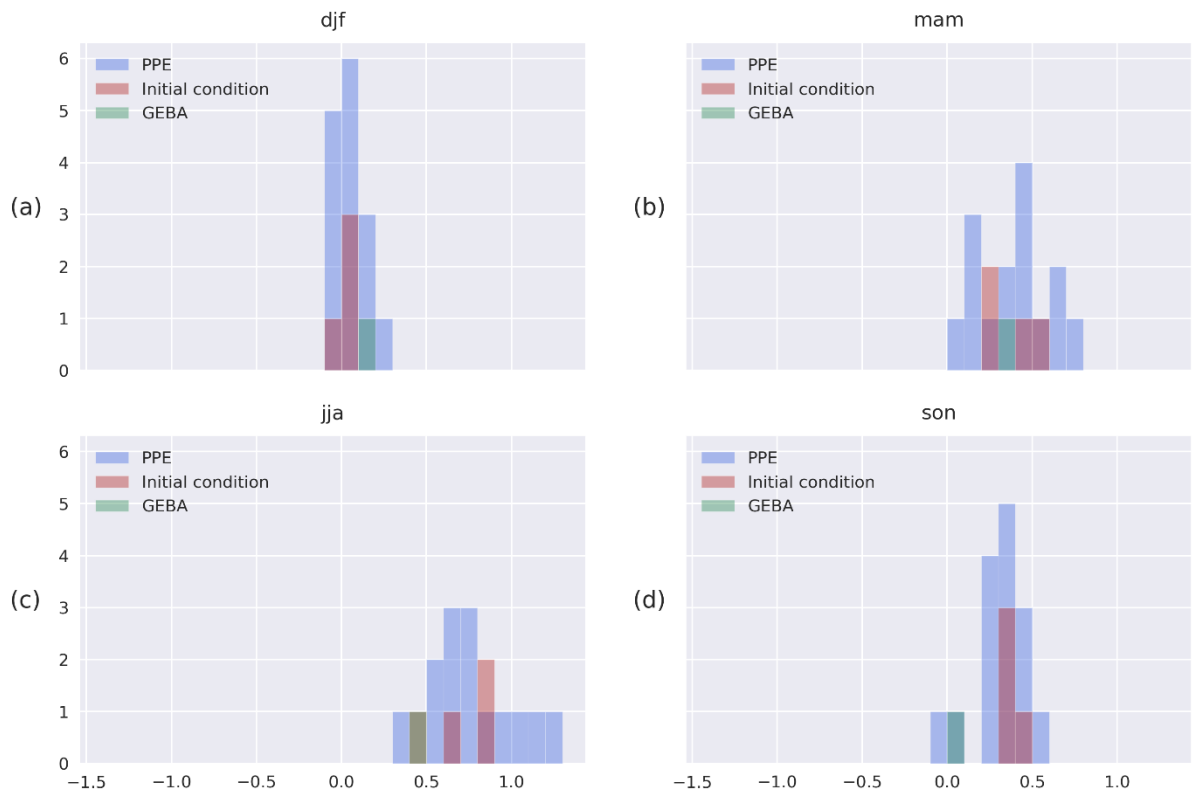


Figure C.6 Histogram of the 1985 to 2005 trend ($W m^{-2} year^{-1}$) in the 5-year rolling mean time series of the anomaly in SSR ($W m^{-2}$) for the average over European GEBA station in a) DJF*, b) MAM, c) JJA and d) SON. *GEBA seasonal mean is calculated over January and February only. Initial condition ensemble is HadGEM3-GC3.1-LL.

Trend in 1960 to 1980 clear-sky SSR anomaly

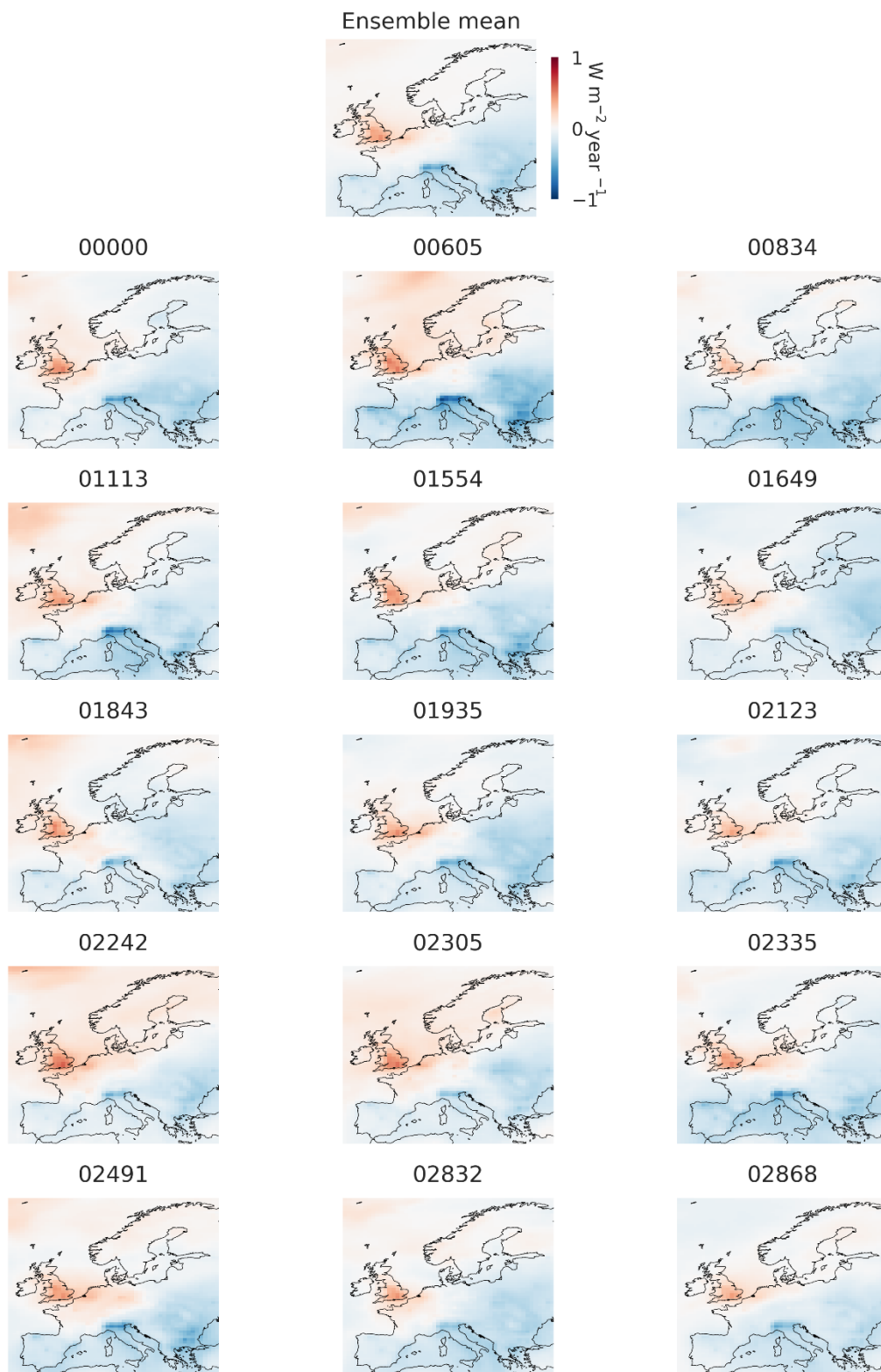


Figure C.7 1960 to 1980 linear trend of the five-year rolling mean annual anomaly (from the 1960 to 1980 mean) in clear-sky SSR ($W m^{-2} year^{-1}$) across Europe. Individual ensemble members are labelled by numbers.

Trend in 1985 to 2005 clear-sky SSR anomaly

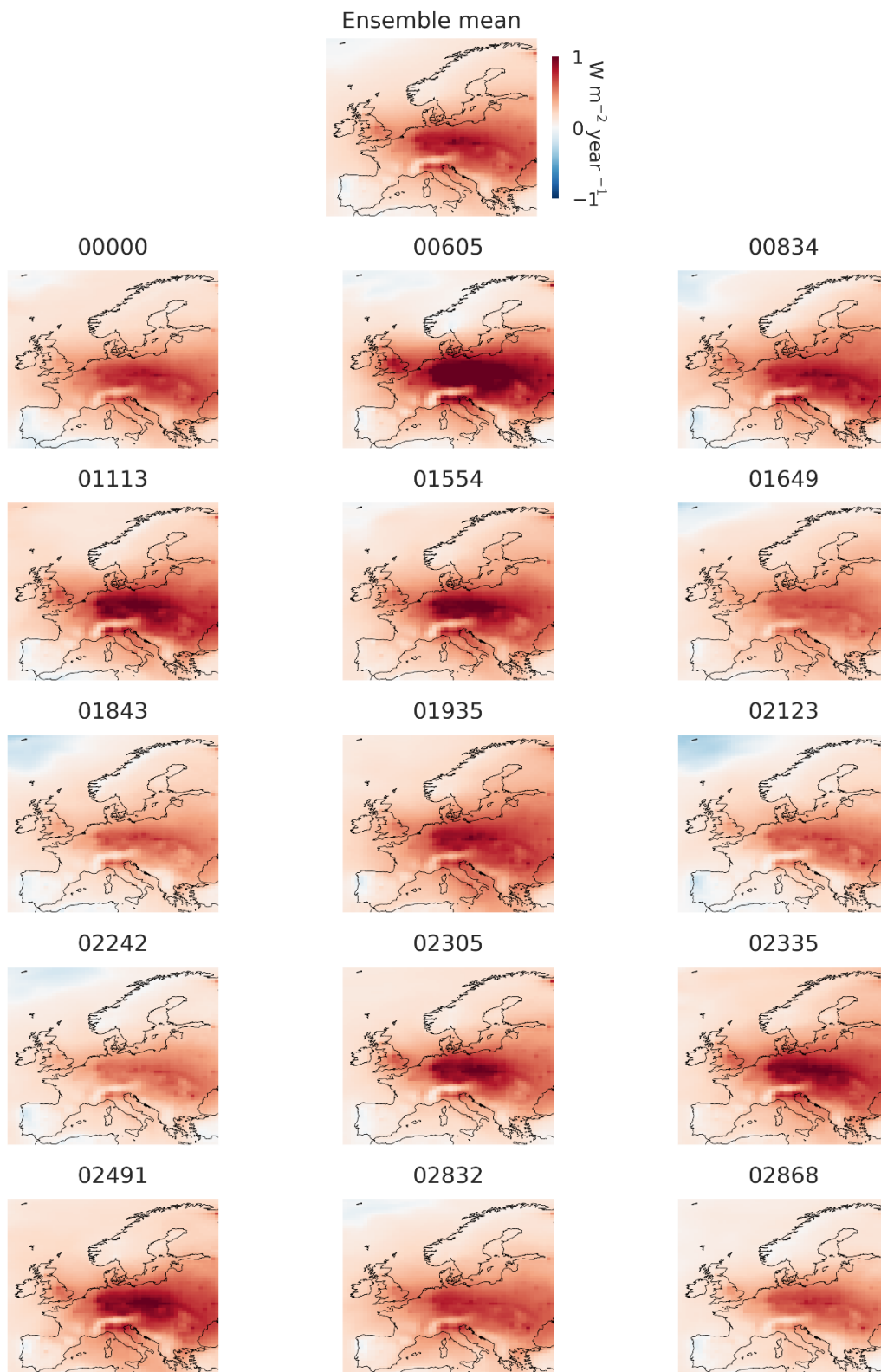


Figure C.8 1985 to 2005 linear trend of the 5-year rolling mean annual anomaly (from the 1985 to 2005 mean) in clear-sky SSR ($W\ m^{-2}\ year^{-1}$) across Europe. Individual ensemble members are labelled by numbers.

Trend in 1960 to 1980 CLT

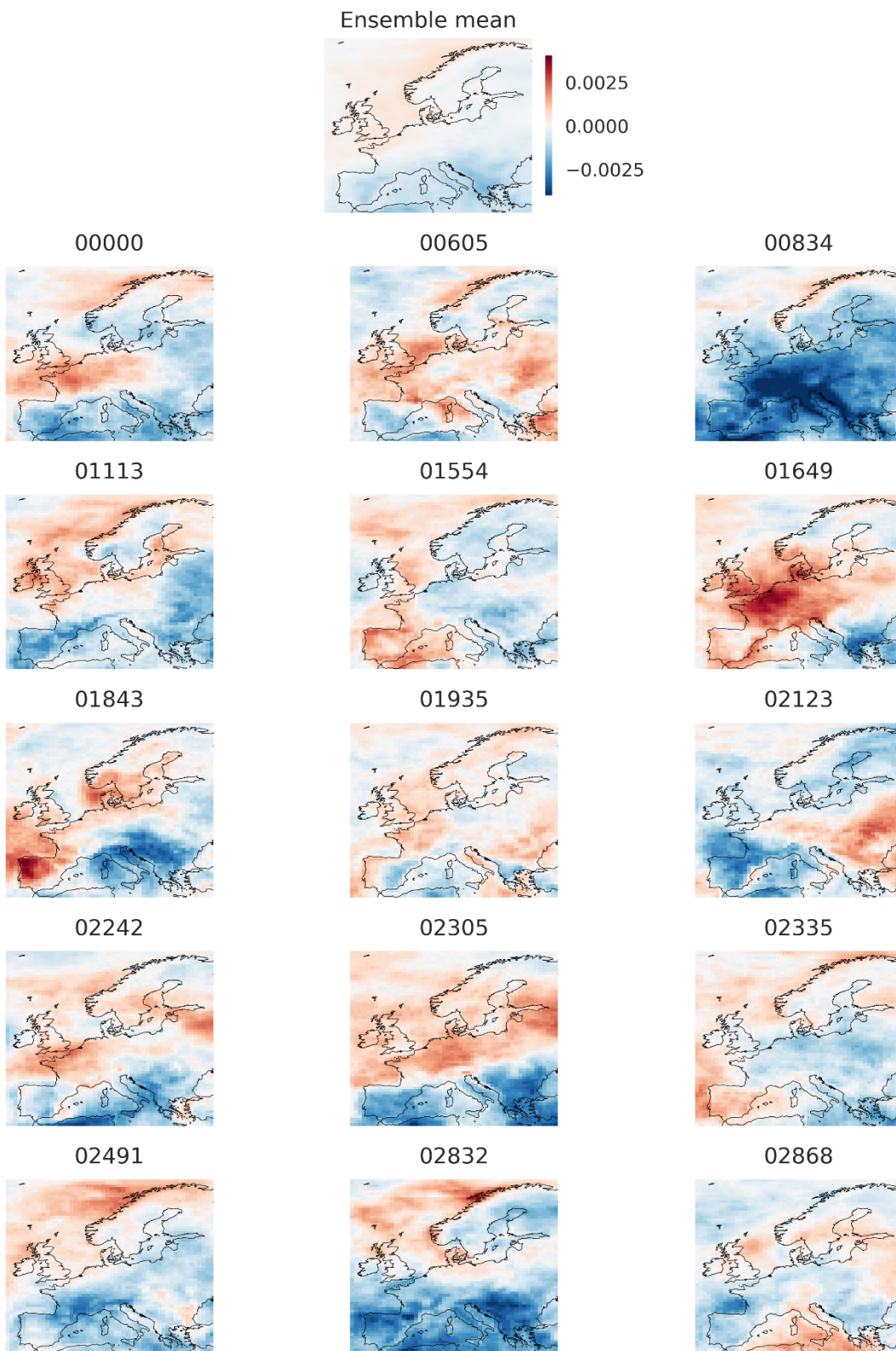


Figure C.9 1960 to 1980 linear trend of the 5-year rolling mean annual cloud fraction anomaly across Europe. Individual ensemble members are labelled by numbers.

Trend in 1985 to 2005 CLT

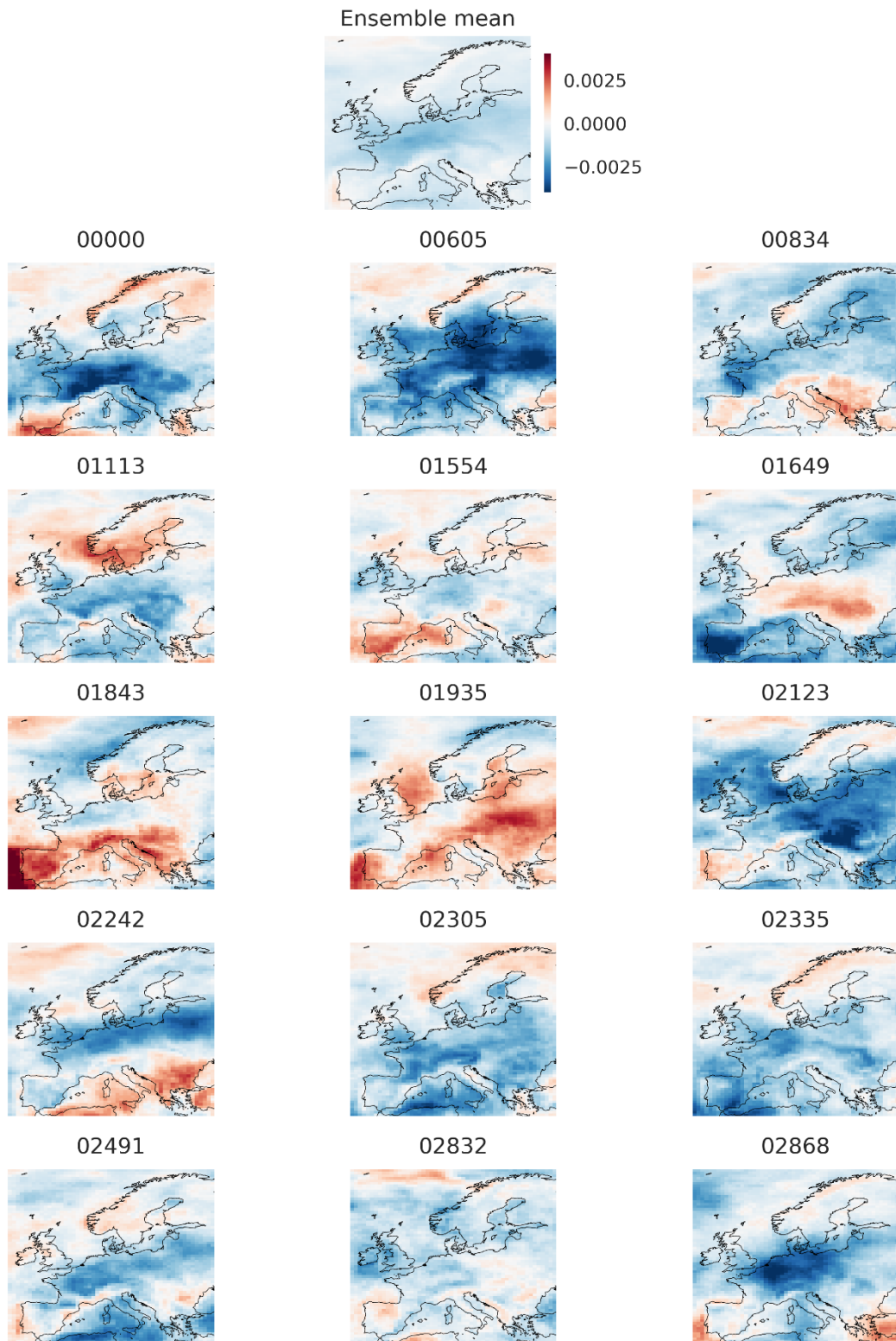


Figure C.10 1985 to 2005 linear trend of the 5-year rolling mean annual cloud fraction anomaly across Europe. Individual ensemble members are labelled by numbers.

Anthropogenic aerosol ERF 1860 to 1975

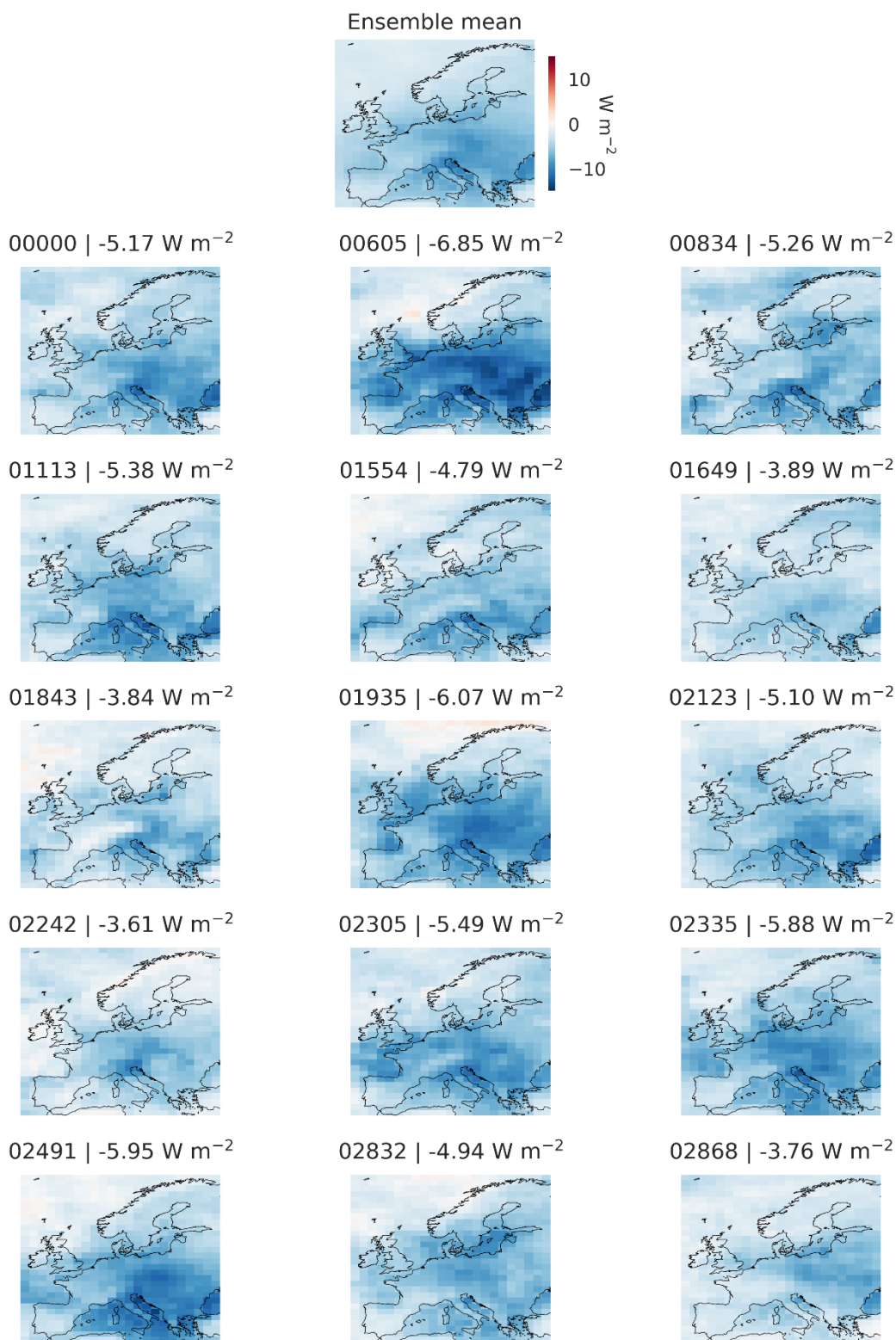


Figure C.11 1860 to 1975 anthropogenic aerosol ERF for PPE members and the ensemble mean. The European mean anthropogenic aerosol ERF is shown next to the realization number.

Anthropogenic aerosol ERF 1975 to 2005

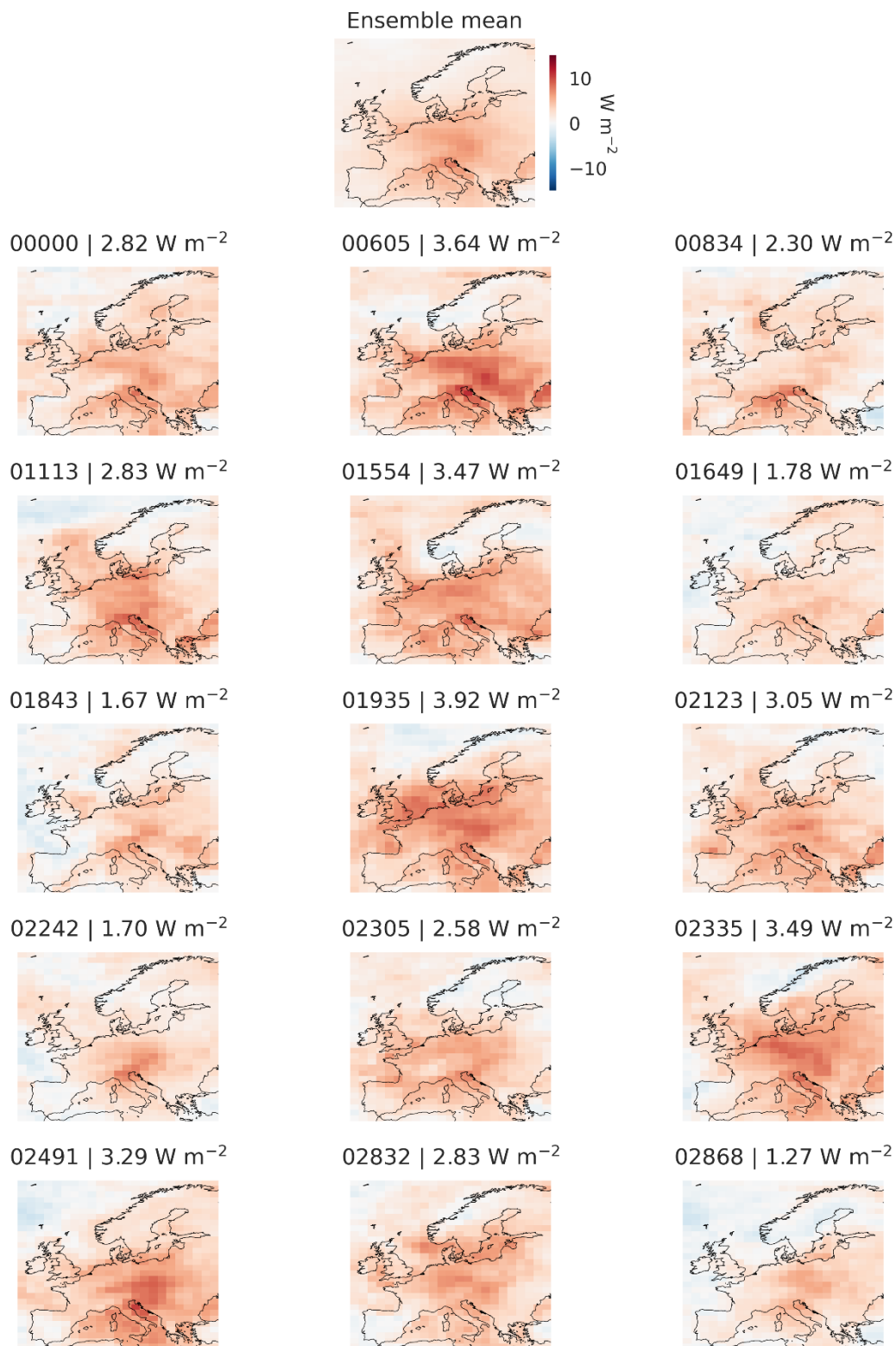


Figure C.12 1975 to 2005 anthropogenic aerosol ERF for PPE members and the ensemble mean. The European mean anthropogenic aerosol ERF is shown next to the realization number.

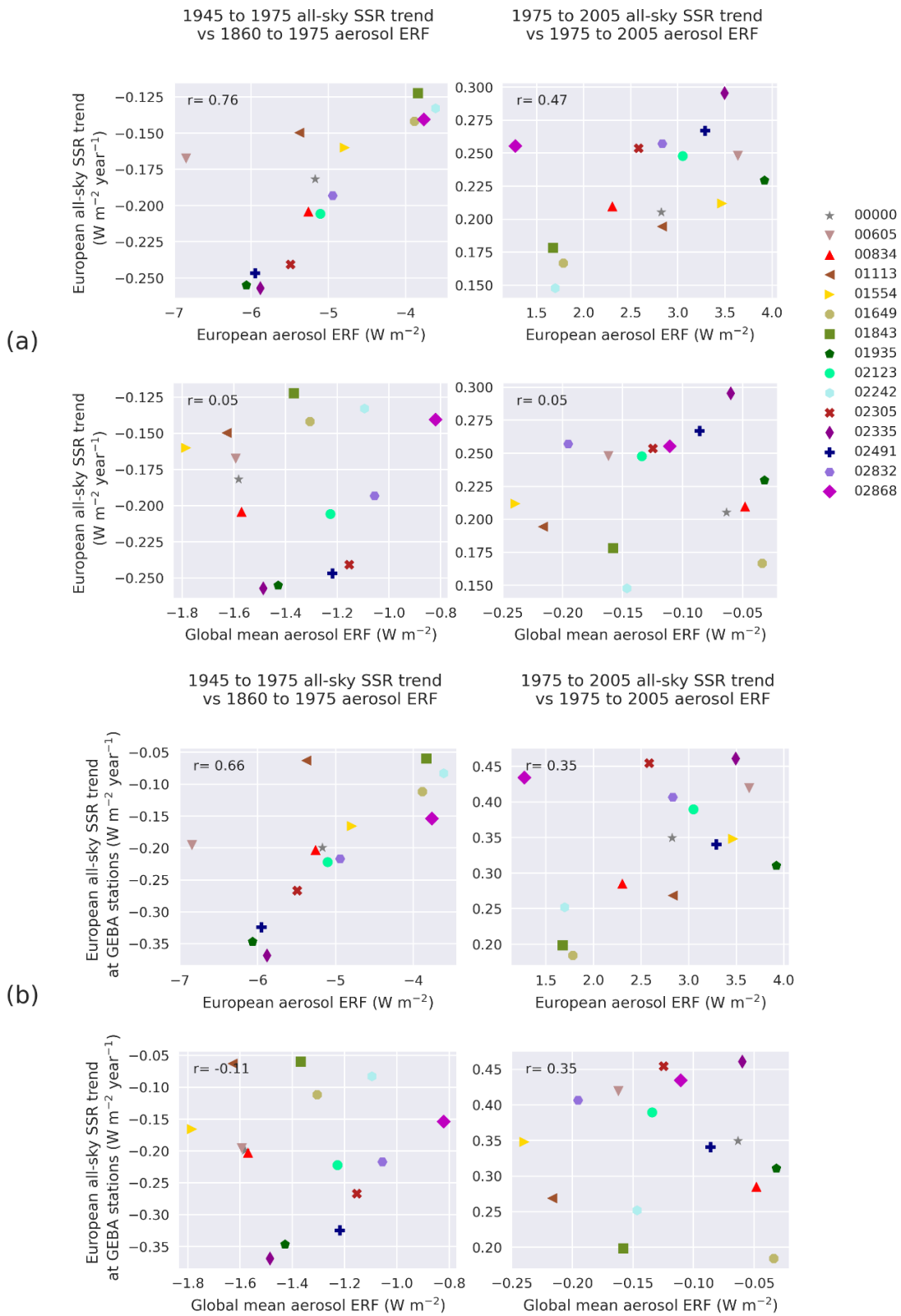


Figure C.13 Scatter plot of the trend in (a) European mean and (b) European mean at GEBA stations all-sky surface solar radiation against anthropogenic aerosol ERF. The left columns shows the 1945 to 1975 trend in SSR against 1860 to 1975 anthropogenic aerosol ERF. The right column shows 1975 to 2005 trend in SSR against 1970 to 2005 anthropogenic aerosol ERF. The Spearman's correlation coefficient is shown in the top left of each subplot.

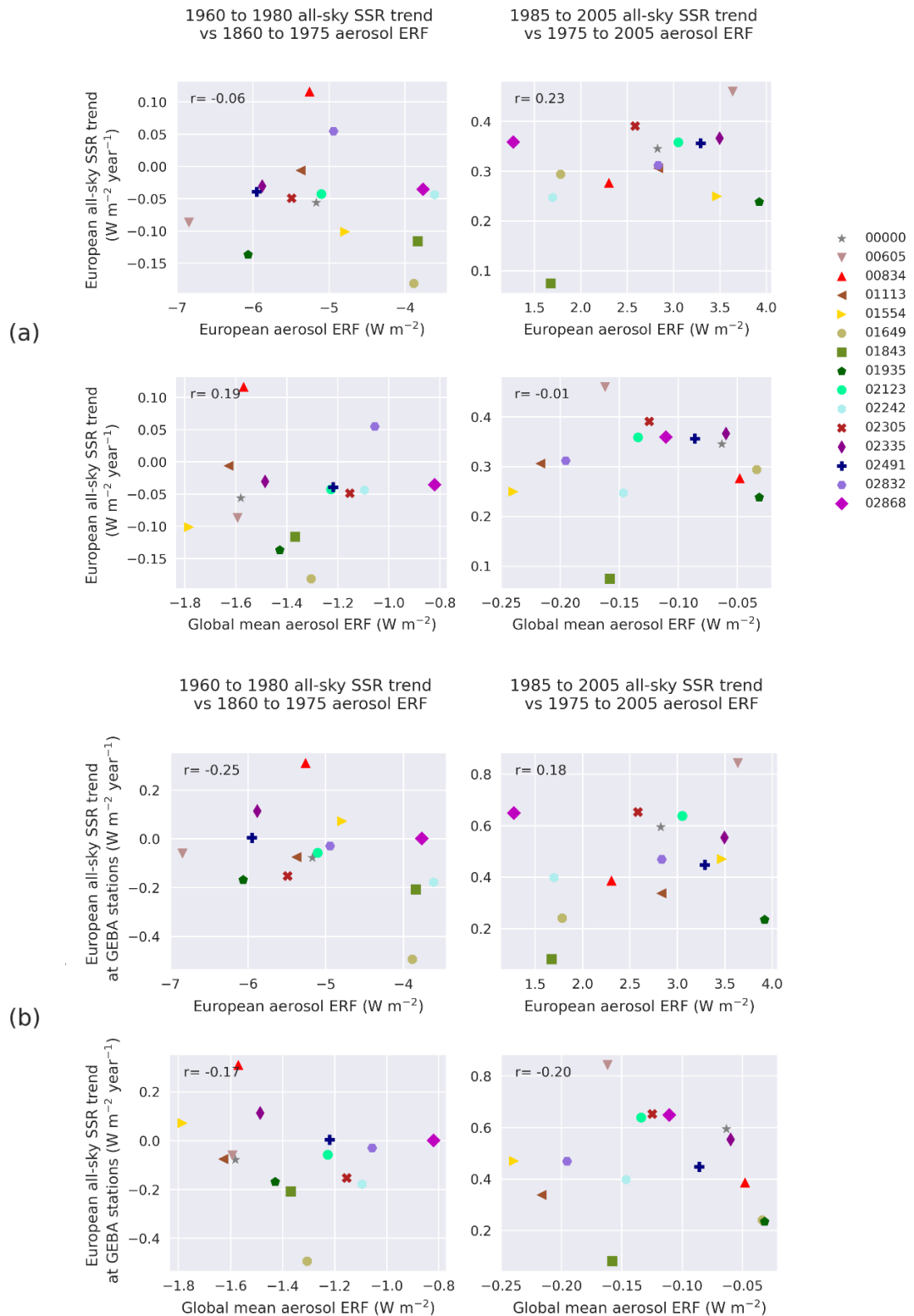


Figure C.14 Scatter plot of the trend in (a) European mean and (b) European mean at GEBA stations all-sky surface solar radiation against anthropogenic aerosol ERF. The left columns shows the 1960 to 1980 trend in SSR against 1860 to 1975 anthropogenic aerosol ERF. The right column shows 1985 to 2005 trend in SSR against 1970 to 2005 anthropogenic aerosol ERF. The Spearman's correlation coefficient is shown in the top left of each subplot.